# Electrode measurements of the net charge on muscle proteins

## Thesis

UNRESTRICTED

# Electrode measurements of the net charge on muscle proteins

by

Elżbieta Anna Bryson, Master, MSc

Submitted for the Degree of
Doctor of Philosophy

Open University
Department of Physics
February 1997

Date of submission: 4th March 1997
Date of award: 6th June 1997

*To my Parents*

# Abstract

Electrode techniques for measuring Donnan potentials in protein solutions were studied and applied to elucidate the effect of methylation on the net charge of heavy meromyosin (HMM) and the effect of $Ca^{2+}$ on the net charge of the thin filament proteins.

Drifts in potentials, observed for macroelectrodes, were examined and their cause established to be KCl leakage out of electrodes. The microelectrode technique was applied to protein solutions and microelectrodes with resistance less than 1 MΩ were used: the conditions for manufacturing and maintaining electrodes functional were established.

HMM was isolated (from rabbit muscle) and methylated; the modification was verified by amino acid analysis. ATPase activity of methylated HMM was found to be significantly elevated in the presence of $Ca^{2+}$ and decreased in the presence of EDTA with respect to the activity of the native protein. Values of the net charge of both proteins were determined at pH 6.7 and no significant difference was found between them. Calculations of the theoretical charge of lysine and $N^{\epsilon}$-dimethyllysine were performed which indicated only 0.5% difference at pH 6.7.

F-actin, tropomyosin-troponin (Tm-tn) and reconstituted thin filaments (RTFs) were isolated from rabbit muscle. Conditions for preserving the binding between F-actin and Tm-tn were established. Net charges of F-actin, Tm-tn, RTFs and BSA (control) were measured in solutions of pCa 3.2–8.7 at ionic strength 0.02 M and pH 7.0. Significant decrease in the negative charge of the RTFs, Tm-tn and F-actin was observed with increasing concentrations of free $Ca^{2+}$, between pCa 6.5 and 3 approximately.

Values of the molecular and specific charge at pH 7.0 and the isoelectric point were calculated from the amino acid sequences of the main muscle proteins.

# Abbreviations and symbols

| | |
|---|---|
| ADP | adenosine 5'-diphosphate |
| $\epsilon$-ADP | 1,$N^6$-ethenoadenosine 5-diphosphate |
| AMP-PNP | adenyl-5'-yl-imidodiphosphate |
| ATP | adenosine 5'-triphosphate |
| Bistris | bis[2-hydroxyethyl]iminotris[hydroxymethyl]methane |
| BSA | bovine serum albumin |
| buffer R | 0.1 M KCl, 5 mM $MgCl_2$, 20 mM potassium phosphate, pH 7.0 |
| $[Ca^{2+}]$ | free $Ca^{2+}$ concentration |
| $c_p$ | protein concentration |
| DMAB | dimethylamine-borane complex |
| DTT | dithiothreitol |
| e | electronic charge $1.602\times10^{-19}$C |
| EDTA | ethylenediaminetetraacetic acid |
| EGTA | ethylene glycol-bis($\beta$-aminoethyl ether)-N,N,N',N'-tetraacetic acid |
| ELC | essential light chain |
| ELC1 | essential light chain, isoform 1 |
| ELC3 | essential light chain, isoform 2 |
| HMM | heavy meromyosin |
| $I$ | ionic strength |
| K | association constant ($M^{-1}$) |
| $K_a$ | dissociation constant (M) |
| $K_{app}$ | apparent binding constant ($M^{-1}$) |
| LMM | light meromyosin |
| m-HMM | methylated HMM |
| MLCK | myosin light chain kinase |
| MOPS | 3-(N-morpholino)propanesulfonic acid |
| MW | molecular weight |
| NTFs | native thick filaments |
| pCa | negative logarithm of the free $Ca^{2+}$ concentration |
| pI | isoelectric point |
| $pK_a$ | negative logarithm of the dissociation constant $K_a$ |
| PMSF | phenylmethylsulfonyl fluoride |
| $PP_i$ | pyrophosphate |
| $q_{mol}$ | molecular charge |
| $q_{spe}$ | specific charge |

| | |
|---|---|
| RLC | regulatory light chain |
| RTFs | reconstituted thin filaments |
| SDS-PAGE | sodium dodecyl sulphate polyacrylamide gel electrophoresis |
| STFs | synthetic thick filaments |
| S1 | subfragment-1 of myosin |
| S2 | subfragment-2 of myosin |
| Tm-tn | tropomyosin-troponin complex |
| $U_D$ | Donnan potential |
| $U_{ref}$ | reference potential |

# Contents

**Abstract** 3

**Abbreviations and symbols** 4

**Table of Contents** 6

**List of Figures** 11

**List of Tables** 15

**Acknowledgements** 17

**Declaration** 18

**1 Introduction** 19

1.1 Structure of muscle . . . . . 19

1.2 Sliding filament model . . . . . 20

1.3 Structure and function of muscle proteins . . . . . 21

1.3.1 Myosin . . . . . 22

1.3.2 Actin . . . . . 24

1.3.3 Tropomyosin and troponin . . . . . 26

1.3.4 Other proteins . . . . . 31

1.4 Intermolecular forces in polyelectrolyte systems . . . . . 32

1.4.1 Electrostatic interactions . . . . . 33

1.4.2 Balance of the intermolecular forces . . . . . 35
1.4.3 Net electric charge approximation . . . . . 36
1.5 Donnan equilibrium . . . . . 36
1.6 Previous studies of electrostatic effects in muscle . . . . . 39
1.6.1 X-ray diffraction studies . . . . . 41
1.6.2 Donnan potential measurements . . . . . 41
1.6.3 Other methods . . . . . 46
1.7 Models of mechanism of muscular contraction . . . . . 47
1.7.1 Model of Elliott and Worthington, 1994 . . . . . 48
1.7.2 Model of Fisher *et al*, 1995 . . . . . 50
1.8 Aims of the thesis . . . . . 51
1.9 Outline of research . . . . . 51

**2 Methods** **54**

2.1 Experimental solutions . . . . . 54
2.2 Protein concentration determination . . . . . 55
2.3 Protein isolation . . . . . 55
2.3.1 Heavy meromyosin . . . . . 56
2.3.2 Methylated heavy meromyosin . . . . . 58
2.3.3 Subfragment-1 of myosin . . . . . 58
2.3.4 Actin . . . . . 59
2.3.5 Tropomyosin-troponin complex . . . . . 61
2.3.6 Reconstituted thin filaments . . . . . 63
2.4 Protein purity assessment . . . . . 63
2.4.1 SDS-PAGE electrophoresis . . . . . 63
2.4.2 ATPase activity assay . . . . . 64
2.4.3 Amino acid analysis . . . . . 64

2.5 Experimental determination of the net electric charge . . . . . 65
2.5.1 Donnan potential macroelectrode measurements . . . . . 65
2.5.2 Donnan potential microelectrode measurements . . . . . 68
2.5.3 Ionic composition of solutions . . . . . 69
2.6 Net charge calculation from the sequence . . . . . 71
2.7 $K_{app}$ method for $[Ca^{2+}]$ calculation . . . . . 71
2.8 Electrode determination of $[Ca^{2+}]$ . . . . . 72
2.9 Viscosity measurements . . . . . 73
2.10 Conductivity measurements . . . . . 74
2.11 Diffusion potentials . . . . . 74
2.11.1 Measurements . . . . . 74
2.11.2 Calculations . . . . . 75
2.12 Experimental error . . . . . 76
2.13 Statistical analysis . . . . . 76

**3 Effect of methylation on the charge of heavy meromyosin** 77
3.1 Introduction . . . . . 77
3.2 Results . . . . . 79
3.2.1 SDS-PAGE electrophoresis . . . . . 79
3.2.2 Amino acid analysis . . . . . 82
3.2.3 ATPase activity . . . . . 83
3.2.4 Donnan potential measurements . . . . . 86
3.2.5 Theoretical charge of lysine . . . . . 90
3.2.6 Sequence analysis . . . . . 92
3.2.7 Structure analysis . . . . . 92
3.3 Discussion . . . . . 96
3.4 Conclusions . . . . . 98

**4 Electrode techniques for protein solutions** 99

4.1 Problems associated with the use of macroelectrodes . . . . . 99
4.1.1 Drifts in potentials . . . . . 99
4.1.2 Requirement of large quantities of protein . . . . . 105
4.1.3 KCl leakage . . . . . 111
4.1.4 Sample compartment geometry dependence . . . . . 112
4.1.5 Discussion . . . . . 115
4.2 Application of the microelectrodes to protein solutions . . . . . 118
4.2.1 Preliminary results with forceps-blunted electrodes . . . . . 119
4.2.2 Grinder bevelled microelectrodes . . . . . 123
4.2.3 Junction-renewable microelectrodes . . . . . 123
4.2.4 KCl leakage . . . . . 124
4.3 Effect of viscosity on electrode measurements . . . . . 131
4.4 Discussion . . . . . 136
4.5 Conclusions . . . . . 142

**5 Calcium effect on thin filament charge** **143**

5.1 Introduction . . . . . 143
5.2 Method . . . . . 145
5.2.1 Experimental solutions . . . . . 145
5.2.2 Protein preparation . . . . . 146
5.2.3 Tropomyosin-troponin binding to actin . . . . . 147
5.3 Results . . . . . 148
5.3.1 Concentration of free $Ca^{2+}$ . . . . . 148
5.3.2 SDS-PAGE protein purity determination . . . . . 154
5.3.3 Tropomyosin-troponin binding to actin . . . . . 160
5.3.4 Net charge measurements . . . . . 162
5.4 Discussion . . . . . 165
5.5 Conclusions . . . . . 174

**6 Conclusions and future studies** **175**

6.1 Conclusions . . . . . 175

6.1.1 Effect of methylation on the charge of HMM . . . . . 175

6.1.2 Effect of $Ca^{2+}$ on thin filament charge . . . . . 177

6.1.3 Electrode techniques for protein solutions . . . . . 178

6.1.4 Summary of the main observations . . . . . 181

6.2 Suggestions for future studies . . . . . 182

**A Stability constants** **184**

**B Sequence derived properties of muscle proteins and BSA** **187**

**C Donnan potentials** **190**

**Bibliography** **195**

# List of Figures


1.1 Schematic diagram of the structure of striated muscle. . . . . 21

1.2 Schematic diagram of the myosin molecule, with the subfragments resulting from the cleavage of the molecule by proteolytic enzymes. . . . 23

1.3 Schematic diagram of the structure of the thick filament. . . . . 24

1.4 Molecular diagram of the structure of subfragment-1 of myosin from chicken, with the residues charged at pH 7.0 indicated. . . . . 25

1.5 Molecular diagrams of the structure of rabbit actin, with the residues charged at pH 7.0 indicated. . . . . 27

1.6 Molecular diagram of the structure of rabbit cardiac tropomyosin, with the residues charged at pH 7.0 indicated. . . . . 28

1.7 Molecular diagram of the structure of troponin C from chicken, with the residues charged at pH 7.0 indicated. . . . . 29

1.8 Schematic diagram of the structure of the thin filament. . . . . 30

1.9 The molecular charge of the ionizable groups in amino acids as a function of pH. . . . . 34

1.10 Theoretical Donnan potential for a protein with the same specific charge as that calculated from the sequence of actin at pH 7.0 as a function of ionic strength and protein concentration. . . . . 40

1.11 A schematic representation of the events during the contraction cycle in the model of Elliott and Worthington, 1994. . . . . 49

2.1 A schematic diagram of the experimental set-up for the Donnan potential macroelectrode measurements. . . . . 66

2.2 A schematic diagram of the experimental set-up for the Donnan potential measurements with a microelectrode as the measuring electrode. . . 70

3.1 15% SDS-PAGE of rabbit HMM and methylated HMM. . . . . 80

3.2 The HPLC chromatogram of $N^{\epsilon}$-methyllysine, $N^{\epsilon}$-dimethyllysine and $N^{\epsilon}$-trimethyllysine used as standards. . . . . 82

3.3 The HPLC chromatograms of HMM and methylated HMM. . . . . 85

3.4 Amount of inorganic phosphate $P_i$ in kmol/mol of protein produced by HMM and methylated HMM during hydrolysis of ATP in the presence of $Ca^{2+}$ and EDTA. . . . . 87

3.5 The calculated molecular charge of lysine ($pK_a$ 10.68) and $N^{\epsilon}$-dimethyllysine ($pK_a$ 10.2 and 9.0). . . . . 90

3.6 The calculated difference $\Delta q_{mol}$ between the molecular charge at pH 6.7 of lysine with $pK_a$ 10.68 and $N^{\epsilon}$-dimethyllysine with $pK_a$ in the range 8–10.68 as a function of $pK_a$ of the $N^{\epsilon}$-dimethyllysine. . . . . 91

3.7 Molecular diagram of the structure of subfragment-1 of myosin from chicken, with the lysine residues and $Cys^{707}$ highlighted. . . . . 93

3.8 Molecular diagram of the structure of subfragment-1 of myosin from chicken, with the residues charged at pH 7.0 and $Cys^{707}$ highlighted. . . 95

4.1 Diffusion potentials for 20, 50 and 80 mM NaCl into 10 mM NaCl recorded using macroelectrodes K422. . . . . 101

4.2 Diffusion potentials for 20 mM NaCl into 10 mM NaCl recorded using macroelectrodes K422, REF401 and REF200. . . . . 102

4.3 Typical example of the potentials recorded during Donnan potential measurements with electrodes REF401. . . . . 104

4.4 12.5% SDS-PAGE of BSA fraction V (from BDH). . . . . 106

4.5 The molecular charge of BSA as a function of pH and sample volume determined using macroelectrodes K422. . . . . 109

4.6 The molecular charge of BSA as a function of pH – experimental and theoretical values. . . . . 110

4.7 Potentials recorded for BSA in 10 mM NaCl, 1 mM Bistris-HCl, pH 6.4 buffer, with electrodes K422 and REF401, using sample compartments with different membrane areas. . . . . 114

4.8 Traces of resistance and potentials registered with forceps-blunted microelectrodes for two samples of BSA in 10 mM NaCl, 1 mM Tris-HCl, pH 8.0 buffer. . . . . 120

4.9 Photographs of the tips of typical sharp, early forceps-blunted and bevelled microelectrodes. . . . . 122

4.10 Potentials $U_{ref}$ and $U_{prot}$ recorded using junction-renewable microelectrodes for Tm-tn in pCa 8.7 buffer with the tightening of the holder indicated. . . . . 125

4.11 Photographs of the tips of typical microelectrodes to which the junction renewal technique was applied during the measurements of Donnan potentials for BSA, Tm-tn, F-actin and RTFs in pCa buffers. . . . . 126

4.12 Distribution of the tip diameters for 'good' and 'bad' microelectrodes (of the junction-renewable type) for Tm-tn, F-actin and RTFs. . . . . 127

4.13 Distribution of the tip diameters for 'good' and 'bad' microelectrodes (of the junction-renewable type) – data pooled for Tm-tn, F-actin and RTFs. . . . . 128

4.14 Example trace of potential and resistance recorded using sharp microelectrodes of resistance less than 1 MΩ for a BSA sample in 1 mM Bistris-HCl buffer, 10 mM NaCl, pH 6.4 to which KCl was gradually added. . . . . 129

4.15 Potential recorded using sharp electrodes of resistance less than 1 MΩ for 4 BSA samples in 1 mM Bistris-HCl, 10 mM NaCl, pH 6.4 to which KCl was introduced to simulate a leakage out of the microelectrode. . . 130

4.16 Example traces of the potentials recorded using junction-renewable microelectrodes for BSA, Tm-tn, F-actin and RTFs in pCa 6.4 buffer. . . 133

4.17 Typical example traces of the Donnan potentials recorded using macroelectrodes K422 for F-actin, RTFs, Tm-tn and BSA in pCa 6.4 buffer. Comparison with the microelectrode values. . . . . 134

4.18 Traces of the Donnan potential for 3 BSA samples recorded using macroelectrodes K422 in pCa 6.4 buffer. Comparison with the microelectrode values. . . . . 135

4.19 Kinematic viscosity of BSA, Tm-tn, F-actin and RTFs determined by capillary viscometry at 20°C in pCa 6.4 buffer as a function of protein concentration. . . . . 138

5.1 The amounts of EGTA in complexes with $Ca^{2+}$, $Mg^{2+}$, $K^{+}$ and $Na^{+}$ in the pCa buffers used for the Donnan potential measurements. . . . . 150

5.2 Potentials recorded with $Ca^{2+}$ sensitive electrode Elit 041 (Merck) for the experimental pCa buffers and standards. . . . . 152

5.3 12.5% SDS-PAGE of rabbit actin – gel photograph and a densitometer scan. . . . . 155

5.4 12.5% SDS-PAGE of rabbit Tm-tn. . . . . 156

5.5 12.5% SDS-PAGE of rabbit RTFs. . . . . 157

5.6 Densitometer scans of 12.5% SDS-PAGE gels of Tm-tn and RTFs. . . . 159

5.7 Protein distribution between supernatant and pellet for RTFs in solutions of various ionic strength. . . . . 161

5.8 12.5% SDS-PAGE of rabbit RTFs immediately after reconstitution and after Donnan potential measurements. . . . . 162

5.9 The specific charge of BSA, F-actin, Tm-tn and RTFs as a function of pCa. . . . . 164

5.10 The molecular charge of F-actin, Tm-tn and RTFs as a function of pCa. 166

5.11 The molecular charge of BSA as a function of pCa. . . . . 167

5.12 Comparison of the directly measured molecular charge of RTFs with a value derived from the measured values of the charge on F-actin and Tm-tn. . . . . 168

5.13 Ratio of the experimental charge to that calculated from the sequences for BSA, F-actin, Tm-tn and RTFs as a function of pCa. . . . . 169

# List of Tables


1.1 The $pK_a$ values of ionizable groups in proteins. . . . . 33

3.1 Molecular weights of the subfragments of HMM and methylated HMM determined from SDS-PAGE gels and calculated from the sequence. . . 81

3.2 Number of residues in HMM and methylated HMM determined by amino acid analysis. . . . . 84

3.3 ATPase activity of HMM and methylated HMM in the presence of $Ca^{2+}$ and EDTA. . . . . 86

3.4 Values of the Donnan potential, protein concentration, temperature and molecular charge for HMM and methylated HMM. . . . . 88

3.5 The molecular charge of HMM and methylated HMM obtained from Donnan potential measurements. . . . . 89

3.6 Relative amounts of lysine residues in various fragments of the HMM molecule from rabbit and chicken expressed as molar percentages. . . . 92

4.1 The molecular charge of BSA as a function of pH and sample volume determined using macroelectrodes K422. . . . . 108

4.2 Experimental values of the isoelectric point pI of BSA from literature. . 108

4.3 Rates of KCl leakage from the K422, REF200 and REF401 macroelectrodes. . . . . 111

4.4 Potentials recorded for BSA in 1 mM Bistris-HCl, 10 mM NaCl, pH 6.4 buffer, with electrodes K422 and REF401, using sample compartments with different membrane areas. . . . . 113

4.5 Rates of KCl leakage from microelectrodes with tip diameters less than 25 $\mu$m. . . . . 131

4.6 Comparison of the Donnan potential and specific charge values obtained with microelectrodes and macroelectrodes, when the potentials at the first plateau are taken from the time course of the macroelectrode potentials. . . . . 136

4.7 Kinematic viscosity of BSA, Tm-tn, F-actin and RTFs determined by capillary viscometry at various protein concentrations. . . . . 137

5.1 Composition of the experimental solutions with varied free $Ca^{2+}$ concentration used for Donnan potential measurements. . . . . 146

5.2 Comparison of the free $Ca^{2+}$ concentration in solutions for the Donnan potential measurements calculated using the PERRIN program and two values of $K_{app}$. . . . . 151

5.3 Comparison of the theoretical and determined by SDS-PAGE protein ratios in the preparation of Tm-tn and RTFs. . . . . 158

5.4 Molecular weight of actin and the components in the preparations of Tm-tn and RTFs determined from 12.5% SDS-PAGE gels and calculated from the sequence. . . . . 160

5.5 The specific charge of BSA, F-actin, Tm-tn and RTFs as a function of pCa. . . . . 163

5.6 The molecular charge of BSA, F-actin, Tm-tn and RTFs as a function of pCa. . . . . 165

5.7 Comparison of the directly measured molecular charge of RTFs with a value derived from the measured values of the charge on F-actin and Tm-tn. . . . . 167

A.1 Stability constants for the formation of the complexes for ligands and metals present in the experimental solutions. . . . . 186

B.1 Protein sequence database OWL codes or literature references for the analysed protein sequences. . . . . 188

B.2 Number of amino acid residues, values of the molecular weight, molecular and specific charge at pH 7.0 and isoelectric point of muscle proteins and BSA as calculated from their amino acid sequences. . . . . 189

C.1 Donnan potential, protein concentration, temperature and specific charge for F-actin in solutions of various pCa. . . . . 191

C.2 Donnan potential, protein concentration, temperature and specific charge for Tm-tn in solutions of various pCa. . . . . 192

C.3 Donnan potential, protein concentration, temperature and specific charge for RTFs in solutions of various pCa. . . . . 193

C.4 Donnan potential, protein concentration, temperature and specific charge for BSA in solutions of various pCa. . . . . 194

# Acknowledgements

I wish to thank my supervisor Prof. Gerald F. Elliott for the supervision of this research project, encouraging scientific curiosity and independent open-minded thinking.

I am indebted to Dr Tony Willis of the MRC Immunochemistry Unit, Department of Biochemistry, University of Oxford for carrying out the amino acid analysis and for discussion of the results. I wish to express my gratitude to Prof. Nigel P. Groome, of the School of Biological and Molecular Sciences, Oxford Brookes University, for access to a freeze-drier in his laboratory on numerous occasions. I am obliged to Dr Christopher C. Ashley of the Department of Physiology, University of Oxford, who kindly allowed me to use a microelectrode grinder in his laboratory. I am also grateful to Janice Henderson for advice and help in the laboratory on many occasions and to Alan Knight for immediate assistance with electrical equipment.

I would like to acknowledge the Engineering and Physical Sciences Research Council for access to the Seqnet computing facility at the Daresbury Laboratory which allowed me to carry out the protein sequence and structure analysis and to create the molecular structure diagrams using the MOLSCRIPT program (Kraulis, 1991). I also wish to show my appreciation to the Open University for providing a research grant.

I am very grateful to all my friends and colleagues at the Oxford Research Unit. Nageena Malik receives particular mention here, for her advice, help and most of all, her friendship. I am grateful to Jason Liggins for, among other things, his patience while advising me on car maintenance and to Alec Goodyear for valuable suggestions and excellent coffee. I would also like to thank Saeed Akhtar who has always been friendly and helpful.

My parents receive my special thanks for, most of all, never stopping to believe in me. And finally I wish to thank my husband Kevin for always being there for me with his knowledge, support and love.

# Declaration

I declare that the work presented in this thesis, except where otherwise stated, is based on my own research and has not been submitted for a degree in this or any other University.

E. Bryson

Elżbieta Bryson

# Chapter 1

# Introduction

The aim of the research of this thesis was to increase the understanding of the electrostatic phenomena in muscle and thus to contribute to the unravelling of the mechanism of muscular contraction at the molecular level. This chapter starts with a brief review of the current state of knowledge of the structure and functioning of muscle (sections 1.1–1.3). The terminology used throughout the thesis is introduced in these sections. The theoretical aspects of the electrostatic effects in a polyelectrolyte medium are discussed in section 1.4, with more detailed analysis of the Donnan equilibrium in section 1.5. Section 1.6 is a review of the achievements in the studies of the electrostatic effects in muscle. Models of the mechanism of muscular contraction are reviewed in section 1.7, and the most recent electrostatic model is described in more detail. Finally, the aims of the thesis and the outline of research are given in sections 1.8 and 1.9 respectively.

## 1.1 Structure of muscle

The structure of the vertebrate skeletal muscle will be considered here. This type of muscle is formed from bundles of multinucleate cells called fibres which vary in length, from a few millimetres to many centimetres, and are 20–100 $\mu$m in diameter. The membrane surrounding each fibre, the sarcolemma, is electrically excitable. The cytosol of the fibres, the sarcoplasm, contains myofibrils which have a diameter of

about 1 $\mu$m each and are arranged longitudinally in the fibre.

A muscle fibre, when examined under a polarizing microscope, displays a striated pattern of isotropic and anisotropic bands (with respect to the refractive index). These bands have been called the I- and A-bands respectively. An electron micrograph of a longitudinal section of a myofibril reveals that the striation results from a regular arrangement of interdigitating sets of filaments within a functional unit, repeating every 2–3 $\mu$m along the myofibril axis. This functional unit has been called a sarcomere. Two sets of filaments can be distinguished: thin filaments, about 9 nm in diameter, and thick filaments, with a shaft diameter about 15 nm. The thick filaments, observed at high magnification, were discovered to have projections, except for the so-called bare zone in their centre. These projections were called cross-bridges since they were seen to connect the thick and thin filaments under rigor conditions. A schematic diagram of the structure of a sarcomere is given in figure 1.1. The regular arrangement of the thick and thin filaments, revealed in electron micrographs of cross-sections of a myofibril, is also shown in this figure. In the I-band there is a hexagonal lattice of the thin filaments, whereas the A-band contains a hexagonal lattice of the thick filaments in the H-zone and a double hexagonal lattice of the thick and thin filaments in the overlap zone.

The thick filament consists mainly of myosin molecules, whereas the thin filament contains mostly actin, tropomyosin, troponin and nebulin.

## 1.2 Sliding filament model

The sliding filament model was proposed by Huxley and Niedergerke (1954) and independently by Huxley and Hanson (1954). In this model, the thick and thin filaments slide past each other during contraction, increasing the degree of their overlap. In a similar way the degree of overlap is decreased when the muscle returns to the resting state or is stretched. The length of the thick or thin filaments, however, remains

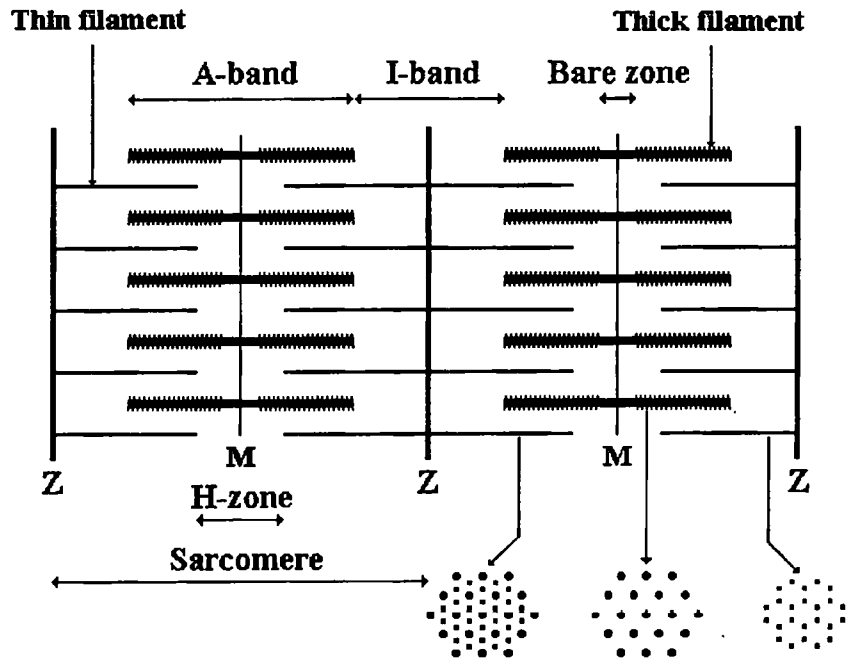


Figure 1.1: Schematic diagram of the structure of striated muscle. The top part represents a longitudinal section of two sarcomeres. In the bottom part of the figure, the arrangement of the filaments in a hexagonal lattice is shown, with circles and squares representing the thick and thin filaments respectively.

constant. It was also postulated that the force of contraction is generated through the formation of cross-bridges between the filaments, the energy for the contraction being delivered by the hydrolysis of ATP by myosin.

## 1.3 Structure and function of muscle proteins

Values of the parameters characterizing the physical properties of all the major muscle proteins are listed in table B.2 in appendix B. These parameters include number of residues, molecular weight, molecular and specific charge at pH 7.0 and isoelectric point. The values of these parameters were obtained from the amino acid sequences of the proteins as described in appendix B and section 2.6. The properties of muscle proteins, relevant to our studies, will be reviewed in this section. In particular, diagrams of the molecular structure of proteins containing the distribution of positively and negatively charged residues at pH 7.0 will be presented. The description of any

system containing charged species would not be complete unless it included both the distribution of matter and the distribution of the electric charge (Elliott *et al.*, 1985).

### 1.3.1 Myosin

Myosin has been a subject of a recent comprehensive review by Sellers and Goodson (1995) and, unless otherwise explicitly given, references to the statements made in this section can be found in the above review. Myosin is the motor protein of muscle. Being an ATPase, the protein utilizes the energy of ATP hydrolysis for its motor activity. The MgATPase activity of myosin is enhanced by actin, typically by a factor of 50–100, depending on the experimental conditions. Another property of the enzymic action of myosin, however, is often utilized as a diagnostic test for assessing the quality of the preparation (Margossian and Lowey, 1982). The intact protein exhibits lower activity in the presence of $Ca^{2+}$ than in the presence of EDTA. Modifications of the sulphydryl groups of $Cys^{707}$ and $Cys^{697}$ are reflected in the reversal of the activities and complete loss of both activities respectively.

Myosin is a hexamer of two heavy and four light chains. The two heavy chains form an $\alpha$-helical coiled coil at their C-termini (rod) and separate to form two globular heads at their N-termini, each of which is called subfragment-1 (S1). There are two light chains attached to each of the myosin heads: one called the regulatory light chain (RLC) and one called the essential light chain, which exists in two isoforms (ELC1 and ELC3). The shape of the molecule is shown schematically in figure 1.2. Myosin can be cleaved into various subfragments by the action of proteolytic enzymes: papain, trypsin and $\alpha$-chymotrypsin. Isolation procedures have been developed to obtain these proteolytic fragments in a homogenous form (described in Margossian and Lowey, 1982). The points of myosin cleavage are indicated in figure 1.2.

The extensive studies of myosin subfragments have led to establishing their structure and function. S1 contains the active and actin binding sites and is able to move actin filaments *in vitro* (Toyoshima *et al.*, 1987) producing the same force as intact

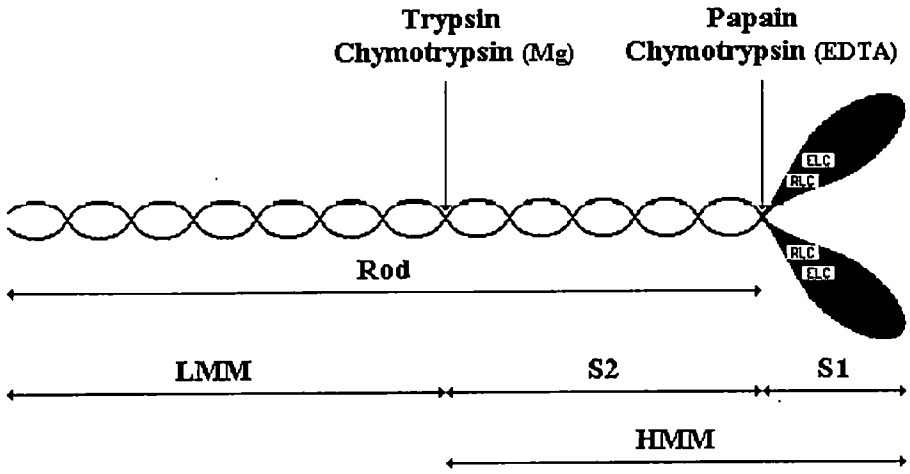


Figure 1.2: Schematic diagram of the myosin molecule. Points of cleavage by proteolytic enzymes are indicated with arrows. The results of the action of papain and $\alpha$-chymotrypsin depend on the medium. In the presence of EDTA, both enzymes produce rod and S1 with the regulatory light chain digested. In the presence of $MgCl_2$, the action of papain produces rod and S1 with both light chains intact, whereas $\alpha$-chymotrypsin produces heavy meromyosin (HMM) and light meromyosin (LMM).

myosin (Kishino and Yanagida, 1988). The role of the light chains has not been clarified yet. Recent studies of Lowey *et al.* (1993) show that the removal of the light chains from myosin reduces the velocity of actin filaments approximately 10-fold, without decreasing the ATPase activity significantly. Under physiological conditions the myosin rod and light meromyosin exhibit the filament forming properties of intact myosin. The analysis of the amino acid sequence of myosin rod reveals how the electrostatic and hydrophobic interactions lead to the formation of the coiled coil and also the thick filament. The sequence consists of repeating 7-residue fragments which contain 2 hydrophobic and 3 charged residues. In the coiled coil the hydrophobic residues of the two strands come together to form the hydrophobic core of the rod. The charged residues are on the outside of the rod and the electrostatic interactions, between the residues from different molecules, probably mediate the packing of the rods into filaments and are responsible for the self-assembly of the thick filament. The resulting structure of the thick filament is shown schematically in figure 1.3. The bare zone is present in both native and synthetic thick filaments.

The atomic structure of myosin S1 from chicken was recently determined using single

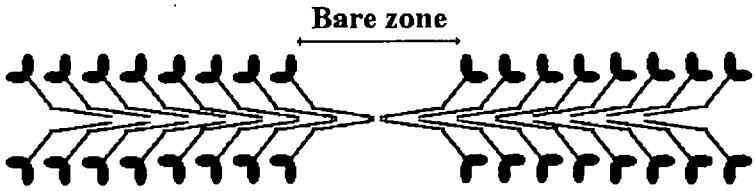


Figure 1.3: Schematic diagram of the structure of the thick filament.

crystal X-ray diffraction for a protein with 97% of the lysine residues reductively methylated (Rayment *et al.*, 1993), this structure is presented in figure 1.4. So far, it has only been possible to crystallize the truncated myosin (consisting of the motor domain) from *Dictyostelium discoideum* without the methylation. The structures of this protein with MgADP·$BeF_x$, MgADP·$AlF_x$, pyrophosphate ($PP_i$) and MgADP-$V_i$ (where $V_i$ denotes vanadate) have been determined (Fisher *et al.*, 1995; Smith and Rayment, 1995, 1996).

### 1.3.2 Actin

A recent comprehensive review on actin can be found in Sheterline and Sparrow (1994). As for myosin, unless explicitly given, the references for the statements in this section can be found in the above mentioned review. Actin exists in two forms: monomeric G-actin and filamentous F-actin. Actin can be extracted at low ionic strength as G-actin and converted to the viscous F-actin by the addition of salt. The polymerization process of actin received significant attention and it was established that *in vitro* G- and F-actin co-exist in a dynamic equilibrium which can be characterized by the so-called critical concentration $c_{cr}$. This is the concentration of G-actin, above which extra actin assembles into filaments. Under physiological conditions the value of $c_{cr}$ is approximately 0.1 $\mu$M and hence the F-actin is the predominant form of the protein. The critical concentration is increased at low ionic strength in the presence of $Ca^{2+}$. This property is the basis of the purification procedure, which was used in this thesis, where G-actin is extracted and F-actin depolymerized under conditions

ORIGINAL IN COLOUR

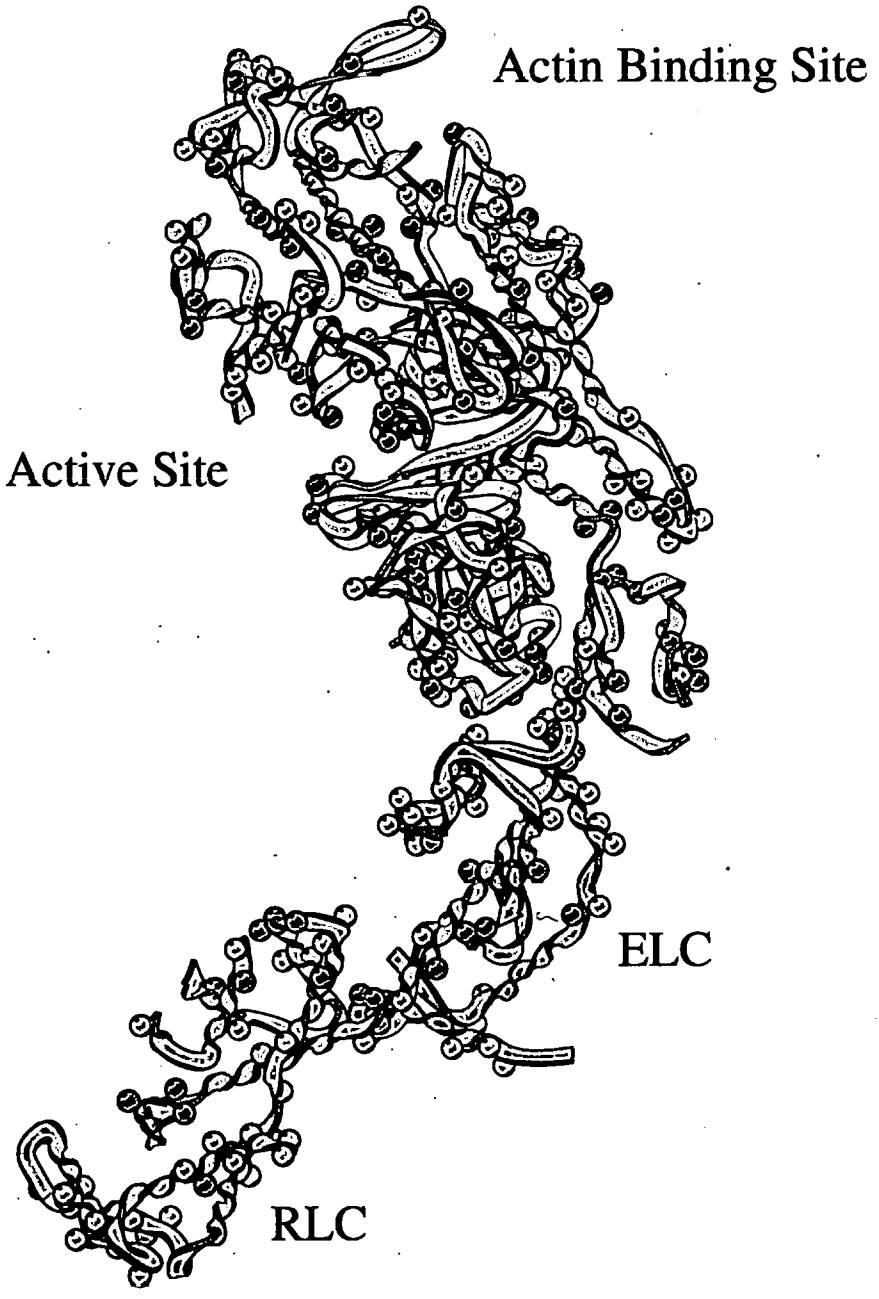


Figure 1.4: Molecular diagram of the structure of subfragment-1 of myosin from chicken. The heavy chain is drawn in grey, the essential light chain (ELC) in green and regulatory light chain (RLC) in yellow. The $\alpha$-carbon atoms in positively charged at pH 7.0 residues (Lys and Arg) are indicated in red and those in negatively charged residues (Glu and Asp) are shown in blue. Also the actin binding and active site are indicated. Created using MOLSCRIPT (Kraulis, 1991) with the S1 structure of Rayment *et al.* (1993). The coordinates were taken from the 2MYS file from the Brookhaven PDB (Bernstein *et al.*, 1977; Abola *et al.*, 1987).

when $c_{cr}$ is approximately 0.1 mM.

Actin is also an ATPase, the activity for rabbit skeletal actin being about 0.07 $s^{-1}$ under the conditions used by Pollard and Weeds (1984). This value is about two orders of magnitude lower than the actin activated activity of rabbit myosin S1 (Margossian and Lowey, 1982; Sellers and Goodson, 1995), with the exact values depending on the experimental conditions. The hydrolysis of ATP accompanies the process of polymerization; the presence of ATP is, however, not essential for the assembly (Cooke, 1975). The slow rate of ATP hydrolysis provides the switch mechanism for the so-called head-to-tail assembly or treadmilling (Wegner, 1976).

The atomic structure of actin monomer has been recently solved (Kabsch *et al.*, 1990). The method of X-ray diffraction was applied to crystals of the complex of actin and DNaseI, in which actin was preserved in the monomeric form. The structure of actin is presented in figure 1.5. The above structure was used to construct an atomic model of F-actin filament by fitting the structure of the monomer to the X-ray pattern observed for oriented gels of actin (Holmes *et al.*, 1990).

### 1.3.3 Tropomyosin and troponin

Tropomyosin and troponin form the regulatory system of vertebrate skeletal muscle. Troponin consists of three components: calcium binding troponin C, tropomyosin binding troponin T and the actomyosin ATPase inhibiting troponin I. The structure of the rabbit cardiac tropomyosin and the structure of chicken skeletal troponin C have been solved (Phillips *et al.*, 1979; Strasburg *et al.*, 1980, respectively). These structures are shown in figures 1.6 and 1.7.

Tropomyosin is an $\alpha$-helical coiled coil, with a residue repeat motif similar to myosin. Troponin C contains two binding sites for $Ca^{2+}$ in each of the two homologous domains, all of them have the E-F hand motif which is characteristic for $Ca^{2+}$ binding proteins (Celio *et al.*, 1996). The two sites in the C-terminus part of the molecule,

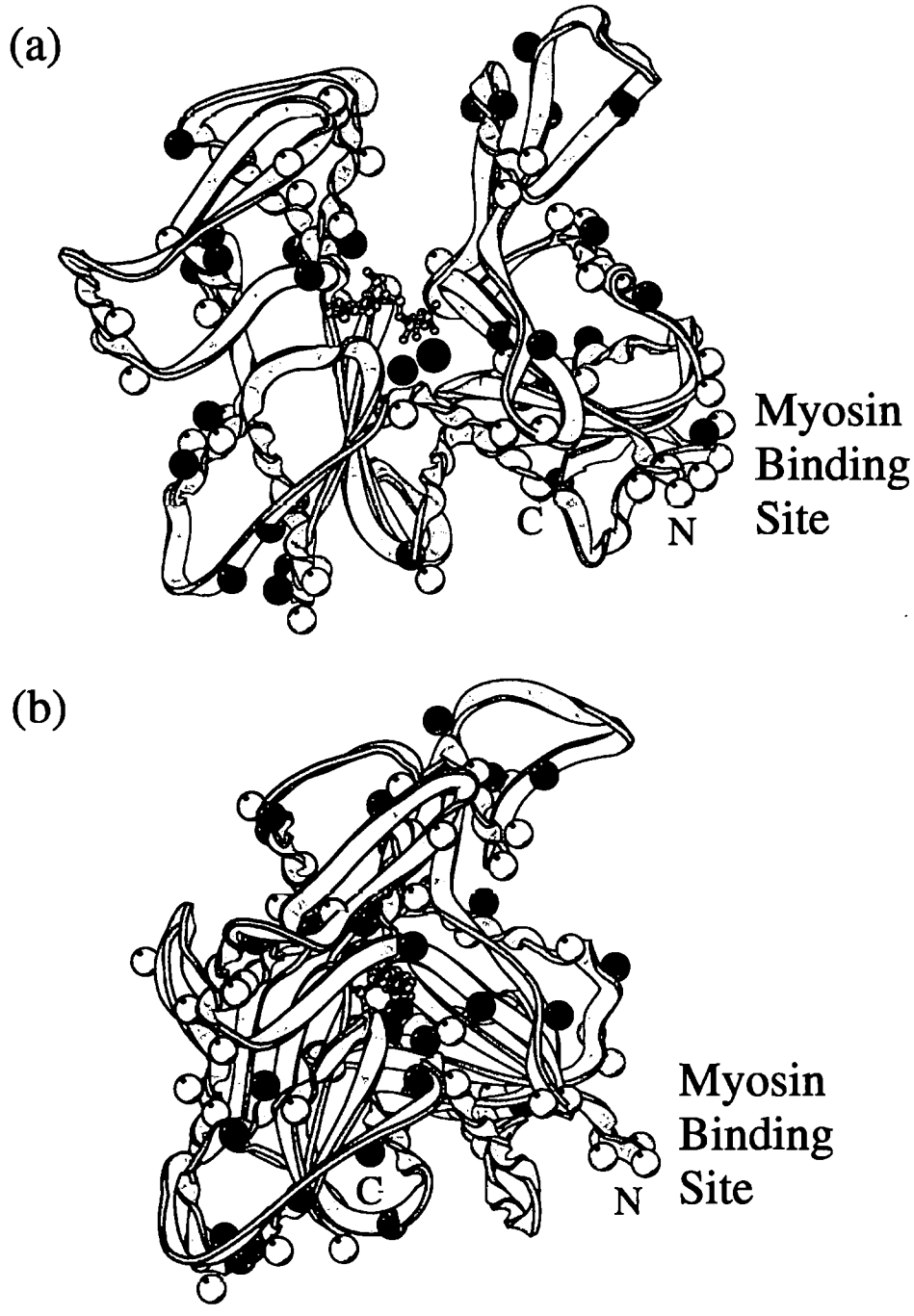


Figure 1.5: Molecular diagrams of the structure of rabbit actin. Structure shown in (b) has resulted from rotating structure (a) by +45° about the vertical axis (pointing upwards) to give a better view of the myosin binding site. The $\alpha$-carbon atoms in positively charged at pH 7.0 residues (Lys and Arg) are indicated in red and those in negatively charged residues (Glu and Asp) are shown in blue. N and C denote the N- and C-termini respectively. Also an ATP molecule and calcium ion bound to the actin molecule are displayed in yellow and green respectively. Created using MOLSCRIPT (Kraulis, 1991) with the structure of Kabsch *et al.* (1990). The coordinates were taken from the 1ATN file from the Brookhaven PDB (Bernstein *et al.*, 1977; Abola *et al.*, 1987).

ORIGINAL IN COLOUR

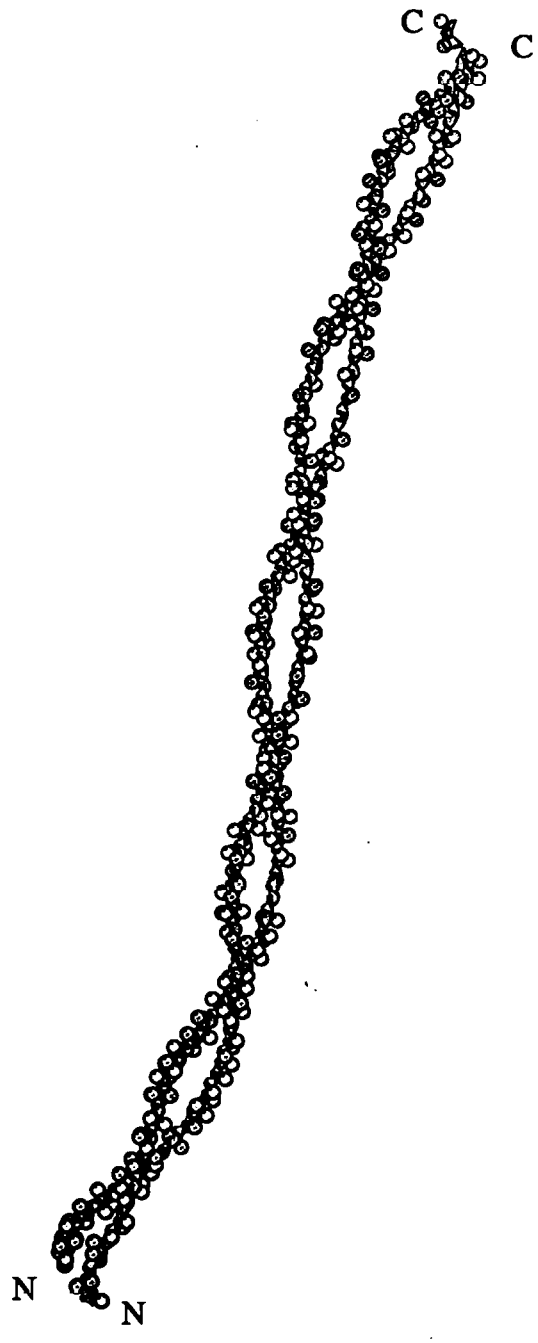


Figure 1.6: Molecular diagram of the structure of rabbit cardiac tropomyosin. The two chains forming the $\alpha$-helix are drawn in grey and yellow. The $\alpha$-carbon atoms in positively charged at pH 7.0 residues (Lys and Arg) are indicated in red and those in negatively charged residues (Glu and Asp) are shown in blue. N and C denote the N- and C-termini respectively. Created using MOLSCRIPT (Kraulis, 1991) with the tropomyosin structure of Phillips *et al.* (1979). The coordinates were taken from the 2TMA file in the Brookhaven PDB (Bernstein *et al.*, 1977; Abola *et al.*, 1987).

ORIGINAL IN COLOUR

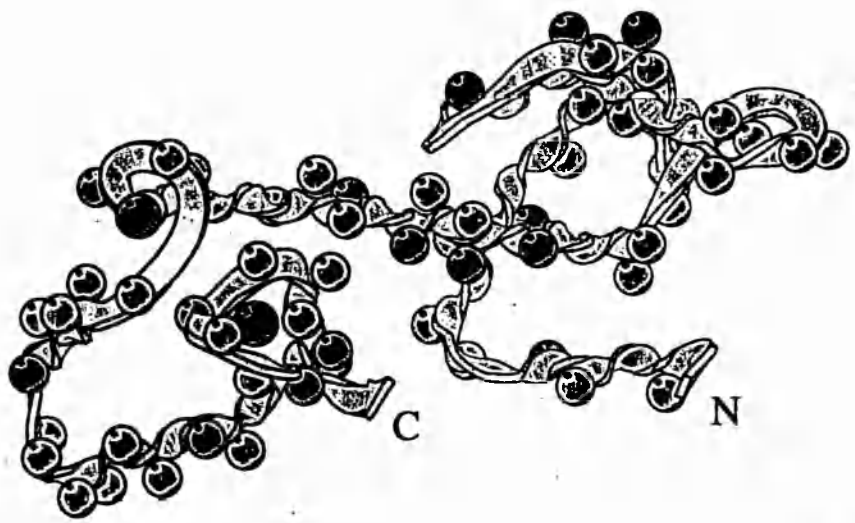


Figure 1.7: Molecular diagram of the structure of troponin C from chicken with two bound $Ca^{2+}$ ions. The $\alpha$-carbon atoms in positively charged at pH 7.0 residues (Lys and Arg) are indicated in red and those in negatively charged residues (Glu and Asp) are shown in blue. Green spheres represent the two bound calcium ions. N and C denote the N- and C-termini respectively. Created using MOLSCRIPT (Kraulis, 1991) with the troponin C structure of Strasburg *et al.* (1980). The coordinates were taken from the 1TOP file in the Brookhaven PDB (Bernstein *et al.*, 1977; Abola *et al.*, 1987).

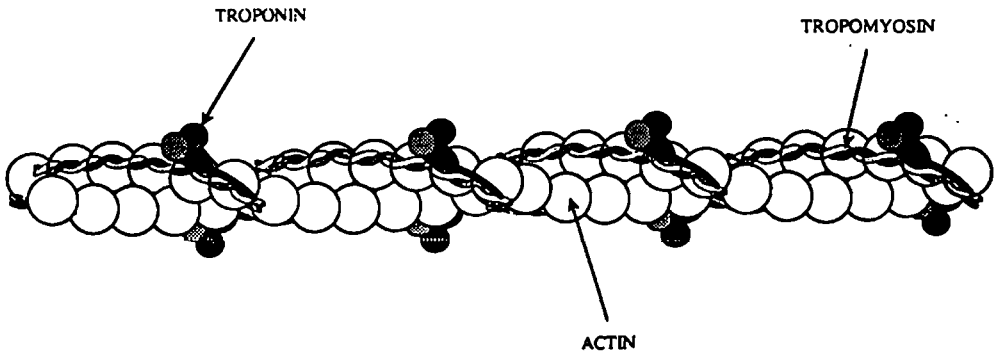


Figure 1.8: Schematic diagram of the structure of the thin filament (reproduced from Bagshaw, 1993).

occupied in the crystal structure, are the high affinity sites which are also occupied in resting muscle at approximately 0.1 $\mu$M concentration of $Ca^{2+}$. The other two sites have lower affinity for $Ca^{2+}$ and become occupied when the concentration of sarcoplasmic calcium increases to approximately 10 $\mu$M. The $Ca^{2+}$ and $Mg^{2+}$ binding to troponin is discussed in more detail in section 5.4.

The schematic diagram of the arrangement of the tropomyosin and troponin in the thin filament is presented in figure 1.8. The thin filament is composed of a double helix of actin monomers. In the grooves of the helix, there are dimers of tropomyosin spanning across seven actin monomers with a troponin complex bound to each tropomyosin dimer, resulting in the periodic arrangement of the troponin complex every 38.5 nm.

Differences in the X-ray diffraction patterns associated with actin between a relaxed and contracting muscle observed by Huxley (1973) and Haselgrove (1973) could be accounted for by the movement of tropomyosin. A steric blocking model was formulated, in which $Ca^{2+}$ binding to troponin C causes a sideways movement of tropomyosin on the surface of actin exposing the myosin binding site (Haselgrove, 1973; Huxley, 1973; Parry and Squire, 1973).

Some structural evidence supporting this model has accumulated recently. A difference between the thin filament structure in the presence of $Ca^{2+}$ and EGTA was observed by Ishikawa and Wakabayashi (1994) using cryo-electron microscopy. It was not determined however if that change was caused by tropomyosin movement or a

transformation of actin. Lehman *et al.* (1994) observed a 25° azimuthal movement of tropomyosin in electron micrographs of thin filaments of *Limulus*. Differences between the X-ray diffraction patterns of rabbit psoas fibres obtained at various $Ca^{2+}$ concentrations (Poole *et al.*, 1994) were accounted for with also a 25° azimuthal movement of tropomyosin. Lorenz *et al.* (1995) obtained an agreement between the X-ray diffraction patterns of unregulated synthetic thin filaments (without troponin) and the patterns of the regulated filaments in the presence of $Ca^{2+}$.

### 1.3.4 Other proteins

#### Titin

Titin has been a subject of recent reviews by Labeit and Kolmerer (1995) and Wang (1996). It is at present the largest known protein. Single molecules are approximately 1 $\mu$m long and extend from the M- to Z-lines, spanning the A- and I-bands of a sarcomere. The titin filament is elastic along most of its length but the segment of the molecule that spans the A-band is prevented from stretching in muscle. The remaining fragment acts as an elastic connector of the thick filaments to the Z-line. Labeit *et al.* (1992) found that fragments of titin bound C-protein and myosin LMM, whereas Koretz *et al.* (1993) showed that titin aggregates did not bind myosin but bound C-protein and AMP-deaminase and that their structural ordering was improved upon binding of these proteins.

#### Nebulin

Nebulin has been recently reviewed by Wang (1996). Immunoelectron microscopy studies suggest that a single nebulin molecule spans the length of the thin filament and that it moves along with actin during contraction. An interesting feature of the amino acid sequence of nebulin is that it consists of approximately 200 repeats of a 35-residue motif. These modules form more than 20 seven-module super-repeats. It has been proposed that each nebulin module is an actin binding domain and each

seven-module unit corresponds to the tropomyosin and troponin binding site. Other studies indicate that nebulin may be a part of the thin filament regulatory system, so far associated only with tropomyosin and troponin.

### C-protein

C-protein is located in the thick filament. It has been shown to bind strongly to the rod portion of myosin (Moos *et al.*, 1975). The structure of the thick filament is disrupted by the addition of the C-protein at high (Moos *et al.*, 1975) and low (Koretz, 1979) molar ratios to myosin. At a ratio of 1 C-protein molecule to 3–4 myosin molecules, ordered synthetic thick filaments are formed, suggesting that there may be 3–4 myosin-specific binding sites on one C-protein molecule (Koretz, 1979). C-protein has been found to increase the resistance of the synthetic thick filaments to pressure-induced dissociation (Tumminia *et al.*, 1989). C-protein plays a part in the organization of the thick filament, but the role of the protein is not yet entirely clear.

## 1.4 Intermolecular forces in polyelectrolyte systems

Muscle is a polyelectrolyte system with a regular hexagonal lattice of the protein filaments. There exist two types of intermolecular forces in such a system: van der Waals and electrostatic forces. Van der Waals forces are attractive and result from the interactions between electric dipoles. The magnitude of the van der Waals forces is proportional to $r^{-6}$, where $r$ is the distance between atoms or molecules. The electrostatic interactions in a polyelectrolyte system will be discussed in more detail in the next section.

Table 1.1: The $pK_a$ values of ionizable groups in proteins at ionic strength 0.1 M. All the $pK_a$ values were taken from Smith and Martell (1989), the values for the N- and C-terminal groups being averaged over 20 amino acids listed as common by Stryer (1988). Also the charge of each group in a fully protonated and deprotonated state is given in electronic charge units ($q_p$ and $q_d$ respectively).

| Residue | Group (protonated state) | $q_p$ | $q_d$ | $pK_a$ |
|---|---|---|---|---|
| Arginine | guanidyl-$NH_2^+$ | 1 | 0 | 12.10 |
| Histidine | imidazolyl-$NH^+$ | 1 | 0 | 6.02 |
| Lysine | $\epsilon$-$NH_3^+$ | 1 | 0 | 10.68 |
| Cysteine | $\beta$-SH | 0 | -1 | 8.16 |
| Tyrosine | phenolic-OH | 0 | -1 | 10.10 |
| Glutamate | $\gamma$-COOH | 0 | -1 | 4.20 |
| Aspartate | $\beta$-COOH | 0 | -1 | 3.70 |
| N-terminal | $\alpha$-$NH_3^+$ | 1 | 0 | 9.38 |
| C-terminal | $\alpha$-COOH | 0 | -1 | 2.14 |

### 1.4.1 Electrostatic interactions

A polyelectrolyte system like muscle contains charged molecules consisting of proteins and mobile ions.

Proteins have a net electric charge equal to zero only at a particular value of pH, which is called the isoelectric point (pI). At other values of pH, proteins possess a net electric charge which is positive at pH values below their pI, and negative at pH values above their pI. This charge results from the electric charge of the component amino acids.

The ionizable groups of amino acids that contribute to the charge of proteins are listed in table 1.1. Some of the groups are positively charged in the protonated form, while the other groups bear no charge in the protonated form and become negatively charged upon hydrolysis of a $H^+$ ion. This is indicated in the table in the values of $q_p$ and $q_d$ representing the charge of the group in electronic charge units in the protonated and deprotonated states respectively. The $pK_a$ values for the dissociation of a $H^+$ ion from the protonated form of each group are also given in the table.

The theoretical net charge of a protein can hence be calculated as a sum of the

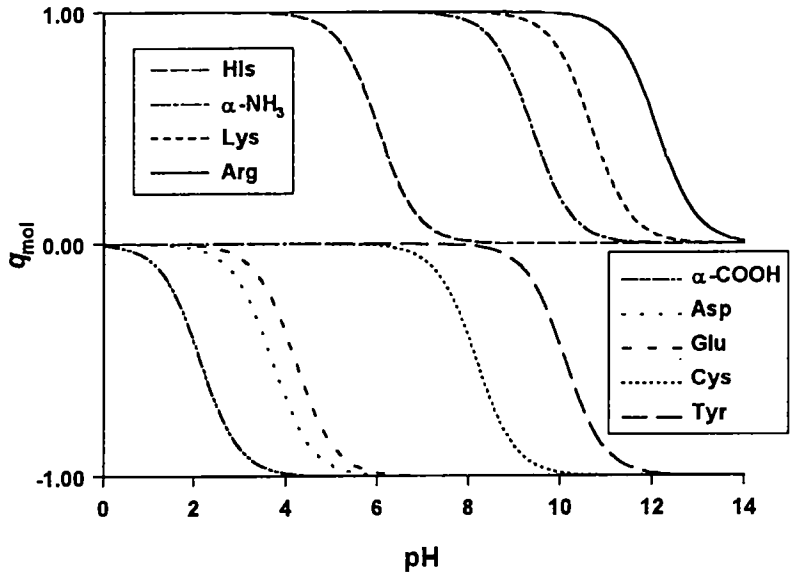


Figure 1.9: The molecular charge $q_{mol}$ of the ionizable groups in amino acids as a function of pH in electronic charge units. The charge was calculated from the $pK_a$ values given in table 1.1 and using equations 1.1 and 1.2.

charges on all of the residues in the protein. This is equal in electronic charge units to the number of protonated residues for which $q_p = 1$ minus the number of deprotonated residues for which $q_d = -1$. The number $n_p^i$ of protonated groups of type $i$ as a function of pH can be obtained from:

$$n_p^i = \frac{n^i[H^+]}{[H^+] + K_a^i} \tag{1.1}$$

where $[H^+]$ is the hydrogen ion concentration, $K_a^i$ is the dissociation constant for the group of type $i$ and $n^i$ is the total number of groups $i$ in the protein sequence. The number of deprotonated residues $n_d^i$ of type $i$ can be calculated as:

$$n_d^i = n^i - n_p^i \tag{1.2}$$

If we take $n^i$ as equal to 1 in equations 1.1 and 1.2, we can calculate the molecular charge of each of the ionizable groups as a function of pH (figure 1.9).

The study of 36 globular proteins by Rashin and Honig (1984) indicated that the majority of the charged groups of a protein are on its surface, with the hydrophobic groups buried inside the molecule. This has also been observed for fibrous proteins

such as myosin rod and tropomyosin (sections 1.3.1 and 1.3.3) . Hence it is appropriate to consider the electrostatic effects in the neighbourhood of such charged surfaces in an electrolyte solution. These phenomena are discussed by Israelachvili (1985). A charged surface attracts counterions and repels co-ions giving rise to a formation of the so-called double layer. Due to this ionic atmosphere, the electrostatic potential of the charged surface decays with distance more sharply than in the vacuum. The potential $\Psi$ at distance $r$ from the surface is given (in the so-called Debye-Hückel approximation) as:

$$\Psi = \Psi_o \, e^{-\kappa r}$$

where $\Psi_o$ is the electric potential at the surface and $\frac{1}{\kappa}$ is the Debye length. The Debye length decreases with the valency of the ions in the solution and is inversely proportional to the square root of the ionic strength. The $\Psi_o$ increases with the surface charge density and decreases with the ionic strength. Divalent counterions have a dramatic effect on the $\Psi_o$, lowering its value about 100 times more effectively than monovalent counterions. The electrostatic forces between charged surfaces of particles thus decay exponentially with the distance between them, with the range of the forces decreasing as the ionic strength and the concentration of divalent counterions increase.

### 1.4.2 Balance of the intermolecular forces

Elliott (1968) has calculated the magnitude of the van der Waals attraction forces and the electrical double-layer repulsion forces for a hexagonal lattice of cylinders with a uniform negative charge in an ionic medium. It was shown that a balance of these two forces could be achieved for certain values of the distance between the cylinders. When parameters appropriate for muscle were taken, the distance for which the balance existed, was found to be close to the value of the separation between the thick filaments in muscle.

### 1.4.3 Net electric charge approximation

It is of particular interest for our studies, in which we are only able to measure the net electric charge on proteins, whether this quantity is of importance in the interactions between proteins. If a surface with a set of discrete charges is considered, with each charge separated by a distance $d$ from the neighbouring charges, then the resulting electric field at a distance $d/2$ from the surface differs only by 17% from the electric field calculated for a surface with a smeared charge of the same surface charge density; at a distance $d$ from the surface the difference between these electric fields is only 0.7% (Israelachvili, 1985).

Barlow and Thornton (1986) studied the distribution of the charged groups in proteins and found that the local surface charge density was 0.5–25 charged groups per 1 $nm^2$ in the analysed group of 32 proteins. This corresponds to the distance of 0.2–1.4 nm between the charged groups on the protein surface, assuming a square lattice. Hence electrostatic interactions between proteins at distances greater than about 1 nm can be approximated by average smeared charges on their surfaces, in which individual charged sites can be neglected. At even larger distances, the magnitude of which is dependent on the protein, local surface charge density can be neglected and only the overall net charge of the protein determines the extent of the interaction (Barlow and Thornton, 1986). The net charge will thus provide the force that will bring the molecules together to enable the interactions between individual sites on the proteins.

## 1.5 Donnan equilibrium

In a system consisting of two phases, with one or more of the ionic components being restricted from passing between the phases, an equilibrium exists which is called the Donnan equilibrium. It was discovered and described by Donnan (1911). In this thesis the considerations will be limited to the case when only one phase contains the nonpermeable molecules which will be proteins. The restriction can be caused

by a semi-permeable membrane in the case of protein solutions or by the structural arrangement of the proteins in the contractile apparatus or in gels. The presence of a membrane is by no means essential for establishing a Donnan equilibrium (Overbeek, 1956).

There are three aspects of the Donnan equilibrium:

1. Unequal distribution of the mobile ions between the phases.
2. The osmotic pressure.
3. The potential difference between the phases.

In the phase containing the macromolecules there is accumulation of the counterions whereas the co-ions are partially excluded from this phase. The bulk of both phases remains electrically neutral.

In the subsequent paragraphs the classical Donnan equilibrium will be considered using ion concentrations rather than ion activities. This approach is justified since the theory is applied to homogenous protein solutions at relatively low concentration (Overbeek, 1956). Concentrations will be used as opposed to ion activities for the reasons given in Elliott and Bartels (1982). The theory could be extended to non-ideal solutions by introducing Debye-Hückel activity coefficients, and replacing the concentrations in the subsequent equation for the Donnan potential by the activities (Overbeek, 1956).

In equilibrium, the concentration ratios between the phases for each type of permeant ion must be such that their Nernst potentials are all equal and equivalent to the potential difference between the two phases, the Donnan potential $U_D$. If $c_j^i$ and $c_j^o$ denote the concentrations of the ion $j$ in the phase containing the macromolecules and the other phase respectively, then:

$$U_D = \frac{RT}{z_j F} ln \frac{c_j^o}{c_j^i} \qquad j = 1, \cdots, n \tag{1.3}$$

where $z_j$ is the valency of ion $j$, $R$ is the gas constant, $T$ absolute temperature, $F$ the Faraday constant and $n$ is the total number of ion types present. The concentrations of the ionic species in the phase containing the macromolecules can thus be determined from the value of the Donnan potential and their concentrations in the other phase.

If $q$ is the net electric charge of the protein at a concentration $c_p$, then the condition of electroneutrality of the bulk of solution containing the protein, takes the form:

$$qc_p + \sum_{j=1}^{n} z_j c_j^i = 0 \tag{1.4}$$

Combining equations 1.3 and 1.4, leads to the equation enabling the calculation of the value of the net charge $q$:

$$q = -\frac{1}{c_p} \sum_{j=1}^{n} z_j c_j^o \exp -\frac{z_j U_D F}{RT} \tag{1.5}$$

The calculations can be simplified by grouping the terms for the same valency:

$$q = -\frac{1}{c_p} \sum_{k=1}^{r} z_k \left( \sum_{l=1}^{s} c_l^o \right) \exp -\frac{z_k U_D F}{RT} \tag{1.6}$$

where $c_l^o$ are concentrations of the $s$ types of ions with valency $z_k$ and $r$ is the total number of different ionic valencies present in solution.

If the protein concentration is expressed as mass per unit volume, then only the so-called specific charge, $q_{spe}$, defined as the net charge per $10^5$ Da, can be known. If the molar concentration of the protein is known, then the molecular charge, $q_{mol}$, defined as the net charge per molecule, can be calculated.

If both phases are electrically neutral, how does an electric potential difference arise between them? The answer is that there are positive and negative excess charges located near the boundary between the phases in a narrow band, whose width is of the order of the Debye length for a given solution. This does not, however, affect the bulk of the solution, which remains electroneutral.

For a protein of certain net charge $q$, the Donnan potential increases with the protein concentration and decreases with the ionic strength of the medium. These proper-

ties, which are of consequence for the experimental determination of the net charge on proteins, are illustrated in figure 1.10. The values of the Donnan potential are plotted as a function of the ionic strength and protein concentration for a protein of the specific charge equal to that calculated from the sequence of actin at pH 7.0 (see table B.2). The protein concentrations range from typical concentrations achieved in protein solutions (several mg/ml), through concentrations in protein gels of about 100 mg/ml (Jennison, 1992), to the concentrations of proteins in the muscle tissue of about 400 mg/ml in the thin filament (Bagshaw, 1993). It should be noted, however, that the real Donnan potentials would be less negative than those plotted in figure 1.10 due to counterion binding. It can be seen that potentials that can be obtained from protein preparations are very much smaller (the absolute value) than those obtained from the muscle, where proteins are highly concentrated. At physiological ionic strength of about 0.15 M, the values of the Donnan potential that can be obtained from samples with concentrations of 10–20 mg/ml would be about 1 mV at the maximum and higher potentials could only be obtained at the expense of using less physiological conditions, i.e. lower ionic strength.

## 1.6 Previous studies of electrostatic effects in muscle

The electrostatic effects in the contractile system have been studied mostly in fibres, whose membranes have been removed, in protein gels and protein solutions.

In living muscle, the sarcolemma acts as a barrier preventing the sarcoplasm from changing with the changes in the external medium. The muscle membrane can be removed chemically or mechanically. The structure of the contractile apparatus is not affected by these procedures (Huxley, 1957). In fibres without the sarcoplasm, as well as in protein gels and solutions, the chemical environment surrounding the contractile proteins can be controlled and varied.

(a)

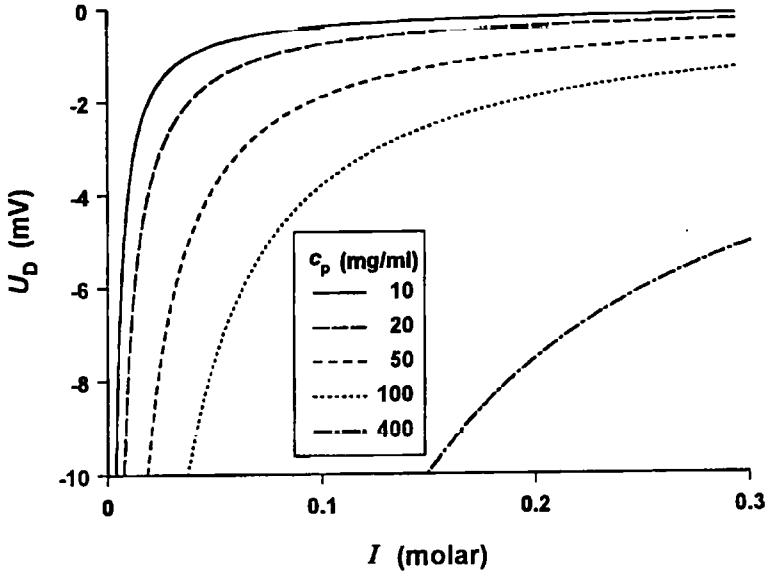


(b)

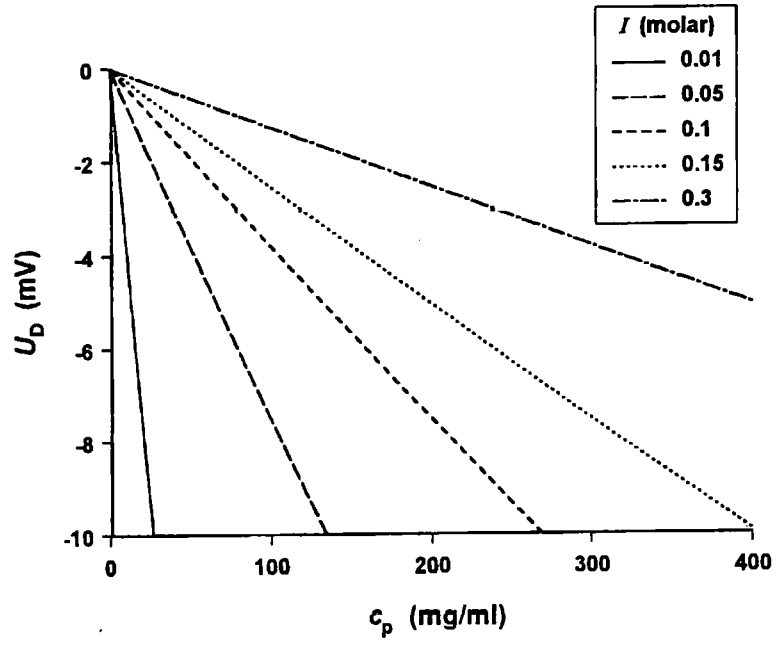


Figure 1.10: Theoretical Donnan potential $U_D$ for a protein with the same specific charge as that calculated from the sequence of actin at pH 7.0 (-29.7e). Dependence (a) on the ionic strength of the solution $I$ and (b) protein concentration $c_p$. Equation 1.6 was used to obtain the curves, only monovalent ions were considered.

The first studies of the electrostatic effects in muscle were performed using the X-ray diffraction technique. This is described in the next section.

### 1.6.1 X-ray diffraction studies

The studies of Rome (1967, 1968) on the glycerinated rabbit psoas muscle fibres, revealed that the thick filament spacing was a function of the pH, ionic strength and valency of the cations in the inter-filament medium. The spacing for short and medium sarcomere lengths decreased continuously as the pH of the medium decreased from pH 9.0 to 3.5, whereas at long sarcomere length there was a minimum value of the spacing at about pH 4.7. This behaviour indicated a negative charge on the filaments at physiological values of the pH. The dependence of the spacing on the pH at long sarcomere length was attributed to the isoelectric point of myosin being 4.7 under those experimental conditions, since at this sarcomere length myosin filaments constitute 70% of the A-band lattice. The spacing was smaller in solutions containing divalent cations, whereas the valency of the anion had no effect on the spacing. This effect, however, could also be caused by stronger binding of the divalent cations to the proteins. These results indicated very clearly the presence of the inter-filament forces in muscle which are of an electrostatic nature.

April *et al.* (1969) observed a 40% increase of the lattice volume of intact crayfish muscle fibres bathed in a medium in which 50% of the NaCl was substituted by KCl. This phenomenon was explained by Elliott (1973) by Donnan and osmotic effects across the sarcolemma.

### 1.6.2 Donnan potential measurements

The Donnan potential studies of the electrostatic phenomena in muscle were pioneered by Collins and Edwards (1971). A potential difference was detected, with microelectrodes filled with 3 M KCl, between the glycerinated muscle fibres and the bathing medium. A glycerinated fibre lacks the sarcolemma which would produce

the membrane potentials observed in earlier microelectrode experiments with intact muscle (Ling and Gerard, 1949; Nastuk and Hodgkin, 1950). The potential obtained by Collins and Edwards (1971) was negative at pH 7.5 and positive at pH 4.0. The magnitude of the potential was reduced if the ionic strength of the medium was increased or if the contractile proteins were partially extracted from the tissue. The magnitude of the potential was the same in NaCl- and KCl-based media. This potential was thus consistent with a Donnan potential resulting from the electric charge on the contractile proteins.

The muscle fibres studied by Collins and Edwards (1971) were in rigor. Pemrick and Edwards (1974) measured the Donnan potentials of glycerinated rabbit psoas muscle fibres in solutions producing rigor, relaxation and contraction. For fibres at rest-length the potentials were significantly more negative in a relaxed state than in rigor or contraction, whereas for fibres stretched to non-overlap, there was no difference between these potentials.

The Donnan potential in glycerinated rabbit psoas muscle was also studied by Naylor (1977) as a function of the sarcomere length for rigor and relaxed muscle. The potentials obtained were independent of the sarcomere length and significantly less negative in the relaxed state than in rigor, thus contradicting some of the results of Pemrick and Edwards (1974).

A progress in the technique was made by Bartels and Elliott (1981) who measured the Donnan potentials from the A- and I-bands. The tip position was observed under light microscope in glycerinated rabbit psoas and skinned barnacle muscles. In rigor the A-band potential was significantly more negative than the I-band potential in both muscles. In relaxation the two potentials did not differ, although in rabbit fibres they were equal to the I-band potential in rigor, whereas in barnacle muscle both potentials became approximately equal to the A-band rigor potential. This difference between the potentials in the relaxed state of the two preparations was found to result from the presence of sarcoplasmic reticulum in the skinned barnacle fibres (Bartels and Elliott,

1982). Skinned rat muscle fibres also gave potentials in the relaxed state equal to the rigor A-band potential whereas skinned fibres treated with detergent and glycerinated fibres gave potentials in the relaxed state equal to the I-band rigor potential. These results confirmed the results obtained by Naylor (1977) for glycerinated fibres. The difference in the potentials between the rigor and relaxation was significant and of the order of the potential in the relaxed state itself. The A-band potential for glycerinated rabbit fibres was found to be -4.7±0.6 mV in rigor and -2.3±0.6 mV in the relaxed state at approximately physiological ionic strength (Bartels and Elliott, 1981).

The technique of selective measurements of the Donnan potentials from individual bands was applied by Aldoroty and April (1984) in skinned crayfish fibres. Random and directed impalements gave reproducible trimodal distributions of potentials, with the modalities representing the A- and I-bands and the Z-line vicinity.

A fascinating development was initiated by the studies of Bartels and Elliott (1983), on the effect of ATP, ADP, AMP-PNP and $PP_i$ on the potentials of the A- and I-bands in glycerinated rabbit psoas muscle. It was found that in the presence of $PP_i$ the A-band potential was lowered in a similar way as in the presence of ATP, whereas in the presence of ADP or AMP-PNP the potentials had the same values as in rigor.

In a subsequent study (Bartels *et al.*, 1984), the Donnan potential microelectrode technique was applied to threads of myosin and also to threads of myosin rods. The potentials recorded in rigor solutions were more negative than the potentials obtained in relaxing solutions. These experiments demonstrated that the effect observed for the A-bands is related to the myosin filament backbone.

The effect of varying concentration of ATP and $PP_i$ on the Donnan potentials from the A-bands and on the charge of myosin and myosin rod, was investigated by Bartels *et al.* (1993). It was established that only 100–200 $\mu$M ATP was needed to initiate the charge decrease between the rigor and relaxed conditions. The difference in charge was most prominent at ionic strength equal to approximately half of the physiological

ionic strength. The negative charge on myosin and the rod decreased by about 30% and 40% respectively, when ATP or $PP_i$ were added to 100 $\mu$M concentration. Also the charge on the light meromyosin fragment of the rod was measured using threads of purified protein. No difference, however, was found between the rigor and relaxing conditions. A possible mechanism for the myosin charge difference in the presence and absence of ATP/$PP_i$ was suggested to be due to ion binding to the charged side chains clustered between the myosin rods in the thick filament or between the polypeptide chains in one rod.

An interesting observation was that the charge density on the filaments in the A-band, obtained from the experiments on glycerinated fibres, was approximately twice the charge density derived from the measurements on synthetic thick filaments in the same solution (Bartels *et al.*, 1993). This large difference was associated with differences in the structure and ion binding properties of the native and synthetic thick filaments, that were observed by Tumminia *et al.* (1989, 1990) in hydrostatic pressure studies. These studies revealed that native thick filaments (NTFs) from rabbit psoas muscle were more resistant to pressure-induced disaggregation than synthetic thick filaments (STFs), with and without C-protein, although the addition of C-protein had a stabilizing effect on the STFs. It was found that the NTFs prepared from glycerinated muscle were less resistant to dissociation than the NTFs obtained from fresh muscle, with the loss of resistance being correlated to the length of the glycerination period. Experiments with varying EGTA concentrations suggested that the loss of NTFs stability could be due to a leaching of cations over time. Results of these studies clearly demonstrated that thick filaments assembled *in vitro* are different from thick filaments assembled *in vivo*. It is not surprising, then, that differences in the electric charge of the NTFs and STFs were observed. The charge measurements of isolated proteins can shed light on the role of the individual proteins in the contraction mechanism. A question arises, however, as to how the values of the electric charge measured for isolated proteins reflect the charge that these proteins have in living muscle. This issue will be discussed in chapter 5.

The electric charge of actin was the subject of studies of Cantiello *et al.* (1991), Jennison (1992) and Deshayes (1994). Cantiello *et al.* (1991) measured the potentials of solutions of F-actin at concentrations of about 5 mg/ml using a chloride-plated silver electrode as the measuring electrode. The value that can be derived from the reported potential (-3.9±1.8 mV), leads to a net negative charge of -370e on a monomer of actin. This value seems impossible for a protein consisting of 377 amino acids, of which approximately 50 could have a negative charge at pH 8.0, as can be determined from the amino acid sequence of rabbit skeletal actin.

Jennison (1992) measured the charge in gels of F actin using the microelectrode technique and obtained a value of -9±4e per actin monomer at physiological ionic strength and pH 7.0. The value of the charge was found to be dependent on the ionic strength, with the charge becoming more negative as the ionic strength was increased. Deshayes (1994) also observed the same tendency in the charge of F-actin with the ionic strength using the same technique. The value obtained at physiological strength, -10±4e per monomer, was in good agreement with the value of Jennison (1992).

The charge on F-actin was noticed to be dependent on the history of the preparation. A gel which was stirred immediately before the measurements gave a significantly more negative charge on the monomer (by about 2e) than a gel that was allowed to rest for a period of hours or a gel that was sonicated (Deshayes *et al.*, 1993).

Experiments with glycerinated rabbit psoas muscle fibres revealed a cooperative change in the Donnan potentials occurring with free $Ca^{2+}$ concentration, $[Ca^{2+}]$, (Coomber and Elliott, 1995, 1996). The experiments were performed using microelectrodes in a rigor solution of ionic strength approximately half of the physiological ionic strength, to which $CaCl_2$ and EGTA in various proportions were added to a total concentration of 2mM. For muscle fibres stretched beyond overlap (with sarcomere length 4.2 $\mu$m), four distinct Donnan potentials were observed which were assigned to the A- and I-bands, Z-line and the gap filament. A change in their values of about 2 mV was reported at pCa 6.0, with the potentials becoming less negative at higher

[$Ca^{2+}$] (Coomber and Elliott, 1996). When fibres stretched towards zero overlap were used (with sarcomere length 3.4 $\mu$m) two Donnan potentials were observed, corresponding to the A- and I-bands for which a cooperative change at pCa of 6.2 was reported (Coomber and Elliott, 1995). The magnitude of the change in the Donnan potentials recorded between pCa 5.5 and 7.0 was 1.7 and 2.1 mV for the A- and I-bands respectively. The effect was significantly reduced (to 0.6 and 0.8 mV for the A- and I-bands respectively) if the Donnan potential measurements were performed after an incubation of the fibres with 1% Triton X-100. This treatment has been found to remove the sarcoplasmic reticulum from skinned crayfish fibres (Aldoroty and April, 1984).

Donnan potential measurements were carried out on gels of F-actin and reconstituted thin filaments, which suggested that there was a change in the charge of these proteins with [$Ca^{2+}$] (Jennison, 1993). Microelectrode measurements were performed in rigor solutions of ionic strength approximately 30 mM, with and without the addition of 1 mM EGTA. The charge on both F-actin and the reconstituted thin filaments was found to be more negative in the presence of EGTA.

The Donnan potential of soluble proteins (rabbit tropomyosin and myosin S1) was measured using the macroelectrode technique of Ojteg *et al.* (1989) by Deshayes (1994).

### 1.6.3 Other methods

Methods other than X-ray diffraction and the Donnan potential technique, have been used to investigate the electrostatic properties of muscle and muscle proteins. These methods include: fluorescence, isotope exchange and mass spectrophotometry.

Scordilis *et al.* (1975) measured the fluorescence of the dye 3,3'-dihexyl-2,2'-oxacarbocyanine in myofibrillar suspensions of rabbit muscle. It was found that the changes in fluorescence were linearly proportional to the changes in the Donnan potentials

measured in rabbit glycerinated fibres under the same conditions. This method was further investigated and applied to protein solutions by Deshayes (1994). The calibration of the method was performed using latex particles with a fixed surface charge density of carboxylic groups. The fluorescence of the dye was found to increase with the absolute value of the charge i.e. the sign of the electric charge could not be determined with this method. The advantage of this method is, however, the requirement of fractions of a milligram of the protein. The method applied to troponin gave a molecular charge of -3e at ionic strength 0.07 M and pH 7.0.

Hinke (1980) measured the cation content in chemically skinned barnacle fibres and the bathing solution, using mass spectroscopy. The theoretical Donnan potential was calculated from the ratio of the cation concentration in the fibre and the bathing medium. This value was in very good agreement with the experimentally measured value which is rather surprising since, the cation content of the fibre determined by mass spectroscopy would be the total cation content, i.e. would include counterions which are tightly bound to the proteins and do not contribute to the Donnan potential. Also the uptake of the isotopes $^{22}Na$, $^{42}K$ and $^{36}Cl$ into the fibres was measured. At pH 7.4 the fibre was found to accumulate $K^+$ and $Na^+$ but exclude $Cl^-$ relative to the bathing solution. At pH 5.4 the anion accumulation was observed while the cation accumulation was greatly reduced. In the isotope exchange experiments, the ions tightly bound to proteins are not differentiated from the ions that can move freely between the two phases.

## 1.7 Models of mechanism of muscular contraction

The sliding filament model for the contraction of a striated muscle is widely accepted. There is no agreement, however, as to the mechanism for the production of the force leading to the power stroke. The proposed models fall into two general categories:

1. Indirectly-coupled models.

2. Directly-coupled models.

In models of the first type, the enzymatic hydrolysis of ATP modulates the relative amounts of time spent by the parts of the myosin molecule in two states. The transition between these two states gives the power stroke. In the second group of models, particular steps of the kinetic scheme are made responsible for the conformational changes of the myosin S1 leading to the power stroke. The recently proposed models of the two types will be characterized in the following sections: the indirectly-coupled model of Elliott and Worthington (1994) and the directly-coupled model of Fisher *et al.* (1995).

### 1.7.1 Model of Elliott and Worthington, 1994

The key feature of this model (Elliott, 1993; Elliott and Worthington, 1994, 1995) is the function of myosin ATPase as an ion pump, moving ions against a potential gradient. This is based on the observations of the decreased net negative charge on the A-band and on the myosin molecule in the presence of ATP (Bartels and Elliott, 1981, 1982, 1983, 1985; Bartels *et al.*, 1984, 1993). The central postulate of the model is that the force producing the power stroke arises from the discharge of the S1 and snapping back of the $\alpha$-helical part of the molecule. The contractile cycle is illustrated in figure 1.11.

The sequence of events during the contractile cycle is as follows:

1. **The binding of S1 to actin.** The contraction events are triggered by the increase of the concentration of free $Ca^{2+}$ in the sarcoplasm. This will affect the depth of the electric potential between the thick and thin filaments, through binding of $Ca^{2+}$ to the troponin located in the thin filament. The S1 will carry an ADP-$P_i$ complex in the active site at that stage of the cycle. The long range electrostatic interactions acting on the negatively charged myosin head will cause its movement towards the thin filament. The local electrostatic interactions will cause the binding of the S1 to actin.

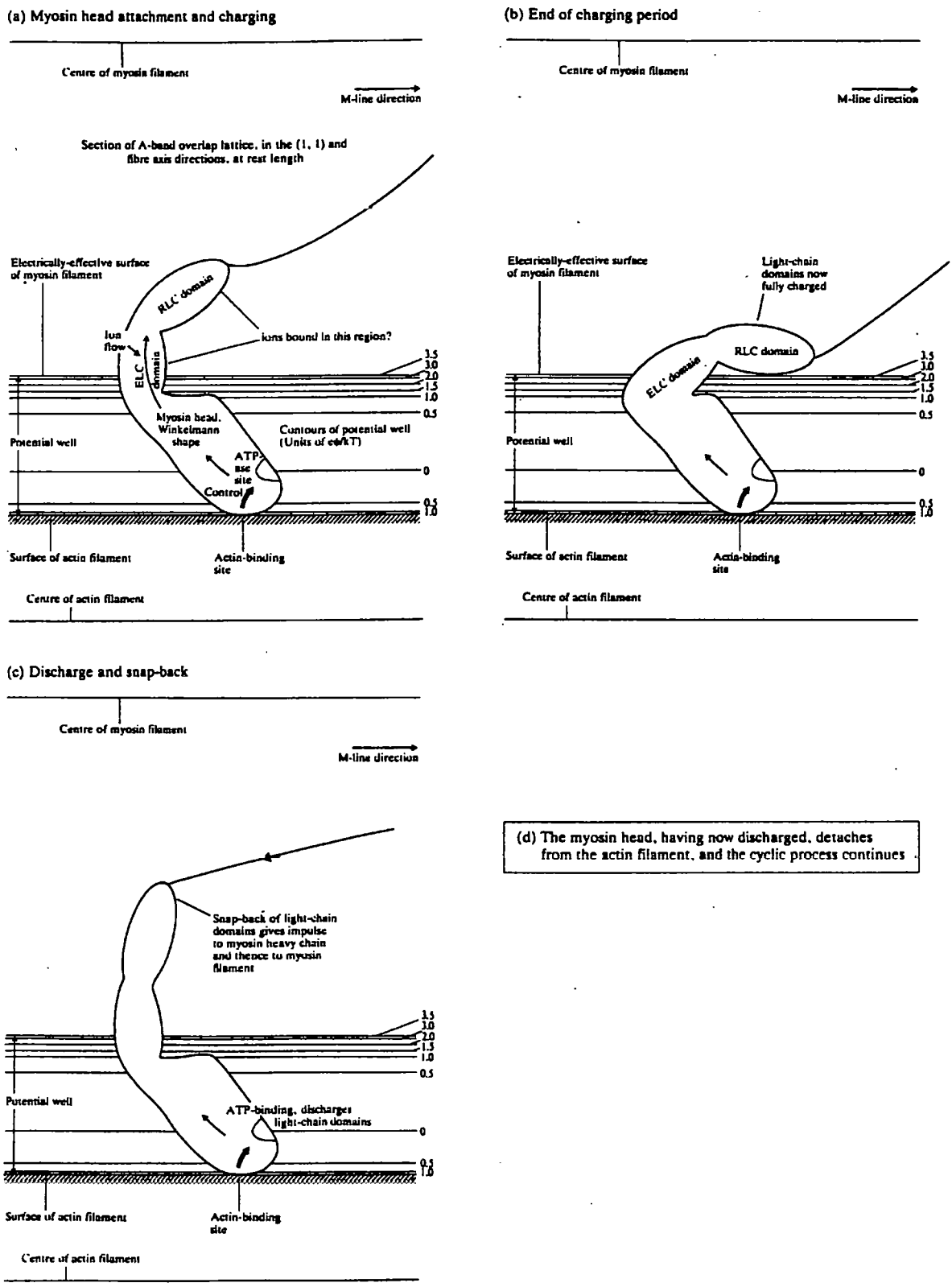


Figure 1.11: A schematic representation of the events during the contraction cycle in the model of Elliott and Worthington (1994) (reproduced from Elliott and Worthington, 1994).

2. **The product release and charging of S1.** When the S1 is attached to actin, the products of ATP hydrolysis are released. The neck region of the S1 charges up (becomes more negatively charged) and the repulsive electrostatic forces between the S1 and the filaments cause the tail of the S1 to curl (figure 1.11a,b). It is possible that the charging up is initiated before the binding to actin.

3. **The power stroke.** When the ATP binds, the S1 discharges and snaps back, producing the power stroke (figure 1.11c).

4. **Detachment of S1 from actin.** It is supposed that the longer and shorter range electrostatic interactions are such that the S1 is released from actin. At that point there will be ATP or ADP-$P_i$ in the active site of S1, but the tail will not be charged up yet (figure 1.11d).

These cycles can be repeated, until the $Ca^{2+}$ level decreases, and then if ATP is still present, the S1 is left with the ATP hydrolysing to ADP and $P_i$ in its active site, bound to actin in the charged state (rigor).

This model agrees with the results of biochemical and structural studies of muscle. It explains many of the puzzling phenomena such as the temperature-jump effects (Davis and Harrington, 1987) and the tension generated at low concentrations of ATP in the absence of $Ca^{2+}$ (Reuben *et al.*, 1971). The explanation for these phenomena is given in Elliott and Worthington (1994).

### 1.7.2 Model of Fisher *et al*, 1995

This model is based on the structure of the methylated chicken S1 (Rayment *et al.*, 1993) and the structures of the truncated *Dictyostelium discoideum* S1 with nucleotide analogues in the active site (Fisher *et al.*, 1995; Smith and Rayment, 1995, 1996).

The conformational changes in this model are associated with the opening and closing of the cleft that splits the 50 kDa fragment of the heavy chain into a lower and upper

domain. These changes are transmitted via the 20 kDa segment to the rest of the molecule. It is suggested that a hinge is formed between the globular and neck region of the S1. The opening of the cleft occurs in response to binding of ATP and its hydrolysis. This reduces the affinity of myosin for actin and is predicted to initiate bending of the S1. The S1 in a fully bent conformation binds to actin, which is suggested to cause the lower 50 kDa domain to move so that the cleft closes again, at the same time the phosphate is released from the nucleotide binding site. The conformational change, induced by closing of the cleft, is proposed to constitute the power stroke.

## 1.8 Aims of the thesis

The following aims were formulated at the onset of this thesis:

1. Calculation of the net electric charge, from the amino acid sequence, for all the main muscle proteins for which the sequences had been determined.

2. Critical evaluation of the electrode techniques for the measurement of the Donnan potential for soluble and filamentous muscle proteins.

3. Determination of any differences in the net electric charge and its distribution between the subfragment-1 of myosin and its methylated form that could account for the ability of the latter to crystallize.

4. Elucidation of the charge of the thin filament and its components as a function of the free $Ca^{2+}$ concentration in order to extend the understanding of the mechanism of the $Ca^{2+}$ regulation of muscular contraction.

## 1.9 Outline of research

**Chapter 2** contains the description of the experimental techniques and computational methods used throughout this thesis.

The results of the studies are presented in **chapters 3, 4** and **5**.

The effect of methylation on the charge of heavy meromyosin (HMM) is investigated in **chapter 3**. The HMM was isolated from rabbit and reductively methylated. The degree of HMM methylation was checked by amino acid analysis and the ATPase activity of HMM and methylated HMM was measured. The molecular charge of both proteins was determined with macroelectrodes using the Donnan potential technique. Also the effect of a difference in the $pK_a$ values of lysine and $N^{\epsilon}$-dimethyllysine on the electric charge of these residues, was considered at various values of pH. The distribution of lysine and other charged residues in the structure of myosin S1, was analysed by visualizing these residues in the S1 structure of Rayment *et al.* (1993).

**Chapter 4** is a study of the macro- and microelectrode techniques for measuring the Donnan potentials in protein solutions. The drifts in potentials, observed for macroelectrodes, were examined and their cause established. The effect of the rate of KCl leakage and sample compartment geometry, on the values of the obtained potentials, was also studied. The possibility of using samples of smaller volume was investigated by measuring the charge of bovine serum albumin (BSA) as a function of pH using two different sample volumes. The microelectrode technique was applied to protein solutions. Microelectrodes with resistance less than 1 MΩ were used; these had been obtained by removing the tips of sharp electrodes. A structural analysis of the tips of microelectrodes was carried out. The KCl leakage rates for microelectrodes of various tip sizes were measured. A procedure for manufacturing lasting microelectrodes giving reproducible results in protein solutions, was developed. The effect of sample viscosity on electrode measurements was also investigated.

The effect of the concentration of free $Ca^{2+}$ on the charge of the proteins of the thin filaments is investigated in **chapter 5**. Also a parallel study was conducted on BSA. Suitable low ionic strength conditions for the preservation of the binding between F-actin and the tropomyosin-troponin complex (Tm-tn) were initially determined. The charge on F-actin, Tm-tn and reconstituted thin filaments (RTFs) was measured using

microelectrodes, whereas the charge on BSA was determined with the macroelectrode technique.

**Appendix B** contains the values of the physical parameters characterizing the main muscle proteins determined from their amino acid sequences. These parameters include: number of residues, molecular weight, molecular and specific charge at pH 7.0 and isoelectric point.

The overall conclusions and suggestions for future work are presented in **chapter 6**.

# Chapter 2

# Methods

## 2.1 Experimental solutions

Analar grade reagents were used to prepare all solutions. All experimental solutions, except for the series with varying pCa, were prepared with water from the Elgastat Option 3 water purification system, which utilizes processes of reverse osmosis, adsorption, deionisation and ultraviolet irradiation to achieve water purity higher than that of distilled water (i.e. of conductivity $\sigma < 1$ $\mu$S·cm$^{-1}$ at 25°C).

Care was taken while preparing solutions with varying pCa in order to obtain the desired concentrations of free $Ca^{2+}$. Water purified in an Elgastat UHQ PS water purification unit was used since it provided a source of greater purity than double distilled water (i.e. of conductivity $\sigma < 0.08$ $\mu$S·cm$^{-1}$ at 25°C). Solutions were prepared and stored in plastic containers since glass is known to release calcium. The solutions were weighed to avoid the use of glass volumetric flasks. Since the experimental solutions were dilute (of ionic strength less than 0.1 M), the difference between the concentration per weight and volume was negligible, hence concentrations were expressed in moles per litre. Since it is impossible to achieve free $Ca^{2+}$ concentrations lower than 0.2 $\mu$M in physiological strength buffers without using EGTA (Celio *et al.*, 1996), a Ca-EGTA buffer system was used to obtain solutions with the desired concentrations of free $Ca^{2+}$.

A frequently used solution was the rigor solution (buffer R). Its composition approximates the composition of the intracellular fluid in the absence of ATP. Buffer R contained 0.1 M KCl, 2.5 mM $MgCl_2$, 20 mM potassium phosphate, pH 7.0 (as in Bartels and Elliott, 1981). The composition of other solutions used will be given in the sections where their use is described.

## 2.2 Protein concentration determination

Two methods were used for protein concentration measurements:

1. The microbiuret method, essentially as described by Goa (1952). The protein sample was made up to 0.5 ml with deionized $H_2O$. The addition of 3.5 ml of 3.4% NaOH was made followed by mixing. After addition of 0.2 ml of Benedict's reagent, the mixture was left for 15 minutes. Following this, absorbance was read at 330 nm in a Cecil 4000 spectrophotometer (Elegant Technology). Protein concentration of all samples was calibrated against BSA protein concentration standard solutions from Sigma. Amounts of protein between 0.1 and 2 mg could be detected with this method.

2. Ultraviolet absorbance at 280 nm. Protein solutions were diluted with an appropriate buffer and the absorbance at 280 nm was measured in 3 ml quartz cuvettes in the Cecil 4000 spectrophotometer. Extinction coefficients used are given in the sections where the application of this method is described.

## 2.3 Protein isolation

Isolation of all the proteins used was performed, except for bovine serum albumin (BSA) which was purchased from BDH. Rabbit heavy meromyosin (HMM) was also purchased from Sigma, its purity was checked by sodium dodecyl sulphate polyacrylamide gel electrophoresis (SDS-PAGE), as described in section 2.4.1, and it proved unsatisfactory. The preparation was a mixture of fragments of various molecular

weights which did not correspond to the fragments that should be present. There was no band corresponding to the heavy chain of molecular weight 140 kDa at all, which suggested that its degradation had taken place. It was therefore decided that I should isolate the protein myself. In the case of actin, the commercially available protein was prohibitively expensive in the quantities required. This meant that a considerable proportion of time would be devoted to protein isolation.

All the proteins were isolated from rabbits which were obtained from the Park Farm, University of Oxford. They were killed by an intravenous injection of 3 ml of 20% sodium pentobarbitone by a member of staff at the Park Farm. After quick skinning, the leg and back muscles were placed on ice for 1 hour during which time they were brought to the Oxford Research Unit.

### 2.3.1 Heavy meromyosin

#### Crude myosin

Myosin was isolated from rabbit leg and back muscles using a procedure modified from Starr and Offer (1982). A Guba-Straub solution (0.3 M KCl, 0.155 M potassium phosphate, pH 6.4) was pre-chilled in an ice-salt bath to about -4°C. All the steps, apart from centrifuging, were carried out in the cold room at 6°C. The muscles were minced twice in a hand mincer that had been pre-chilled on ice. After adding three volumes of Guba-Straub solution, the suspension was stirred gently in an ice-salt bath with a motor driven overhead stirrer for 10 minutes (Silverson laboratory mixer-emulsifier that had been modified to stir solutions slowly) and centrifuged at 5 000×g at 2°C in a Beckman 16 rotor for 10 minutes (average centrifugal forces are always given). The supernatant was filtered through 4 layers of sterile gauze and its volume was measured. Fourteen volumes of pre-chilled solution of 2 mM $\beta$-mercaptoethanol, 0.1 mM EDTA, pH 7.5, were added to the supernatant. After 2 hours the precipitate was collected by syphoning off as much of the supernatant as possible and centrifuging the rest at 5 000×g at 2°C in a Beckman 16 rotor for 10 minutes. The same bottles

were reused until all the precipitate was collected. The pellet was dissolved in 20 ml of 0.5 M potassium phosphate buffer (pH 6.7), 3 M KCl, containing freshly added 2 mM DTT. This was followed by a dilution with 2 mM DTT up to 200 ml and 1 hour centrifugation at 100 000×g at 2°C in a Beckman 90Ti rotor. The supernatant was filtered through 4 layers of gauze and the filtrate was diluted with 6.5 volumes of cold water. After 25 minute centrifugation at 5 000×g at 2°C in a Beckman 16 rotor, the pellet was dissolved in 20 ml of MOPS buffer (3 M KCl, 5 mM $MgCl_2$, 30 mM MOPS, pH 7.0 with 10 mM DTT added on the day of use). The solution was then made up to 100 ml with cold water and centrifuged for 2 hours at 125 000×g at 2°C in a Beckman 90Ti rotor. Only the top 1/3 of the supernatant was used for further purification. At this stage the concentration of myosin was measured spectrophotometrically at 280 nm using an extinction coefficient $5.3\times10^2$ $cm^2 \cdot g^{-1}$ (Margossian and Lowey, 1982) and the yield was determined. The myosin was left on ice overnight.

### Isolation of HMM from crude myosin

HMM was obtained by myosin digestion with $\alpha$-chymotrypsin (Sigma, type VII from bovine pancreas). The myosin solution was warmed up to 25°C. Chymotrypsin was dissolved in the above MOPS buffer at the concentration 1.1 mg/ml and added to myosin in the ratio 1:800 by weight. Digestion was stopped after 8 minutes by adding 0.2 M PMSF in ethanol to a concentration of 0.5 mM with stirring and placing the solution on ice. Subsequently the solution was dialysed overnight in the cold room against 2*l* of 30 mM KCl, 5 mM MOPS, pH 7.0 buffer in order to precipitate light meromyosin (LMM) and undigested myosin. Digestion products were separated by a 2 hour centrifugation at 125 000×g at 2°C in a Beckman 90Ti rotor: the supernatant contained the HMM. Protein concentration was determined spectrophotometrically at 280 nm using an extinction coefficient $6.0\times10^2$ $cm^2 \cdot g^{-1}$ (Margossian and Lowey, 1982). The yield was about 0.3 g per gram of crude myosin used, which is approximately 40% of the maximum theoretical yield. Aliquots of 5 and 10 mg were frozen in an

ethanol/$CO_2$ bath and stored frozen until further required. The protein was used within 5 months.

### 2.3.2 Methylated heavy meromyosin

The methylation was carried out following the procedure for the subfragment-1 of myosin (S1) as outlined in Rayment *et al.* (1993), with minor modifications. Heavy meromyosin, obtained as described in section 2.3.1, was thawed and diluted to 5 mg/ml. It was then dialysed against 1 *l* of 1 mM $MgCl_2$, 0.2 M potassium phosphate, pH 7.5 at 6°C. A 1 M solution of dimethylamine-borane complex (DMAB, Aldrich Chemical Co.) and a 1 M solution of formaldehyde (purchased as 37% solution from Sigma) were freshly prepared before use. 20 $\mu$l of 1 M DMAB and 40 $\mu$l of 1 M formaldehyde per ml of protein were added with rapid stirring and the solution was left at 4°C. This step was repeated after 2 hours and then, after a further 2 hours, 10 $\mu$l of DMAB per ml of protein were added. The reaction mixture was incubated at 4°C in the dark (in a fridge). The reaction was stopped after 18 hours by addition of 3.8 M ammonium sulphate to a concentration of 1 M. The protein solution was dialysed exhaustively to remove traces of ammonium sulphate against 30 mM KCl, 5 mM MOPS, pH 7.0 buffer and concentrated by adding polyethylene glycol (of MW 20 kDa) to the dialysis buffer. Aliquots of methylated HMM were frozen and stored as for the HMM.

### 2.3.3 Subfragment-1 of myosin

S1 was obtained by enzymatic digestion of myosin that had been isolated using the method of Starr and Offer (1982), in its original form or with the modifications described in section 2.3.1. Papain digestion was attempted according to the method of Margossian and Lowey (1982) in the presence of $MgCl_2$ in order to obtain the S1 with all the light chains intact. Also, the digestion in the presence of EDTA was tried in order to obtain S1 without the regulatory light chain. In both cases, how-

ever, degradation of the heavy chain occurred, resulting in the preparation containing mostly a fragment of a molecular weight approximately 70 kDa, as determined by SDS-PAGE. The $\alpha$-chymotryptic digestion according to the method of Weeds and Taylor (1975) also gave an unsatisfactory result. These preparations were not used for any measurements.

### 2.3.4 Actin

#### Acetone powder

The procedure of Pardee and Spudich (1982) was used, with just one modification in the initial myosin extraction. The back and leg muscles were obtained in the usual way as described in section 2.3. All the steps, except for the centrifugation, extractions with acetone and drying of the powder, were carried out in the cold room at about 8°C. The muscles were minced in a hand mincer and after adding three volumes of 0.3 M KCl, 0.15 M potassium phosphate, pH 6.5 solution, pre-chilled on ice, the suspension was stirred gently with a motor driven overhead stirrer for 15 minutes and centrifuged at 2 500×g at 4°C in a Beckman 16 rotor for 10 minutes. The pellet from this centrifugation was extracted with 2 $l$ of 0.05 M $NaHCO_3$ by stirring for 10 minutes with an overhead motor stirrer. This and subsequent extraction solutions had been pre-chilled to 4°C, except for acetone which had been cooled to below 20°C. The muscle suspension was filtered through 3 layers of sterile gauze and the residue was extracted with 1 $l$ of 1 mM EDTA, pH 7.0, by stirring for 10 minutes. It was filtered as previously and then extracted twice with 2 $l$ of water for 5 minutes. Finally the muscle was extracted 5 times with 1 $l$ of acetone, filtering through 4 layers of gauze each time. The residue was placed in large glass dishes, covered with filter paper and left to dry overnight in a fume cupboard at room temperature. The next morning the acetone powder was weighed and placed in bottles that were stored in a freezer at -20°C in sealed bags containing silica gel. The yield was about 8 g of powder per 100 g of muscle mince.

### Isolation of actin from the acetone powder

Actin was isolated from powder using the procedure of Pardee and Spudich (1982). Two protocols were followed: one for faster isolation of smaller quantities of the protein (starting from 4 g of acetone powder) and the other one for isolation of larger quantities (starting from 10 g of acetone powder). The latter involved longer centrifugations of larger volumes at lower speeds. In one isolation the powder was blended in the Magimix 2000 blender (Robot Coupe, France) by applying three 2 s pulses, but this did not increase the yield and was not used in other isolations. A solution of 0.2 mM $Na_2ATP$, 0.5 mM $\beta$-mercaptoethanol, 0.2 mM $CaCl_2$, 0.005% $NaN_3$, 2 mM Tris-HCl, pH 8.0 (at 25°C) was prepared. The pH of this solution was adjusted with 1 M HCl before adding $\beta$-mercaptoethanol. Acetone powder was stirred manually with 20 ml of the above Tris-HCl buffer per gram of powder in an ice-salt bath (at 0–0.5°C) for 30 minutes in order to extract actin in the monomeric form (G-actin). The mixture was centrifuged at 10 000×g in a Beckman 16 rotor for 15 minutes at 4°C. The pellet was re-extracted with 15–20 ml of the same Tris-HCl buffer per gram of powder and filtered through 4 layers of sterile gauze into the supernatant from the centrifugation. All subsequent steps were carried out at 4°C. The combined extract was centrifuged at 19 000×g in a Beckman 16 rotor for 50 minutes to clarify the solution of G-actin. The supernatant was decanted and its KCl concentration was brought up to 50 mM, $MgCl_2$ to 2 mM and $Na_2ATP$ to 1 mM. This solution was left in the fridge for 2 hours during which time polymerization of G-actin into filamentous F-actin took place. Solid KCl was then slowly added to a final concentration of 0.6 M and the solution was stirred with a magnetic stirrer for a further 30 minutes in order to dissociate tropomyosin. If only 4 g of powder were used initially, then the solution was centrifuged in a Beckman 90Ti rotor at 155 000×g for 1.5 hours. If larger quantities of powder were used, as the starting material, then an 11 hour centrifugation in a Beckman 16 rotor at 22 000×g was required. The pellet from this centrifugation, containing F-actin, was homogenized into 10 ml (per gram of powder) of the Tris-HCl buffer containing also 50 mM KCl, 2 mM $MgCl_2$ and it was re-sedimented

in a Beckman 90Ti rotor at 155 000×g for 1.5 hours. This wash was performed to remove any proteases before the depolymerization of F-actin into G-actin, which is more susceptible to proteolysis. The pellets from this centrifugation were thoroughly rinsed with the Tris-HCl buffer and then gently homogenized with 3 ml of the same buffer per gram of acetone powder. The homogenate was dialysed against Tris-HCl buffer with 5 changes at about 12 hours intervals. After the dialysis, the protein solution was centrifuged in a Beckman 90Ti rotor at 155 000×g for 1.5 hours: the supernatant contained G-actin. Its concentration was measured spectrophotometrically at 280 nm using an extinction coefficient $1.097 \times 10^3$ $cm^2 \cdot g^{-1}$ (Rees and Young, 1967). The typical yield was about 10 mg of G-actin per gram of acetone powder used.

At this stage G-actin could be used to form reconstituted thin filaments as described in section 2.3.6. Otherwise G-actin was polymerized by addition of KCl up to 50 mM, $MgCl_2$ to 1 mM and $Na_2ATP$ to 1 mM. The concentration of $NaN_3$ was increased to 0.02% at this stage. After polymerizing for 2 hours in the fridge, the solution was centrifuged in a Beckman 90Ti rotor for 1.5 hours at 155 000×g. The pellet contained F-actin.

### 2.3.5 Tropomyosin-troponin complex

The procedure of Murray (1982) was used to dissociate the tropomyosin-troponin complex from the thin filament at very low ionic strength.

#### Crude tropomyosin-troponin

Muscle mince was obtained as described in section 2.3.4. It was extracted with 2 *l* of 0.3 M KCl, 0.02 M EDTA, 5 mM $MgCl_2$, 1 mM $Na_2ATP$, 0.15 M potassium phosphate, pH 6.5 per kilogram of mince for 15 minutes using a motor driven overhead stirrer. The mixture was then diluted 4-fold with cold water at 4°C and filtered through 3 layers of gauze. The residue was re-suspended in 3 ml of 20 mM KCl, 0.2 mM $NaHCO_3$ per gram of muscle, stirring for 10 minutes with the motor stirrer and filtered through 4

layers of gauze. This was repeated once with 20 mM KCl, 0.2 mM $NaHCO_3$ and twice with cold water. Subsequently the washed residue was mixed with an equal volume of cold water and the suspension was blended in the Magimix 2000 blender for 5 s. After adding $NaN_3$ to a 1 mM concentration, the suspension was stirred slowly with the motor stirrer for 4 hours at room temperature and then left at 4°C overnight. The following day the solution was centrifuged at 16 000×g for 15 minutes in a Beckman 16 rotor at 4°C. The supernatant was subsequently freeze-dried in an Edwards Modulyo freeze-drier and stored at -20°C. The yield of crude tropomyosin-troponin complex was about 0.6 g from 100 g of muscle mince.

### Purified tropomyosin-troponin

Freeze-dried crude protein complex was dissolved in 0.2 mM DTT, 10 mM Tris-HCl, pH 7.4 buffer at a concentration of 10 mg/ml. KCl was added to 0.1 M and $MgCl_2$ to 2 mM in order to polymerize the G-actin present in the solution. Under these rigor conditions, myosin remained bound to actin and it was possible to remove the F-actin, together with myosin and insoluble material by a 2 hour centrifugation at 150 000×g in a Beckman 90Ti rotor at 4°C. $NaN_3$ was added to the supernatant to the concentration of 0.005%. Partially denatured actin that did not polymerize in the previous step could be polymerized by addition of $Na_2ATP$ to 0.1 mM concentration and removed by centrifuging at 155 000×g in a Beckman 90Ti rotor at 4°C. The typical yield of tropomyosin-troponin complex in the supernatant was approximately 300 mg per gram of crude preparation as determined with the microbiuret method described in section 2.2. The protein was either used immediately for the reconstitution of thin filaments (next section) or stored on ice until further required. The storage period was no longer than three weeks for the protein used in the Donnan potential and viscosity measurements of chapter 4. The protein used in the Donnan potential measurements described in chapter 5 was used within one week.

### 2.3.6 Reconstituted thin filaments

The procedure of Murray (1982) was implemented, with one modification. The ratio of tropomyosin-troponin to G-actin used for the reconstitution, was 1.5 by weight. G-actin was isolated as described in section 2.3.4. Tropomyosin-troponin complex in 0.1 M KCl, 0.1 mM $Na_2ATP$, 2 mM $MgCl_2$, 0.2 mM DTT, 10 mM Tris-HCl, pH 7.4, was combined with the G-actin solution. The composition of the medium was adjusted to contain 0.1 M KCl, 2 mM $MgCl_2$ and 10 mM Tris-HCl, pH 7.0. The mixture was stirred briefly and incubated at 15°C for 45 minutes. It was then centrifuged at 155 000×g for 1.5 hours at 4°C in a Beckman 90Ti rotor. The pellets contained reconstituted thin filaments which were used in experiments. The supernatant, containing the excess tropomyosin-troponin complex which had not been incorporated into thin filaments, was discarded.

## 2.4 Protein purity assessment

### 2.4.1 SDS-PAGE electrophoresis

A dissociating discontinuous buffer system based on the method of Laemmli, as described in Hames and Rickwood (1981), was used.

Mini gels of 0.75 mm thickness were cast in a Mini-Protean II electrophoresis cell and the electrophoresis was performed using a Biorad Powerpac 300 at 200 V and constant power for about 45 minutes. Coomassie brilliant blue R250 in 7% acetic acid, 40% methanol was used to fix and stain gels. Gels were scanned with an LKB Bromma Ultroscan XL laser densitometer and photographed with Polaroid MP-4 camera on Polaroid 665 films using a yellow filter from the MP-4+ filter kit.

The ratios of the protein components in a preparation were determined by cutting and weighing corresponding peaks from the gel scan. Only the values obtained from the linear range of the relationship between the peak area and protein quantity for

all the protein bands considered were taken.

### 2.4.2 ATPase activity assay

The amount of inorganic phosphate produced in ATP hydrolysis was measured by the method of Pollard & Korn as given in Pollard (1982). The ATP hydrolysis reaction conditions were as used by Margossian and Lowey (1982) except that the protein concentration was approximately 25 $\mu$g/ml as opposed to 50 $\mu$g/ml in the original assay. This modification was made in order to obtain a suitable range of absorbance values. The hydrolysis reaction conditions were:

- in the presence of $Ca^{2+}$:
  0.23 M KCl, 2.5 mM $CaCl_2$, 2.5 mM $Na_2ATP$, 50 mM Tris-HCl, pH 7.9,
- in the presence of EDTA:
  0.6 M KCl, 1 mM EDTA, 2.5 mM $Na_2ATP$, 50 mM Tris-HCl, pH 7.9.

### 2.4.3 Amino acid analysis

Amino acid analysis was performed on HMM and methylated HMM in order to verify whether the desired modification had actually taken place.

500 picomols of nor-leucine were added to samples as an internal standard prior to hydrolysis with HCl at 110°C for 22 hours. Samples were then applied to an Applied Biosystems 420A derivatiser/analyser where phenylthiocarbamyl amino acids were formed by derivatisation with phenylisothiocyanate. These were automatically applied to a C-18 reversed phase high performance liquid chromatography column which had been equilibrated at 34°C in 7% of buffer B in buffer A, where buffer A was 150 mM sodium acetate, pH 5.5, and buffer B was 70% acetonitrile in water. Elution was carried out with eluent B in 3 steps of linear gradients to 100% of B over 25 minutes. Absorbance at 269 nm was recorded and the amino acid content in the sample was calculated using an ABI 920A data analysis system.

Methylated derivatives of lysine were used as external standards. $N^{\epsilon}$-methyllysine and $N^{\epsilon}$-trimethyllysine were purchased from Sigma and $N^{\epsilon}$-dimethyllysine was purchased from Bachem, California.

## 2.5 Experimental determination of the net electric charge

The net electric charge of a protein was determined from its Donnan potential, protein concentration and ionic composition of the solution in which the Donnan potential was measured. Equation 1.6, given in section 1.5, was used to calculate the net electric charge of a protein.

The Donnan potential and protein concentration were determined experimentally whereas the ionic composition was calculated using the PERRIN program (Abbott, 1976) with the stability constants given in appendix A. The techniques used for the Donnan potential measurements and ionic composition calculations are described in detail in sections that follow. The protein concentration was determined using the microbiuret method described in section 2.2.

### 2.5.1 Donnan potential macroelectrode measurements

A macroelectrode technique developed by Ojteg *et al.* (1989) was used to measure the Donnan potential that exists between two compartments separated by a semi-permeable membrane when one of the compartments contains charged non-permeating protein molecules. A schematic diagram of the experimental set-up, with both the reference and measuring electrodes surrounded by sacks made of semi-permeable membrane, is given in figure 2.1. The original set up of Ojteg *et al.* (1989), with the measuring electrode inside a dialysis sack and the reference electrode in the outer buffer, was also used. The beaker with the buffer, samples and electrodes were placed inside an earthed Faraday's cage.

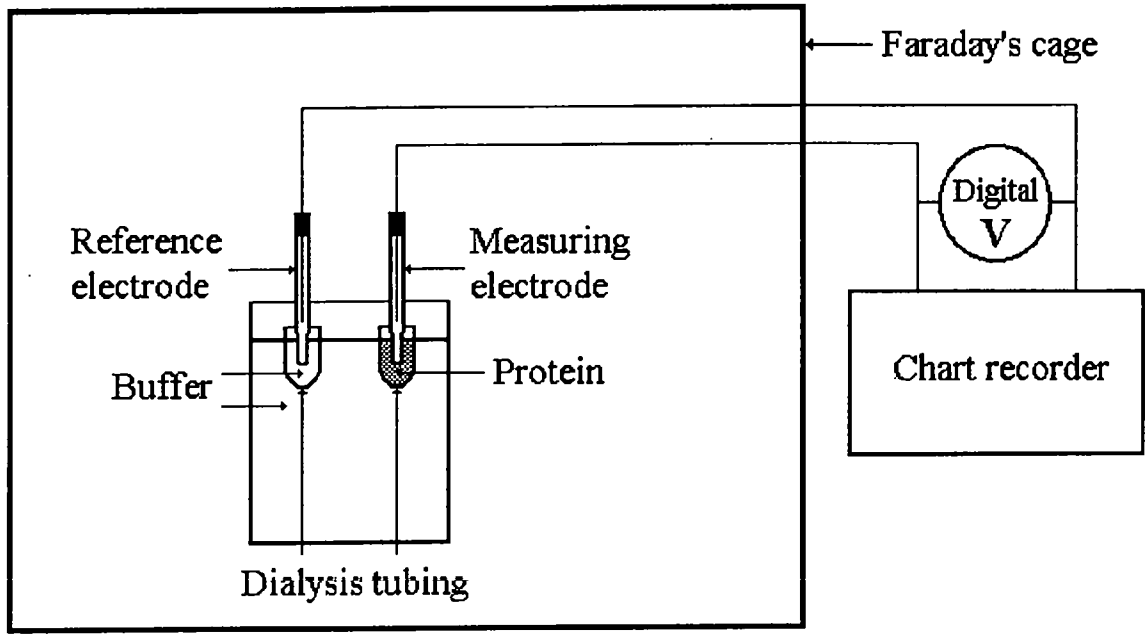


Figure 2.1: A schematic diagram of the experimental set-up for the Donnan potential macroelectrode measurements.

The set-up with both the reference and measuring electrodes in the dialysis sacks was introduced in the expectation that the potentials resulting from the KCl outflow through the porous pin of the electrodes filled with saturated KCl would cancel out due to the symmetry of the system. Later though, we decided to investigate these phenomena and went back to the original one sack system.

Protein solutions were dialysed at 0–8°C against 1 *l* of the appropriate buffer overnight, in cellulose dialysis tubing with 12–14 kDa cut-off. The measurements were made with a set of two calomel electrodes (K422 or REF401 from Radiometer Copenhagen) connected to a Servogor 120 chart recorder (BBC Goerz Metrawatt) and a Metex M-4600 multimeter (Testlab).The chart recorder and multimeter had impedance of approximately 10 MΩ each. The resistance of the electrodes was approximately 9 kΩ as measured with the Metex M-4600 multimeter in a solution of ionic strength around 20 mM. Two types of dialysis tubing were used to make the semi-permeable sacks: 14.3 mm in diameter from Medicell International, for 1 ml samples, and 6 mm in diameter from Sigma, for samples with 0.25 ml volume. Both types of tubing had a

MW cut-off of 12–14 kDa. The tubing was prepared in the standard way and stored in deionized water at 4°C with addition of 1 ml of chloroform per litre. It was soaked in 0.5 $l$ of the appropriate buffer at 4°C at least overnight before use.

Initially the electrodes were placed in the outer buffer to equilibrate for approximately 10 minutes. The Donnan potential $U_D$ was obtained as:

$$U_D = U_{prot} - U_{ref}$$

The reference potential $U_{ref}$ was taken as the potential recorded when the measuring electrode was in a dialysis sack with buffer and the reference electrode was either in the outer buffer (in the set-up with one sack) or in a dialysis sack with buffer (in the set-up with 2 sacks). $U_{prot}$ was the potential recorded when the buffer in the compartment, where the measuring electrode was immersed, was replaced with protein solution. Aliquots of the protein solution (50–100 $\mu$l) were withdrawn and used for protein concentration determination.

In the experiments described in chapter 3 after the first Donnan potential was measured, only one aliquot (50–100 $\mu$l) of the protein solution was withdrawn. Then the potential $U_{prot}$ was measured again. The second Donnan potential was calculated using the reference potential value recorded at the beginning of the experiment. It was assumed that the reference potential was a result of the electrodes not being identical and was a feature of the pair of electrodes that would not change during the course of the experiment. We took no more than two measurements with each sample since transferring the electrode between the two media caused dilution of the protein, and taking aliquots for protein concentration determination, decreased the volume of the sample.

The volume of the solution inside the dialysis tubing was either 0.25 ml or 1 ml whereas the volume of the external buffer was 1 $l$. The protein concentrations were around 10 mg/ml and the recorded Donnan potentials were of the order 1–3 mV.

### 2.5.2 Donnan potential microelectrode measurements

The macroelectrode technique enables measurement of the net charge of proteins in solution but we experienced difficulties while using it, the most prominent problem being the interpretation of the unstable potentials which is described in detail in section 4.1. I therefore looked for modifications of the method or for an alternative method to determine the net charges on proteins.

The immediate candidates were microelectrodes, which had been used by our laboratory before, in work with intact muscle fibres and protein gels. The microelectrodes were made from borosilicate glass capillary tubing with external diameter 1.5 mm and length 65 mm (type GC150f-6.5) obtained from Clark Electromedical Instruments, England. They were pulled using a vertical microelectrode puller from Scientific and Research Instruments Ltd, England. The end of the electrode was removed in order to obtain electrodes with larger tip size. This was done either by breaking the tip off with forceps or using a microelectrode grinder. Initially a grinder in the laboratory of Dr Christopher C. Ashley in the Department of Physiology, University of Oxford, was tried. Then a grinder built by Ted Beaver of the Oxford Research Unit was used. No difference was observed in the performance of the microelectrodes produced with those two grinders. Electrodes were secured in a micromanipulator and lowered to the surface of the grinding disk at an angle. While the disk was moving the electrode was gradually lowered, the position of the tip and its bending could be seen under a travelling microscope. After the tip was removed, the electrodes were filled with 3 M KCl and mounted in Ag/AgCl microelectrode holders from Clark Electromedical Instruments, England. A REF200 Ag/AgCl electrode from Radiometer, Copenhagen was used as a reference electrode. The two electrodes were connected to a resistance and voltage meter of high impedance ($10^{14}$ $\Omega$) constructed by A. Tuddenham of the Meat Research Institute, Bristol, this meter being a development of the original design by Naylor (1978).

A schematic diagram of the experimental set-up for the microelectrode measurements

is given in figure 2.2. The beaker with buffer, samples, electrodes and the analog resistance and voltage meter were placed inside an earthed Faraday's cage. Initially Amicon microconcentrators, with a membrane of MW cut-off 10 kDa at the base, were used as sample compartments. They proved, rather costly however, and dialysis sacks, made of dialysis tubing (6 mm in diameter with MW cut-off of 12–14 kDa from Sigma), were subsequently used. The dialysis tubing sacks were used in all the experiments conducted in solutions with varied free $Ca^{2+}$ concentrations. The tubing was equilibrated and protein samples were dialysed, as for the macroelectrode measurements. Unlike in the macroelectrode method, the same potential difference appeared to exist between the two electrodes, irrespective of whether the microelectrode was outside or inside the sack or Amicon microconcentrator, when they contained buffer. Hence a decision was made, to use the potential recorded when both electrodes were in the outer buffer as the reference potential $U_{ref}$. The protein sample was placed in the sample compartment and the potential $U_{prot}$ measured. The Donnan potential was taken as the difference between $U_{prot}$ and $U_{ref}$. It was possible to repeat the measurements as both $U_{ref}$ and $U_{prot}$ could be recorded more times. Also, due to the small size of the microelectrode tip, the protein transfer to the outside buffer and dilution of the sample, were negligible. The microelectrode was transferred between the outer buffer and protein sample a number of times (usually 10–20) for each electrode and the protein concentration was determined afterwards. Each measurement was typically taken for about 20 seconds, but even if the microelectrode was left in the sample compartment for several minutes, no drifts in potentials were observed.

### 2.5.3 Ionic composition of solutions

Concentrations of ionic species in solution required for equation 1.6 were calculated using the computer program PERRIN (Abbott, 1976) which is based on the method of Perrin and Sayce (1967).

In this method equilibrium concentrations of metal ions, ligands and their complexes

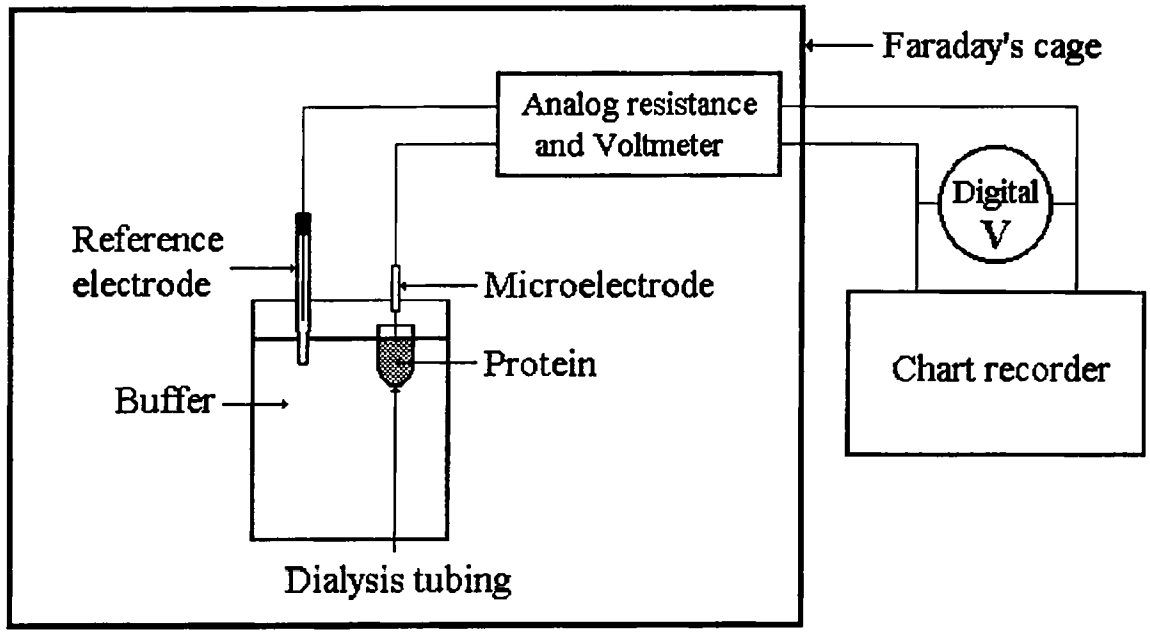


Figure 2.2: A schematic diagram of the experimental set-up for the Donnan potential measurements with a microelectrode as the measuring electrode.

are calculated from the pH of the solution, the total concentrations of metals and ligands and the stability constants for the formation of the complexes. The calculations utilize an iterative algorithm outlined in Perrin and Sayce (1967) which allows the simultaneous solution of the equilibrium equations for all the considered complexes. With a large and increasing number of stability constants available in literature, the composition of solutions with many species can nowadays be known with accuracy, provided that stability constants used were accurately determined. Hence for our calculations, whenever possible, we used the so-called critical stability constants. Critical stability constants are values selected from literature by the authors compiling the tables as satisfying rigorous selection criteria. The values of stability constants that we used to determine the composition of our experimental solutions are listed in appendix A.

## 2.6 Net charge calculation from the sequence

The net charge of a protein in electronic charge units was calculated as a sum of the number of protonated lysine, arginine and histidine residues and amino termini minus the number of deprotonated tyrosine, cysteine, glutamate and aspartate residues and carboxyl termini, since these are the main ionizable groups that contribute to the charge of a protein. The numbers of protonated and deprotonated residues were calculated from equations 1.1 and 1.2, respectively. Calculations were performed using the program ISOELECTRIC contained in the GCG package (Devereux *et al.*, 1984) on the Seqnet computer at Daresbury Laboratory using the $pK_a$ values given in table 1.1. It should be noted that these calculations did not take into account the neutralization of the charges by counterions that are present in the double layer. Hence the values of the charge calculated in this manner are the values of the net charge of the protein without any bound counterions.

## 2.7 $K_{app}$ method for $[Ca^{2+}]$ calculation

The concentrations of free $Ca^{2+}$, $[Ca^{2+}]$, in our series of experimental solutions for Donnan potential measurements, were calculated using the apparent binding constant method as well as the method of Perrin and Sayce (1967). In the $K_{app}$ method one association constant, called the apparent binding constant $K_{app}$, is used to describe the formation of a Ca-EGTA complex as if it was the only reaction involving calcium in solution. The concentration of free $Ca^{2+}$ can be calculated from the following set of equations:

$$\begin{aligned} K_{app} &= \frac{[Ca - EGTA]}{[Ca^{2+}] \cdot [EGTA]} \\ [Ca^{2+}_{total}] &= [Ca^{2+}] + [Ca - EGTA] \\ [EGTA_{total}] &= [EGTA] + [Ca - EGTA] \end{aligned} \tag{2.1}$$

where $[Ca^{2+}]$ and [EGTA] denote concentrations of uncomplexed $Ca^{2+}$ and EGTA respectively, [Ca-EGTA] is the concentration of the Ca-EGTA complex, $[Ca^{2+}_{total}]$ and

$[EGTA_{total}]$ are total concentrations of calcium and EGTA.

One value of the apparent binding constant is used to describe the formation of the many different complexes that involve calcium in multicomponent solutions (see table A.1). It is thus important, that for a given experimental solution, an apparent binding constant, that had been determined under similar experimental conditions, is used. It is rarely the case that such a value is available. However, a correction can usually be made for differences in ionic strength, pH and temperature.

## 2.8 Electrode determination of $[Ca^{2+}]$

The free $Ca^{2+}$ concentration, $[Ca^{2+}]$, in our experimental solutions was determined from the potential difference between a reference and $Ca^{2+}$ sensitive electrode. Two types of $Ca^{2+}$ sensitive electrodes were used: IS 561-Ca (Müller, Switzerland) and Elit 041 (Merck, England). An Ag/AgCl electrode REF200 (Radiometer, Copenhagen) was the reference electrode and the potential difference was measured with a Metex M-4600 multimeter (with 10 MΩ impedance).

Standard and experimental solutions were prepared with special care, as described in section 2.1. The standard solutions contained 10 mM KCl (from BDH with $Ca^{2+}$ content less than 0.001%) and from $10^{-9}$ to $10^{-2}$ mM $CaCl_2$ added. This meant that 10 mM KCl alone could contain as much as $10^{-7}$ mM $CaCl_2$ from its impurities if no calcium-EGTA buffer was included. This was, however, the purest KCl found and it was also used to prepare the experimental buffers. KCl was introduced into the standards as it was the main component of our experimental solutions that would interfere with the response to calcium – this is the recommended practice for calibrating ion specific electrodes (Ammann, 1986). The selectivity coefficient, defined as the ratio between an activity of the selected ion and the activity of an interfering ion that would give an identical electrode response, was $2\times10^{-4}$ for $K^+$ for the Müller electrode, resulting in the electrode responding to 10 mM KCl as to $2\times10^{-6}$ mM $Ca^{2+}$.

The selectivity data were not available for the Merck electrode.

The measurement was performed by placing the reference and $Ca^{2+}$ sensitive electrodes into 100 ml of solution and recording the value of the potential difference after allowing the electrodes to equilibrate for about 1 minute after which time the readings became stable. The same sample was used for the measurement with the Müller and subsequently the Merck electrode for direct comparison. The resistance of the circuit was 2.5 MΩ (with the Müller electrode) and 1 MΩ (with the Merck electrode) in a 10 mM KCl solution.

## 2.9 Viscosity measurements

The capillary viscometry method was used to determine the apparent kinematic viscosity, $\eta^{kin}$, of our protein solutions. The apparent kinematic viscosity is defined as the dynamic viscosity of a liquid divided by its density and measured at particular shear rate. Protein solutions are in generally non-Newtonian fluids, for which the dynamic viscosity varies with shear rate.

The time of flow of the sample through a section of a capillary tube under hydrostatic pressure was measured with a Weber BS748 capillary viscometer. The temperature was maintained at 20.0±0.5°C by placing the samples on a water bath and equilibrating them before starting measurements. The capacity of the viscometer and sample volume were 0.37 ml and 0.5 ml respectively. A timing device with accuracy to hundredths of a second was used. For protein solutions, a series of dilutions was made in the following way: after measuring the flow times for a protein solution, 100 $\mu$l was withdrawn and replaced with the same volume of buffer. The viscometer was then rinsed three times with the diluted protein solution in order to mix it well with any protein that was left in the instrument and then the flow of the solution was timed. Following this, a specified amount of protein solution was again withdrawn and replaced with buffer. This procedure was continued in order to obtain a series of

dilutions of the initial solution. The buffer used in these experiments was 10 mM KCl, 0.5 mM $MgCl_2$, 0.4 mM $CaCl_2$, 0.6 mM EGTA, 2 mM potassium phosphate, pH 7.0. The viscometer was cleaned thoroughly between the measurements for different proteins and standards. The viscometer was calibrated with aqueous solutions of glycerol using the data from Weast (1974) to obtain the apparent kinematic viscosities for the protein solutions.

## 2.10 Conductivity measurements

The electrical conductivity method was applied to determine the rate of outflow of KCl from inside the electrodes through a macroelectrode porous pin and microelectrode tip. The electrodes were left with their ends immersed in 12 ml of 10 mM KCl at 25°C for 1 hour, this volume of the solution was used due to the size of the conductivity probe. Subsequently the electrical conductivity of the solutions and KCl standards was measured using a digital conductivity meter PTI-18 from Data Scientific. The accuracy of the meter was better than 0.5% over the whole range.

## 2.11 Diffusion potentials

### 2.11.1 Measurements

Diffusion potentials of NaCl were measured with macroelectrodes initially in order to check whether the method of Ojteg *et al.* (1989) was being applied correctly. Since it was not possible to reproduce the diffusion potentials obtained by Ojteg *et al.* (1989), the problem was investigated. NaCl diffusion potentials were measured using different concentration gradients, electrodes and preparation procedure of the dialysis tubing.

NaCl solutions of different concentrations were prepared and the dialysis tubing was always equilibrated (at least overnight) in the weaker one of the two solutions, intended to create the concentration gradient. The reference potential for these measurements

was taken as the potential recorded when both electrodes were in $1\,l$ of the weaker solution. Potentials $U_o$ and $U_{dif}$ were recorded when 1 ml of the weaker and stronger solution was placed inside the dialysis sack, respectively. The potentials were recorded with a chart recorder and digital multimeter, mentioned in section 2.5.1.

### 2.11.2 Calculations

All equations and the values of parameters used were taken from Ammann (1986).

The diffusion potentials $U_{dif}$ were calculated using the Henderson equation:

$$U_{dif} = \frac{\sum_{i=1}^{n} z_i u_i (a_i - a_i')}{\sum_{i=1}^{n} z_i^2 u_i (a_i - a_i')} \frac{RT}{F} ln \frac{\sum_{i-1}^{n} z_i^2 u_i a_i'}{\sum_{i=1}^{n} z_i^2 u_i a_i} \tag{2.2}$$

where $z_i$, $u_i$, $a_i$, $a_i'$ denote the valency, mobility, activity in the first phase and activity in the second phase of ion $i$, respectively, with $n$ being the total number of ion types present, $R$ is the gas constant, $T$ absolute temperature and $F$ is the Faraday constant.

The concentrations were multiplied by the activity coefficients $\gamma$ to obtain the activities. The activity coefficients were calculated from the Hückel equation:

$$log_{10}\gamma = \frac{-A|z_+ z_-|\sqrt{I}}{1 + Ba\sqrt{I}} + CI \tag{2.3}$$

where $I$ is the ionic strength, $z_+$, $z_-$ are valencies of the cation and anion of the electrolyte, $a$ and $C$ are Debye-Hückel parameters for a given electrolyte, $A$ and $B$ are constants for a particular solvent.

The potential difference measured between two electrodes separated by a semi-permeable membrane, across which a potential difference exists, is a sum of the potential across the membrane and two diffusion potentials at the electrodes (Ammann, 1986). These potential differences are inseparable. Hence in order to compare the experimental values of the diffusion potentials with those predicted by theory, the theoretical values were corrected by also considering the two additional potentials on the electrodes.

## 2.12 Experimental error

Most of the results are expressed as mean values ± standard deviation (SD). The standard deviation was always calculated from replicate values, with one exception. In the case of the molecular charge of the RTFs derived from the measured values of the charge for F-actin and Tm-tn, the error was calculated using the propagation of error formula:

$$\Delta y = \sqrt{(\frac{\partial f}{\partial x_1})^2(\Delta x_1)^2 + \cdots + (\frac{\partial f}{\partial x_n})^2(\Delta x_n)^2} \tag{2.4}$$

where $\Delta y$ is the error of the quantity $y$ derived as $y = f(x_1, \cdots, x_n)$, $f$ is a function of $n$ quantities $x_i$ with standard deviations $\Delta x_i$, where $i = 1, \cdots, n$.

## 2.13 Statistical analysis

It was assumed that the variables had normal distributions. Population variances were compared using two-sided Fisher test. The significance of difference between two means was tested using two-sided Student t-test for means with equal or unequal variances, depending on the result of the Fisher test. The values of the slope of linear regression curves were also compared using Student t-test.

# Chapter 3

# Effect of methylation on the charge of heavy meromyosin

## 3.1 Introduction

The structure of subfragment-1 of chicken myosin was solved by Rayment *et al.* (1993), using crystals of reductively methylated protein. In the process of reductive methylation, 97% of the lysine residues were converted to $N^{\epsilon}$-dimethyllysine.

This modification affects the kinetic properties of the S1 ATPase. The steady state rate of MgATP hydrolysis is increased 4- to 5-fold in the absence of actin whereas the maximum steady state rate in the presence of saturating actin, is decreased 10-fold, as has been reported for the S1 from chicken (White and Rayment, 1993) and for the S1 and heavy meromyosin (HMM) from rabbit (Phan *et al.*, 1994). The $Ca^{2+}$-ATPase activity is almost 4 times higher for methylated rabbit S1 and the $K^{+}$(EDTA)-ATPase is lowered to only 8% of the value for the native protein (Phan *et al.*, 1994).

*In vitro* motility assays of rabbit HMM reveal that the methylated protein suffers complete loss of ability to move actin filaments (Phan *et al.*, 1994). Since the MgATPase activity and actin activated activity of methylated rabbit HMM and S1 are changed in the same way in relation to the activities of the native proteins (Phan *et al.*, 1994), it is highly likely that the methylated S1 also would be unable to support actin movement.

It is interesting to note that the methylated S1 can be crystallized whereas it has not been possible to crystallize the native S1 so far. An important question arises as to whether the structure of the methylated S1 is a valid model for the structure of the native protein. A study of Rypniewski *et al.* (1993) showed that this kind of modification had little effect on the structure of hen egg-white lysozyme. The methylated lysozyme, however, retains almost full catalytic activity (Fretheim *et al.*, 1979).

The $pK_a$ values for lysine and $N^{\epsilon}$-dimethyllysine have been measured by proton magnetic resonance spectroscopy by Bradbury and Brown (1973) as 10.9 and 10.3 respectively. The same method applied to methylated hen egg-white lysozyme, resulted in distinct resonances for the six $N^{\epsilon}$-dimethyllysine residues with $pK_a$ values ranging from 9.6 to 10.2 (Bradbury and Brown, 1973). $^{13}C$ NMR studies of bovine ribonuclease A resulted in $pK_a$ values for $N^{\epsilon}$-dimethyllysine residues ranging from 9.0 to 10.2 (Jentoft *et al.*, 1979) and similar studies of bovine $\alpha$-lactalbumin gave a range of $pK_a$ values from 9.1 to 10.8 (Gerken, 1984). These findings indicate that $N^{\epsilon}$-dimethyllysine residues can have $pK_a$ values shifted down by as much as 2 units depending on the local environment. Such a $pK_a$ shift would be expected to increase the net negative charge of the protein molecule at pH values around these $pK_a$s, since it would reduce the positive contribution of the lysine residues that had been modified.

An investigation was performed as to the effect of reductive methylation on the charge of a protein. An initial consideration involved using chicken myosin S1. However, Rayment *et al.* (1993), reported problems with obtaining chicken S1 without proteolytic cleavages in the essential and regulatory light chains due to the lack of specificity of papain. An improved isolation protocol, which was applied to prepare the crystals used for solving the structure, was not published at the time. Since the methylation was shown to have a similar effect on the MgATPase and the actin-activated ATPase of chicken and rabbit S1 as well as rabbit HMM, those two proteins were candidates for our experiments. An attempt was made to isolate rabbit S1, using both papain

and $\alpha$-chymotrypsin, as described in section 2.3.3, but in all cases a proteolytic degradation of the heavy chain (to a fragment of MW approximately 70 kDa) was detected by SDS-PAGE. A decision was made to purchase rabbit HMM from Sigma. The purity of the protein was checked by SDS-PAGE and it was unacceptable (see section 2.3). Rabbit HMM was therefore isolated, following the procedure described in section 2.3.1. The protein obtained was of high purity.

The experiments described in this chapter were performed on isolated rabbit HMM, part of which was methylated, the methylation procedure was carried out in two batches. The extent of methylation was confirmed by amino acid analysis of HMM and methylated HMM (m-HMM). The $Ca^{2+}$ and $K^{+}$(EDTA)-ATPase activities were determined and measurements of the net electric charge of HMM and m-HMM were performed. Analysis of the S1 and HMM sequence and of the S1 structure was made.

## 3.2 Results

### 3.2.1 SDS-PAGE electrophoresis

The purity of isolated proteins was checked by SDS-PAGE using the system described in section 2.4.1 at a number of gel concentrations (7.5%, 10%, 12.5% and 15%). At concentrations lower than 15%, some or all of the light chains migrated with the buffer front. A photograph of a 15% gel is presented in figure 3.1. One can notice that the HMM light chains have travelled significantly longer distances than the corresponding chains of the methylated protein. This is consistent with the mass increase due to methylation and gives confidence that the methylation procedure has been successful.

The molecular weights determined from the gels are given in table 3.1 together with the molecular weights calculated from the sequence for comparison. The molecular weights of the light chains were calculated from 15% gels and of the heavy chains from 7.5% and 10% gels.

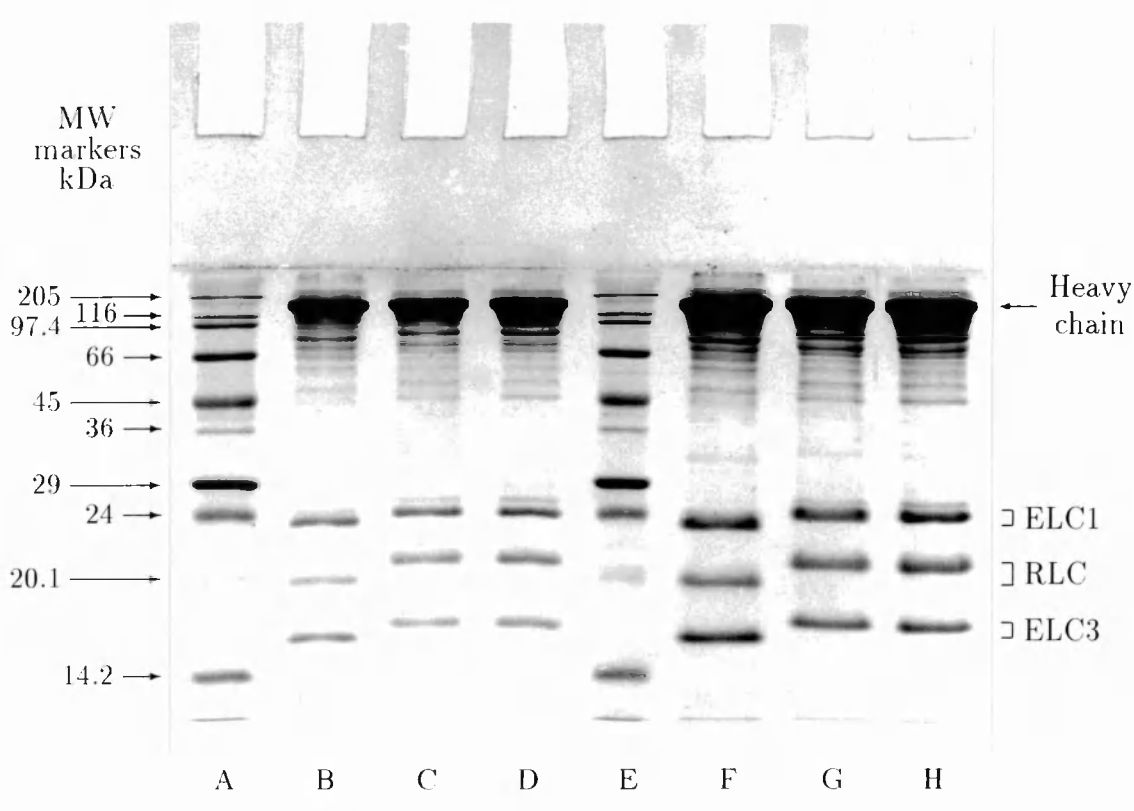


Figure 3.1: 15% SDS-PAGE of rabbit HMM and m-HMM (two batches). Lanes: A and E. MW markers, B and F. HMM, C and G. m-HMM (1st batch), D and H. m-HMM (2nd batch). The molecular weights of the markers are shown on the left and fragments of the HMM and m-HMM are indicated on the right. The quantities of protein applied were: 3 $\mu$g for lanes B, C and D and 6 $\mu$g for lanes F, G and H.

Table 3.1: Molecular weights of the subfragments of HMM and m-HMM determined from SDS-PAGE gels and calculated from the sequence in kDa. The values obtained from the gels are mean values ± SD, with the number n of gel lanes used indicated in each case. ELC1 and ELC3 denote the two essential light chain isoforms, RLC denotes the regulatory light chain.

| Fragment | HMM | | m-HMM | |
|---|---|---|---|---|
| | SDS-PAGE | Calculated | SDS-PAGE | Calculated |
| Heavy chain | 144.2±3.5 n=7 | 140.9 | 150.8±5.0 n=8 | 144.7 |
| ELC1 | 24.5±0.3 n=8 | 20.8 | 25.4±0.3 n=16 | 21.4 |
| RLC | 19.7±0.3 n=8 | 18.9 | 21.3±0.4 n=16 | 19.3 |
| ELC3 | 15.9±0.2 n=8 | 16.5 | 16.9±0.3 n=16 | 16.8 |

The relationship between the $\log_{10}$MW and the distance migrated by a protein from the beginning of the resolving gel ($D_m$), was found to be linear for molecular weights up to 36 kDa for the 15% gels. Hence the molecular weights of the light chains were determined using a linear regression for the relationship of $\log_{10}$MW versus $D_m$ for markers with weights up to 36 kDa.

The molecular weight of the heavy chain of HMM and m-HMM could not be determined in the same way since, even in the 7.5% gel, the $\log_{10}$MW versus $D_m$ relationship was linear only for molecular weights up to 116 kDa. There was not a large deviation from linearity, if only the three heaviest markers were considered for the 7.5% and 10% gels. Hence we calculated the molecular weight of the heavy chain of HMM and m-HMM using linear regression for the $\log_{10}$MW versus $D_m$ relationship for the markers with MW 205, 116 and 97.4 kDa.

There is good agreement between the values determined from our gels and the true molecular weights as calculated from the sequence, with one exception: the molecular weights that we determined from the gels for the ELC1 chains (essential light chains, isoform 1) in case of both proteins, are higher than the calculated values. The same discrepancy however has been noted in literature: Wagner (1982) gives the value of

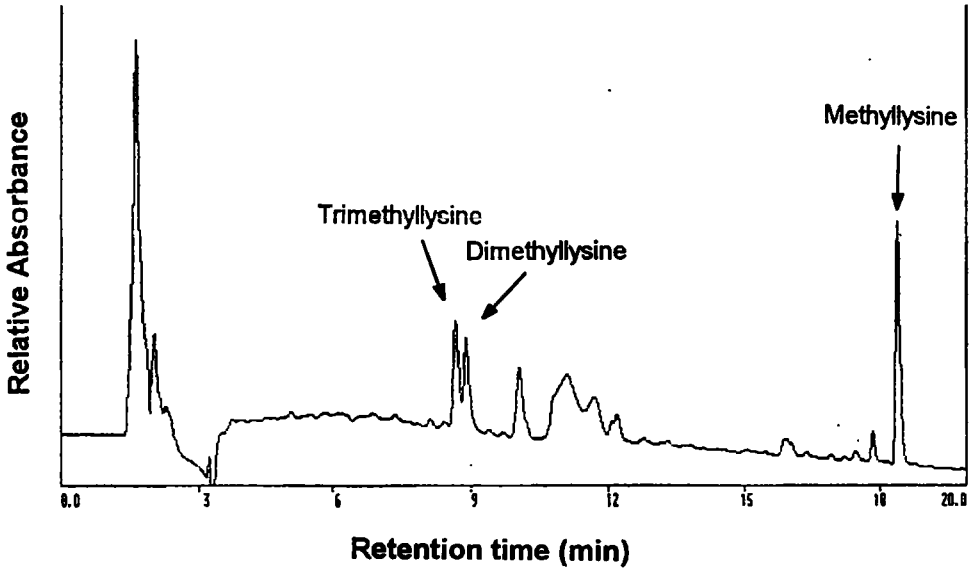


Figure 3.2: The HPLC chromatogram of methylated derivatives of lysine used as standards: $N^{\epsilon}$-methyllysine, $N^{\epsilon}$-dimethyllysine and $N^{\epsilon}$-trimethyllysine.

25 kDa as the molecular weight observed on SDS-PAGE gels for rabbit ELC1, and this is close to the value obtained from my experimental data.

It seems, therefore, that this single exception does not indicate any imprecision in the preparative methods, used in this thesis. It can be concluded, therefore, that by the criteria of SDS-PAGE, the purity of the isolated HMM and m-HMM was satisfactory. The samples were subsequently analysed for their amino acid content in order to check whether the lysine residues were selectively methylated and converted into $N^{\epsilon}$-dimethyllysine residues.

### 3.2.2 Amino acid analysis

Amino acid analysis was performed as described in section 2.4.3. The chromatogram of $N^{\epsilon}$-methyllysine, $N^{\epsilon}$-dimethyllysine and $N^{\epsilon}$-trimethyllysine, which were used as standards, is shown in figure 3.2.

One batch of HMM and two batches of m-HMM were analysed. Two runs were performed for each sample. The experimentally determined numbers of amino acids were

obtained by normalizing data to the number of valine residues in the sequence. Due to the discrepancies between the computed and experimentally obtained values from the first runs for HMM and the 1st batch of m-HMM, the second runs were carried out on samples which were transferred to 10 mM $Na_2EDTA$, pH 7.0 prior to the amino acid analysis since it was suspected that metal ions were responsible for this discrepancy. Metal ions can interfere in the derivatisation reaction with phenylisothiocyanate (Applied Biosystems Inc., 1989). The results obtained from the second runs were in good agreement with the computed values. $N^{\epsilon}$-methyllysine and $N^{\epsilon}$-trimethyllysine residues were not detected, i.e. they could have been present only in very small numbers. The results of the amino acid analysis for the proteins are presented in table 3.2.

The chromatograms from the second runs for HMM and two batches of m-HMM are presented in figure 3.3. They are very similar except for two regions. A peak corresponding to lysine is present in the chromatogram of HMM and essentially absent in the chromatograms of the m-HMM. A peak corresponding to $N^{\epsilon}$-dimethyllysine is present in the chromatogram of the methylated protein in figure 3.3c. It is not resolved in figure 3.3b where it merges with the threonine peak but a larger peak at this position indicates a presence of $N^{\epsilon}$-dimethyllysine.

It is clear from table 3.2 and figure 3.3 that very little native lysine was present in the methylated protein samples. About 98% of lysine residues were converted into $N^{\epsilon}$-dimethyllysine.

### 3.2.3 ATPase activity

The ATPase activity was measured to check whether the protein preparations were active and to verify the effect of activity reversal observed by Phan *et al.* (1994) for the HMM and m-HMM in the presence of $Ca^{2+}$ and EDTA.

The conditions under which the activities were measured were given in section 2.4.2. The amount of inorganic phosphate produced during hydrolysis of ATP is plotted in

Table 3.2: Number of residues from an amino acid analysis $N_{aa}$ of HMM and m-HMM. Residues whose numbers could not be determined from the analysis are denoted by stars $\star$. Two analysis runs were carried out for each protein. Also the amino acid composition computed from the sequence, based on a 2:1 ratio of ELC1 to ELC3 (Wagner, 1982), is given.

| Amino acid | $N_{aa}$ (amino acid analysis) | | | | | | $N_{aa}$ (computed) |
|---|---|---|---|---|---|---|---|
| | HMM | | m-HMM | | | | |
| | | | 1st batch | | 2nd batch | | |
| | Run 1 | Run 2[a] | Run 1 | Run 2[a] | Run 1 | Run 2 | |
| Asx | 244 | 310 | 246 | 309 | 340 | 330 | 314 |
| Glx | 370 | 578 | 374 | 639 | 565 | 586 | 530 |
| Ser | 128 | 139 | 133 | 149 | 147 | 140 | 147 |
| Gly | 188 | 160 | 191 | 174 | 179 | 170 | 172 |
| His | 50 | 49 | 54 | 51 | 53 | 54 | 50 |
| Arg | 139 | 125 | 139 | 129 | 135 | 129 | 122 |
| Dimethyl-Lys | 0 | 0 | $\star$[b] | $\star$[b] | $\star$[b] | $\star$[b] | 0 |
| Thr | 123 | 150 | $\star$[c] | $\star$[c] | 147 | 150 | 173 |
| Ala | 295 | 263 | 294 | 268 | 277 | 285 | 286 |
| Pro | 107 | 104 | 108 | 100 | 95 | 96 | 90 |
| Tyr | 84 | 79 | 85 | 79 | 79 | 81 | 78 |
| Val | 157 | 157 | 157 | 157 | 157 | 157 | 157 |
| Met | 122 | 90 | 120 | 87 | 94 | 99 | 102 |
| Cys[d] | 18 | 0 | 8 | 0 | 5 | 6 | 26 |
| Ile | 141 | 149 | 145 | 148 | 148 | 153 | 158 |
| Leu | 269 | 283 | 262 | 284 | 278 | 262 | 275 |
| Phe | 132 | 142 | 130 | 145 | 138 | 140 | 136 |
| Lys | 125 | 341 | 6 | 7 | 6 | 6 | 330 |
| Trp[e] | $\star$ | $\star$ | $\star$ | $\star$ | $\star$ | $\star$ | 12 |

[a]Due to the discrepancies between the computed and obtained experimentally values from the first runs for HMM and 1st batch of m-HMM, the second runs were carried out on samples which were transferred to 10 mM $Na_2EDTA$, pH 7.0 prior to the amino acid analysis in order to eliminate metal ion interference.

[b]It was only possible to calibrate the amino acid analyser in respect to the retention time for the standards of mono-, di- and tri-methyllysine. It was not possible to quantitate the peak intensities for these standards, except when they were not detected.

[c]It was impossible to determine the number of these residues due to the closeness of threonine and $N^{\epsilon}$-dimethyllysine peaks.

[d]Cysteine was partially destroyed by hydrolysis.

[e]Tryptophan was destroyed by hydrolysis.

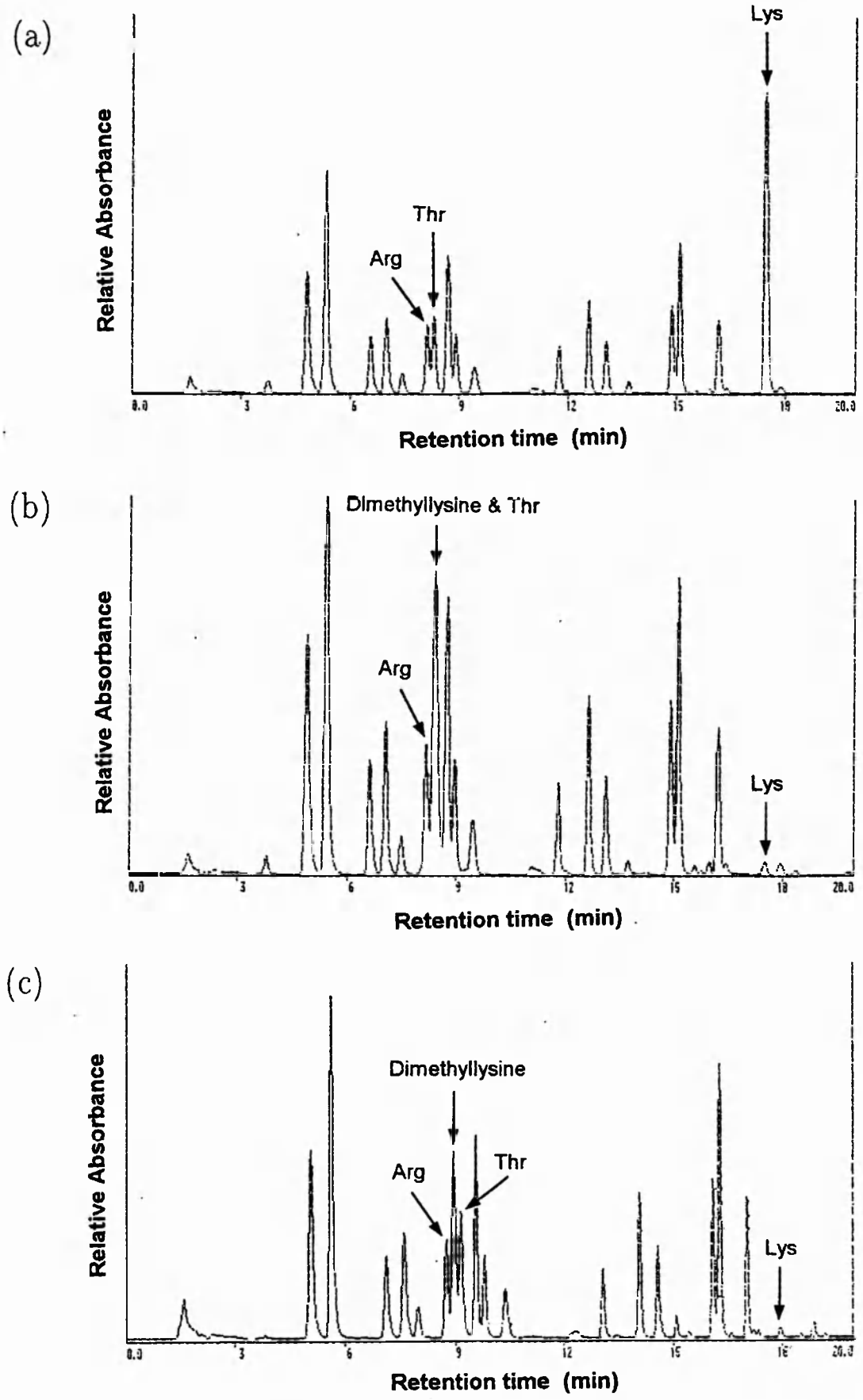


Figure 3.3: The HPLC chromatograms from the second runs of (a) HMM, (b) m-HMM (1st batch) and (c) m-HMM (2nd batch).

Table 3.3: ATPase activity of HMM and m-HMM in $s^{-1}$ in the presence of $Ca^{2+}$ and EDTA.

| Protein | $Ca^{2+}$ | EDTA |
|---|---|---|
| HMM | 3.7±0.5 | 13.0±0.7 |
| m-IIMM | 16.6±0.9 | 3.0±0.2 |

figure 3.4 with data pooled for four samples of HMM and also for four samples of m-HMM. Linear regression was used to fit the data to a line (with intercept not being forced to be zero). The slopes determined are the values of ATPase activity and are given in table 3.3. The intercepts were found to be close to zero.

The activity values obtained for the native HMM agree with the values given by Margossian and Lowey (1982): 4.6 $s^{-1}$ in the presence of $Ca^{2+}$ and 20.6 $s^{-1}$ in the presence of EDTA. These activities are reversed for m-HMM i.e. the $Ca^{2+}$-ATPase activity is elevated and $K^{+}$(EDTA)-ATPase activity is depressed. The difference between the ATPase activities for HMM and m-HMM is significant ($p < 0.001$). Such reversal of activities has been correlated with the modification of the so-called SH1 sulphydryl group within the $Cys^{707}$ residue (Margossian and Lowey, 1982).

### 3.2.4 Donnan potential measurements

The HMM and m-HMM were dialysed against 1 *l* of 10 mM KCl, 1 mM Bistris-acetate buffer, pH 6.7 overnight on ice. This pH was chosen as it is the pH at which methylated S1 was successfully crystallized (Rayment *et al.*, 1993). Bistris buffer was selected as it has $pK_a$ value 6.56 (Smith and Martell, 1989), and this is especially important when working at low buffer concentrations. The Donnan potentials were measured with calomel macroelectrodes K422 using a set-up with two sacks, as was described in section 2.5.1. The recorded values of the Donnan potential, protein concentration, temperature and calculated molecular charge are given in table 3.4. Data which were obtained from one protein sample are grouped together, in the order in which the Donnan potential was measured.

(a)

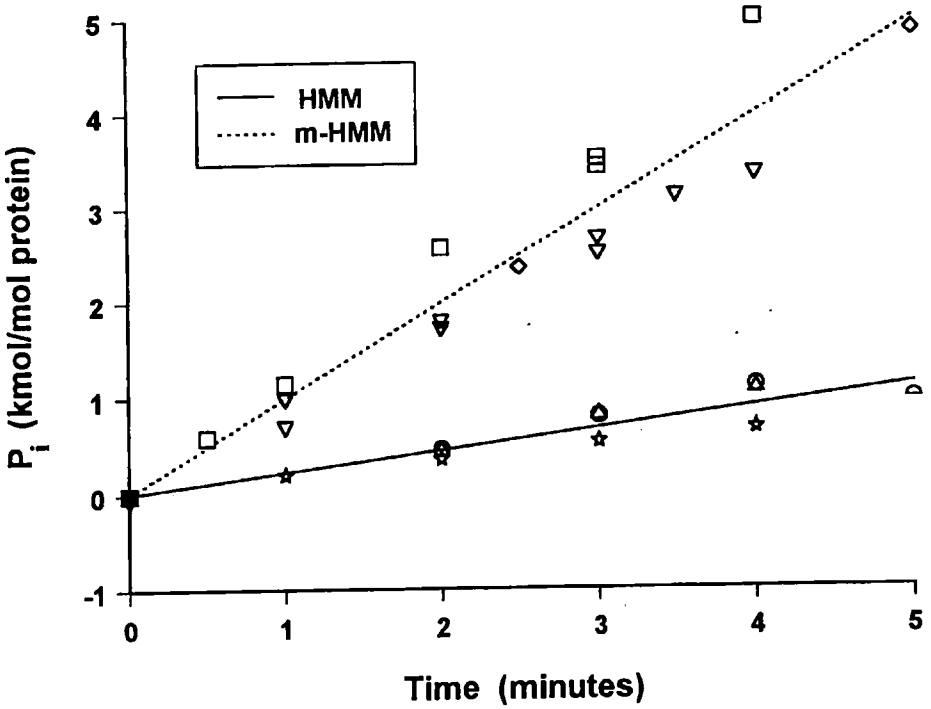


(b)

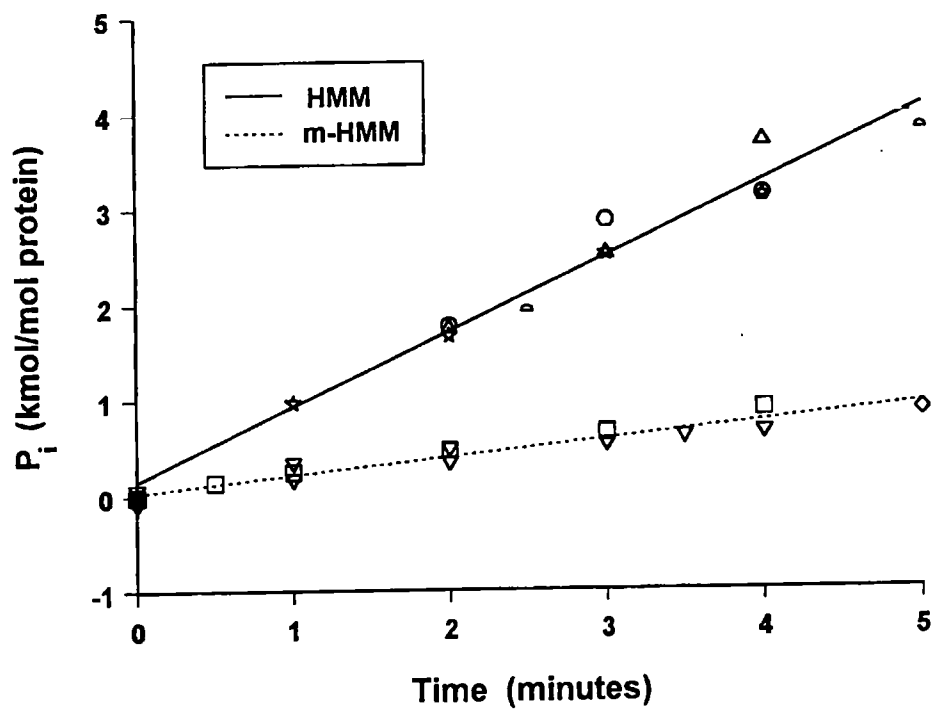


Figure 3.4: Amount of inorganic phosphate $P_i$ in kmols per mol of protein produced by HMM and m-HMM during hydrolysis of ATP in the presence of (a) $Ca^{2+}$ and (b) EDTA. Data points are single observations, different symbols mark different samples.

Table 3.4: Donnan potential $U_D$ values in mV, protein concentration $c_p$ in mg/ml, temperature $T$ in °C and calculated values of the molecular charge $q_{mol}$ in electronic charge units for HMM and m-HMM.

| Protein | $U_D$ (mV) | $c_p$ (mg/ml) | $T$ (°C) | $q_{mol}$ |
|---|---|---|---|---|
| HMM | -0.92 | 6.1 | 19.8 | -44.4 |
| | -1.10 | 6.2 | 20.3 | -52.5 |
| | -0.98 | 7.5 | 19.2 | -38.7 |
| | -0.93 | 7.0 | 19.3 | -39.3 |
| | -1.20 | 7.6 | 19.6 | -46.6 |
| | -1.26 | 7.2 | 20.0 | -51.8 |
| | -0.74 | 7.9 | 20.0 | -27.6 |
| | -1.35 | 7.7 | 20.0 | -52.1 |
| | -1.14 | 8.1 | 19.5 | -41.9 |
| | -1.40 | 8.0 | 19.5 | -52.1 |
| m-HMM | -0.56 | 5.3 | 17.8 | -31.7 |
| | -1.28 | 5.2 | 18.5 | -73.5 |
| | -1.20 | 7.2 | 19.9 | -49.3 |
| | -1.24 | 6.7 | 19.9 | -54.8 |
| | -0.84 | 7.3 | 17.2 | -34.3 |
| | -1.24 | 7.1 | 17.2 | -52.0 |
| | -1.12 | 7.5 | 19.7 | -44.0 |
| | -1.32 | 7.5 | 19.7 | -52.0 |
| | -1.22 | 7.7 | 20.6 | -46.4 |
| | -1.72 | 7.6 | 20.3 | -67.0 |

Table 3.5: The molecular charge of HMM and m-HMM obtained from Donnan potential measurements ± SD in electronic charge units. The number of measurements was n.

| Dataset | n | HMM | m-HMM |
|---|---|---|---|
| All measurements | 10 | -44.7±8.1 | -50.5±12.9 |
| 1st measurements | 5 | -39.8±7.5 | -41.1± 7.7 |
| 2nd measurements | 5 | -49.5±5.7 | -59.9± 9.8 |

The mean values of the molecular charge ± SD for HMM and m-HMM are presented in table 3.5. The statistical comparison of the means, calculated from all the 10 measurements for each type of protein, gives a p value of 0.2, indicating no significant difference. It was noticed during the experiments that the second value of the Donnan potential was usually more negative than the first (in 9 out of the 10 experiments). This could not have been caused by a change in the protein concentration of the sample, as the sample could only get diluted by transferring the electrode between the buffer and the protein solution. After measuring the protein concentration of the samples and calculating the molecular charge, the same tendency in the values of the charge emerged, i.e. the second value of the charge was always more negative than the first. The mean values of the molecular charge determined in the first and second measurements are also given in table 3.5. On comparison of the values of the molecular charge for HMM and m-HMM from the first measurements, the t-test revealed p value of 0.8, whereas the p value for the comparison of the results from the second measurements was 0.08. A highly significant difference, however, was found between the mean values from the first and second measurements for each protein (p values equal 0.05 and 0.01 for HMM and m-HMM respectively). This indicated clearly either a systematic error arising from the experimental procedure or changes occurring in the system over time. A possible explanation emerged from the studies described in chapter 4. The differences between the values obtained from the first and second measurement on a sample were determined to result from the KCl leakage out of the electrodes. The full explanation is given in section 4.1.5.

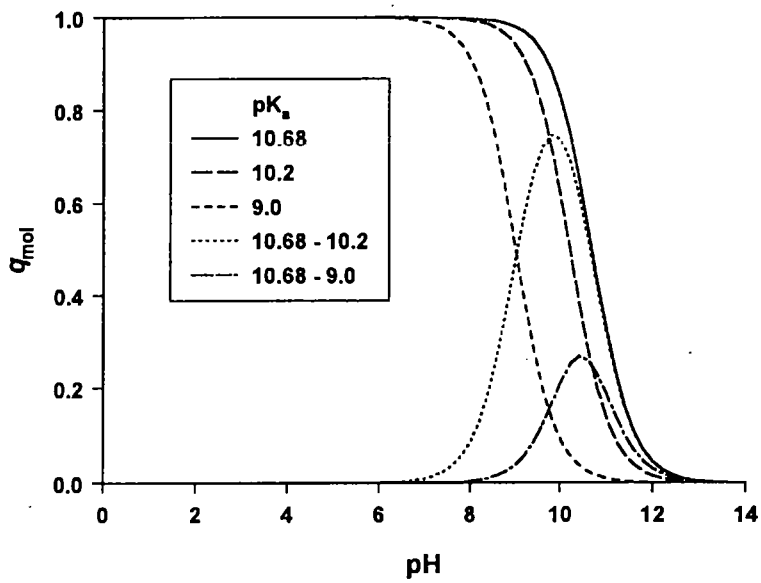


Figure 3.5: The calculated molecular charge $q_{mol}$ of lysine ($pK_a$ 10.68) and $N^{\epsilon}$-dimethyllysine ($pK_a$ 10.2 and 9.0) in electronic charge units. Also the difference between the charge for $pK_a$ 10.68 and the charge for the $pK_a$ values 10.2 and 9.0 is plotted.

### 3.2.5 Theoretical charge of lysine

The charge of lysine and $N^{\epsilon}$-dimethyllysine was calculated as a function of pH using equation 1.1. The $pK_a$ value for lysine was taken as 10.68 (Smith and Martell, 1989). Two values were taken for $N^{\epsilon}$-dimethyllysine : 10.2 and 9.0 as values giving a possible range based on the data for ribonuclease A (Jentoft *et al.*, 1979), lysozyme (Bradbury and Brown, 1973) and bovine $\alpha$-lactalbumin (Gerken, 1984). The charge of lysine and $N^{\epsilon}$-dimethyllysine is plotted as a function of pH in figure 3.5. The difference between the charge of lysine with $pK_a$ 10.68 and a residue with a $pK_a$ in the range 8–10.68 at pH 6.7 is plotted in figure 3.6.

The charge on lysine with $pK_a$ 10.68 is +1e for pH up to approximately 9, at higher pH it decreases to zero, with the value of +0.5e for pH 10.68. The $N^{\epsilon}$-dimethyllysine would have a lower positive charge than lysine at pH values approximately 8–12 (figure 3.5).

Typical shifts in $pK_a$ observed for lysine upon methylation in other proteins (Bradbury

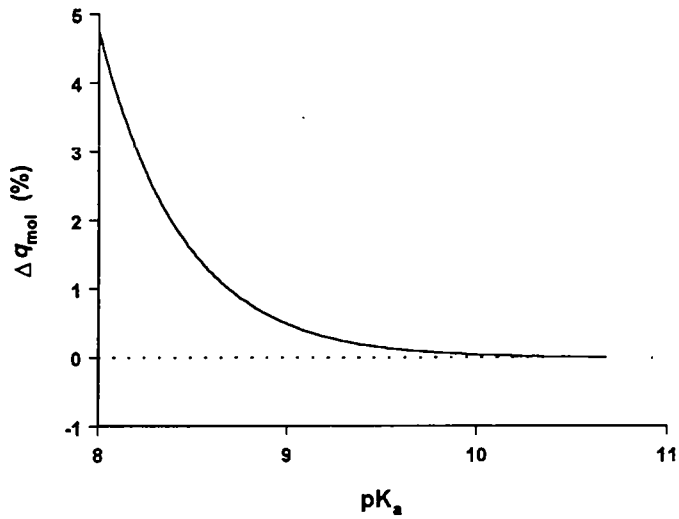


Figure 3.6: The calculated difference $\Delta q_{mol}$ between the molecular charge at pH 6.7 of lysine with $pK_a$ 10.68 and $N^{\epsilon}$-dimethyllysine with $pK_a$ in the range 8–10.68 as a function of $pK_a$ of the $N^{\epsilon}$-dimethyllysine.

and Brown, 1973; Jentoft *et al.*, 1979; Gerken *et al.*, 1982), would cause a very small change in the charge of the residue at pH 6.7 (figure 3.6): a shift to $pK_a$ 10.2 would result in a change of 0.02%. Chicken S1 (with a 1:1 ratio of ELC1 to ELC3 chains) contains 108 lysine residues, so the difference between the charge of methylated and native S1 would be approximately 0.02e at pH 6.7. In the case of a molecule of rabbit HMM this difference in charge would be about 0.07e. It is unlikely that many lysine residues would exhibit larger shifts in their $pK_a$ values on methylation. Even if all the lysine residues in the S1 and HMM molecules had their $pK_a$ values shifted by as much as it was observed for $Lys^{41}$ in an active site of ribonuclease A (Jentoft *et al.*, 1979, $pK_a$ 9.0), their net negative charge at pH 6.7 would be increased by only 0.5e and 1.6e for the S1 and HMM, respectively. In order to change the charge on a lysine residue at this pH by 5% the $pK_a$ would have to be as low as 8.0, values lower than 9.0, however, have not been observed in proteins. The calculations suggest that the charge on the methylated S1 and HMM is more negative than the charge of the native protein only by a fraction of an electronic charge at pH 6.7.

Table 3.6: Relative amounts of lysine residues in various fragments of the HMM molecule from rabbit and chicken expressed as molar percentages. The 23 kDa fragment of the heavy chain of S1 contains residues 1-204, the 50 kDa fragment contains residues 205-646. The 20 kDa fragment contains residues 647-809 of the rabbit protein and 647-843 of the protein from chicken. The relative amount of lysine residues in the S1 and HMM has been calculated for a protein with a 1:1 ratio of ELC1 to ELC3 in chicken and a 2:1 ratio of ELC1 to ELC3 chains in rabbit (Wagner, 1982).

| Protein type | ELC1 | ELC3 | RLC | S1 heavy chain | | | Whole S1 | S2 | HMM |
|---|---|---|---|---|---|---|---|---|---|
| | | | | 23 kDa | 50 kDa | 20 kDa | | | |
| Rabbit | 10.5 | 7.4 | 9.5 | 8.8 | 10.0 | 8.6 | 9.4 | 13.8 | 10.6 |
| Chicken | 10.5 | 7.4 | 9.6 | 8.8 | 9.7 | 7.6 | 9.1 | 14.2 | 10.5 |

### 3.2.6 Sequence analysis

The relative amount of lysine residues in various subfragments of rabbit and chicken HMM was calculated from their sequences in order to see how uniformly these residues were distributed in the molecules (table 3.6). There is not much difference between the relative amounts of lysine in the corresponding subfragments of the protein from rabbit and chicken (not more than 1%). The percentages are between 7.4% and 10.5% for the S1 fragments, with a slightly higher value, around 14%, for the S2 fragment. As far as can be seen from the sequence, the distribution is fairly uniform. In order to investigate this issue further, we visualized the structure of the chicken S1.

### 3.2.7 Structure analysis

Figure 3.7 contains the chicken S1 structure drawn using the crystal structure data of Rayment *et al.* (1993) in ribbon representation with highlighted lysine residues and the SH1 group. The structure contains 1072 residues out of the total of 1158. It can be seen that the distribution of lysine residues is fairly uniform and that there is one lysine residue, $Lys^{709}$, very close to the SH1 group of $Cys^{707}$.

A striking feature is the presence of a number of places of potential flexibility, one of them being at the beginning of the long $\alpha$-helix in the tail domain. It is in this

ORIGINAL IN COLOUR

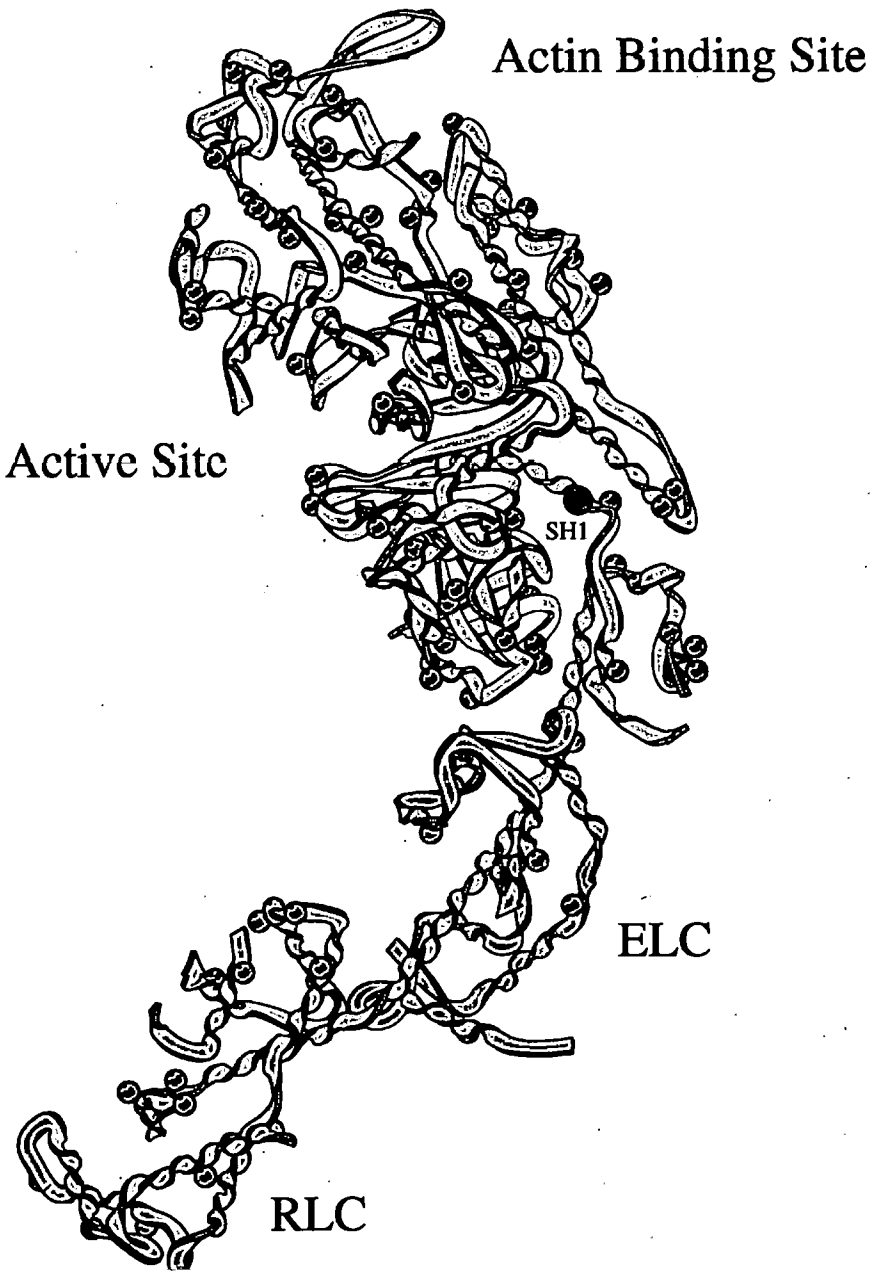


Figure 3.7: Molecular diagram of the structure of subfragment-1 of myosin from chicken. The heavy chain is drawn in grey, the essential light chain (ELC) in green and regulatory light chain (RLC) in yellow. The $\alpha$-carbon atoms in lysine residues are indicated in red. The violet sphere represents the $\alpha$-carbon atom of $Cys^{707}$ where the sulphydryl group SH1 is located. Also the actin binding site and the active site are indicated. Created using MOLSCRIPT (Kraulis, 1991) with the S1 structure of Rayment *et al.* (1993). The coordinates were taken from the 2MYS file in the Brookhaven PDB (Bernstein *et al.*, 1977; Abola *et al.*, 1987).

region that the *Dictyostelium discoideum* myosin has been cleaved and subsequently crystallized without reductive methylation of the lysine residues (Fisher *et al.*, 1995; Smith and Rayment, 1995, 1996). It is thus possible that the flexibility, leading to multiple conformations in solution, stops the nontruncated S1 from crystallizing and that the methylation stabilizes one of the conformations of the flexible molecule.

The distribution of all the positive and negative charges in the chicken S1 was also analysed in order to see how the electrostatic bonds within the molecule could be affected by the methylation. Figure 3.8 contains the structure of the chicken S1 of Rayment *et al.* (1993), where the negatively charged residues (Asp and Glu), lysine and other positively charged residues (Arg), are all highlighted.

Although the charge calculations suggest no differences between the charge on lysine and $N^{\epsilon}$-dimethyllysine at pH 6.7, the electrostatic bonds could be weakened within the methylated molecule. This may result from the additional methyl groups increasing the distance between the $N^{\epsilon}$-dimethyllysine and negatively charged groups. This could affect the overall structure since several lysine residues can be seen to be close to negatively charged residues in neighbouring domains (figure 3.8). The weakening of these interactions would have a destabilizing effect on the structure of the methylated protein and hinder its crystallization.

Phan *et al.* (1994) have reported a faster rate of dissociation of $\epsilon$-ADP from the methylated S1 than from the native protein. This, together with their observation of increased reactivity of the SH1 group towards thiol reagents, led them to the conclusion that the vicinity of the SH1 group becomes more open in the methylated S1. The lysine residue nearest to the SH1 group ($Lys^{709}$), is in close contact with negatively charged $Glu^{499}$, $Glu^{501}$ and $Glu^{502}$ on the loop seen to the right of $Lys^{709}$ in figure 3.8. The changes in the vicinity of the SH1 group, that were associated with a more open conformation of this region by Phan *et al.* (1994), could be caused by a weakening of the attraction between the $Lys^{709}$ and those three residues.

ORIGINAL IN COLOUR

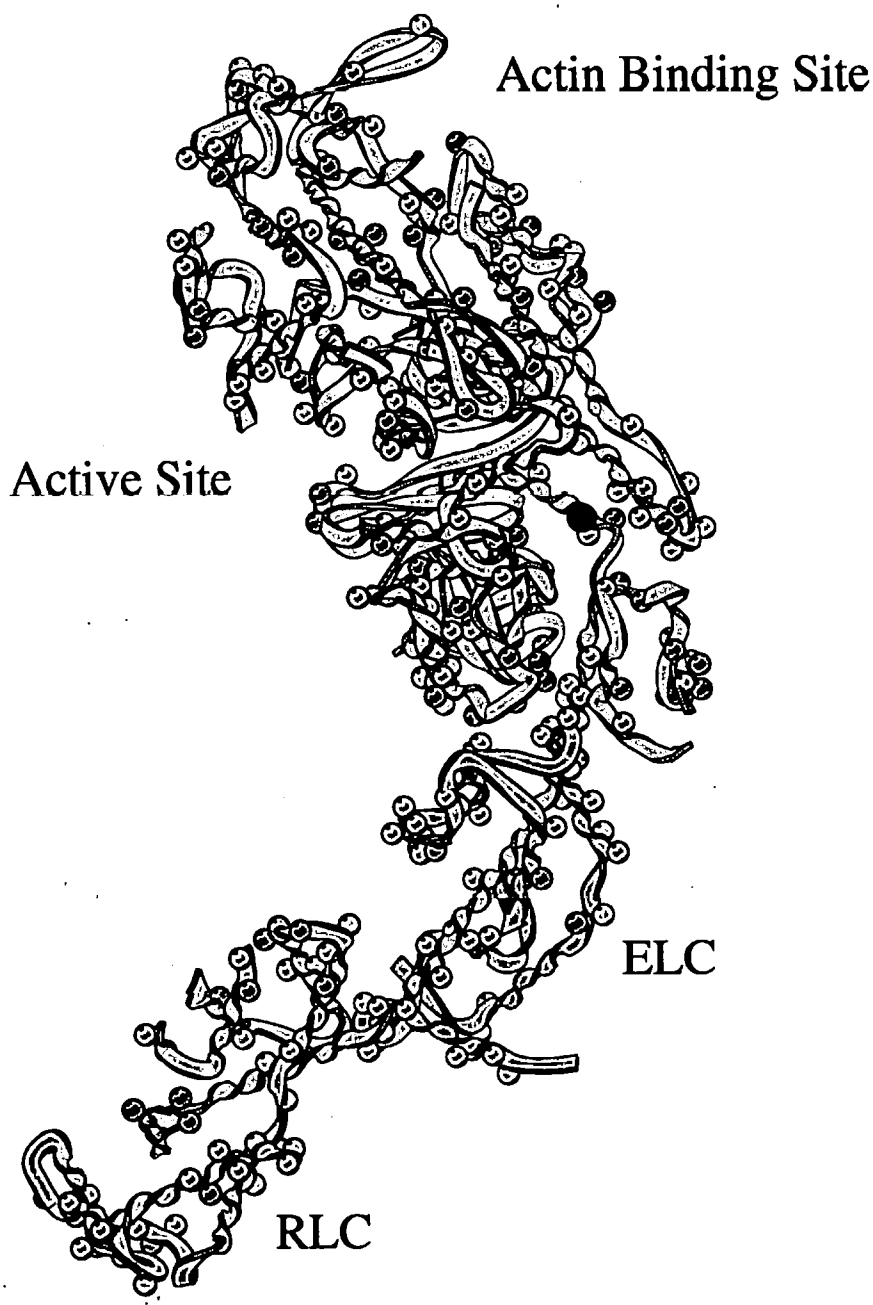


Figure 3.8: Molecular diagram of the structure of subfragment-1 of myosin from chicken. The heavy chain is drawn in grey, the essential light chain (ELC) in green and regulatory light chain (RLC) in yellow. The $\alpha$-carbon atoms in positively charged at pH 7.0 residues are indicated in red (Lys) and orange (Arg) whereas those in negatively charged residues (Glu and Asp) are shown in blue. The violet sphere represents the $\alpha$-carbon atom of $Cys^{707}$ where the sulphydryl group SH1 is located. Also the actin binding site and the active site are indicated. Created using MOLSCRIPT (Kraulis, 1991) with the S1 structure of Rayment *et al.* (1993). The coordinates were taken from the 2MYS file in the Brookhaven PDB (Bernstein *et al.*, 1977; Abola *et al.*, 1987).

It is possible that the presence of two additional methyl groups on each $N^{\epsilon}$-dimethyl-lysine increases the packing density of the protein. This would make the structure more rigid and could facilitate its crystallization.

## 3.3 Discussion

The reductive methylation of lysine residues must have a dramatic effect on the S1 properties since it is necessary for its crystallization. An important question is whether this modification affects the structure of the molecule. A parallel study on egg-white lysozyme showed that this modification did not have much effect on the structure of the crystallized protein (Rypniewski *et al.*, 1993). The lysozyme, however, has only six lysine residues which constitute 5% of the total number of residues, which is less than in the case of myosin S1 (9% for chicken S1). It could be as a result of the difference in the composition of lysozyme and S1, that the former retains almost full catalytic activity (Fretheim *et al.*, 1979) while the latter does not.

The ATPase activity of HMM is elevated in the presence of $Ca^{2+}$ and lowered in the presence of EDTA. A similar effect was reported by Phan *et al.* (1994) for the methylated S1. This is in agreement with the results of the investigation of kinetic behaviour of HMM and S1 which revealed no difference between the proteins, both native and with SH1 groups modified (Sleep *et al.*, 1981). Such a reversal of activities accompanies modifications in the vicinity of the SH1 group (Margossian and Lowey, 1982). Indeed an increased reactivity of the SH1 groups towards thiol reagents and faster dissociation rate of $\epsilon$-ADP have been observed for S1 upon methylation (Phan *et al.*, 1994).

Our charge measurements did not reveal a statistically significant difference between the net charge of the native and methylated HMM at pH 6.7. The values of the net charge for both proteins could be divided into two groups, depending upon whether they were obtained from the first or second Donnan potential measurement on a

sample. The values obtained from the second measurements were significantly more negative. Subsequent studies, described in chapter 4, identified the source of these differences as the KCl leakage out of the electrodes. The full explanation is given in section 4.1.5. The obtained values of charge, however, have an experimental error of about 20%. Hence, on the basis of the Donnan potential measurements, a smaller than about 20% difference in charge between HMM and m-HMM at this pH, cannot be excluded.

The analysis of the charge of lysine and $N^{\epsilon}$-dimethyllysine, calculated from the $pK_a$ values taken from literature, reveals that the modified amino acid would have lower positive charge at pH values approximately 8 to 12. Even if all the lysine residues had their $pK_a$ values shifted to 9.0, which was observed for $Lys^{41}$ in the active site of ribonuclease A (Jentoft *et al.*, 1979), the net negative charge at pH 6.7 on the S1 and HMM would increase by only 0.5e and 1.6e, respectively. A 5% change in charge of the lysine residue at pH as low as 6.7 would result from a larger shift in $pK_a$ down to 8.0. Such shifts in the value of $pK_a$ have not been observed in proteins for which the effect of methylation on the $pK_a$ of lysine residues was studied (Bradbury and Brown, 1973; Jentoft *et al.*, 1979; Gerken, 1984). The results of these calculations agree thus with the results of the Donnan potential experiments, which were performed at pH 6.7.

The presence of two additional methyl groups on lysine residues may weaken the electrostatic bonds within the molecule by increasing the distance between the lysine and negatively charged groups. This would agree with the suggestion of Phan *et al.* (1994) that the methylated S1 has a more open conformation in the vicinity of the SH1 group. This could result from a weakening of the bond between $Lys^{709}$ and the three glutamic acid residues $Glu^{499}$, $Glu^{501}$ and $Glu^{502}$.

A possible explanation as to why the methylation facilitates the crystallization is that the molecule becomes more rigid as a result of closer packing of lysine residues with two additional methyl groups occupying more space.

The problem in the experimental procedure for the macroelectrode measurements of the Donnan potentials, revealed during the experiments described in this chapter, set out a goal for our work. One of the aims was to identify the sources of the experimental error in the technique and determine whether and how its accuracy could be improved. This is described in the next chapter.

## 3.4 Conclusions

The following overall conclusions can be drawn:

1. The ATPase activity of m-HMM is elevated in the presence of $Ca^{2+}$ and reduced in the presence of EDTA compared to the native HMM. Both the increase and decrease are approximately 4-fold and the differences are highly significant ($p < 0.001$). Such a reversal of activities is indicative of modifications in the close vicinity of the SH1 group.

2. On the basis of the calculations of the charge of lysine and $N^{\epsilon}$-dimethyllysine from the $pK_a$ values from literature, one can predict an increased negative charge on the methylated S1 and HMM at pH approximately 8–12. The predicted difference at pH 6.7 would be not more than 0.5e for methylated S1 and 1.6e for the methylated HMM.

3. Our Donnan potential measurements do not reveal a statistically significant difference between the values of the net electric charge of the HMM and methylated HMM at pH 6.7. The results have a large experimental error of about 20%, hence a smaller than 20% change in charge cannot be excluded on the basis of these experiments.

4. The macroelectrode technique should be refined to give more accurate results.

# Chapter 4

# Electrode techniques for protein solutions

## 4.1 Problems associated with the use of macroelectrodes

As soon as the use of the macroelectrode method of Ojteg *et al.* (1989) was made, several difficulties were encountered leading to puzzling results which were initially difficult to explain. We think it is worth describing them here in detail so that anyone wishing to apply this technique in future can benefit from the experiences gained. This is especially important since it was discovered that, under certain circumstances, one may obtain very reduced values of the electric charge, or indeed a positive charge, for a negatively charged protein.

### 4.1.1 Drifts in potentials

The potentials given in this section are expressed relative to the value of the potential when both electrodes were in the outer solution. Such a reference was chosen in order to demonstrate the potentials arising when an electrode was placed in the sample compartment with 1 ml of the same solution as was outside the compartment. These potentials will be denoted as $U_o$.

The work with macroelectrodes was started by trying to reproduce the experiment

of Ojteg *et al.* (1989) with NaCl diffusion potentials in order to check whether the method was being applied correctly. The experiments were performed as described in section 2.11. Initially calomel electrodes K422 were used to measure the potential when 1 ml of 20 mM NaCl was placed inside the dialysis sack and the outer solution was 1 *l* of 10 mM NaCl. The experiment was repeated 4 times and a value of 1.0±0.1 mV was obtained for the maximum observed potential (at temperature 20±2°C). Ojteg *et al.* (1989) obtained a potential of approximately 3 mV, in good agreement with the value of 3.1 mV that can be calculated from equation 2.2. This discrepancy was further investigated and diffusion potentials for other NaCl gradients were measured. This is shown in figure 4.1 for 20, 50 and 80 mM NaCl applied inside the dialysis sack. The values obtained: 2.7 and 6.5 mV for 50 and 80 mM NaCl respectively, were again much lower than the corresponding values calculated from equation 2.2: 7.1 and 9.1 mV. It was suspected that NaCl was diffusing out of the dialysis sack very quickly and, before the diffusion potential was fully established, a large part of NaCl had already diffused through the membrane to the outer solution. This seemed likely since Ojteg *et al.* (1989) were using dialysis tubing that had not been prepared in the standard way for dialysis but had only been soaked in 10 mM NaCl for 48 hours. However, a potential of only 1.1 mV was obtained for 20 mM NaCl when using such tubing.

It was decided, at this point, to measure the diffusion potentials with different electrodes – two Ag/AgCl electrodes REF200 and two calomel electrodes REF401 were used, but the values obtained with them were very similar to the values obtained with electrodes K422 (figure 4.2). Only when more concentrated solutions of NaCl were used, was it possible to obtain potential values closer to those predicted by theory. For example, when 0.1 M NaCl was the outer solution and 0.2 M NaCl was applied inside the dialysis sack, the diffusion potential recorded was 2.7 mV in good agreement with the value of 2.8 mV calculated from equation 2.2.

As different types of electrodes were used, it was noted that there was an interesting

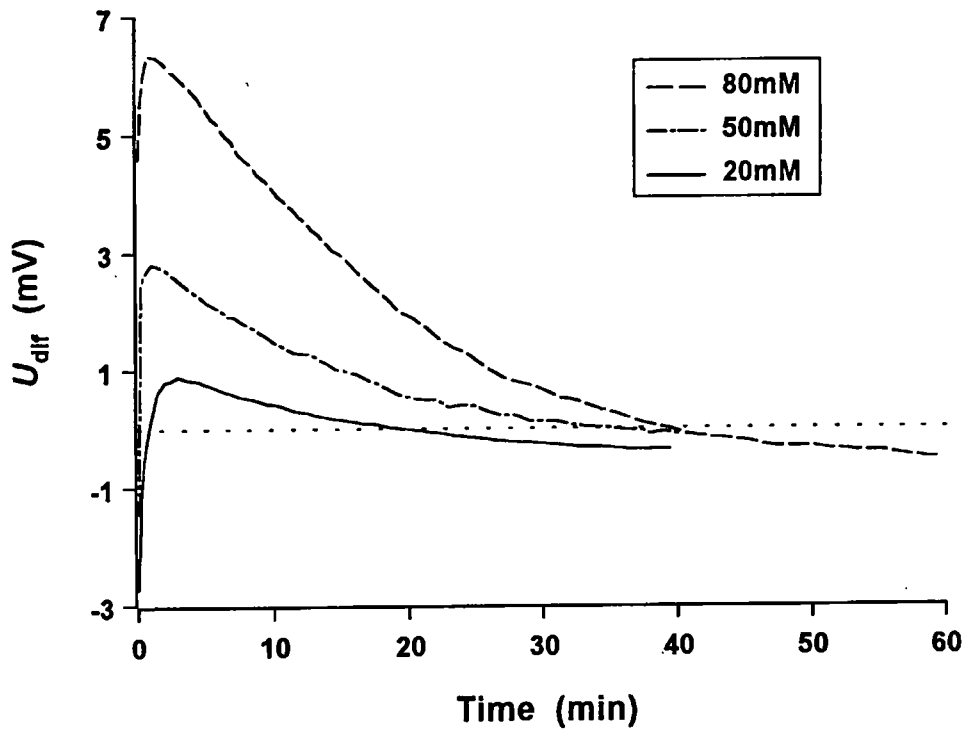


Figure 4.1: Diffusion potentials $U_{dif}$ for 20, 50 and 80 mM NaCl into 10 mM NaCl recorded using macroelectrodes K422 at temperature 20±2°C.

(a)

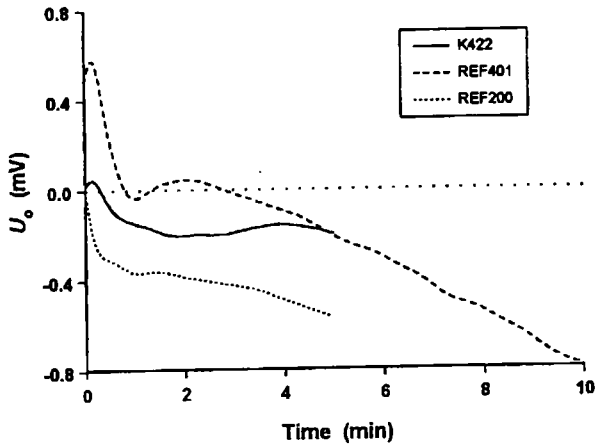


(b)

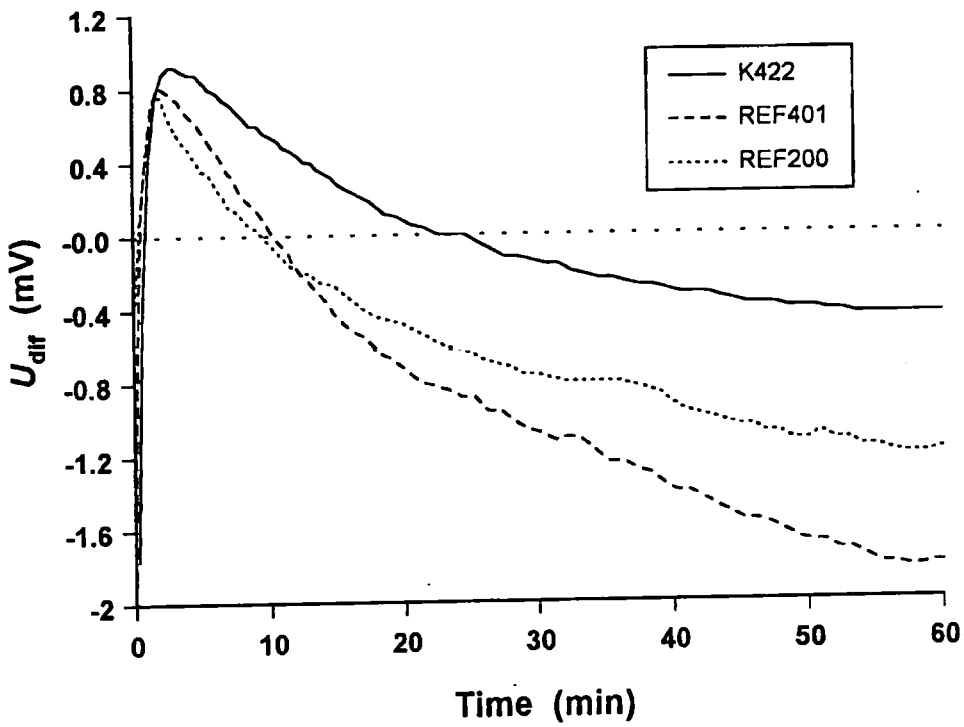


Figure 4.2: Diffusion potentials for 20 mM NaCl into 10 mM NaCl recorded using calomel macroelectrodes K422 and REF401 and Ag/AgCl macroelectrodes REF200 at temperature 20±2°C. Potentials (a) $U_o$ and (b) $U_{dif}$ recorded when the measuring electrode was placed in the dialysis sack containing 1 ml of 10 mM NaCl and 1 ml of 20 mM NaCl, respectively.

difference in their behaviour. When one of the electrodes of the pair was immersed in the dialysis sack containing 1 ml of 10 mM NaCl and the other was outside, there should theoretically have been the same potential difference between them as when they were both outside. This was the case only for electrodes K422, for the other electrodes the potential was drifting towards more negative values (figure 4.2a), the drift being most prominent for electrodes REF401. When the diffusion potential was recorded for 60 minutes, the potential at the end of that time was markedly lower than the starting potential for both electrodes REF200 and REF401 (figure 4.2b).

Drifts were also observed in Donnan potentials when the method was applied to bovine serum albumin (BSA). This is demonstrated in figure 4.3, where potentials recorded for BSA in 10 mM NaCl, 1 mM Bistris-HCl buffer, pH 6.4 are plotted. The potentials are again expressed relative to the potential when both electrodes were in the outer buffer. The original set-up of Ojteg *et al.* (1989) with one sack was used. The sample volume was 1 ml and protein concentration 12 mg/ml. Electrodes REF401 were used. The potentials recorded were changing towards more negative values for a period of about 20 minutes. The potential $U_o$ recorded when the measuring electrode was in the dialysis sack containing 1 ml of buffer, was about -2 mV. The potential measured when the protein was placed in the dialysis sack was initially about -3 mV and changed to about -4 mV after 20 minutes.

It was not possible to explain this phenomenon at that point. Whenever we tried to use electrodes REF200 or REF401 in future, under various conditions, the drifting of potentials occurred when one or both electrodes were placed inside a small compartment. In the case of electrodes K422 there were also drifts in potentials but very much smaller than for the other electrodes. It was suspected that this could have been caused by the difference in the KCl outflow rate through the porous pin, this was given by the manufacturer Radiometer Copenhagen to be 5 $\mu$l/hr for electrodes REF200 and 10 $\mu$l/hr for electrodes REF401, whereas it was not specified for electrodes K422.

It therefore seemed sensible, at the time, to use two dialysis sacks for Donnan potential

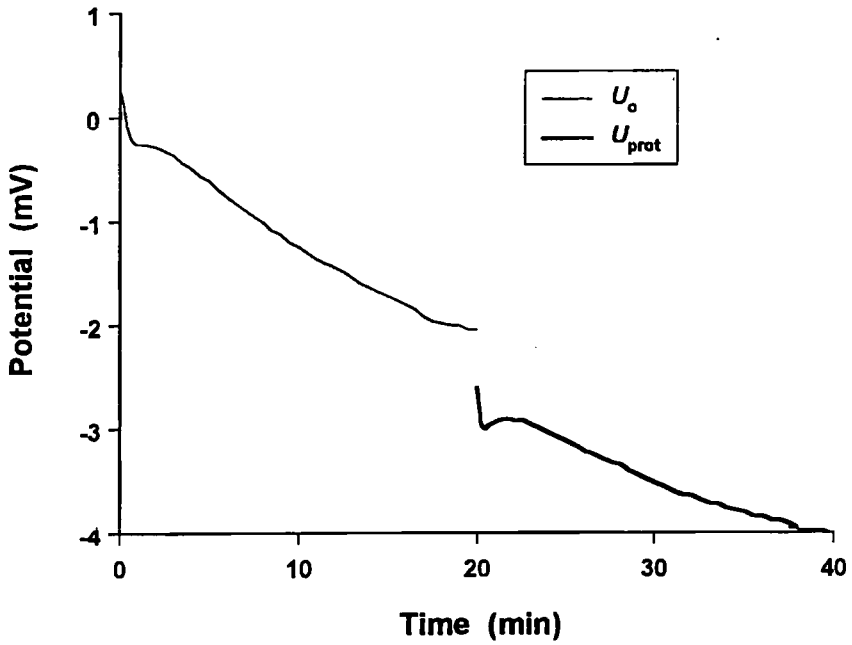


Figure 4.3: Typical example of the potentials recorded during Donnan potential measurements with electrodes REF401. The protein was BSA and the buffer was 10 mM NaCl, 1 mM Bistris-HCl, pH 6.4. $U_o$ and $U_{prot}$ are potentials recorded when the measuring electrode was placed in the sample compartment containing buffer and protein, respectively. Potentials are expressed relative to the potential recorded when both electrodes were in the outer buffer. The set-up with one sack was used, the sample volume was 1 ml and protein concentration was 12 mg/ml.

measurements: one with the reference buffer and the other initially with reference buffer and then with protein solution. It was expected that any drifts that were making the results less accurate would have been cancelled out due to the symmetry of the system. Experiments with heavy meromyosin were then performed, described in the previous chapter, using a set-up with two dialysis sacks. In those experiments the value of the charge obtained from the second Donnan potential measurement on a sample was significantly more negative than the value from the first measurement. Clearly changes affecting the potentials were occurring over time. The reference potential in the 2-sack set-up was measured when both electrodes were placed in the sacks containing buffer. In this particular case the reference potential was only taken prior to a number of measurements and it was assumed to remain fairly constant. To alleviate any variation that may be occurring in the reference potential with time, it was decided that reference potential measurements should be taken prior to each sample measurement. In the experiments described in the next section, the reference potential was therefore measured just prior to each sample measurement.

It also occurred that an important limitation of the method of Ojteg *et al.* (1989) is the fact that it requires relatively large quantities of proteins whose isolation and purification is usually a time consuming process, as indeed they pointed out. The higher the ionic strength of the solution, which usually means the closer to physiological conditions, the more concentrated are the protein samples needed to obtain Donnan potentials measurable with reasonable accuracy. This is why a decision was made to investigate the possibility of using sample volumes smaller than the 1.0 ml that was used by Ojteg *et al.* (1989). This is described in the next section.

### 4.1.2 Requirement of large quantities of protein

The idea of using protein volumes smaller than 1.0 ml seemed viable because the electrodes K422 and REF200 had smaller diameter (4.5 mm) than the electrodes used by Ojteg *et al.* (1989) (7.5 mm). The charge of a selected protein was determined as a

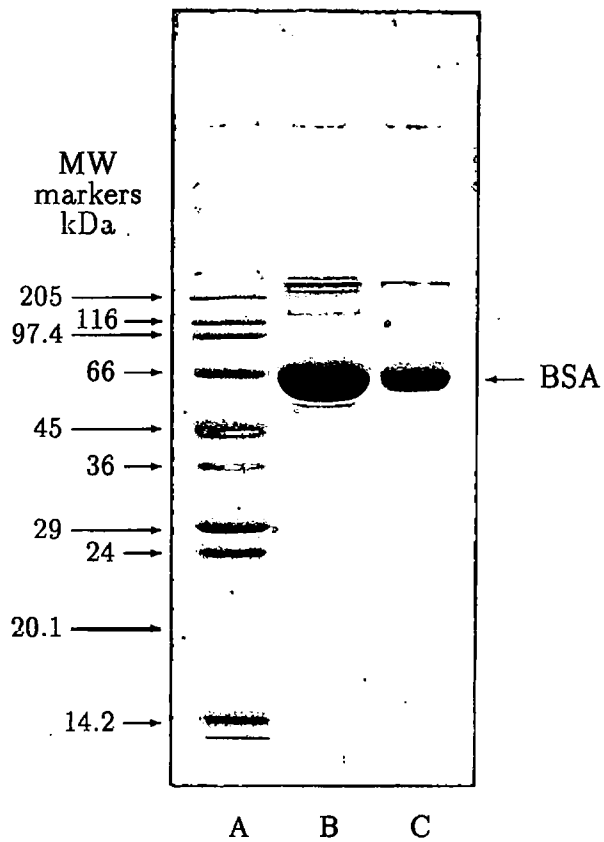


Figure 4.4: 12.5% SDS-PAGE of BSA fraction V (from BDH). The molecular weights of the markers are indicated. Lanes: A. MW markers, B and C. BSA, 7.5 and 1.8 $\mu$g respectively.

function of pH using sample volumes 1.0 and 0.25 ml in order to be able to relate the results to the isoelectric point of the protein obtained using other methods. In this experiment it was desirable to use a protein that could be available in large quantities, for which there are experimental values of the isoelectric point in the literature and whose amino acid sequence has been determined so that calculation of the theoretical net charge could be made. BSA fulfilled the above conditions and was therefore the protein chosen. BSA fraction V was purchased from BDH and its purity was checked by SDS-PAGE (figure 4.4).

The following buffer solutions were used to cover pH range from 3.4 to 8.0:

- 1 mM sodium citrate buffer, 10 mM NaCl (pH 3.4, 4.0, 4.5, 4.9)
- 1 mM Bistris-HCl, 10 mM NaCl (pH 5.6, 6.4, 7.2)

- 1 mM Tris-HCl, 10 mM NaCl (pH 8.0)

The pH range was deliberately not broader since at more extreme pH values denaturation of BSA could take place (Kanal *et al.*, 1994), due to high positive (at low pH) or negative (at high pH) electric charge. Strong repulsive electrostatic interactions lead to protein unfolding and denaturation.

The experiment was carried out as described in section 2.5.1 using the experimental set-up with two dialysis sacks. The protein was dissolved in an appropriate buffer and dialysed against it overnight in the cold room at 8°C. When protein samples of 1 ml volume were used, two 100 $\mu$l aliquots of the protein solution were taken for protein concentration determination after the Donnan potential measurement whereas the rest was returned to the protein solution from which subsequent samples were taken. This was done in a similar way as in the Ojteg *et al.* (1989) method, with the exception of the protein being diluted to a different concentration by Ojteg *et al.* (1989). For each of the buffers, its ionic composition was determined using the PERRIN program (Abbott, 1976) with stability constants given in appendix A. Then the molecular charge was determined using equation 1.6. The values of the molecular charge together with the t-test p values (for a comparison of the values of the charge obtained for the two sample volumes) are given in table 4.1. The molecular charge of BSA is plotted against pH in figure 4.5. Also indicated is the range of experimental values of isoelectric point determined in NaCl based solutions with other methods and available in literature (as listed in table 4.2).

The molecular charge of BSA as a function of pH was calculated from its sequence, in the manner described in section 2.6. A fragment was used, with residues 25–607, of BSA precursor sequence ALBU_BOVIN from the OWL database (Bleasby and Wootton, 1990). The theoretical molecular charge is plotted in figure 4.6 together with the experimental curve for volume 1.0 ml.

Table 4.1: The molecular charge $q_{mol}$ (in electronic charge units) for BSA determined with macroelectrodes K422 in solutions with various pH using sample volumes 1.0 and 0.25 ml. The number of measurements with one volume was 12 for pH 6.4 and pH 8.0 whereas 6 measurements were made for the remaining values of pH. Mean values of the charge are presented ± SD. The last column contains p values of the t-test for comparison of the mean values obtained using the two sample volumes.

| pH | Molecular charge $q_{mol}$ ± SD | | p |
|---|---|---|---|
| | Volume 1 ml | Volume 0.25 ml | |
| 3.4 | 17.9±2.0 | 17.1±2.1 | 0.6 |
| 4.0 | 5.7±1.5 | 5.5±1.2 | 0.8 |
| 4.5 | 0.7±0.7 | 1.1±1.1 | 0.5 |
| 4.9 | -2.6±0.3 | -2.4±0.3 | 0.3 |
| 5.6 | -5.9±0.2 | -6.6±0.4 | 0.005 |
| 6.4 | -8.8±0.3 | -9.3±0.6 | 0.03 |
| 7.2 | -11.3±0.1 | -11.8±0.4 | 0.02 |
| 8.0 | -12.5±0.7 | -11.5±1.2 | 0.02 |

Table 4.2: Experimental values of the isoelectric point pI of BSA from literature.

| pI | Method | Medium | Reference |
|---|---|---|---|
| 4.63 | Moving boundary | 0.01 M NaCl | Bull (1971) |
| 4.59 | Moving boundary | 0.08 M NaCl, 0.02 M sodium acetate | Longsworth and Jacobsen (1949) |
| 4.6 | Osmotic pressure | 0.1 M NaCl buffered with sodium acetate | Kanal *et al.* (1994), Minton (1995)* |

⋆ Data of Kanal *et al.* (1994) in interpretation of Minton (1995).

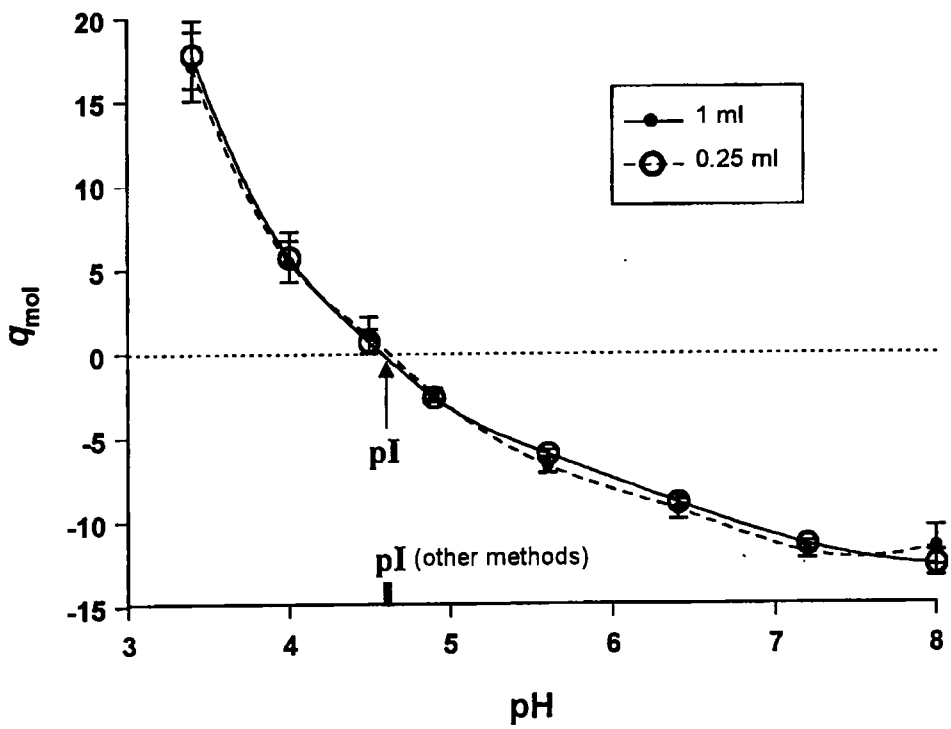


Figure 4.5: The molecular charge of BSA (in electronic charge units) as a function of pH determined using macroelectrodes K422. For all pH values 6 measurements were performed with volume 1.0 ml and 0.25 ml except for pH 6.4 and 8.0 for which measurements were repeated 12 times. The data points are mean values through which smooth curves are drawn, bars represent standard deviations. The isoelectric point that can be determined from our data is indicated with an arrow (pH 4.6) and the range of isoelectric point in NaCl based solutions determined with other methods from literature is shown for comparison (black rectangle).

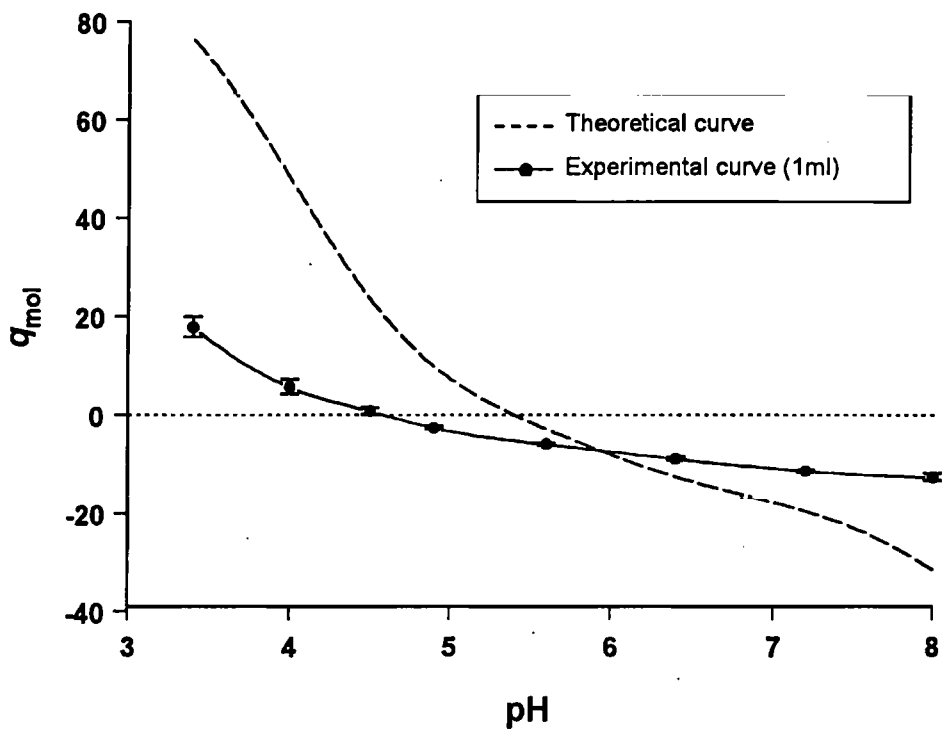


Figure 4.6: The molecular charge of BSA (in electronic charge units) as a function of pH – experimental and theoretical values. For clarity the experimental curve for sample volume 1 ml is only drawn.

Table 4.3: Rates of KCl leakage from macroelectrodes K422, REF200 and REF401 (Radiometer Copenhagen) immersed for 1 hour in 12 ml of 10 mM KCl at 25°C and determined with a conductivity meter. Electrode filling holes were either opened (○) or closed with parafilm (⊗). Two electrodes of each type (denoted a and b) were used.

| Electrode type | Electrode | Filling hole open ○ closed ⊗ | KCl leakage rate ($nmol \cdot s^{-1}$) | | | | |
|---|---|---|---|---|---|---|---|
| | | | Experiment | | | | Mean ± SD |
| | | | 1 | 2 | 3 | 4 | |
| K422 | a | ○ | 1.7 | 1.5 | 1.5 | 1.6 | 1.5±0.1 |
| | | ⊗ | 4.1 | 1.4 | 5.7 | 1.5 | 3.2±2.1 |
| | b | ○ | 1.1 | 1.0 | 1.0 | 1.1 | 1.0±0.1 |
| | | ⊗ | 1.0 | 1.2 | 1.9 | 1.0 | 1.3±0.4 |
| REF200 | a | ○ | 1.8 | 2.1 | 3.8 | 1.7 | 2.3±1.0 |
| | | ⊗ | 1.5 | 1.1 | 3.9 | 1.1 | 1.9±1.4 |
| | b | ○ | 6.7 | 6.6 | 6.8 | 6.0 | 6.5±0.4 |
| | | ⊗ | 8.9 | 6.0 | 7.1 | 5.7 | 6.9±1.5 |
| REF401 | a | ○ | 7.6 | 7.5 | 7.6 | 7.7 | 7.6±0.1 |
| | | ⊗ | 4.9 | 7.0 | 8.6 | 13.6 | 8.5±3.7 |
| | b | ○ | 7.6 | 8.2 | 8.3 | 7.6 | 7.9±0.4 |
| | | ⊗ | 4.1 | 2.9 | 9.6 | 8.3 | 6.2±3.2 |

### 4.1.3 KCl leakage

An investigation of the rates of leakage of KCl from the macroelectrodes was made in order to see whether these could account for the problems with drifts in potentials. The electrodes were left with their ends in 12 ml of 10 mM KCl for 1 hour after which the electrical conductivity of the solution, that the electrode was immersed in, was measured as described in section 2.10. The experiment was repeated 4 times for each electrode. The filling hole was either opened as it was normally during Donnan potential measurements or covered with parafilm. The filling hole was covered in order to see whether the decrease in hydrostatic pressure would reduce the rate of KCl leakage as one could expect. The rates of KCl leakage are presented in table 4.3.

For electrodes with filling holes covered, there was a larger variation in the leakage rates between experiments than for electrodes with filling holes opened. This is reflected in generally higher standard deviations for the leakage rates determined for electrodes with filling holes covered. The covering caused a decrease in the leakage

rate for 2 electrodes and increase for 4; this was not expected. The rate of leakage of an electrode placed in 10 mM KCl with the filling hole opened appears to be a characteristic of each electrode.

Electrodes K422 had the lowest KCl leakage rate, whereas electrodes REF401 had the highest rate. This correlates well with the drifts in potentials observed in the diffusion experiment (figure 4.2) and also in Donnan potential measurements. The approximate leakage rates given by the electrode manufacturer, as 5 and 10 $\mu$l/hr of saturated (4.2 M KCl approximately) for electrodes REF200 and REF401 respectively, correspond to about 6 and 12 nmol$\cdot$s$^{-1}$. These values are in agreement with the experimental data presented.

In view of these results, it could be suggested that, if the KCl leaking out of the electrode was unable to diffuse quickly out of the sample compartment, then the reference potentials could be quite large, i.e. of the same order as the Donnan potentials. This was shown to be the case in the following section where a 1-sack set-up was used.

### 4.1.4 Sample compartment geometry dependence

Sample compartments, for measurements described in this section, were made of plastic cylinders which are normally used for column filtration. The compartments possess a fitting ring at the base which enables housing of a membrane. The diameter at the base of the plastic cylinder was 8 mm, resulting in a membrane area of approximately 0.5 cm$^2$. The dialysis membrane was the same as that used for the sacks for sample volume 1 ml. The tubing was equilibrated in 10 mM NaCl, 1 mM Bistris-HCl, pH 6.4 buffer, and BSA was dialysed against the above solution. Electrodes K422 and REF401 were used for the measurements, electrodes marked 'a' in table 4.3 were the reference electrodes, whereas electrodes marked 'b' were the measuring electrodes. Such a selection of electrodes was made in order to obtain a pair with the lowest and highest KCl leakage rate from the measuring electrode (electrodes K422 and REF401 respectively). The set-up with one sample compartment was used. Figure 4.7a rep-

Table 4.4: Values of the potentials recorded for BSA in 1 mM Bistris-HCl, 10 mM NaCl, pH 6.4 buffer with electrodes K422 and REF401. Potentials are expressed relative to the potential when both electrodes were in the outer buffer. $U_D$ is the Donnan potential taken as $U_{prot} - U_o$. The set-up with one sample compartment was used, sample volume was 1 ml, protein concentration 12 mg/ml, temperature 20°C. The sample compartment was either a sack made of dialysis tubing with the membrane area ≈3 $cm^2$ or a plastic cylinder with a membrane area ≈0.5 $cm^2$ at the base.

| Potential (mV) | Membrane area | | | |
|---|---|---|---|---|
| | ≈3 $cm^2$ | | ≈0.5 $cm^2$ | |
| | K422 | REF401 | K422 | REF401 |
| $U_o$ | -0.2 | -0.3 → -2.0 | -0.8 | -2.3 |
| $U_{prot}$ | -2.5 | -2.9 → -4.0 | -2.6 | -3.3 |
| $U_D$ | -2.3 | -2.6 → -2.0 | -1.8 | -1.0 |

resents the potentials recorded when the measuring electrode was first placed in the compartment containing buffer ($U_o$) and then in the compartment containing protein solution ($U_{prot}$). These potentials are expressed relative to the potential when both electrodes were in the outer buffer. Potentials recorded using a sack made of the same dialysis tubing, are plotted in figure 4.7b for comparison. The values of the potentials obtained are given in table 4.4.

The potential $U_o$ had a value close to zero for the electrodes with low KCl outflow rate (K422) in a compartment with the larger membrane area. The same electrodes gave a more negative reference potential (-0.8 mV) in the other type of compartment. The electrodes with higher rate of KCl outflow (REF401) gave a reference potential which was close to zero initially and then drifted to a value of -2.0 mV when the dialysis sack was used. The value of that potential was -2.3 mV only 1 minute after immersing the electrode into the compartment with a small membrane area. Potentials $U_{prot}$ were more negative when obtained with electrodes REF401 than with electrodes K422. They were stable except for the potential recorded with electrodes REF401 in the compartment with a larger membrane area. The resulting Donnan potentials varied from -1.0 mV to -2.3 mV or even -2.6 mV when the initial values of the potentials recorded with electrodes REF401 were taken as opposed to the values after 20 minutes.

(a)

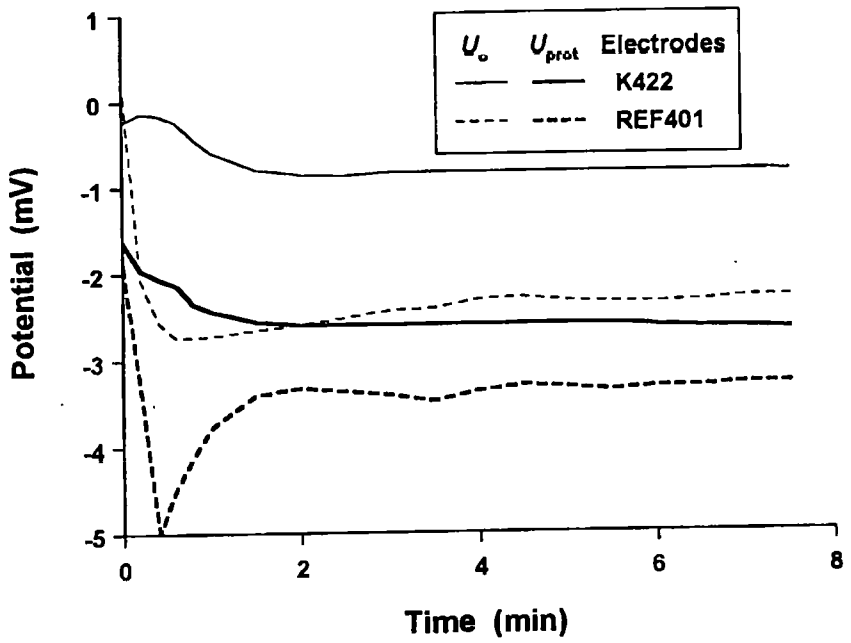


(b)

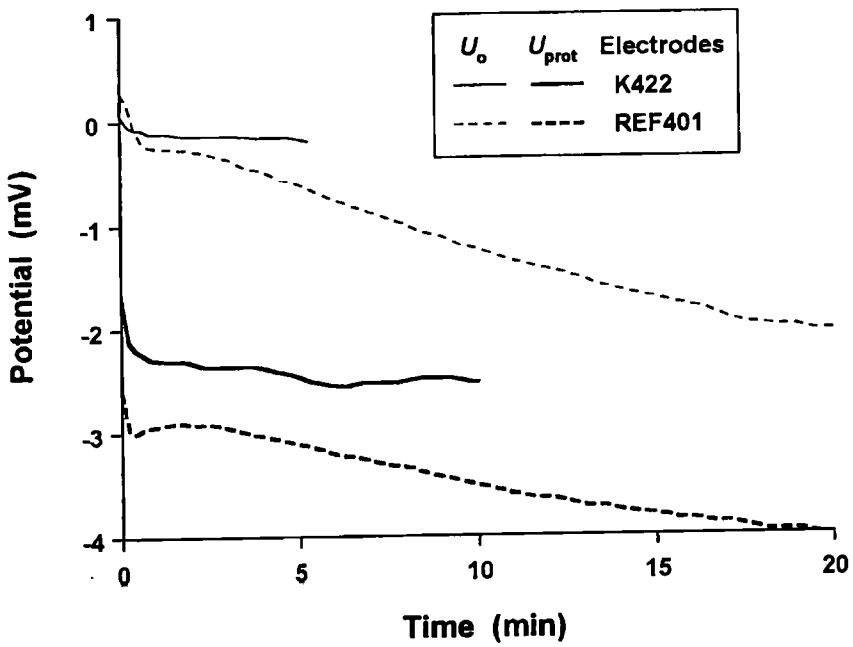


Figure 4.7: Potentials recorded for BSA in 10 mM NaCl, 1 mM Bistris-HCl, pH 6.4 buffer, with electrodes K422 and REF401. Potentials are expressed relative to the potential when both electrodes were in the outer buffer. The set-up with one sample compartment was used, sample volume was 1 ml, protein concentration 12 mg/ml, temperature 20°C. The sample compartment was (a) plastic cylinder with a membrane of $\approx$0.5 cm$^2$ area at the base, (b) dialysis sack with a membrane area $\approx$3 cm$^2$.

### 4.1.5 Discussion

It has not been possible to explain the discrepancy between the experimental and theoretical diffusion potentials at low ionic strength.

There are some differences between the net charge of BSA determined using 1.0 and 0.25 ml sample volume but they are quite small although, according to the t-test, they are significant for pH values 5.6 to 8.0. Certain observations were made which may explain these results.

Firstly, the buffers were weak (1 mM) so as to keep the ionic strength low and obtain larger Donnan potentials. It is possible that the pH of the Tris buffer was not maintained at 8.0 but was lower due to $CO_2$ absorption from the air. This was discovered after the Donnan potential measurements when looking for possible explanations for the differences in the net charge determined with the two sample volumes. The initial pH of the Tris buffer was 8.0, but ten and eighteen days after preparation the pH was 7.8 and 7.3, respectively. It should be noted that the pH of the experimental solution was not checked whilst measuring the potentials. A plot of the net charge obtained as a function of the measurement number (not shown in the thesis) indicated a trend towards less negative values with time. Since the potential was measured for samples with a volume of 1.0 ml first, this could account for the difference.

Secondly, a large increase of the reference potential was noted after the first measurement for pH 3.4 and 4.0 (of about 1 mV). The potentials recorded in the protein, however, were approximately constant for consecutive measurements. This resulted in the first Donnan potential having a larger value than the potentials subsequently measured. This was probably caused by the absorption of the positively charged protein onto the negatively charged surface of the glass electrode as glass has many sites available for hydrogen bonding (Bull, 1971). No values were rejected, hence results for low pH carry larger error which would increase the p value of the t-test.

In spite of these small differences between the values of the charge obtained for the

two sample volumes, both curves in figure 4.5 give an isoelectric point value of 4.6. This value agrees very well with the isoelectric point values determined in NaCl based solutions using other methods available from the literature, which were given in table 4.2.

A comparison of the experimental results with the molecular charge calculated from the sequence indicates counterion binding leading to a decrease in the absolute value of the net charge (figure 4.6). It is interesting that the intersection point of the experimental and theoretical curves is not at the zero charge line. This could suggest that there is preferential binding of anions (which are in this case predominantly $Cl^-$ ions) to a negatively charged protein.

On the basis of a reasonable agreement between the results obtained for the two sample volumes, one can conclude that it is possible to use volumes as small as 0.25 ml for this type of measurement. Agreement with the isoelectric point values from literature encourages the view that the technique is sound. One has to bear it in mind though, that the series of measurements for BSA at various pH values, was carried out with electrodes K422 for which the leakage rate of KCl is relatively small.

Larger leakages of KCl can cause anomalous potentials and drifts (figure 4.7 and table 4.4). The effect of using electrodes with different rates of KCl leakage and sample compartments with small and large membrane areas on the observed potentials, suggests that the following phenomena take place when an electrode is placed in a sample compartment. If the KCl leakage rate out of the electrode exceeds the diffusion rate through the semi-permeable membrane, an accumulation of KCl inside the compartment will take place to a concentration at which these rates will be equal. The KCl leaking out of the electrodes gives rise to negative potentials, whose magnitude is proportional to the KCl concentration.

The observed more negative values of the charge obtained for HMM and m-HMM from the second Donnan potential measurement on a sample, described in chapter 3, can be

explained within the above model. The reference potential was measured first, during which time some accumulation of KCl could have occurred in both compartments. In most of the experiments the buffer in one of the compartments was replaced with protein and the buffer in the other compartment was not changed at the same time. The potential was measured with the reference electrode in the buffer (containing some KCl) and the measuring electrode in fresh protein solution. This would have made the resulting Donnan potential less negative. When the second measurement was made, the buffer in the reference compartment was changed. Hence the second $U_{prot}$ was measured between fresh buffer and protein solution, in which the electrode had been immersed for the period of the first measurement. The accumulation of KCl in the protein sample would give rise to a more negative potential. Hence the negative value of the charge from the first measurement is reduced (less negative) and from the second measurement increased (more negative) with respect to the true value of the charge. This resulted in the bimodal distribution of the data and overall large experimental error.

This effect was not observed for BSA, for which the protein solution was also reused, with the difference though that the buffer was always changed at the same time as the protein was applied and the protein solution was returned to the solution from which samples were taken. The reference potential was, however, measured prior to each measurement for protein. Also electrodes were immersed for much shorter periods of time in the compartments. In the experiments with BSA these times were usually not longer than about 5 minutes whereas in the experiments with HMM electrodes were kept in sample compartments until there were no further changes in the potentials, for as long as 20–30 minutes. No trend towards more negative values was observed between consecutive measurements for BSA, from which it can be inferred that no significant change in the KCl concentration in the protein samples took place. Possibly the leakage affects more the potential when the electrode is placed in buffer than when it is in protein, and it could be expected that the leakage rate would be lower for a solution of higher viscosity. This can also be seen in figure 4.3, where the change in

the potential $U_o$ is larger than the change in potential $U_{prot}$ over the same period of time. These observations clearly indicate that the reference electrode should not be placed in an environment that can change. Hence the set-up with one dialysis sack was used in subsequent measurements (for BSA described in chapter 5).

Quite significant drifting in potentials occurred for the macroelectrode technique applied to BSA. When an attempt was made to apply the technique to other proteins such as F-actin other problems arose. It was observed that F-actin would initially give zero or even slightly positive potentials at pH 7.0, which would slowly change towards negative values over tens of minutes. This was noted for more than one preparation even though actin should be negatively charged at neutral pH. There was no way of knowing the true value of the equilibrium Donnan potential without having an alternative and accurate method for its determination. Since the interest was in measuring the charge of F-actin as well as the charge of tropomyosin-troponin complex (Tm-tn) and reconstituted thin filaments (RTFs) at various free $Ca^{2+}$ levels, a different technique was required. The application of microelectrodes to protein solutions is described in the next section.

## 4.2 Application of the microelectrodes to protein solutions

The microelectrode technique has been used in this laboratory to measure the Donnan potentials in muscle fibres (Elliott *et al.*, 1978; Bartels and Elliott, 1981, 1982, 1983; Naylor *et al.*, 1985; Bartels and Elliott, 1985) and protein gels (Bartels *et al.*, 1984; Elliott *et al.*, 1985; Jennison, 1992; Bartels *et al.*, 1993; Deshayes, 1994). Sharp electrodes with diameter 0.5–1.0 $\mu$m were used for muscle fibres and protein gels and blunt electrodes with the external diameter 20–100 $\mu$m were introduced by Jennison (1992) for protein gels. The latter electrodes were obtained from the sharp electrodes by breaking usually less than 1 mm off the tip with forceps. The reason for breaking the electrode tips was to prevent clogging taking place when the sharp electrodes were

inserted into protein gels. The latter technique was considered as suitable for applying to protein solutions.

### 4.2.1 Preliminary results with forceps-blunted electrodes

The materials and equipment used for these measurements were described in section 2.5.2. The Donnan potentials were measured for 0.25 ml BSA samples in 1 mM Tris-HCl, 10 mM NaCl, pH 8.0 buffer in order to compare the results with those obtained using macroelectrodes (this was prior to discovery that the pH of the Tris buffer may not have been 8.0 at all times).

Microelectrodes whose resistance was of the order of several MΩ produced very unstable readings: the traces had a high noise level, were 'wandering' and the resistance of the circuit, which was also recorded all the time, did not remain constant. It was not until the use of electrodes with much lower resistance was made (lower than 1 MΩ), that the traces of both the potentials and the resistance became more stable and the results more reproducible.

The potentials recorded with the same electrode did not always give similar values for consecutive measurements. It was noticed that, for some electrodes, the potential recorded when the electrode was placed in the protein sample for the first time, changed in a characteristic manner as shown in figure 4.8. If the electrode was taken out before the potential came to an equilibrium value this trend would continue during the second measurement. If a new electrode was used with the same sample the observed potential differences would be as for the previous electrode at the end of its use. It was suspected that sample contamination was taking place, with the KCl leaking through the tips since the electrodes of lower resistance were affecting samples in this way. This is also demonstrated in figure 4.8, where the first electrode has resistance of only 0.13 MΩ and the other two (which give stable readings) have higher resistance (0.2 MΩ and 0.27 MΩ).

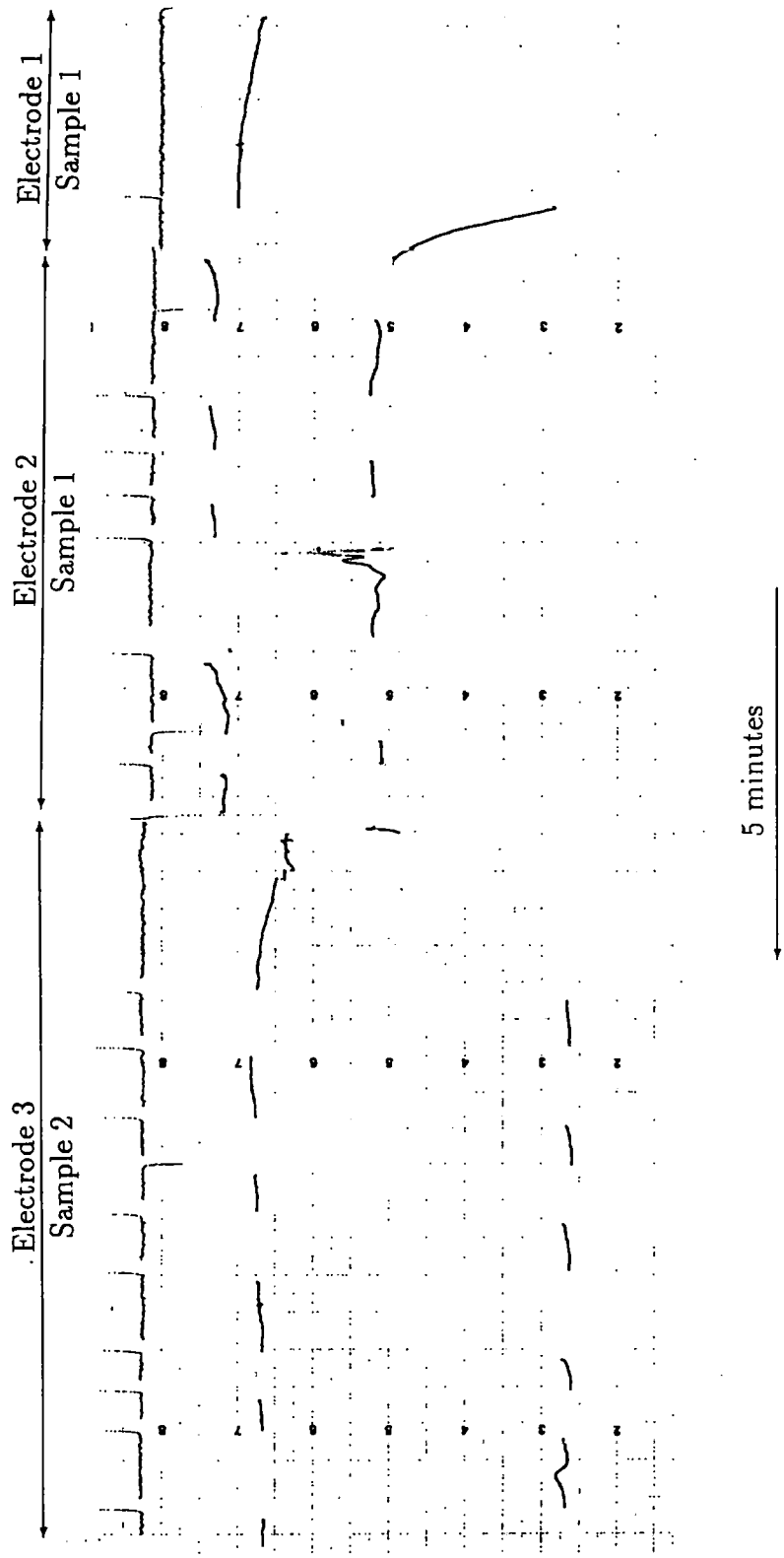


Figure 4.8: Traces of resistance $R$, potentials $U_{ref}$ and $U_{prot}$ (from left to right) registered with forceps-blunted microelectrodes for two samples of BSA in 10 mM NaCl, 1 mM Tris-HCl, pH 8.0 buffer. Microelectrodes of resistance 0.13 MΩ, 0.2 MΩ and 0.27 MΩ were used (electrodes 1,2 and 3 respectively). Protein concentration 14.4 mg/ml, sample volume 0.25 ml. Time flows from top to bottom.

Potentials obtained only with electrodes for which the first potential did not drop provided the value of the molecular charge -12.3±0.5e (from 12 measurements collected with 3 electrodes for 3 samples). Comparison with the value obtained with macroelectrodes (-12.5±0.7e and -11.5±1.2e for 1 ml and 0.25 ml respectively) yields t test p values 0.34 and 0.05. The blunted microelectrodes gave results agreeing with the results obtained using macroelectrodes. This also indicated that the reduced values of potential observed for some electrodes were not true Donnan potentials.

Subsequently, forceps-blunted microelectrodes were used for the measurements of Donnan potentials for F-actin and RTFs. During these experiments however, only very few of the microelectrodes were found to last for more than about 3 measurements, after which their resistance would increase to several tens of MΩ and the potential would become erratic. This usually happened while the microelectrode was in the protein and must have been caused by the protein clogging up the electrode. In practice it meant that many electrodes had to be made and tried, and only very few of them would last for 10 or 20 measurements. The fact that such electrodes did exist however, encouraged attempts to find out what distinguished these 'good' electrodes from the 'bad' ones and how to manufacture consistently 'good' electrodes.

In order to find out what features distinguished 'good' and 'bad' microelectrodes, the electrodes used while carrying out measurements on F-actin and RTFs were collected and their tips examined under microscope at 1250× magnification. Most electrodes were found to have 'jagged' ends and some had cracks along them. It, at first, appeared that the electrodes that had performed best however, had smoother ends and no cracks. Typical examples of these early electrodes are given in figure 4.9b,c. At this stage a method of manufacturing low resistance microelectrodes with smooth ends was explored.

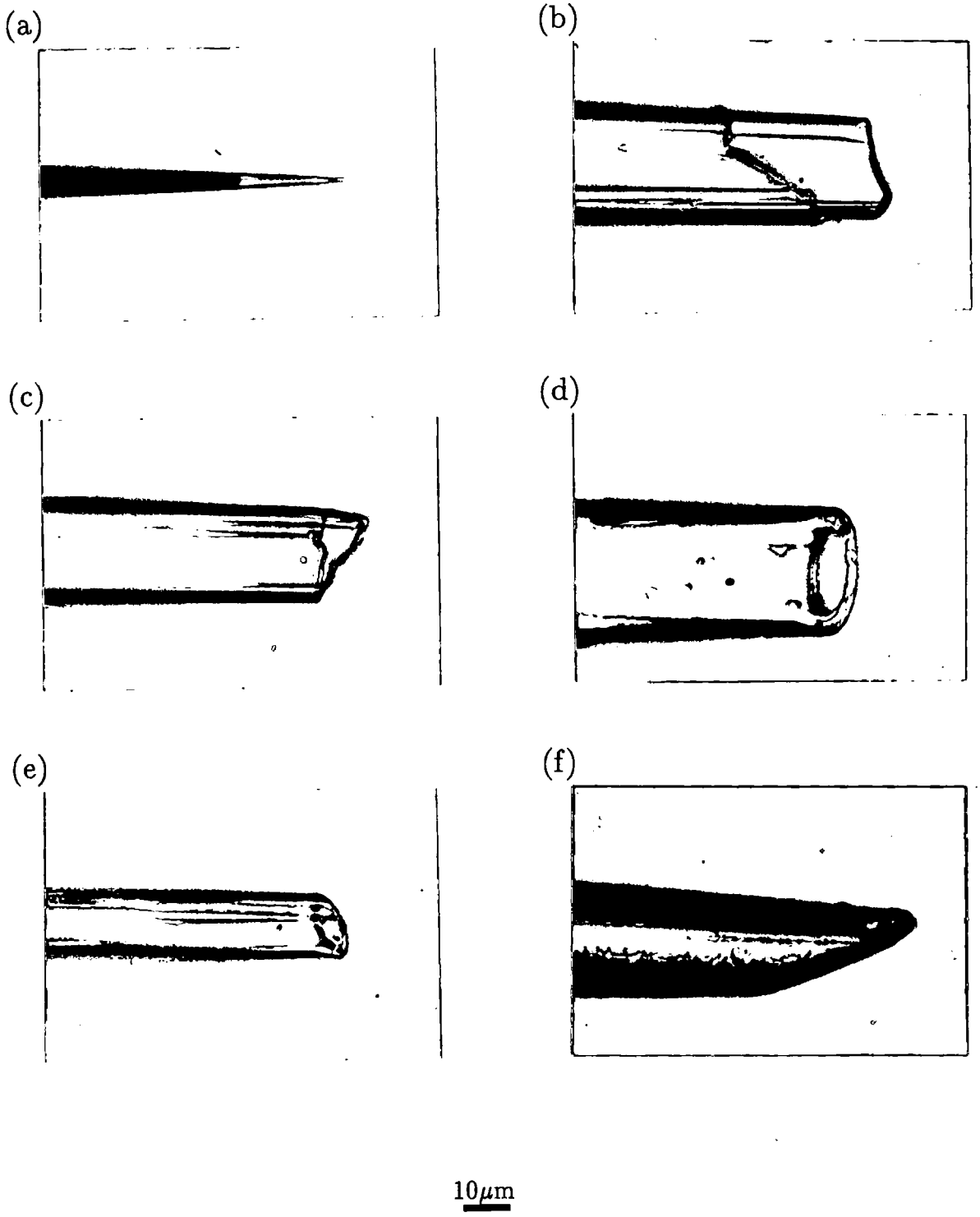


Figure 4.9: Photographs of the tips of microelectrodes. (a) Sharp electrode. (b)-(c) Typical early forceps-blunted electrodes: electrode (b) drifting in protein (5 measurements), (c) very good electrode (20 measurements). (d)-(f) Typical examples of bevelled electrodes: electrode (d) clogged in protein after 5 measurements, (e) performed well giving 19 readings, (f) gave drifting and unstable readings. Tip sizes were 24, 20, 28, 13 and 20 $\mu$m for electrodes (b) to (f) respectively. Photographs at 750× magnification.

### 4.2.2 Grinder bevelled microelectrodes

The method that seemed suitable for the bevelling of microelectrodes employed a microelectrode grinder as described in section 2.5.2. Photographs of electrodes that were obtained are shown in figure 4.9d,e,f. These electrodes were tested again in 1 mM Tris-HCl buffer, 10 mM NaCl, pH 8.0. A molecular charge of -12.0±0.5e was obtained for BSA with 3 electrodes from the total of 21 measurements. The bevelling however did not improve performance of the electrodes, on average they did not last longer than the 'jagged' electrodes.

### 4.2.3 Junction-renewable microelectrodes

After examining a large number of electrode tips and relating the tip structure to the potential and resistance traces, it became apparent that most of the electrode tips had similar diameter (typically around 20–40 $\mu$m) whether they were good or bad and there were no structural features that distinguished them within that range of tip sizes. We were almost ready to accept the fact that it might not be possible to find out what makes so few electrodes last for many measurements giving stable, reproducible results thus making them a reliable tool. On close examination of the potential and resistance traces I concluded that blockage of the tip (usually with the protein) was the event ending functioning of most electrodes. After examining an open liquid junction macroelectrode with a glass sleeve (from Radiometer Copenhagen) a simple solution to this problem occurred to me. The loosening of the sleeve of the macroelectrode was enabling some of the filling solution to drip out of the end of the electrode thus renewing the liquid junction. The electrode was very large (tip size about 1 cm) and was leaking KCl when left in a vertical position even with the sleeve tightened. It was completely useless for small samples which were affected so strongly by KCl leakage. But it gave me an idea that perhaps one could renew the microelectrode liquid junction in a similar way, possibly by tightening its holder slightly. I tried it every time an electrode resistance jumped, and it worked! The resistance would go

back to the initial value and so would the potential. To be on the safe side the holder was always tightened when the tip of the microelectrode was immersed in the buffer. Even when performed while the electrode tip was in the protein compartment, to see if this would push out much KCl, the potential was not affected by the tightening. Such junction-renewable electrodes were used in the Donnan potential measurements for F-actin, Tm-tn and RTFs described in chapter 5. These measurements were carried out in pCa buffers whose composition is given in table 5.1. Some example traces of potentials and resistance for Tm-tn in pCa 8.7 buffer are given in figure 4.10 with the tightening of the holder indicated. Also photographs of the tips of the electrodes used are presented in this figure.

Using this technique the lifetime of a majority of electrodes could be extended to obtain 20 or more measurements. Most importantly, the microelectrodes for which blockages could be removed by this simple procedure, became reliable tools. There were some electrodes that produced noisier traces and clogged up more often than others. Their examination under microscope did not reveal any structural feature that they shared: neither in size nor in shape. Photographs of typical electrodes to which the junction renewal technique was applied are shown in figure 4.11. Histograms of the tip sizes are given in figure 4.12 for Tm-tn, F-actin and RTFs. The pooled data for these 3 proteins form the histogram given in figure 4.13. These electrodes had tip sizes smaller (up to 15 $\mu$m with average value about 12 $\mu$m) than the early electrodes to which the junction renewal technique was not applied (20–40 $\mu$m).

### 4.2.4 KCl leakage

An investigation into the cause of the characteristic behaviour of the potential obtained with some of the, mostly early, electrodes was made. This behaviour was described in section 4.2.1 and illustrated with traces in figure 4.8. A hypothesis was formed that KCl leakage was responsible for the characteristic drop in potential for some electrodes, especially with larger tip diameters.

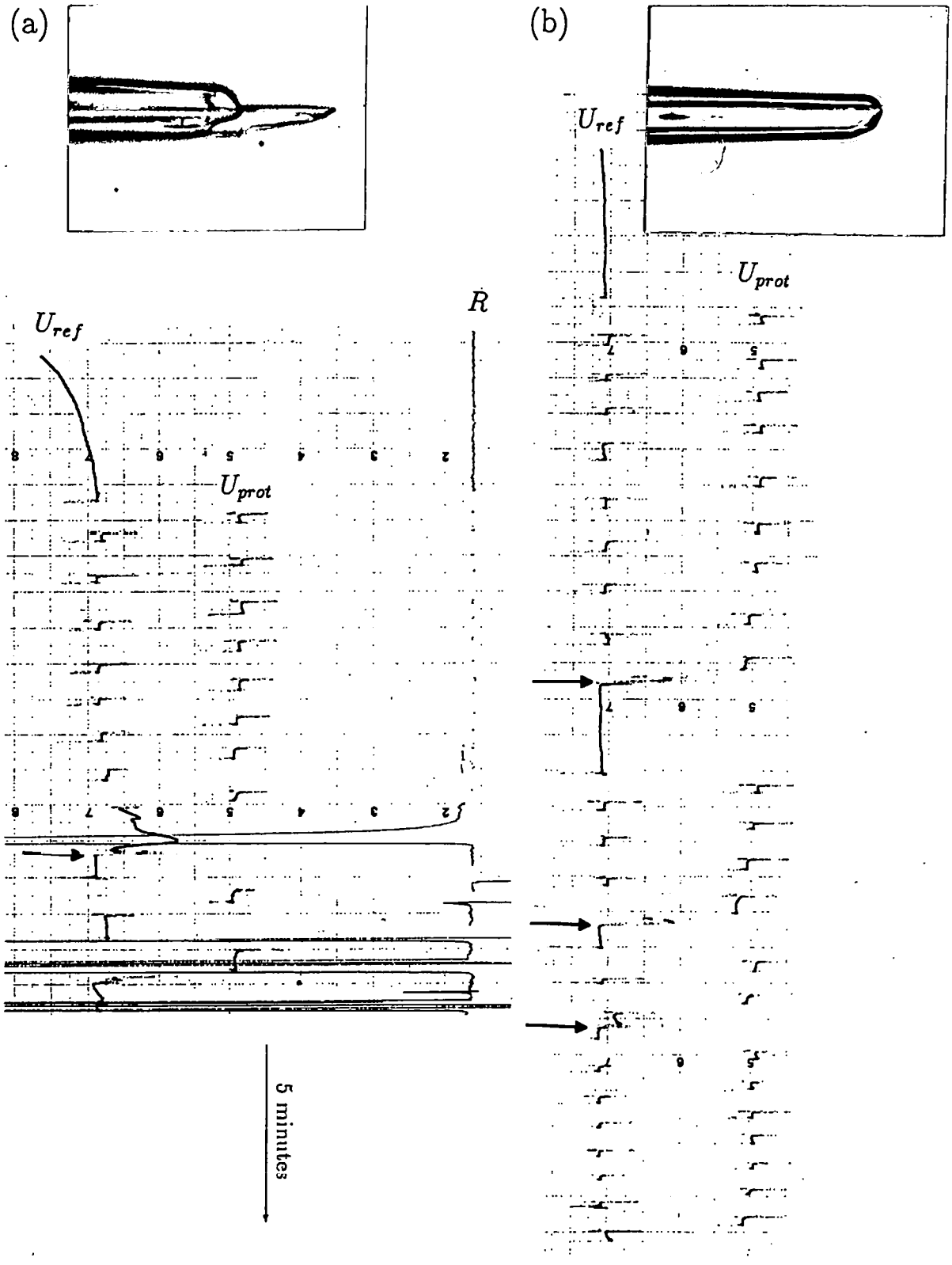


Figure 4.10: Potentials $U_{ref}$ and $U_{prot}$ recorded using junction-renewable microelectrodes for Tm-tn in pCa 8.7 buffer. Arrows indicate when the microelectrode had its holder tightened to renew the blocked junction. Traces for 2 samples at very similar protein concentration (9.6 and 9.3 mg/ml) recorded with 2 microelectrodes are shown. Resistance ($R$) trace is given for one of the samples (on the left) to illustrate the increase in resistance accompanying the blockage. Time flows from top to bottom. Also photographs of the tips of the electrodes used are presented (at magnification 750×).

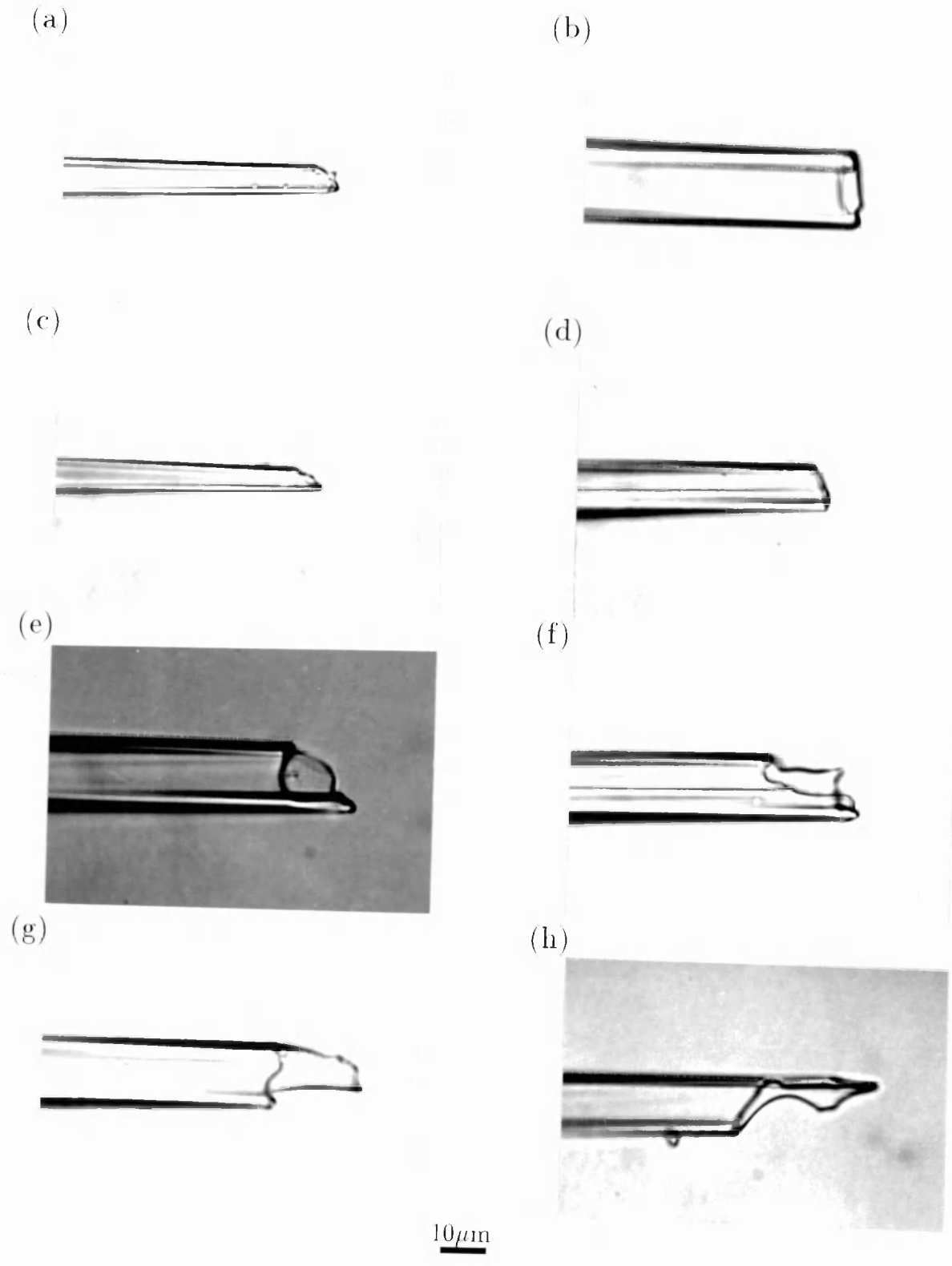


Figure 4.11: Photographs of the tips of typical microelectrodes to which the junction renewal technique was applied during the measurements of Donnan potentials for BSA, Tm-tn, F-actin and RTFs in pCa buffers. (a) and (b) electrodes clogging both in buffer and protein (6 and 17 $\mu$m tips). (c) to (h) electrodes performing very well: (c) narrow tip electrode (5 $\mu$m), (d) smoothly broken electrode (10 $\mu$m), (e) and (f) typical jagged electrodes (15 and 14 $\mu$m tips), (g) and (h) very jagged electrodes (14 and 13 $\mu$m tips). Photographs at 750$\times$ magnification.

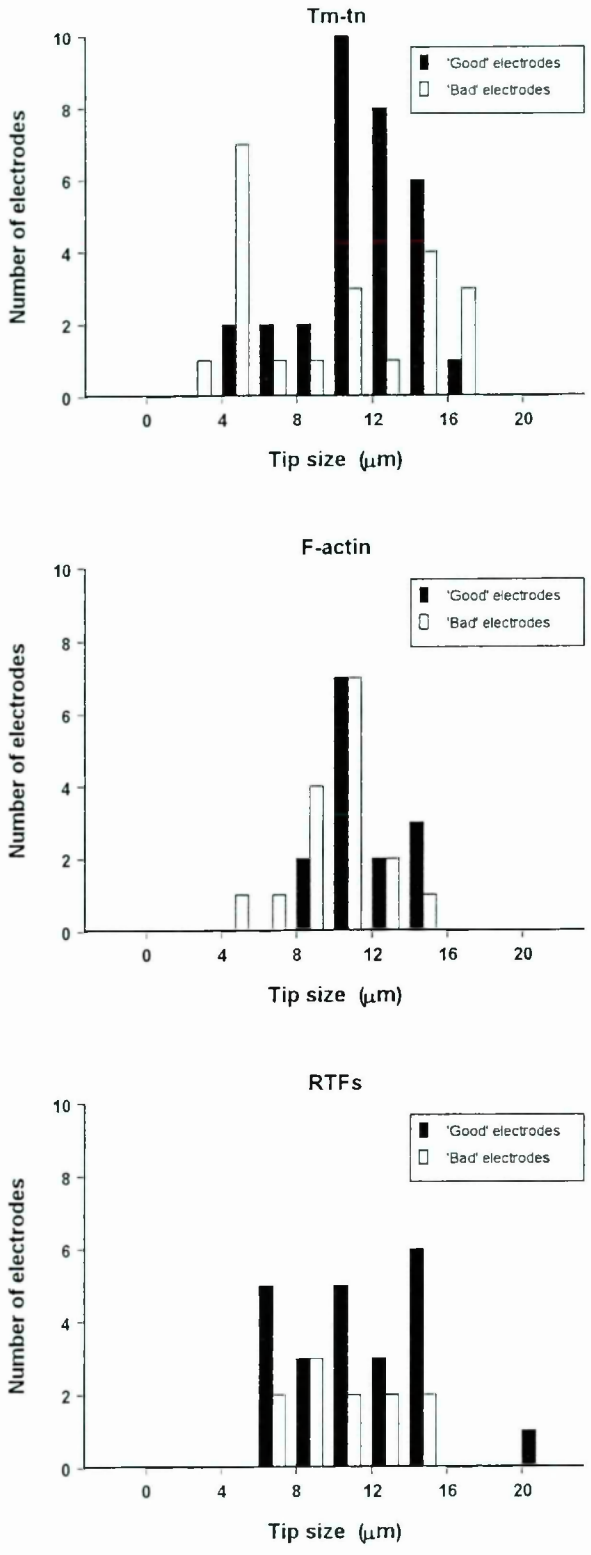


Figure 4.12: Distribution of the tip diameters for 'good' and 'bad' microelectrodes (of the junction-renewable type) for Tm-tn, F-actin and RTFs.

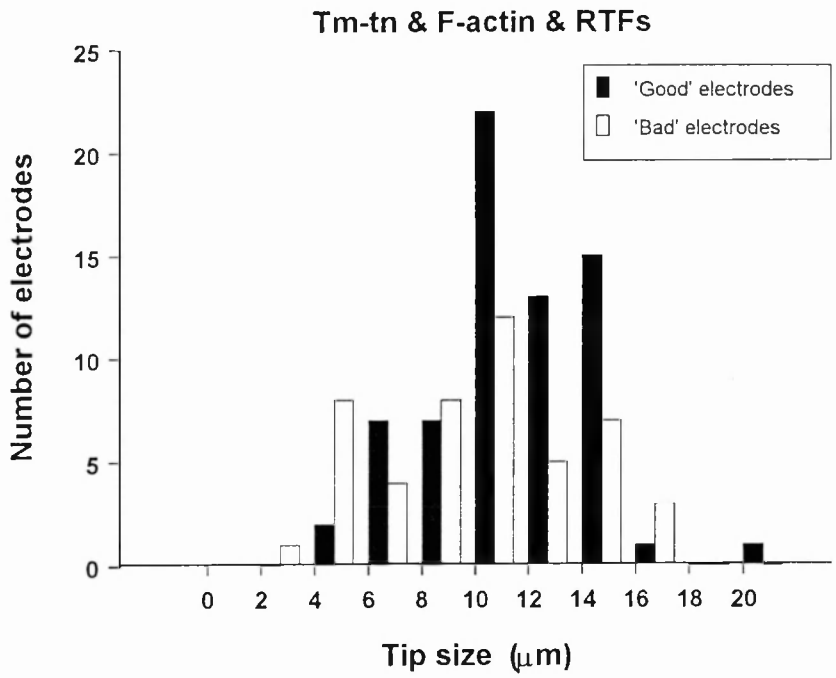


Figure 4.13: Distribution of the tip diameters for 'good' and 'bad' microelectrodes (of the junction-renewable type) - data pooled for Tm-tn, F-actin and RTFs.

It was desirable to use microelectrodes which would have minimal leakage themselves and introduce small amounts of concentrated KCl into the protein sample. In view of the problems with pH stability of Tris buffers at pH 8.0, work was performed at lower pH. The pH chosen was 6.4, since the charge of BSA was also measured with macroelectrodes at this pH twelve times for each of the sample volumes. Various settings of the microelectrode puller were tried and it was found that, at low values of pull and furnace, it was possible to obtain electrodes with resistance under 1 MΩ which would not clog in BSA or buffer and gave stable potentials. These electrodes had very short tips. Initially the Donnan potentials for BSA were measured without introducing any KCl in order to check whether such sharp electrodes of low resistance were giving values of the charge in agreement with macroelectrodes. The potentials for 5 samples of BSA were measured (20 measurements of potential in total) and produced a molecular charge of -9.8±0.4e as compared to the values obtained with the macroelectrodes (-8.8±0.3e for 1 ml and -9.3±0.6e for 0.25 ml). The agreement was assumed good enough to carry out the experiment with simulated KCl leakage.

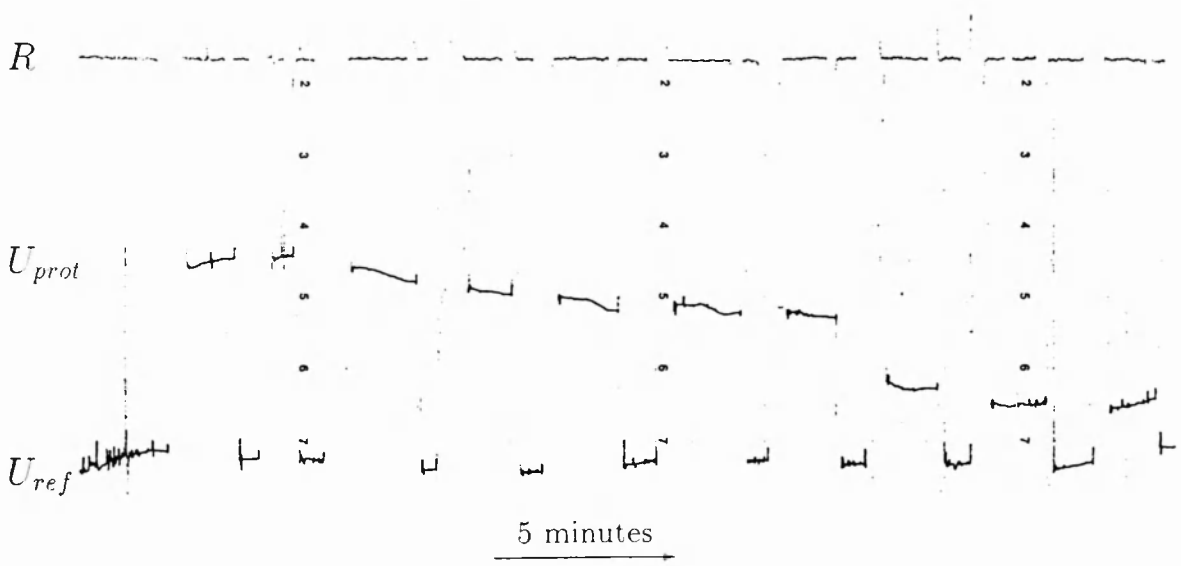


Figure 4.14: Example trace of potential $U_{ref}$ and $U_{prot}$ and resistance $R$ recorded using sharp microelectrodes of resistance less than 1 MΩ (0.77 MΩ) for a BSA sample in 1 mM Bistris-HCl, 10 mM NaCl, pH 6.4 buffer to which KCl was added. Initial protein concentration 12.5 mg/ml. final 11.5 mg/ml. Initial sample volume 250 $\mu$l, final 273 $\mu$l.

The experiment was performed in the following way. The potential was measured twice for 0.25 ml sample of BSA in 1 mM Bistris-HCl, 10 mM NaCl, pH 6.4 buffer to determine whether an electrode was suitable. Then microlitre amounts of initially 0.1 M KCl and later 0.5 M KCl in 1 mM Bistris-HCl, pH 6.4 buffer, were added, and after each addition, potentials $U_{prot}$ and $U_{ref}$ were measured. If the electrode clogged before the final concentration of KCl was achieved the procedure was started again. An attempt was made to carry out the measurements in the time frame of 1 minute in buffer and 2 minutes in BSA bearing in mind that the added KCl would diffuse out of the sample. An example trace of the potential and resistance is shown in figure 4.14. The results from 4 samples are shown graphically in figure 4.15 – the potentials were averaged as the protein concentration differences between samples were small (less than 5%).

A measurement of the leakage rates for 12 microelectrodes into 10 mM KCl was made using the conductivity method as used for macroelectrodes in section 4.1.3. Microelectrodes, blunted with forceps were checked in 1 $l$ of 10 mM KCl to confirm

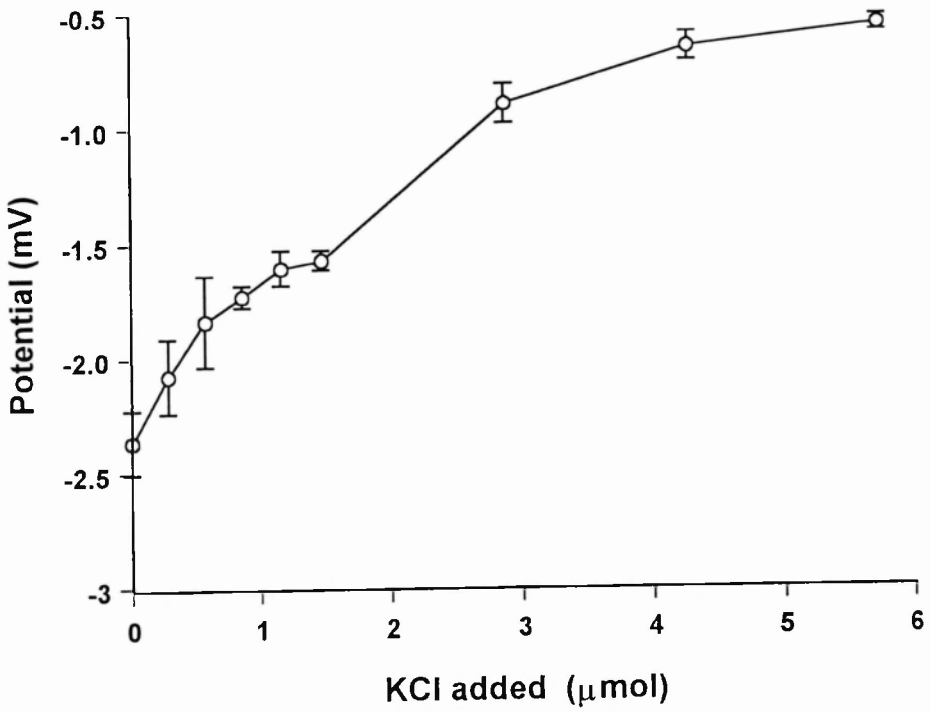


Figure 4.15: Potential ($U_{prot} - U_{ref}$) recorded using sharp electrodes of resistance less than 1 MΩ for BSA samples in 1 mM Bistris-HCl, 10 mM NaCl, pH 6.4 buffer to which KCl was introduced to simulate a leakage out of the microelectrode. Initial sample volume 250 $\mu$l, final 273 $\mu$l. BSA dilution during the experiment (from 12.5 to 11.5 mg/ml) does not account for the large potential change. Data points are mean values of 4 measurements with standard deviations indicated.

Table 4.5: Rates of KCl leakage from microelectrodes whose tips were immersed for 1 hour in 12 ml of 10 mM KCl at 25°C (determined with a conductivity meter).

| Microelectrode | Tip size ($\mu$m) | Resistance (M$\Omega$) | KCl leakage rate (nmol·s$^{-1}$) |
|---|---|---|---|
| 1 | 4.8 | 0.62 | $\star$ |
| 2 | 5.6 | 0.50 | $\star$ |
| 3 | 5.6 | 0.53 | 0.15 |
| 4 | 6.8 | 0.33 | 0.17 |
| 5 | 9.6 | 0.40 | 0.07 |
| 6 | 12.0 | 0.40 | 0.27 |
| 7 | 16.0 | 0.22 | 0.17 |
| 8 | 18.4 | 0.20 | 0.44 |
| 9 | 19.2 | 0.20 | 0.15 |
| 10 | 19.2 | 0.35 | 0.54 |
| 11 | 21.6 | 0.12 | 0.24 |
| 12 | 24.0 | 0.18 | 0.47 |

$\star$ Not detectable.

whether they were working and had suitable resistance prior to the determination of their leakage rates. Also the sizes of the electrodes tips were determined under microscope at magnification 1250×. The results are presented in table 4.5.

## 4.3 Effect of viscosity on electrode measurements

In the early macroelectrode experiments with solutions of F-actin potentials obtained were unusual and difficult to interpret as described in section 4.1.5. It was suspected that this was due to the viscosity of the samples. The potentials establishing soon after placing the electrode in protein solution, were stable for a few minutes, after which time the potential would slowly change, becoming more negative. These, initially stable potentials could easily have been taken as the Donnan equilibrium potentials, with the subsequent changes in the potentials interpreted as caused by the KCl outflow from the macroelectrode. It was not clear whether this was the case.

Both macroelectrodes and microelectrodes were therefore used to measure the potentials for 4 proteins differing in viscosity: BSA, Tm-tn, F-actin and RTFs. The protein solutions were dialysed into pCa 6.4 buffer overnight on ice, then each protein solution

was divided into 4 (F-actin and RTFs) or 6 (BSA and Tm-tn) samples of 0.25 ml each depending on how much of the protein was left over from measurements at various $Ca^{2+}$ levels described in chapter 5. Each sample was placed in a dialysis tubing sack and its Donnan potential was measured with either macro- or microelectrodes.

Junction-renewable microelectrodes were used and example potential traces for the 4 proteins are given in figure 4.16. Macroelectrodes K422 were used and the potentials were recorded until no further change in potential was observed. Examples of macroelectrode traces for the 4 proteins are presented in figure 4.17. The potentials recorded during the first 10 minutes after placing an electrode into protein solution are plotted in figure 4.17a. Traces recorded until no further change was observed, are plotted in figure 4.17b. The samples used for the macro- and microelectrode measurements for a given protein had similar concentrations, since they were taken from the same protein solution and no significant dilution occurred when the samples were placed in the dialysis sack compartment, as was confirmed in a protein concentration assay (microbiuret). The values of the potentials obtained with microelectrodes were nevertheless scaled to match exactly the protein concentrations of the samples used for macroelectrode measurements, for direct comparison. It was checked that the potentials were linear with the protein concentrations for these experimental conditions. These scaled values are represented by horizontal lines in figure 4.17.

Figure 4.18 contains 3 traces for BSA showing the reproducibility of the complex time course of the potentials. The horizontal lines represent the corresponding microelectrode potential values. Numerical values of the potentials, protein concentrations, specific charge and equilibration times are given in table 4.6.

When the Donnan potentials and protein concentrations were determined, the kinematic viscosity of the above four proteins was measured using the method described in section 2.9. For each protein concentration 6 measurements of the flow time were performed, except for the most concentrated sample of RTFs, for which only 2 measurements were made. The mean values of the kinematic viscosities obtained are listed

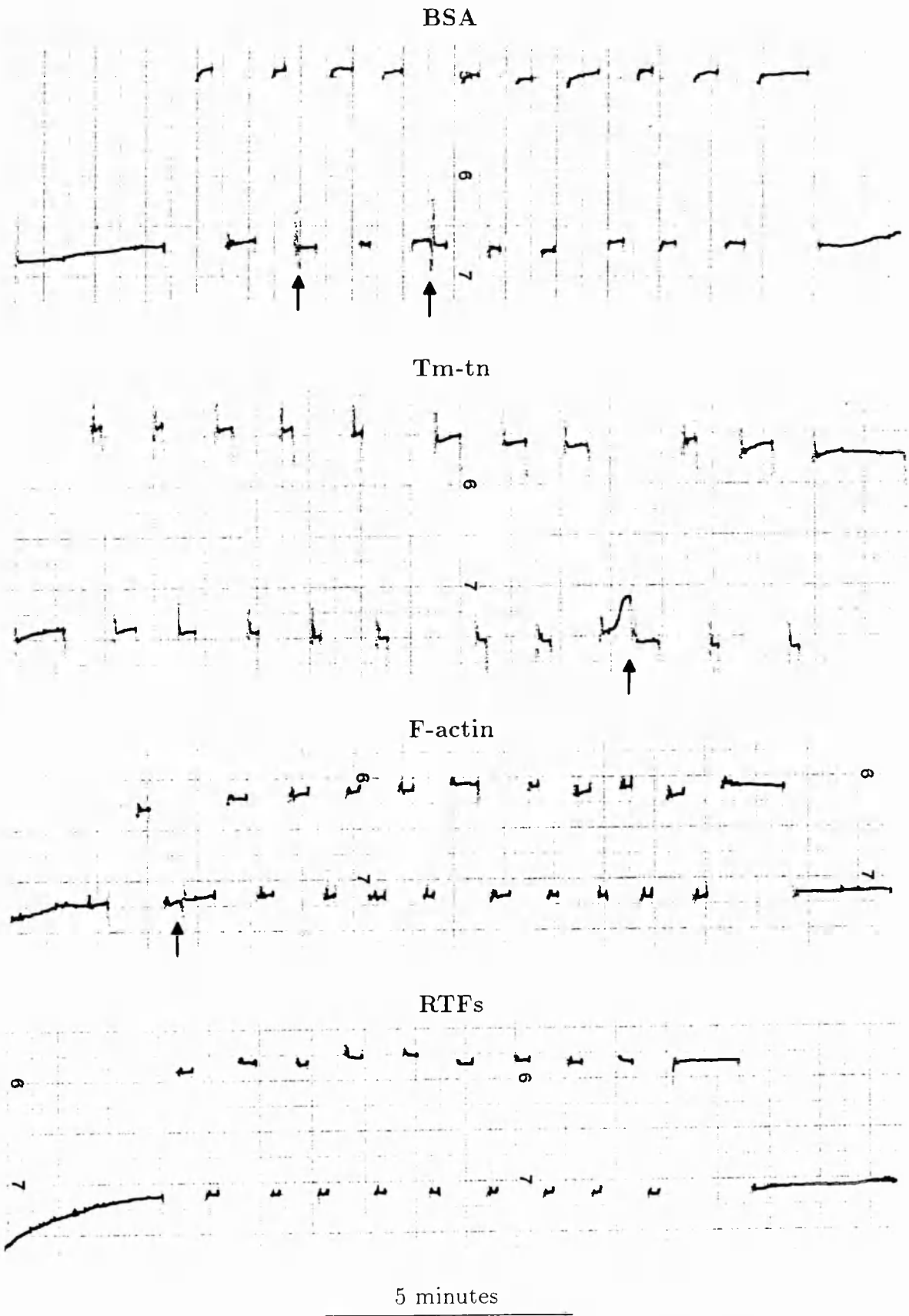


Figure 4.16: Example traces of the potentials $U_{ref}$ (bottom) and $U_{prot}$ (top) recorded using junction-renewable microelectrodes for BSA, Tm-tn, F-actin and RTFs in pCa 6.4 buffer. The tightening of the electrode holder is indicated with arrows.

(a)

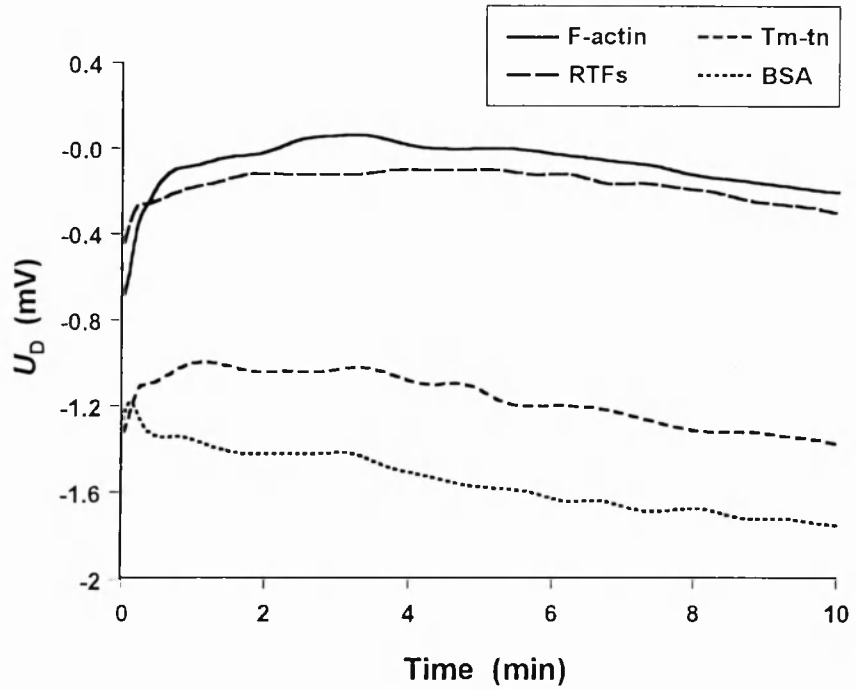


(b)

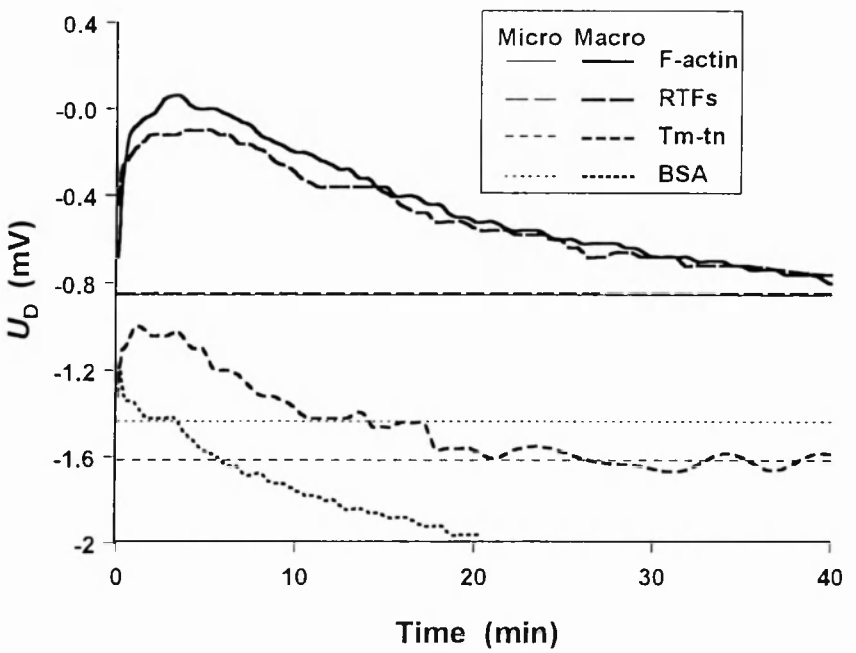


Figure 4.17: Typical example traces of the Donnan potentials $U_D$ recorded using macroelectrodes K422 for F-actin, RTFs, Tm-tn and BSA in pCa 6.4 buffer. Sample volume 0.25 ml. (a) First 10 minutes after placing the electrode into protein sample. (b) Full traces i.e. recorded till there was no further change in the potential. Horizontal lines are values of the potentials obtained with microelectrodes scaled to the protein concentrations for the samples used for macroelectrode measurements.

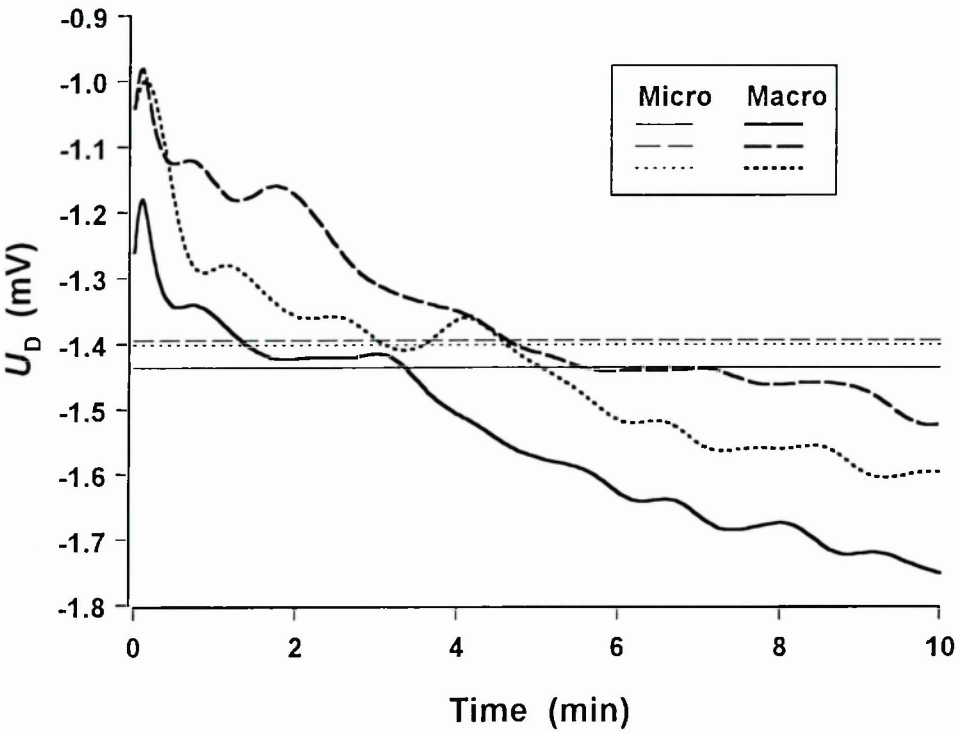


Figure 4.18: Traces of the Donnan potential for 3 BSA samples recorded using macroelectrodes K422 in pCa 6.4 buffer. Sample volume 0.25 ml. Horizontal lines are values of the potentials obtained with microelectrodes scaled to the protein concentrations for the samples used for macroelectrode measurements.

Table 4.6: Comparison of the Donnan potential $U_D$ and specific charge $q_{spe}$ values obtained with microelectrodes and macroelectrodes, if the potentials at the first plateau are taken from the time course of the macroelectrode potentials. Measurements were performed on BSA, Tm-tn, F-actin and RTFs in pCa 6.4 buffer. The times after which the macroelectrode potential value was taken are denoted $t_{eq}$, n is the number of Donnan potential measurements with microelectrodes, $c_p$ is the protein concentration.

| Protein | Microelectrodes | | | | Macroelectrodes | | | |
|---|---|---|---|---|---|---|---|---|
| | $c_p$ (mg/ml) | $U_D \pm$ SD (mV) | n | $q_{spe}$ | $c_p$ (mg/ml) | $U_D$ (mV) | $t_{eq}$ (min) | $q_{spe}$ |
| BSA | 11.1 | -1.40±0.03 | 10 | -18.5 | 11.1 | -1.41 | 3 | -18.6 |
| | 11.2 | -1.43±0.04 | 10 | -18.8 | 11.1 | -1.44 | 5 | -19.1 |
| | 11.4 | -1.41±0.05 | 13 | -18.3 | 11.4 | -1.42 | 2 | -18.3 |
| Tm-tn | 9.1 | -1.59±0.05 | 15 | -25.5 | 9.6 | -1.65 | 20 | -25.3 |
| | 9.3 | -1.58±0.05 | 14 | -25.1 | 9.9 | -1.46 | 15 | -21.8 |
| | 9.7 | -1.56±0.04 | 12 | -23.7 | 10.1 | -1.49 | 17 | -21.6 |
| F-actin | 5.6 | -0.87±0.03 | 10 | -22.8 | 5.5 | -0.74 | 30 | -19.7 |
| | 5.7 | -0.82±0.04 | 11 | -21.1 | 5.7 | -0.86 | 40 | -21.0 |
| RTFs | 6.4 | -0.99±0.07 | 12 | -22.6 | 5.4 | -0.75 | 32 | -20.4 |
| | 6.6 | -1.04±0.03 | 10 | -23.2 | 6.2 | -0.86 | 26 | -20.4 |

in table 4.7 and shown graphically as a function of protein concentration in figure 4.19. BSA was found to have very low kinematic viscosity even at concentrations as high as 90 mg/ml. The kinematic viscosity of the other 3 proteins was strongly dependent on the protein concentration in the range measured. For the same concentration the most viscous were the RTFs, then F-actin, followed by Tm-tn with BSA being the least viscous of the 4 proteins.

## 4.4 Discussion

The KCl leakage rate out of the macroelectrodes that were used was about an order of magnitude larger than for microelectrodes with diameters up to about 25 $\mu$m. After an immersion of a macroelectrode into a sample compartment containing the same buffer as the buffer outside the compartment, negative potentials were usually observed relative to the potential recorded when both electrodes were in the outer buffer. The magnitude of these potentials was correlated to the KCl leakage rate out

Table 4.7: Kinematic viscosity $\eta^{kin}$ of BSA, Tm-tn, F-actin and RTFs determined by capillary viscometry at various protein concentrations. Mean values of 6 measurements are given ± SD except for the sample of the RTFs at highest concentration, for which the flow time was only measured twice. Measurements were performed at 20±0.5°C in pCa 6.4 buffer.

| Protein | $c_p$ (mg/ml) | $\eta^{kin} \times 10^6$ ($m^2 \cdot s^{-1}$) | SD |
|---|---|---|---|
| BSA | 91.4 | 1.463 | 0.014 |
| | 73.2 | 1.294 | 0.007 |
| | 54.9 | 1.167 | 0.009 |
| | 36.6 | 1.059 | 0.023 |
| | 18.3 | 0.951 | 0.008 |
| | 10.9 | 0.984 | 0.048 |
| | 9.1 | 0.923 | 0.014 |
| | 8.8 | 0.924 | 0.022 |
| | 6.6 | 0.905 | 0.006 |
| | 4.4 | 0.899 | 0.025 |
| | 2.2 | 0.884 | 0.014 |
| | 1.1 | 0.881 | 0.008 |
| Tm-tn | 9.5 | 38.22 | 0.56 |
| | 7.6 | 19.74 | 0.11 |
| | 5.7 | 9.44 | 0.18 |
| | 3.8 | 4.091 | 0.063 |
| | 1.9 | 1.576 | 0.035 |
| | 1.0 | 1.087 | 0.022 |
| F-actin | 5.3 | 17.32 | 0.28 |
| | 4.2 | 10.69 | 0.20 |
| | 3.2 | 6.46 | 0.15 |
| | 2.1 | 3.42 | 0.11 |
| | 1.1 | 1.75 | 0.17 |
| | 0.5 | 1.75 | 0.39 |
| RTFs | 6.1 | 301.2 | 5.2 |
| | 4.0 | 73.6 | 1.1 |
| | 3.2 | 24.90 | 0.46 |
| | 2.4 | 7.92 | 0.11 |
| | 1.6 | 2.821 | 0.041 |
| | 0.8 | 1.314 | 0.020 |

(a)

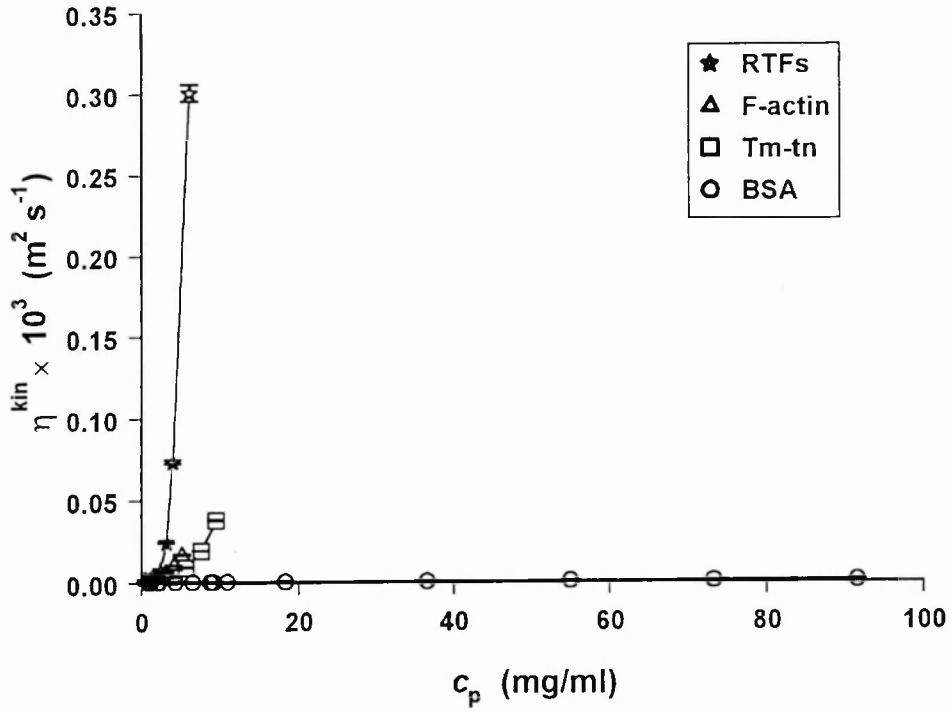


(b)

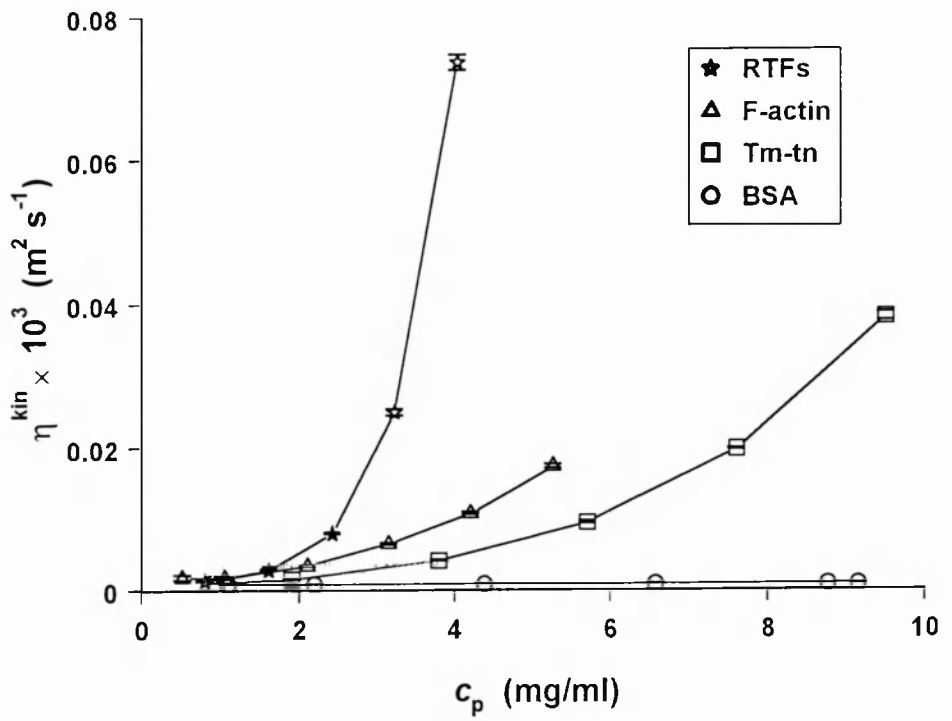


Figure 4.19: Kinematic viscosity $\eta^{kin}$ of BSA, Tm-tn, F-actin and RTFs determined by capillary viscometry at 20±0.5°C in pCa 6.4 buffer as a function of protein concentration. Diagram (b) is an enlargement of the bottom left part of diagram (a).

of the macroelectrode and it also depended on the membrane area and volume of the solution in the compartment. When a microelectrode was immersed in the sample compartment containing buffer solution, a constant potential was observed equal to the potential when both the reference electrode and the microelectrode were in the outer buffer. This was found to occur whether Amicon microconcentrators or dialysis tubing sacks were used.

Our experiments suggest that the KCl leakage out of macroelectrodes placed in protein solution causes additional potentials to the Donnan potential. The time course of the potential observed when the reference electrode remains in the outer buffer and the measuring electrode is placed into protein solution appears to be dependent on the KCl leakage rate from the electrode, the type and volume of the sample and the membrane area of the sample compartment. Drifts towards more negative values were usually observed whose rate seemed to be dependent on the sample viscosity. For more viscous proteins the potentials changed so slowly that the transient potentials could be interpreted as the equilibrium value of the Donnan potential and lead to reduced values of the net charge or even positive values for negatively charged proteins. Comparison of the potentials obtained with micro- and macroelectrodes for the same protein at similar concentration reveals that an agreement between the values is obtained if the potential value recorded with macroelectrodes at the first plateau is taken. It would be impossible, however, to know which value of the potential recorded with macroelectrodes, which was changing over time, is the true Donnan equilibrium potential without the microelectrode measurement. It is not clear, however, if the slow rate of the changes in the potentials recorded for viscous solutions (F-actin, Tm-tn, RTFs) is due to long response time of the electrode or KCl leakage and accumulation. For the BSA samples, which are less viscous, there is not such an ambiguity in the interpretation of the results since the potentials soon after placing the electrode in the protein solution are in agreement with the microelectrode potentials. Thus macroelectrodes can provide accurate measure of the equilibrium Donnan potential provided that the time course of the potential is obtained and interpreted correctly.

In order to minimize the errors on the resulting values of the charge, electrodes with minimum KCl leakage rates (1 $nmol \cdot s^{-1}$ or less) and sample compartments made entirely of semi-permeable membrane should be used. The use of the set-up with two compartments does not eliminate the problems stemming from the KCl outflow. The rates of leakage are likely to be different for the compartment with buffer and the protein sample. Having the reference electrode inside a compartment, where KCl accumulation can occur, obscures the phenomena occurring in the experimental system.

Some of the early microelectrodes exhibited a characteristic drop in potential towards more positive values when the electrode was placed in the protein sample for the first time and then reduced negative potentials were obtained. If a new electrode was used for the same sample, reduced potentials were also obtained, suggesting that sample contamination had taken place. The experiment with simulated leakage showed that the addition of $\mu$molar amounts of KCl to the BSA sample caused large changes in the registered potentials similar to those observed for some forceps-blunted electrodes. These combined observations suggest that very large outflow of KCl took place when these drops in potential were observed. Taking into account time scale of the changes in potentials observed, one obtains the outflow rate approximately 3 orders of magnitude larger than in case of later electrodes. This suggests that those microelectrodes were leaking KCl much more than later electrodes for which the rates were measured. It is in agreement with the fact that the earlier electrodes had tips of larger diameters, although not all of the electrode tips were measured. To prevent clogging larger fragments were broken off the tip. Interestingly, the additions of KCl to the sample compartment caused the potential recorded with microelectrodes to become more positive as opposed to the changes seen in the potentials registered with macroelectrodes and associated with leakage of KCl.

The microelectrode technique was found to be very suitable for use with low viscosity protein solutions of BSA, viscous protein solutions of Tm-tn and dilute gels of F-actin

and RTFs. Microelectrodes with tip diameters approximately 5–20 $\mu$m and resistance less than 1 M$\Omega$, give reproducible results. Most electrodes with this tip size give stable readings unless they get clogged up by the protein which leads to an increase in resistance and erratic values of potential. This usually occurred after only a few measurements for both the 'jagged' and bevelled electrodes, the bevelled electrodes not lasting on average longer than the 'jagged' ones.

An important observation was that the problem of microelectrode clogging can be overcome by renewing their liquid junction and making most of the electrodes last as long as was required for the measurements. This was discovered to be achieved by tightening the electrode holder a very small fraction of a turn which slightly increased the pressure of the filling solution inside the holder and electrode and pushed the clogging protein out of the tip. This procedure was very successful when applied to electrodes blunted with forceps. Since it is much easier and faster to manufacture blunted electrodes by breaking their tip off with forceps than to bevel them with an electrode grinder and since the performance of 'jagged' electrodes was very satisfactory with an occasional junction renewal, I decided to use this type of electrode for my measurements described in chapter 5.

The microelectrode technique has an advantage in comparison to the macroelectrode technique that the size of the measuring electrode is very small in relation to the sample size and also the KCl leakage rate is lower than for macroelectrodes. Hence a microelectrode does not affect the sample as much as a macroelectrode and the readings are stable instantly after immersion of the electrode into the sample. Since the transfer of the microelectrode between the outer buffer and the protein causes negligible protein dilution and the immersion of the electrode in the protein sample does not cause KCl accumulation that would lead to observable additional potentials, one can repeat the measurements of the potentials to achieve greater accuracy and determine the protein concentration afterwards.

## 4.5 Conclusions

The following main conclusions can be drawn:

1. The macroelectrode technique is more suited for protein solutions of low viscosity like BSA. In higher viscosity samples such as F-actin or RTFs the initial potentials registered after placing an electrode in the protein sample can be interpreted as Donnan potentials. This can lead to obtaining very reduced negative or even positive value of charge for negatively charged proteins. In case of low viscosity samples, KCl leakage from macroelectrodes can cause large errors in the Donnan potentials. These can be minimized if electrodes with leakage rates of 1 $nmol \cdot s^{-1}$ or less are used in a set-up with one sample compartment entirely made of dialysis tubing. The analysis of the time course of the potentials is crucial for the detection of the effects caused by KCl leakage and accumulation.

2. Reproducible values of the Donnan potentials can be obtained with microelectrodes for protein solutions of low and high viscosity. Electrodes of resistance less than 1 M$\Omega$ and tip size approximately 5–20 $\mu$m can be used for protein solutions. Microelectrodes do not affect the samples in the same way as macroelectrodes do: the KCl outflow rate is an order of magnitude lower for microelectrodes of tip sizes up to 25 $\mu$m and, due to the small tip size, the transfer of the electrode between the outer buffer and the protein sample does not cause its dilution. Microelectrodes, however, tend to clog up in protein solutions, which leads to an increase in resistance and erratic potential values. This can be overcome by renewing the microelectrode liquid junction by slight tightening of the holder.

# Chapter 5

# Calcium effect on thin filament charge

## 5.1 Introduction

Calcium is the triggering factor for muscular contraction. In a resting muscle the free calcium concentration in the sarcoplasm is maintained at approximately 0.1 $\mu$M by the operation of an ATP driven $Ca^{2+}$ pump. A nerve impulse stimulates a release of $Ca^{2+}$ from the sarcoplasmic reticulum into the sarcoplasm raising its concentration to about 10 $\mu$M. The role of the tropomyosin-troponin complex in the calcium regulation of muscle contraction was reviewed in section 1.3.3. The mechanism of calcium regulation at the molecular level, however, still remains unexplained and as challenging as the mechanism of muscular contraction itself.

Experiments with glycerinated rabbit psoas muscle fibres in our laboratory revealed a cooperative change in the Donnan potentials occurring with changes in the free $Ca^{2+}$ concentration, $[Ca^{2+}]$, (Coomber and Elliott, 1995, 1996). Also Donnan potential measurements were carried out on gels of F-actin and reconstituted thin filaments in our laboratory, which suggested that there was a change in the charge of these proteins with $[Ca^{2+}]$ (Jennison, 1992). The results of these studies were described in section 1.6.2.

The aim of the work described in this chapter was to measure the net electric charge on

the tropomyosin-troponin complex (Tm-tn), F-actin and reconstituted thin filaments (RTFs) as a function of the concentration of free $Ca^{2+}$. Also a parallel experiment was to be conducted on a protein known to bind $Ca^{2+}$ and $Mg^{2+}$ in a non-specific manner. For the control protein, BSA was chosen since albumins bind $Ca^{2+}$ and $Mg^{2+}$ ions with low affinities. Human serum albumin binds $Ca^{2+}$ with association constant, K, approximately $1\times10^{3}$ $M^{-1}$ at pH 7.4 and ionic strength 0.15, whereas it binds $Mg^{2+}$ with K approximately $1\times10^{2}$ $M^{-1}$ (Peters, 1996).

The difference in Donnan potentials with changes in $[Ca^{2+}]$, observed in our laboratory for rabbit muscle fibres, was of the order of 0.5–2mV at ionic strength 72 mM (Coomber and Elliott, 1995, 1996). The protein concentration in muscle is high, for example actin concentration in the thin filament is approximately 400 mg/ml as can be calculated from the data in Bagshaw (1993). It was not possible experimentally to isolate pure proteins in quantities producing concentrations of this magnitude in samples of sufficient size for Donnan potential measurements. Even if the effects observed in the whole muscle were to be manifest in reconstituted thin filaments or their components, it would not be possible to detect them using samples of concentrations at least an order of magnitude lower since Donnan potential is proportional to protein concentration (see figure 1.5b). Another feature of Donnan potential needed to be exploited, namely its dependence on ionic strength (see figure 1.5a). One can obtain higher values of the Donnan potential if the ionic strength of the solution is lowered, although this may mean that the measurements are carried out under less physiological conditions.

An important consideration is that both Tm-tn and F-actin are negatively charged at neutral pH (see table B.2) and one could expect a strong electrostatic repulsion between the two, especially at lower ionic strength, when the Debye length becomes larger. Indeed Tm-tn dissociates from F-actin at low ionic strength, and this effect is used in the isolation of Tm-tn from muscle acetone powder described in section 2.3.5, where the separation is carried out in water. Eisenberg and Kielley (1970) found

that the inhibition, in the presence of EGTA, of the acto-HMM and acto-S1 ATPase by Tm-tn disappeared at a KCl concentration below 15 mM. They attributed this effect to a possible dissociation of Tm-tn from F-actin. Jennison (1992) carried out a reconstitution of thin filaments using a 1:1 ratio of Tm-tn and actin (w/w) and found that when the reconstitution took place in the rigor buffer or its 2-fold dilution, the percentage of Tm-tn in the gel was approximately 33%. If the reconstitution was carried out in a 5-fold dilution of buffer R, the percentage was only about 15%.

Therefore, before attempting to measure the Donnan potentials, it was necessary to establish how low an ionic strength could be used without causing a dissociation of Tm-tn from F-actin. It was anticipated that use of lower ionic strength solutions could be made than a 2-fold dilution of the rigor buffer, if the thin filaments were reconstituted under standard conditions and the ionic strength was lowered later.

## 5.2 Method

### 5.2.1 Experimental solutions

The solutions with various [$Ca^{2+}$] used for the experiments described in this chapter were prepared with special care as outlined in section 2.1. A Ca-EGTA buffer system was used to achieve a wide range of free $Ca^{2+}$ concentrations down to nanomolar levels. The total concentration of $CaCl_2$ and EGTA used was 1 mM, and the proportion of their concentrations was varied. The base solutions, to which the Ca-EGTA buffer and $NaN_3$ were added, were dilutions of the rigor buffer (buffer R).

The use of several n-fold dilutions of buffer R (where n = 2,4,5,6,7,8,9,10 and 20) was made for the determination of the ionic strength sufficient to maintain the bonding between Tm-tn and F-actin. Also, 0.005% $NaN_3$ was added to the R/2 solution which was the starting solution for subsequent dilutions. Two series of the dilutions were prepared i.e. with high and low [$Ca^{2+}$] (containing 0.6mM $CaCl_2$ and 0.4 mM EGTA or 0.01 mM $CaCl_2$ and 0.99 mM EGTA, respectively).

Table 5.1: Composition of the experimental solutions with varied free $Ca^{2+}$ concentration used for Donnan potential measurements (pCa buffers). All solutions contained 10 mM KCl, 0.5 mM $MgCl_2$, 0.002% $NaN_3$, 2 mM potassium phosphate, pH 7.0.

| Total concentration (mM) | | Concentration of free ions | | Ionic strength |
|---|---|---|---|---|
| $CaCl_2$ | EGTA | $Ca^{2+}$ (pCa) | $Mg^{2+}$ (mM) | (mM) |
| 0.01 | 0.99 | 8.7 | 0.42 | 19.0 |
| 0.05 | 0.95 | 7.9 | 0.42 | 19.0 |
| 0.20 | 0.80 | 7.1 | 0.43 | 18.8 |
| 0.40 | 0.60 | 6.4 | 0.44 | 18.6 |
| 0.50 | 0.50 | 5.1 | 0.44 | 18.5 |
| 0.60 | 0.40 | 3.9 | 0.44 | 18.4 |
| 1.00 | 0.00 | 3.2 | 0.45 | 18.0 |

The base solution for the Donnan potential measurements was a 10-fold dilution of buffer R (10 mM KCl, 0.5 mM $MgCl_2$, 2 mM potassium phosphate buffer, pH 7.0) with the addition of 0.002% $NaN_3$. The concentrations of $CaCl_2$ and EGTA which were added to these solutions are given in table 5.1. The table also contains the free $Ca^{2+}$ and $Mg^{2+}$ concentrations and ionic strength which were calculated using the PERRIN program (Abbott, 1976) with the stability constants listed in table A.1 in appendix A. The concentration of free $Mg^{2+}$ and ionic strength varied very little between the solutions of the series.

### 5.2.2 Protein preparation

**F-actin** was isolated following the procedure described in section 2.3.4 (Pardee and Spudich, 1982). Tm-tn and RTFs were prepared according to the method of Murray (1982) as described in sections 2.3.5 and 2.3.6 respectively. BSA fraction V was purchased from BDH.

F-actin pellets were covered with 2 ml of the solution that they were in at the final stage of isolation (50 mM KCl, 1 mM $MgCl_2$, 1 mM $Na_2ATP$, 0.2 mM $CaCl_2$, 0.5 mM $\beta$-mercaptoethanol, 0.02% $NaN_3$, 2 mM Tris-HCl, pH 8.0). They were then stored on ice and used within 2 weeks. After 1 week, when the pellets became less

firm, they were re-centrifuged in a Beckman 90Ti rotor at 155 000×g for 1.5 hours at 4°C. In order to transfer the protein into a pCa buffer, the pellet was re-suspended in the desired pCa buffer and subsequently the protein solution was dialysed against 1 *l* of the buffer overnight with rapid stirring on ice. The protein solution was then divided into six 0.25 ml samples which were used for Donnan potential measurements.

Pellets of **RTFs** were treated in the same way as pellets of F-actin, except for the medium used to cover them during storage which was 0.1 M KCl, 2 mM $MgCl_2$, 0.2 mM DTT, 10 mM Tris-HCl, 0.02% $NaN_3$, pH 7.0.

**Tm-tn** was initially concentrated by dialysis against a pCa 7.1 buffer to which polyethylene glycol (of MW 20 kDa) was gradually added. The concentration process typically took several hours, the initial and final protein concentrations were approximately 3 and 10 mg/ml respectively. The concentrated protein solution was stored on ice and used within a week. Aliquots of 1.8 ml of the protein solution were dialysed against 1 *l* of a pCa buffer overnight on ice and then each of them was divided into six 0.25 ml samples which were used for Donnan potential measurements.

**BSA** was dissolved in a pCa buffer at a concentration approximately 10 mg/ml. The protein solution was then dialysed against 1 *l* of that buffer overnight on ice.

### 5.2.3 Tropomyosin-troponin binding to actin

The protein concentration was determined in the pellet and supernatant after centrifuging RTFs that had been incubated in solutions of various ionic strengths. The microbiuret method (described in section 2.2) was used for the protein determination.

RTFs in R/2 buffer with 0.005% $NaN_3$ and high or low $[Ca^{2+}]$ (containing 0.6mM $CaCl_2$ and 0.4 mM EGTA or 0.01 mM $CaCl_2$ and 0.99 mM EGTA, respectively) were used for the experiment. 50 $\mu$l protein samples were transferred to 2 ml centrifuging tubes and diluted to obtain a series of n-fold dilutions of the R buffer (where n = 2,4,5,6,7,8,9,10 and 20), the $CaCl_2$ and EGTA concentrations were, how-

ever, maintained as in the starting solutions. The resulting pCas for these solutions were calculated with the PERRIN program (Abbott, 1976). There was a negligible increase in the pCa values with dilution for the low $[Ca^{2+}]$ series (from 8.63 for the R/2 solution to 8.66 for the R/20 solution), with the average of 8.6 for this series. There was some decrease in the pCa values with dilutions for the high $[Ca^{2+}]$ series (from 4.3 for the R/2 solution to 3.8 for the R/20 solution), with the average pCa of 4.0 for this series.

The concentrations of the diluted samples were around 1.7 mg/ml. The samples were mixed on a rotary stirrer at 8°C for 1 hour and then they were left on ice for the night. The following morning the samples were centrifuged at 100 000×g in a Beckman 90Ti rotor for 2 hours at 2°C. After removing and reserving the supernatant, the pellet was gradually transferred into 3.5 ml of NaOH, used in the microbiuret assay, by adding initially 0.5 ml and then three times of 1 ml, of NaOH to the tube and vortexing the contents. The mass of the pellet was determined for the low $[Ca^{2+}]$ series, these pellets contained slightly more protein than the high $[Ca^{2+}]$ series samples (on average 0.87 mg compared to 0.82 mg for the other series). The empty tubes were weighed as well as the tubes with the pellet. The mass difference was between 10 and 20 mg, the exact mass of pellet was difficult to determine due to some moisture on the walls of the tubes and also a small amount of solution left on the surface of the pellet. The mass of the pellet, however, could not have been greater than 10 or 20 mg, and in the calculations of the relative amount of protein in the pellet and supernatant, the supernatant volume was assumed to be 0.5 ml and the pellet volume negligible.

## 5.3 Results

### 5.3.1 Concentration of free $Ca^{2+}$

Two methods were used to verify the concentrations of free $Ca^{2+}$ obtained using the PERRIN program: a calculation method utilizing an apparent binding constant $K_{app}$

and an experimental method involving the use of $Ca^{2+}$ sensitive electrodes.

### Calculation of $[Ca^{2+}]$ from $K_{app}$

The apparent binding constant ($K_{app}$) method (described in section 2.7) is a method widely used throughout literature to calculate the concentrations of free $Ca^{2+}$ in solutions.

Two values of the apparent binding constant $K_{app}$ were taken from literature: $4.8\times10^{6}$ $M^{-1}$ (Reuben *et al.*, 1971) and $4.2\times10^{6}$ $M^{-1}$ (derived from Harafuji and Ogawa, 1980). The former had been calculated from individual stability constants for pH 7.0. The latter value was obtained by adjusting an experimental $K_{app}$ $9.72\times10^{5}$ $M^{-1}$ of Harafuji and Ogawa (1980) which had been determined in a solution containing 0.1 M KCl, 10 mM potassium phosphate buffer (pH 6.8), of ionic strength 0.12 M. This value was adjusted to ionic strength 18.6 mM and pH 7.0. The adjustment for ionic strength was made using the Hückel equation (equation 2.3) with the parameters as given in Harafuji and Ogawa (1980). The adjustment for pH was made according to the relationship obtained by Harafuji and Ogawa (1980): $\Delta \log_{10} K_{app} = 2 \times \Delta\text{pH}$. These corrections gave the final value of $K_{app}$ equal to $4.2\times10^{6}$ $M^{-1}$, which was used.

The effect of $Mg^{2+}$ on the $K_{app}$ for Ca-EGTA was neglected. In order to estimate whether this was justified, the data from the PERRIN program output files was used to calculate the concentrations of the EGTA complexes with the metal ions present in solutions. The results are plotted in figure 5.1. It can be seen that EGTA forms complexes predominantly with $Ca^{2+}$ as would be expected. At very high pCas however, the concentration of the complexes of EGTA with $Ca^{2+}$ decreases to become slightly lower than the concentration of the EGTA complexed with $Mg^{2+}$. The presence of monovalent ions could certainly be neglected, whereas neglecting the presence of $Mg^{2+}$ may cause some inaccuracies at pCas above 8.

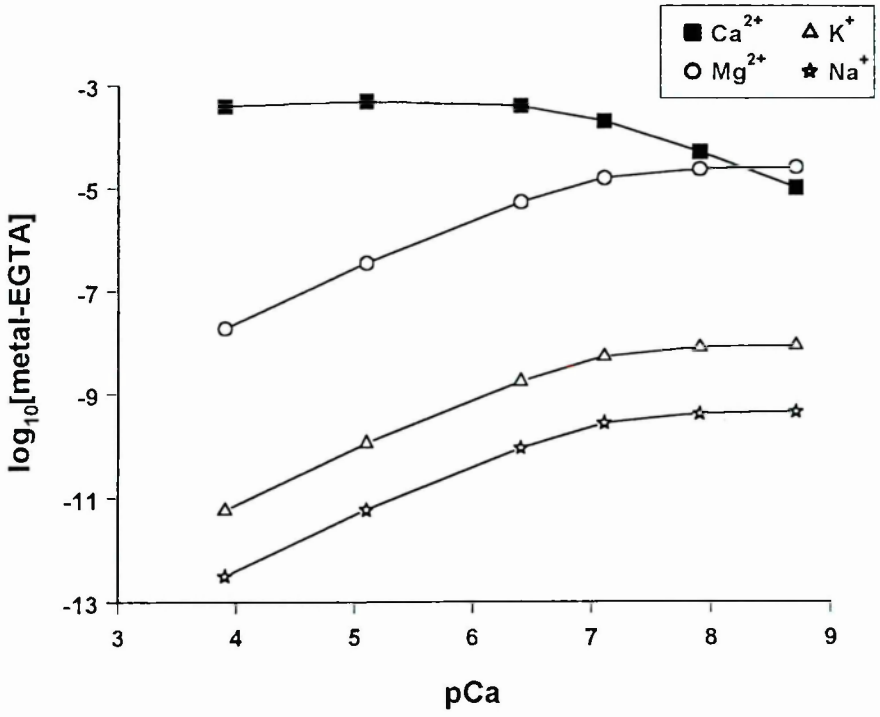


Figure 5.1: The amounts (on a logarithmic scale) of EGTA in complexes with $Ca^{2+}$, $Mg^{2+}$, $K^{+}$ and $Na^{+}$ in the pCa buffers used for the Donnan potential measurements.

The pCa values obtained for our experimental solutions by solving the set of equations 2.1 using two values of apparent binding constants are given in table 5.2. An excellent agreement between the values obtained using the PERRIN program and the apparent binding constants can be seen.

A calculation was also made to determine the pCa of the solution used by Coomber and Elliott (1995, 1996), whose pCa was reported to be 6.2, in order to be able to relate our results to the results obtained with muscle fibres. The PERRIN program was also used in their calculations, however, different sets of stability constants were used. The pCa obtained for this solution was 6.8. The discrepancy can be explained by the fact that a formation of six calcium containing complexes in our set of stability constants was considered, as opposed to three complexes that were considered in their set of stability constants. Hence $[Ca^{2+}]$ obtained using the set of 6 stability constants was lower.

Table 5.2: Comparison of the free $Ca^{2+}$ concentration in solutions whose composition was given in table 5.1 calculated using the PERRIN program (Abbott, 1976) and two values of apparent binding constants $K_{app}$.

| Concentration of free $Ca^{2+}$ (pCa) | | |
|---|---|---|
| Calculated with PERRIN | Calculated from $K_{app}$ | |
| | $K^{\star}_{app}$ $4.8\times10^{6}$ $M^{-1}$ | $K^{\dagger}_{app}$ $4.2\times10^{6}$ $M^{-1}$ |
| 8.7 | 8.7 | 8.6 |
| 7.9 | 7.9 | 7.9 |
| 7.1 | 7.2 | 7.1 |
| 6.4 | 6.4 | 6.3 |
| 5.1 | 5.0 | 5.0 |
| 3.9 | 3.7 | 3.7 |
| 3.2 | 3.0 | 3.0 |

$\star$ $K_{app}$ calculated from stability constants for pH 7.0 by Reuben *et al.* (1971).

$\dagger$ $K_{app}$ obtained from a value determined experimentally at pH 6.8, ionic strength 0.12 M, 20°C by correcting it to ionic strength 18.6 mM and pH 7.0 (Harafuji and Ogawa, 1980).

### Electrode determination of $[Ca^{2+}]$

The measurements were performed as described in section 2.8. Potentials for the pCa buffers and standards ($CaCl_2$ solutions in 10 mM KCl) were measured with two types of $Ca^{2+}$ sensitive electrodes: IS 561-Ca (Müller, Switzerland) and Elit 041 (Merck, England).

The data obtained with the Müller electrode indicated a loss of sensitivity of this electrode as the range of potentials recorded for the pCa buffers decreased from about 120 mV in the first experiment to about 65 mV in the second experiment which was carried out a week after the first one. The other electrode (from Merck) gave more reproducible results and these results are presented here.

Values of the potentials obtained with the Merck electrode for the pCa buffers are plotted against the calculated values of pCa in figure 5.2. In this figure the potentials recorded for standards are also drawn as a function of the concentrations of $CaCl_2$ added to the 10 mM KCl solutions.

There is not such a good agreement between the potentials recorded for the standard

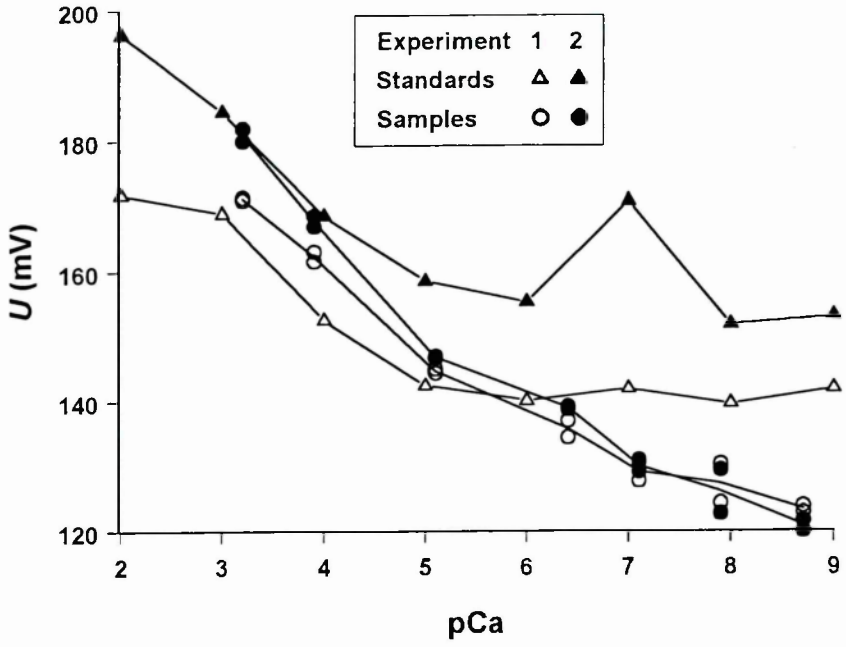


Figure 5.2: Potentials recorded with $Ca^{2+}$ sensitive electrode Elit 041 (Merck) for the experimental pCa buffers and standards. Standards were 10 mM KCl solutions containing various amounts of added $CaCl_2$ and the potentials for the standards are plotted against the pCa of added $CaCl_2$. The potentials for pCa buffers are plotted against the pCa values calculated using the PERRIN program (Abbott, 1976).

solutions in the two experiments as there is for the solutions with the Ca-EGTA buffering system. The same standard solutions gave potential values much higher after being stored for one week in plastic containers in a refrigerator. The plastic must have released some calcium in that period of time. The flattening of the curve, for the standards at about 1–10 $\mu$M of $CaCl_2$ added, is not a result of the electrode detection limit having this value, since the electrode gave lower potentials for three pCa buffers. It can be concluded that all the standard solutions contained a high background level of free $Ca^{2+}$. This was about 1–10 $\mu$M (in the first experiment), as might be expected for solutions not containing EGTA. Hence only the standards with $CaCl_2$ concentrations $10^{-3}$, $10^{-4}$, $10^{-5}$ M could be used to calibrate the pCa buffers. The lack of reproducibility in the measurements for the standards, however, proves their very limited value.

The relationship between the potentials recorded for the pCa buffers and the values of pCa has a curve shape typical for the so-called electrode function curve of an ion selective electrode (Ammann, 1986). It has a linear range at higher free ion concentrations (or strictly speaking activities), according to the Nernst equation. At lower activities of the ion, the curve flattens out until there is no further change of the recorded potentials with the changes in the ion activity. All the pCa buffers had $[Ca^{2+}]$ above the detection limit of the electrode. Different potentials obtained from the buffers with different calculated pCas confirm that there were differences in the pCa values between them.

The overall conclusion is that the actual concentrations of free $Ca^{2+}$ could not be determined accurately using the $Ca^{2+}$ sensitive electrodes, even at millimolar level, due to a lack of available standards with precise and stable concentrations of calcium. Since the pCa values obtained with the PERRIN program could be verified satisfactorily with another method, those pCa values will be used as accurate measures of the free $Ca^{2+}$ concentrations in the experimental solutions.

### 5.3.2 SDS-PAGE protein purity determination

12.5% SDS-PAGE gels were run to check all the protein preparations, the system described in section 2.4.1 was used. The interpretation of the band pattern is based on Bagshaw (1993).

Figure 5.3 contains a photograph of an actin gel together with a densitometer scan of an overloaded lane (lane B of the gel). The densitometer scan is plotted as the relative absorbance (normalized to the absorbance of the strongest peak) against relative mobility $R_f$ (defined as the ratio of the distance, from the start of the resolving gel, migrated by the protein divided by the distance migrated by the buffer). This method of presenting the densitometer scans was chosen in order to allow direct comparison between gels.

A photograph of a gel with two batches of Tm-tn is shown in figure 5.4. Only the 1st batch was used in the microelectrode measurements presented in this chapter, the 2nd batch was used in earlier macroelectrode measurements, whose results are not given in this thesis. These protein preparations were not pure, the main impurity was actin, whose band is of similar intensity to the bands of tropomyosin and troponin T. Other bands that correspond to contaminants are also quite pronounced – one running close to the buffer front and several bands with proteins of higher molecular weight than actin, possibly fragments of the heavy chain of myosin.

Figure 5.5 contains a photograph of a gel where RTFs, as well as G-actin and Tm-tn used for the reconstitution, are shown. Tm-tn was not pure and contained impurities similar to other preparations of this protein complex (shown in figure 5.4). In the process of the reconstitution however, only the desired proteins from the preparation had bound to actin since the RTFs were purer than Tm-tn.

Figure 5.6a contains densitometer scans of lanes B and D from the Tm-tn gel shown in figure 5.4. A scan of a lane containing RTFs (lane G from the RTFs gel presented in figure 5.5) is shown in figure 5.6b. A comparison of the scans of Tm-tn and RTFs

(a)

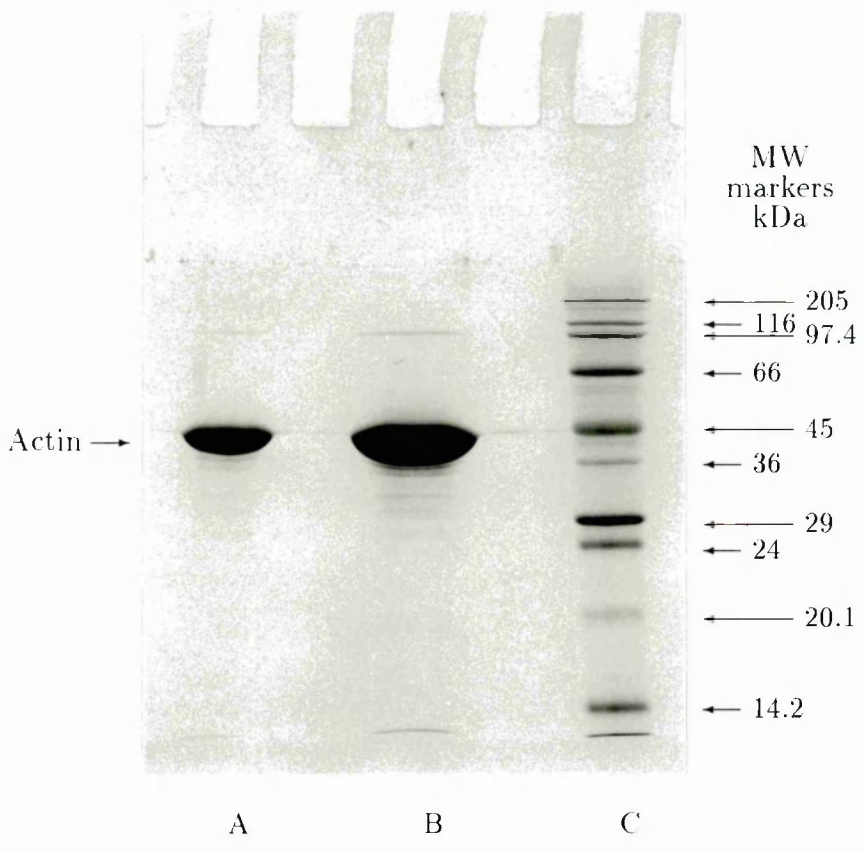


(b)

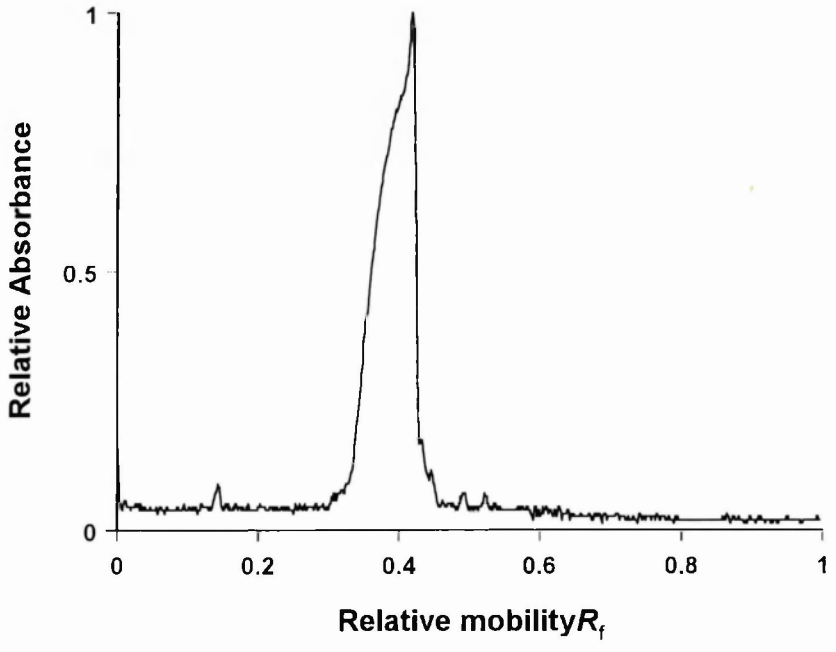


Figure 5.3: (a) 12.5% SDS-PAGE of rabbit actin. The molecular weights of the markers are given on the right. Gel lanes: A. and B. actin (6.5 and 19 $\mu$g respectively), C. MW markers. Diagram (b) shows a densitometer scan of lane B of the above gel.

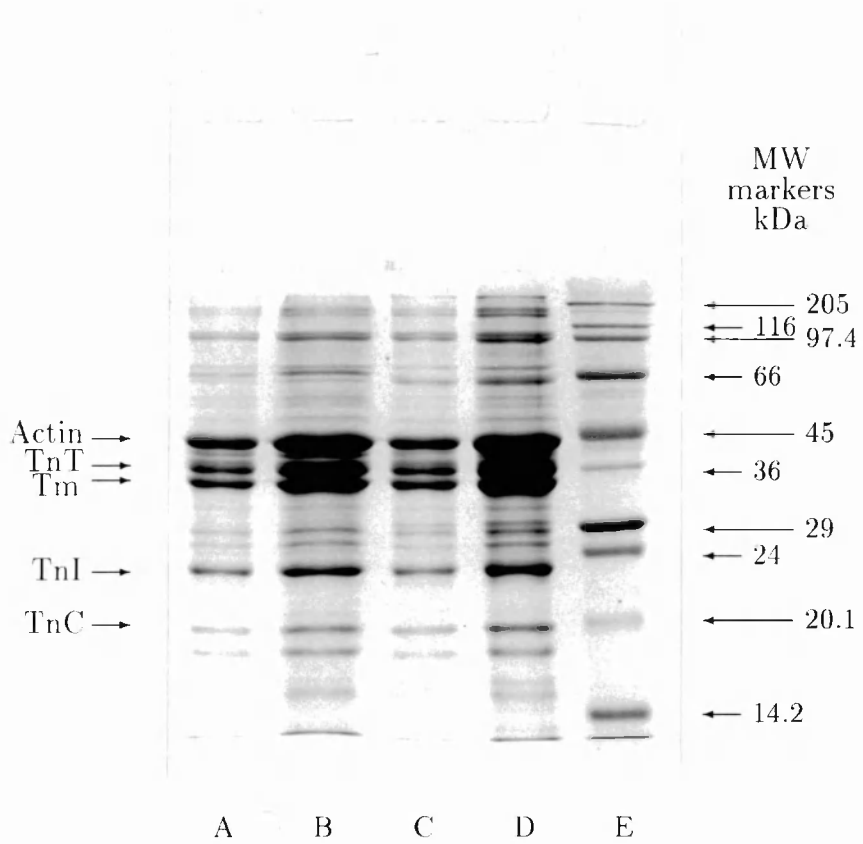


Figure 5.4: 12.5% SDS-PAGE of rabbit Tm-tn. The molecular weights of the markers are given on the right and the bands in the protein preparation are indicated on the left. Lanes: A. and B. Tm-tn (1st batch), C. and D. Tm-tn (2nd batch), E. MW markers. The quantity of Tm-tn applied was: 3 $\mu$g for lanes A,C and 9 $\mu$g for lanes B,D. Only the 1st batch was used in the microelectrode measurements presented in this chapter, the 2nd batch was used in earlier macroelectrode measurements, whose results are not given in this thesis.

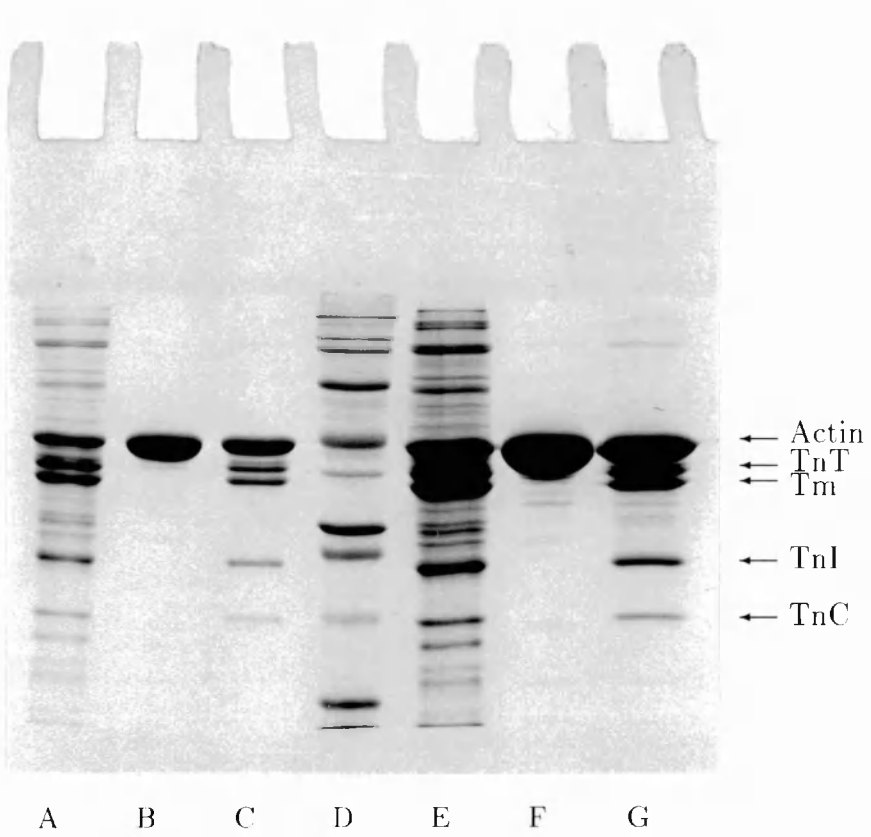


Figure 5.5: 12.5% SDS-PAGE of rabbit RTFs. The bands in proteins under study are indicated, MW markers were as in figure 5.4. Lanes: A. Tm-tn used for the reconstitution (3 $\mu$g), B. G-actin used for the reconstitution (3.7 $\mu$g), C. RTFs (7 $\mu$g), D. MW markers, lanes E,F,G are a repeat of the first 3 lanes with the protein amount increased 3-fold.

Table 5.3: Comparison of the theoretical and experimental protein ratios in the preparation of Tm-tn and RTFs. The experimental values were determined by SDS-PAGE with respect to the amount of tropomyosin present and are means of 6 ratios ± SD.

| Protein band | Protein preparation | | | |
|---|---|---|---|---|
| | Tm-tn | | RTFs | |
| | SDS-PAGE | Theory | SDS-PAGE | Theory |
| Actin | 2.0 ±0.1 | 0 | 5.4 ±0.5 | 7 |
| TnT | 1.9 ±0.1 | 1 | 2.4 ±0.1 | 1 |
| Tm | 1 | 1 | 1 | 1 |
| TnI | 1.1 ±0.1 | 1 | 1.2 ±0.2 | 1 |
| TnC | 0.31±0.05 | 1 | 0.48±0.13 | 1 |

lanes reveals a good agreement between the $R_f$ values of the corresponding peaks. Also the purifying effect of the reconstitution procedure can be clearly seen.

The ratios of the proteins in the preparations of Tm-tn and RTFs were determined as described in section 2.4.1 and are presented in table 5.3 together with the theoretical values. Six lanes in the linear range of the relationship between the peak area and protein amount were taken from 12.5% gels for the determination of the ratios for both Tm-tn and RTFs.

The molecular weights of the proteins were determined using linear regression. The relationship of the $\log_{10}$MW versus the distance of migration from the beginning of the resolving gel, $D_m$, was determined to be linear up to 45 kDa in the 12.5% gels, although there was slight indication of a deviation from linearity for the 45 kDa marker. Hence the markers with MW up to 45 kDa were used to determine the MW of actin, whereas markers with MW up to 36 kDa were used for the determination of the MW for the other proteins which had higher mobility than the 36 kDa marker (Tm, TnT, TnI, TnC). For each protein, six protein lanes taken from 4 gels were analysed. The results are presented in table 5.4 together with the values of the true MW calculated from the sequence (from table B.2).

There is generally a reasonable agreement between the experimental and true molecular weights for the proteins isolated, except for troponin T, for which the MW, deter-

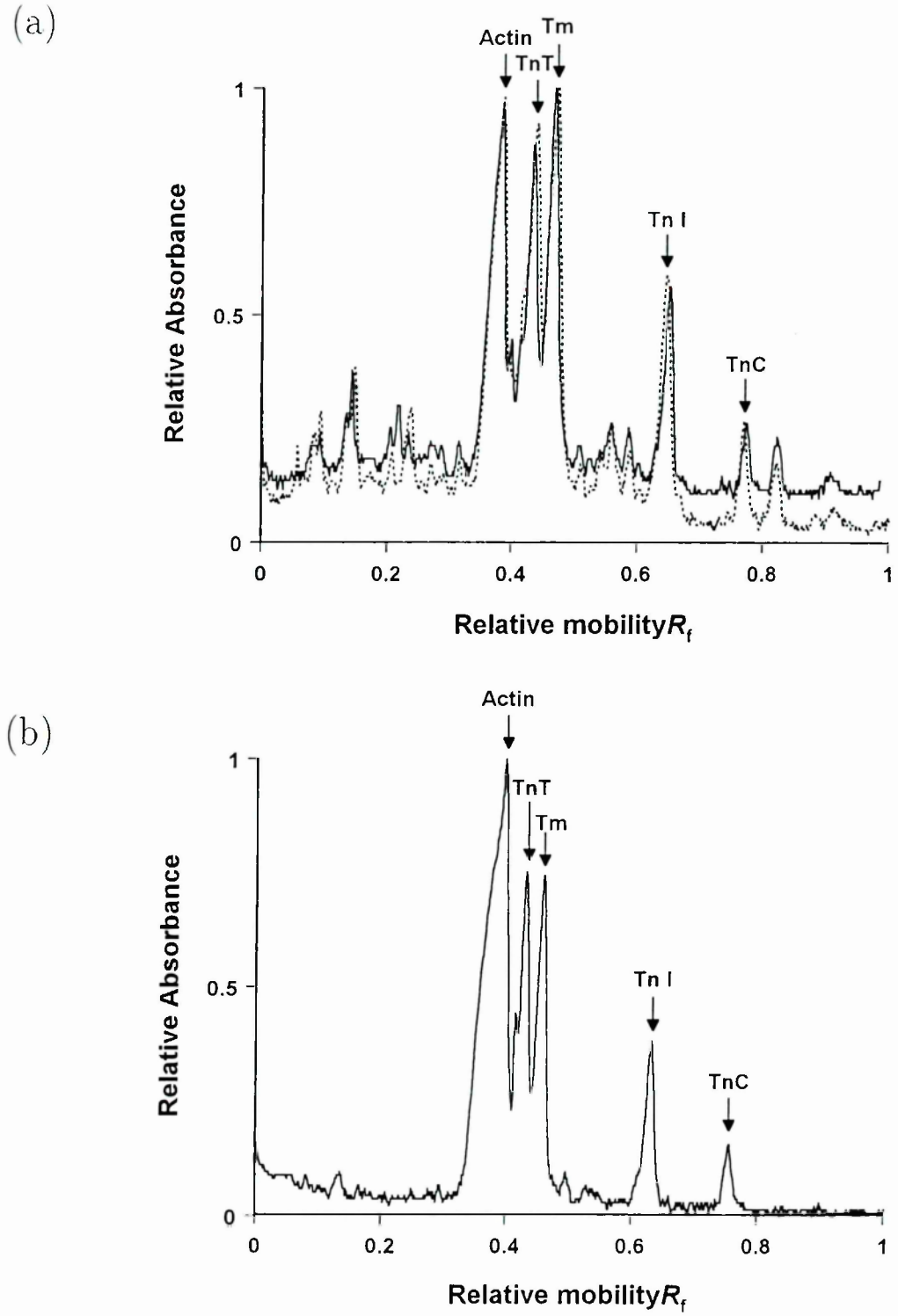


Figure 5.6: Densitometer scans of 12.5% SDS-PAGE gels. (a) Tm-tn (lanes B and D from the gel shown in figure 5.4 are plotted with the solid and dotted lines respectively). (b) RTFs (lane G from the gel presented in figure 5.5).

Table 5.4: Molecular weight of actin and the components in the preparations of Tm-tn complex and RTFs determined from 12.5% SDS-PAGE gels and calculated from the sequence in kDa. The molecular weights determined from the gels are means ± SD of values obtained from 6 protein lanes collected from 4 gels for each preparation.

| Protein band | Protein preparation | | | Calculated MW (fast muscle) |
|---|---|---|---|---|
| | Actin | Tm-tn | RTFs | |
| Actin | 40.5±1.2 | 40.7±0.6 | 39.8±1.0 | 42.1 |
| TnT | - | 35.3±0.5 | 35.5±0.8 | 30.6 |
| Tm($\alpha$) | - | 33.5±0.4 | 33.7±0.7 | 32.7 |
| TnI | - | 24.2±0.3 | 24.5±0.6 | 21.1 |
| TnC | - | 19.3±0.2 | 19.6±0.5 | 18.0 |

mined from gels, is higher. In fact troponin T has a lower true MW than tropomyosin but it displays lower mobility in the gel than tropomyosin. This phenomenon has been observed in SDS-PAGE gels of rabbit myofibrils (Bagshaw, 1993; Wang, 1982).

### 5.3.3 Tropomyosin-troponin binding to actin

A centrifuging study was carried out as described in section 5.2.3. The relative amounts of protein in the supernatant and pellet, after centrifuging the RTFs incubated in solutions of various ionic strength, are plotted in figure 5.7. A complete dissociation of the Tm-tn from actin would result in the presence of the dissociated protein in the supernatant fraction. In that case, the relative amounts of protein would be approximately 31% and 69% for the supernatant and pellet fractions respectively. This was not observed even at the lowest ionic strength, for all samples the relative amount of protein in the supernatant was lower than 10%. On the basis of these results it was decided to carry out Donnan measurements at lower ionic strength than those performed with muscle fibres. A 10-fold dilution of buffer R was chosen as the base solution for our buffers with varied $[Ca^{2+}]$.

A comparison was made of the SDS-PAGE band pattern of RTFs immediately after reconstitution and after completing the Donnan potential measurements at low ionic strength. The filaments that were left over from Donnan potential measurements were

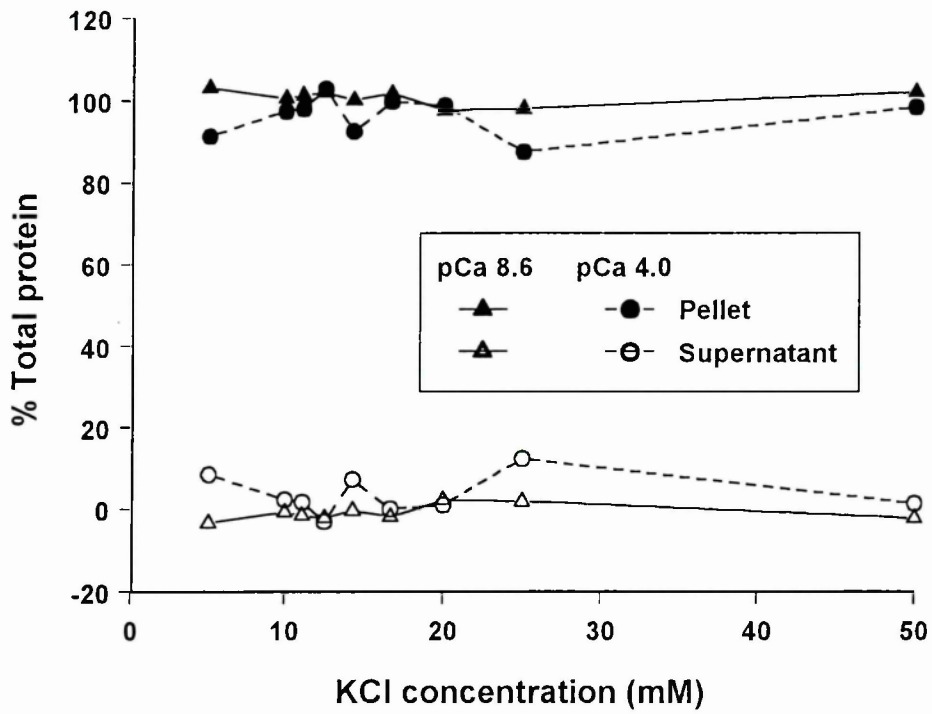


Figure 5.7: Protein distribution between supernatant and pellet for RTFs in solutions of various ionic strength, which were dilutions of buffer R (0.1 M KCl, 5 mM $MgCl_2$, 20 mM potassium phosphate, pH 7.0). RTFs were incubated at concentrations approximately 2mg/ml in the appropriate solutions overnight on ice and centrifuged at 100 000×g for 2 hrs at 2°C.

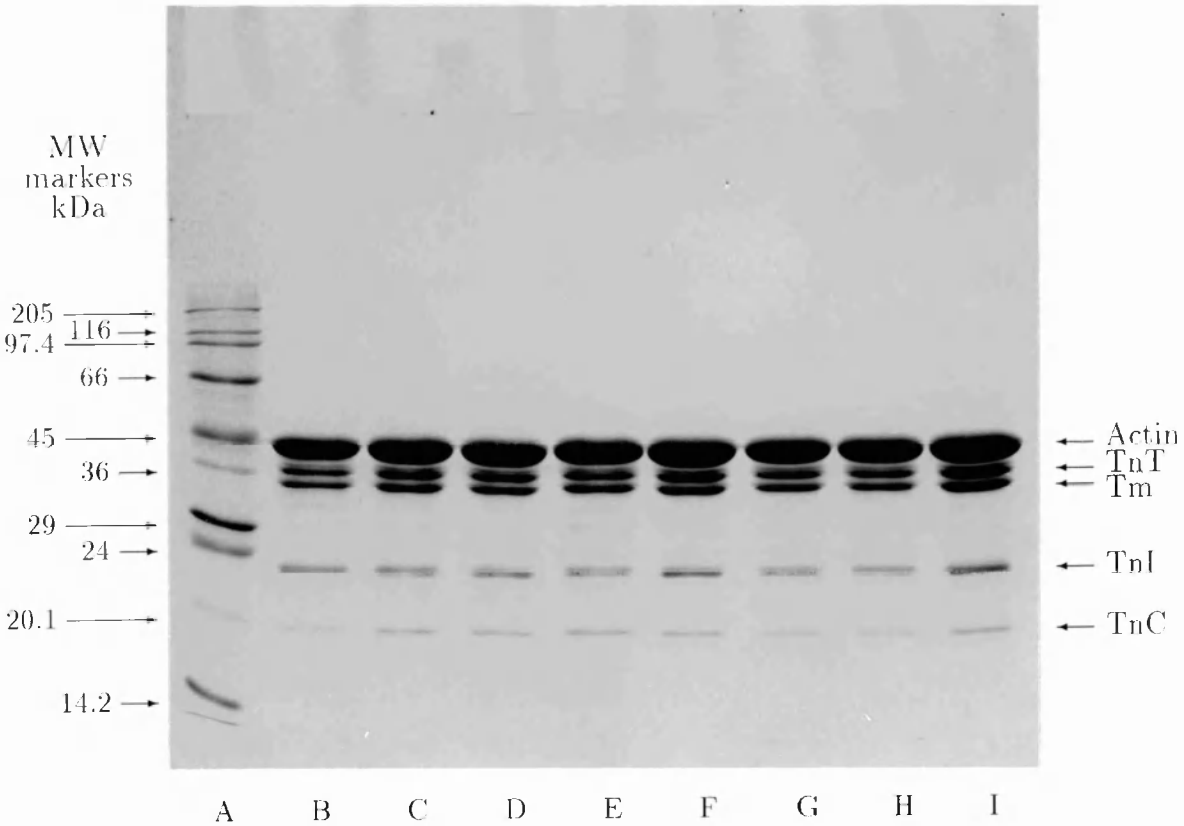


Figure 5.8: 12.5% SDS-PAGE of rabbit RTFs immediately after reconstitution and after Donnan potential measurements. Lanes: A. MW markers, B. RTFs immediately after reconstitution, C. to I. pellet fraction from the centrifugation of RTFs in buffers of pCa 3.2, 3.9, 5.1, 6.4, 7.1, 7.9 and 8.7 (from left to right). The amount of RTFs applied was 12 $\mu$g.

diluted 20-fold with the appropriate pCa buffers to concentration 0.3 mg/ml. This was performed directly before spinning the samples at 100 000×g for 2 hours at 4°C. The pellets from this centrifugation were dissolved directly into the sample buffer for electrophoresis. Figure 5.8 represents a photograph of a 12.5% gel of the RTFs immediately after reconstitution and after Donnan potential measurements. There are no detectable differences between the samples. This confirms that the composition of the samples used remained unchanged during the Donnan potential measurements.

### 5.3.4 Net charge measurements

The Donnan potentials were measured for six 0.25 ml samples of each of the four proteins (F-actin, Tm-tn, RTFs and BSA). Buffers listed in table 5.1 were used. The sample compartments were made of dialysis tubing with 6 mm diameter, the reference

Table 5.5: The specific charge $q_{spe}$ of BSA, F-actin, Tm-tn and RTFs in electronic charge units. Each value is a mean of 6 determinations ± SD.

| pCa | Specific charge $q_{spe}$ ± SD | | | |
|---|---|---|---|---|
| | BSA | F-actin | Tm-tn | RTFs |
| 8.7 | -16.4±1.2 | -24.0±1.3 | -25.2±2.6 | -29.7±2.1 |
| 7.9 | -17.1±1.7 | -24.0±1.5 | -25.4±1.3 | -29.5±2.4 |
| 7.1 | -16.3±0.4 | -23.9±2.3 | -26.9±0.9 | -24.8±1.8 |
| 6.4 | -15.7±1.2 | -23.6±1.4 | -26.3±0.9 | -32.1±2.8 |
| 5.1 | -16.9±1.3 | -23.2±3.3 | -25.2±1.3 | -27.8±3.9 |
| 3.9 | -16.1±0.5 | -23.7±3.5 | -24.7±1.0 | -24.1±2.4 |
| 3.2 | -15.0±0.7 | -18.3±1.9 | -22.2±0.8 | -18.5±2.3 |

electrode was immersed in the outer buffer. Calomel macroelectrodes K422 were used for BSA, whereas the microelectrode technique was used for the other proteins. The Donnan potentials recorded in the pCa buffers, protein concentration of the samples, temperature and calculated values of the specific charge are given in tables C.1 - C.4 in appendix C. The mean values of the specific charge obtained are given in table 5.5 and plotted in figure 5.9.

It would be useful to express the net charge of the proteins as the charge per molecule or complex of molecules, i.e. as a molecular charge $q_{mol}$. In the case of single component preparations like F-actin or BSA the value of the molecular charge can be obtained from the specific charge and molecular weight of the protein. In the case of protein complexes like Tm-tn and RTFs the molar ratios of the components must also be known. The molecular weights from table B.2 (for fast muscle) and the molar ratios from table 5.3 were used in order to convert the specific charge into a molecular charge. A molecule of tropomyosin was taken to be an $\alpha.\alpha$-tropomyosin dimer since the $\alpha$ form is predominant in rabbit fast muscle (Smillie, 1982). The Tm-tn complex for which the molecular charge was calculated consists of 1 tropomyosin, 1.9 TnT, 1.1 TnI, 0.3 TnC and 2.0 actin molecules. In the case of RTFs, $q_{mol}$ is used to represent the charge per 1 tropomyosin, 5.4 actin, 2.4 TnT, 1.2 TnI and 0.5 TnC molecules. The resulting values of the molecular weight were 238.546 kDa for the Tm-tn complex and 399.297 kDa for the RTFs. The mean values of the molecular charge at various

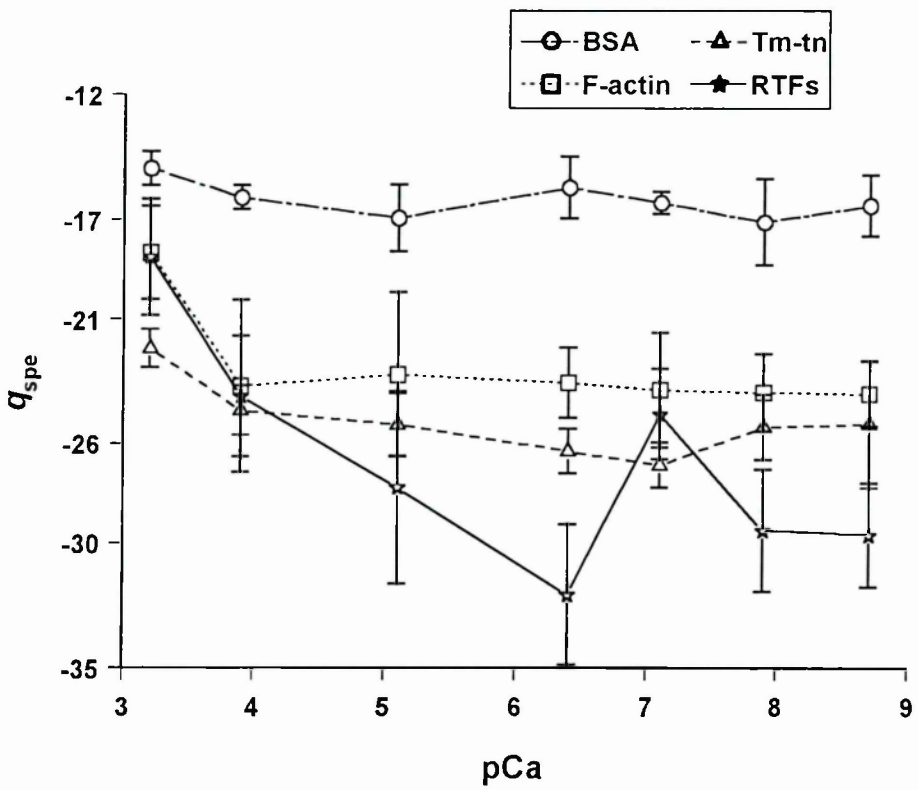


Figure 5.9: The specific charge $q_{spe}$ of BSA, F-actin, Tm-tn and RTFs as a function of pCa. Each data point is a mean of measurements for 6 samples and standard deviations are indicated. Donnan potentials were measured with macroelectrodes for BSA and with microelectrodes for the other proteins.

Table 5.6: The molecular charge $q_{mol}$ of BSA, F-actin, Tm-tn and RTFs as a function of pCa in electronic charge units. The charge of Tm-tn and RTFs is expressed per protein complex containing 1 tropomyosin molecule with the molar ratios of the proteins as given in table 5.3. Each value is a mean of 6 determinations ± SD.

| pCa | Molecular charge $q_{mol}$ ± SD | | | |
|---|---|---|---|---|
| | BSA | F-actin | Tm-tn | RTFs |
| 8.7 | -10.9±0.8 | -10.1±0.6 | -60.2±6.1 | -118.6± 8.3 |
| 7.9 | -11.4±1.1 | -10.1±0.7 | -60.5±3.1 | -117.8± 9.7 |
| 7.1 | -10.8±0.3 | -10.0±1.0 | -64.1±2.1 | -99.2± 7.2 |
| 6.4 | -10.4±0.8 | -9.9±0.6 | -62.8±2.1 | -128.0±11.2 |
| 5.1 | -11.2±0.9 | -9.8±1.4 | -60.2±3.0 | -110.9±15.4 |
| 3.9 | -10.7±0.3 | -10.0±1.5 | -58.9±2.4 | -96.3± 9.7 |
| 3.2 | -9.9±0.5 | -7.7±0.8 | -52.9±1.8 | -73.9± 9.3 |

pCas are given in table 5.6 and presented graphically in figures 5.10 and 5.11.

A calculation was also made as to the charge on RTFs were it to be a simple sum of the charge on actin molecules and on the tropomyosin-troponin complex. Taking into account the molar ratios of proteins in Tm-tn and RTFs given in table 5.3 the following approximations were made. The charge of Tm-tn was added to the charge of actin multiplied by 3.4, since there were approximately two actin molecules in the Tm-tn complex. Differences in the troponin T,I and C content of Tm-tn and RTFs were neglected. The error of the derived charge was calculated using equation 2.4. The two types of the molecular charge of RTFs are given in table 5.7 and plotted in figure 5.12.

The ratio of the experimental charge to that calculated from the sequence is plotted in figure 5.13. The experimentally determined molar ratios of the proteins in Tm-tn and RTFs (given in table 5.3) were used to obtain the calculated values of the charge.

## 5.4 Discussion

$Ca^{2+}$ sensitive electrodes proved to be of limited value for the determination of the free $Ca^{2+}$ concentrations. Accurate results were not expected at micromolar $[Ca^{2+}]$,

(a)

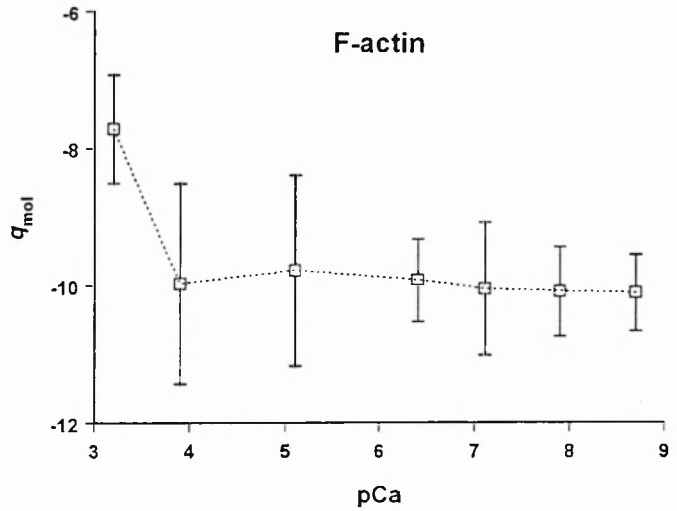


(b)

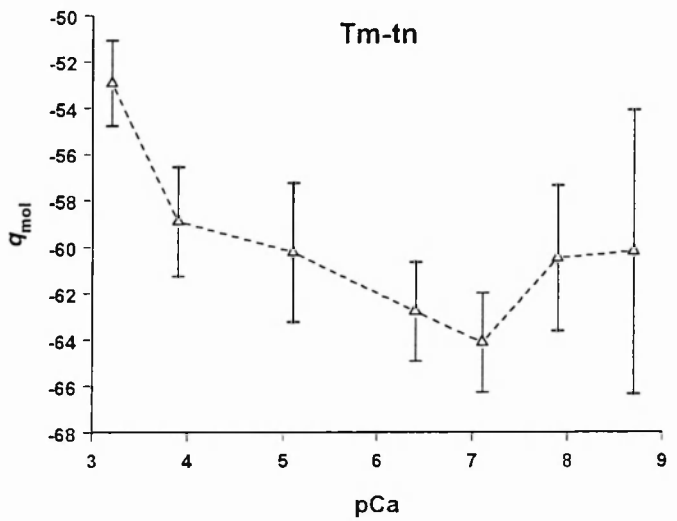


(c)

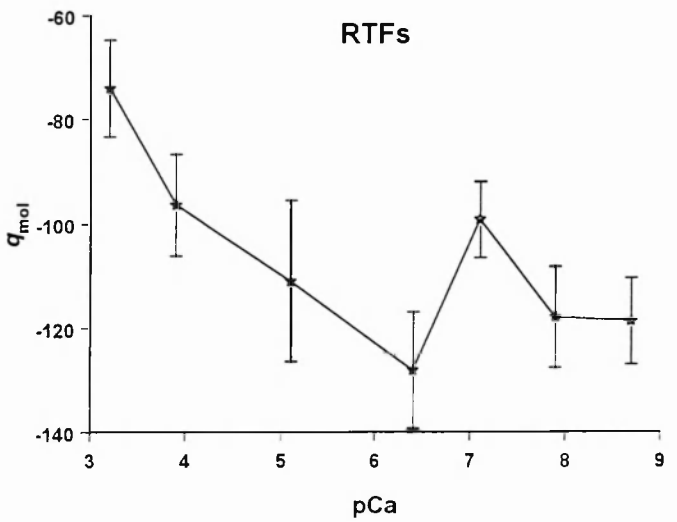


Figure 5.10: The molecular charge $q_{mol}$ in electronic charge units as a function of pCa for (a) F-actin, (b) Tm-tn and (c) RTFs. The charge of Tm-tn and RTFs is expressed per protein complex containing 1 tropomyosin molecule with the molar ratios of the proteins as given in table 5.3. The data points are mean values of measurements for 6 samples with bars representing standard deviations. Donnan potentials were measured with microelectrodes.

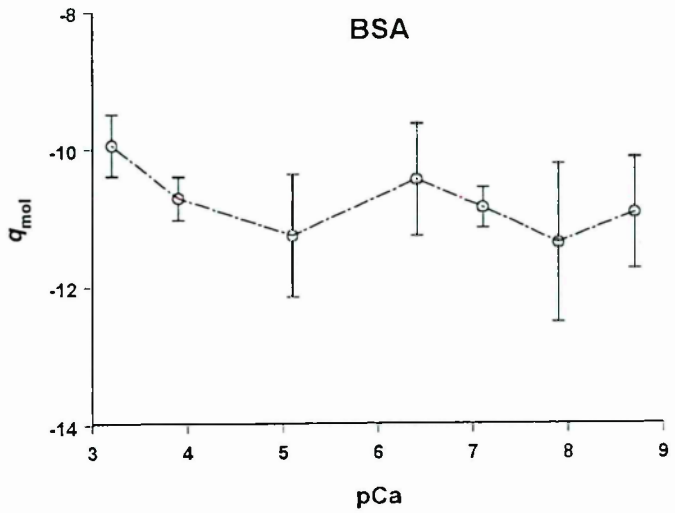


Figure 5.11: The molecular charge $q_{mol}$ in electronic charge units for BSA as a function of pCa. The data points are mean values of 6 determinations and the bars represent standard deviations. The Donnan potentials were measured with macroelectrodes.

Table 5.7: Comparison of the directly measured molecular charge $q_{mol}$ of RTFs with a value derived from the measured values of the charge on F-actin and Tm-tn. The derived charge was calculated as the sum of the charge on 1 Tm-tn complex and 3.4 molecules of actin to take into account the molar ratios of the proteins in the preparations of Tm-tn and RTFs. Charges are expressed in electronic charge units.

| pCa | Molecular charge $q_{mol}$ ± SD | |
|---|---|---|
| | Measured | Derived |
| 8.7 | -118.6± 8.3 | -94.5±6.4 |
| 7.9 | -117.8± 9.7 | -94.7±3.8 |
| 7.1 | -99.2± 7.2 | -98.2±3.9 |
| 6.4 | -128.0±11.2 | -96.5±2.9 |
| 5.1 | -110.9±15.4 | -93.5±5.6 |
| 3.9 | -96.3± 9.7 | -92.8±5.5 |
| 3.2 | -73.9± 9.3 | -79.1±3.3 |

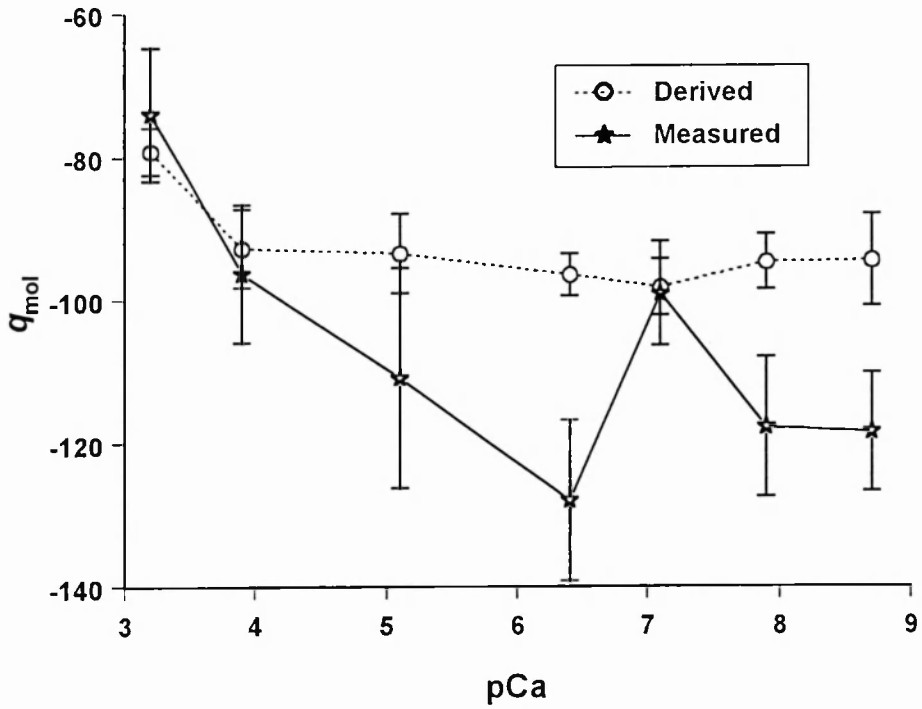


Figure 5.12: Comparison of the directly measured molecular charge $q_{mol}$ of RTFs with a value derived from the measured values of the charge on F-actin and Tm-tn. The derived charge was calculated as the sum of the charge on 1 Tm-tn complex and 3.4 molecules of actin to take into account the molar ratios of the proteins in the preparations of Tm-tn and RTFs. Charges are expressed in electronic charge units.

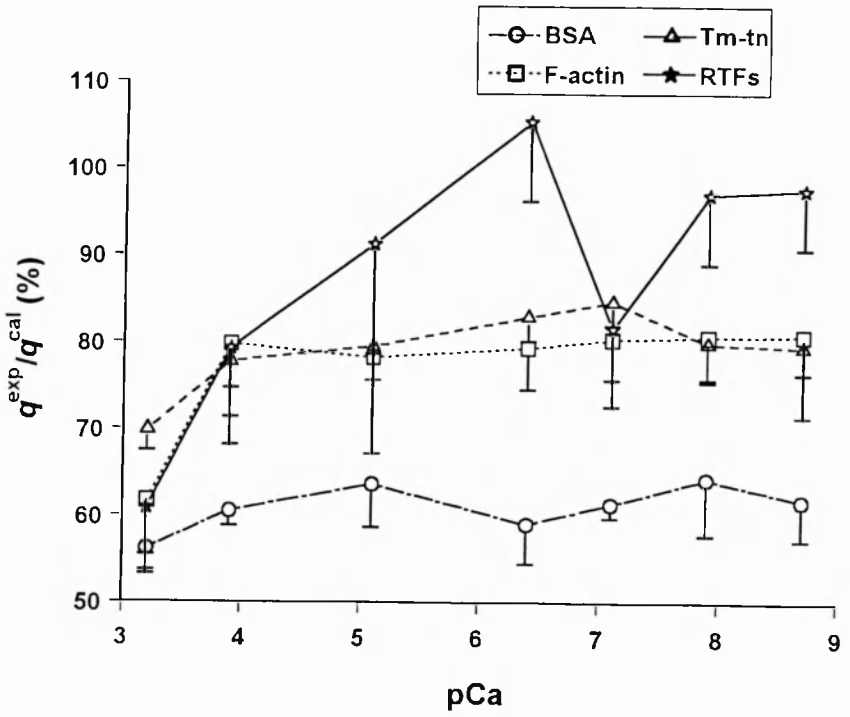


Figure 5.13: Ratio of the experimental charge to that calculated from the sequences $q^{exp}/q^{cal}$ for BSA, F-actin, Tm-tn and RTFs as a function of pCa. Specific charge values were used to calculate the ratios. The sequence derived values of the specific charge were taken as -26.6e, -29.7e, -31.7e and -30.4e for BSA, F-actin, Tm-tn and RTFs respectively. These values were obtained from table B.2 using the molar ratios of proteins given in table 5.3. Each data point represents a mean of values obtained from measurements for 6 samples and standard deviations are indicated.

however, it was found that even at millimolar levels the results were not reproducible for the standards used. Perhaps, if standards containing a Ca-EGTA buffering system, for which the free $Ca^{2+}$ concentrations had been determined independently, were used, one would be able to verify experimentally the calculated pCa values with $Ca^{2+}$ sensitive electrodes.

The pCa values for the buffers used for Donnan potential measurements calculated using the PERRIN program, agree very well with the values obtained from two values of the apparent binding constants in the whole range of pCas (table 5.2). Thus, when certain free $Ca^{2+}$ levels are referred to, one can be confident that they agree with generally accepted values.

On the basis of the centrifuging study described in section 5.3.3 the Donnan potential measurements were performed in solutions based on a 10-fold dilution of buffer R. One could argue however that, even though there was no detectable protein in the supernatant resulting from a full dissociation of Tm-tn from F-actin, there could have been a partial dissociation, where Tm-tn was not in close contact with actin. This could be detected by carrying out actomyosin ATPase assay in the presence of high and low levels of free $Ca^{2+}$.

The molecular charge for **BSA** is constant, within experimental error, in the whole range of pCas. It is approximately -11e for pCas 8.7 to 3.9, with a small change to approximately -10e for pCa 3.2 (table 5.6, figure 5.11). This is consistent with a low affinity of albumins for $Ca^{2+}$ and $Mg^{2+}$ (see section 5.1).

The molecular charge for **F-actin** is constant, within experimental error, for pCas down to 3.9 (approximately -10e). When $[Ca^{2+}]$ is increased to pCa 3.2, the charge becomes -8e (table 5.6, figure 5.10), the difference being significant with $p = 0.008$. This could be due to binding of a single divalent cation, in this case $Ca^{2+}$. Actin has one high affinity cation binding site and three or more intermediate and lower affinity cation binding sites (Sheterline and Sparrow, 1994). The high affinity binding site has

higher affinity for $Ca^{2+}$ ($K = 5\times10^{8}$ $M^{-1}$) than for $Mg^{2+}$ ($K = 1\times10^{8}$ $M^{-1}$), whereas the other sites do not show preference for $Ca^{2+}$ or $Mg^{2+}$ and also bind monovalent cations (Sheterline and Sparrow, 1994). Thus the experimental data suggest that actin had the high affinity site occupied with a $Mg^{2+}$ ion at all pCas and the change of 2e in charge occurring between pCas 3.9 and 3.2 could be interpreted as due to binding of one $Ca^{2+}$ ion to one of the low affinity sites.

In the case of the **tropomyosin-troponin** complex, a gradual change was observed towards less negative values from the charge of approximately -64e at pCas 7.1 to the charge of -53e at pCa 3.2 (table 5.6, figure 5.10). The difference between these values is highly significant with $p = 2\times10^{-6}$.

The troponin complex contains six divalent cation binding sites: two high affinity $Ca^{2+}$ sites which also bind $Mg^{2+}$ (competitively), two $Ca^{2+}$ specific lower affinity sites and two $Mg^{2+}$ specific lower affinity sites (Potter and Gergely, 1975). The actual affinity constants for the above sites depend on the concentration of free $Ca^{2+}$ and $Mg^{2+}$. In the absence of $Mg^{2+}$ the association constant, K, for the two high affinity $Ca^{2+}$ sites is $5\times10^{8}$ $M^{-1}$ and for the lower affinity sites is $5\times10^{6}$ $M^{-1}$ (Potter and Gergely, 1975). In the presence of 2 mM $MgCl_2$ the binding of $Ca^{2+}$ to these four sites is with $K = 5\times10^{6}$ $M^{-1}$, this change in the affinity for $Ca^{2+}$ of the $Ca^{2+}/Mg^{2+}$ site indicates that the affinity of troponin for $Mg^{2+}$ is around $K = 5\times10^{4}$ $M^{-1}$ (Potter and Gergely, 1975). Hence the Tm-tn probably had four sites occupied with $Mg^{2+}$ at pCas around 8.7 to 5, below this pCa a competition between $Ca^{2+}$ and $Mg^{2+}$ probably caused an exchange of $Mg^{2+}$ to $Ca^{2+}$ in the high affinity sites. This would not have caused noticeable change of the charge of the protein. The observed changes in the charge could be due to the binding of two $Ca^{2+}$ ions to the lower affinity sites on troponin C and binding of one $Ca^{2+}$ ion to the actin (also present in the preparation). However, this would only account for a change of about 5e, which is smaller than the observed change.

Larger changes with pCas can be seen in the case of the **reconstituted thin fila-**

ments (table 5.6, figure 5.10). The molecular charge at pCa 7.1 is significantly less negative than the charge at pCas 7.9 or 6.4 (p values less than 0.005). One would however have to measure the charge at pCa values close to pCa 7.1 to confirm that the obtained charge results from a real effect and is not an artefact. When $[Ca^{2+}]$ is increased from pCa 6.4 to pCa 3.2 a gradual change in the molecular charge, from a charge of approximately -128e at pCa 6.4 to a charge of -74e at pCa 3.2, is observed. The 40% difference in charge between pCa 6.4 and 3.2 is highly significant ($p = 4 \times 10^{-6}$). This change cannot be explained by $Ca^{2+}$ binding to the same sites as for Tm-tn and F-actin in isolation, since this would only account for a change of about 17e. Whether the data point at pCa 7.1 is included in the analysis or not, no change towards less negative values at pCa around 6.8 observed in muscle fibres by Coomber and Elliott (1995, 1996), was seen in the charge on the isolated RTFs.

Table 5.7 and figure 5.12 reveal that the charge measured on the RTFs is more negative, by approximately 20–30e, than the charge derived from the charge on F-actin and Tm-tn complex, for pCas 8.7, 7.9 and 6.4. This cannot be due to the slightly higher TnT content in the RTFs than in the Tm-tn, since TnT carries a positive charge at neutral pH (see table B.2). At other pCas there is good agreement between the measured and derived values of the charge. At these pCas the charge of the RTFs is a simple sum of the charges on its components.

It can be seen from figure 5.13 that the measured charge on F-actin, Tm-tn and BSA is equal to about 60–80% of the charge calculated from the sequence, i.e. the charge that the protein would carry in the absence of bound counterions. For RTFs this ratio changes much more with pCa, in the range of approximately 60–100%, with the maximum value at pCa 6.4.

The cooperative change in charge, found in muscle fibres (Coomber and Elliott, 1995, 1996), was not observed in RTFs or their components. This is possibly due to differences in the ionic strength, molar ratios of the proteins, protein concentration and arrangement between these systems. Alternatively, the cooperative change observed

in muscle fibres may not be a manifestation of the calcium regulation of muscular contraction, since an effect of the same order of magnitude is observed for the Donnan potentials recorded from all the regions of the sarcomere. This, together with the fact that the potential difference is very reduced after an incubation of the fibres with 1% Triton X-100, and that the effect disappears when the muscle is stretched beyond overlap, suggests two possible explanations. One is that the source of the potential change is a protein spanning the whole length of the sarcomere i.e. titin. This explanation for the effect has been suggested by S.J. Coomber (private communication). The second possibility is that some membrane proteins involved in the transport of calcium, that were not entirely removed by the glycerination procedure, gave rise to the observed effect by accumulating $Ca^{2+}$ at its higher concentrations in some small membrane compartments. Stretching the muscle would cause these membranes to tear and consequently the calcium could not be accumulated. The treatment with detergent would also abolish the effect if it was due to the membrane proteins.

The charge of F-actin has been measured before, although not under the same conditions. In solutions which were a 5-fold dilution of buffer R, values of -6±3e and -7±3e were obtained for F-actin gels with microelectrodes by Jennison (1992) and Deshayes (1994) respectively. One cannot directly compare these results with the results in this thesis since there is uncertainty as to the levels of free $Ca^{2+}$ in the R/5 buffer. One can assume that the R/5 buffer, which did not contain EGTA, had a similar $Ca^{2+}$ level to our standard solutions, i.e. pCa approximately 5–6. The charge of F-actin obtained in this thesis was slightly more negative, around -9.8±1.4e. This could be caused by the dependence of F-actin charge on the history of the preparation (see section 1.6.2). The value of charge given by Jennison (1992) as -6±3e was obtained mostly from undisturbed pellets (8 out of the 9 samples used).

If the values of the charge on the RTFs at pCa 7.1 and 6.4 could be verified, then the observed change in charge between these pCas could have interesting implications. The pCa value of 7.1 approximately corresponds to the free $Ca^{2+}$ concentration in

resting muscle. It is interesting to note that the charge on RTFs is a simple sum of the charge on actin and Tm-tn at this pCa. If an increase in $[Ca^{2+}]$ causes the charge on the thin filament to become more negative, it could provide the mechanism for the conformational changes accompanying calcium activation. An increase in the net negative charge on the thin filament would cause a strong repulsive interaction within it and could facilitate the movement of the Tm-tn complex away from F-actin, enabling the binding of the myosin subfragment-1 to F-actin. This would mean, however, that the binding of two $Ca^{2+}$ ions to the $Ca^{2+}$-specific low affinity sites on troponin C makes the charge on the thin filaments more negative. A similar phenomenon of 'charge reversal and amplification' has been observed for myosin (Elliott *et al.*, 1985; Bartels and Elliott, 1985; Bartels *et al.*, 1993).

## 5.5 Conclusions

A significant change in the charge of the RTFs, F-actin and Tm-tn complex has been observed to occur with changes in $[Ca^{2+}]$. The charge on these proteins becomes less negative as $[Ca^{2+}]$ is increased from pCa 6.5 to 3 (approximately), the change is more striking for RTFs and Tm-tn than for actin alone, for which the charge only changes between pCa 4 and 3. This effect might well be enhanced and become cooperative, in the conditions of high protein concentration and high ionic strength, that pertain in intact muscle. The Donnan potential method applied to isolated proteins, however, does not allow us to approach these conditions. Also differences in protein stoichiometry of intact muscle and our preparations, particularly the lower troponin C content in the latter, could explain the gradual and uncooperative nature of the observed changes in charge.

# Chapter 6

# Conclusions and future studies

## 6.1 Conclusions

### 6.1.1 Effect of methylation on the charge of HMM

The ATPase activity of the methylated HMM is elevated in the presence of $Ca^{2+}$ and decreased in the presence of EDTA with respect to the activity of the native protein. Both the increase and decrease are approximately 4-fold and the differences are highly significant ($p < 0.001$). A similar effect was reported by Phan *et al.* (1994) for the methylated S1. The observed reversal of activities upon methylation suggests modifications in the vicinity of the SH1 sulphydryl group of $Cys^{707}$ (Margossian and Lowey, 1982). This is in agreement with the increased reactivity of the SH1 groups towards thiol reagents and faster dissociation rate of $\epsilon$ADP that were observed for S1 upon methylation (Phan *et al.*, 1994).

Our Donnan potential measurements do not reveal a statistically significant difference between the values of the net electric charge of the HMM and methylated HMM at pH 6.7, at which the methylated S1 was crystallized. The values of the net charge for both proteins could be divided into two groups, depending on whether they were obtained from the first or second Donnan potential measurement on a sample. The values obtained from the second measurement were significantly more negative. This suggested that there were changes in the experimental system occurring with time.

These changes were subsequently determined to be associated with the KCl leakage out of the electrodes. The obtained values of charge have an experimental error of about 20%. Hence, on the basis of the Donnan potential measurements, a less than 20% difference in charge between HMM and methylated HMM at pH 6.7, cannot be excluded.

The calculations of the theoretical charge of lysine and $N^{\epsilon}$-dimethyllysine as a function of pH indicate that the methylated residue would have a lower positive charge at pH values approximately 8–12. Typical shifts in $pK_a$ observed for lysine upon methylation in other proteins (Bradbury and Brown, 1973; Jentoft *et al.*, 1979; Gerken *et al.*, 1982), would cause a change of only 0.02e in the net charge on the S1 molecule and a change of 0.07e in the charge on the HMM molecule at pH 6.7. Even if all the lysine residues in the S1 and HMM molecules had their $pK_a$ values shifted by as much as it was observed for $Lys^{41}$ in the active site of ribonuclease A ($pK_a$ 9.0, Jentoft *et al.*, 1979), the net negative charge on the S1 and HMM at pH 6.7 would be increased by only 0.5e and 1.6e respectively. A 5% change in the charge on a lysine residue at this pH would require the $pK_a$ value to be as low as 8.0. Values lower than 9.0 , however, have not been observed in proteins. The calculations suggest that the charge on the methylated S1 and HMM is more negative than the charge on the native proteins by only a fraction of an electronic charge at pH 6.7. This finding is in agreement with the results of the Donnan potential measurements.

The following conclusions can be drawn from the analysis of the crystal structure of methylated S1. There are several places of potential flexibility within the molecule. Additional methyl groups present on the $N^{\epsilon}$-dimethyllysine residues may increase the packing density of the protein. This would result in a more rigid structure which may explain its ease of crystallization. The changes in the vicinity of the SH1 group, that were associated with a more open conformation of this region by Phan *et al.* (1994), may be due to the additional methyl groups on $Lys^{709}$ forcing it further apart from three negatively charged glutamic acid residues on a neighbouring loop.

### 6.1.2 Effect of $Ca^{2+}$ on thin filament charge

A significant change in the net charge of the reconstituted thin filaments (RTFs), tropomyosin-troponin complex (Tm-tn) and F-actin has been observed with changes in the free $Ca^{2+}$ concentration $[Ca^{2+}]$ at ionic strength 0.02 M and pH 7.0. The charge on these proteins becomes less negative as $[Ca^{2+}]$ increases, with some differences between the proteins relating to the extent of the changes in charge and to the range of pCas over which these changes occur. The net charge of BSA is constant, within experimental error, in the whole range of pCas (3.2–8.7).

The charge of F-actin is constant within experimental error, for pCas from 8.7 down to 3.9. When $[Ca^{2+}]$ is increased to pCa 3.2, the charge becomes less negative by approximately 2e, the change is significant with $p = 0.008$. This can be interpreted as resulting from binding of one $Ca^{2+}$ ion to one of the low affinity sites of actin. The charge of Tm-tn and RTFs changes gradually between pCa 6.4 and 3.2. The change of charge in this range is approximately 10e for Tm-tn and 54e for the RTFs (where the charges are expressed per protein complex containing 1 tropomyosin molecule). The changes are significant with p less than 0.00001. In the case of Tm-tn, the 16% change in charge is larger than could be expected to result from binding of two $Ca^{2+}$ ions to the lower affinity sites on troponin C and binding of one $Ca^{2+}$ ion to actin, which was also present in the preparation. The 40% change in charge of the RTFs cannot be explained by $Ca^{2+}$ binding to the same sites as for Tm-tn and F-actin in isolation, since this would only account for a change of about 17e. Elliott *et al.* (1985) have suggested that a 'charge amplification' effect occurs in native and synthetic thick filaments, perhaps a similar phenomenon is being observed here in reconstituted thin filaments.

The highly cooperative change in charge found in glycerinated muscle fibres at pCa approximately 6.0 (Coomber and Elliott, 1995, 1996), was not observed for the RTFs, Tm-tn or F-actin. However, this is possibly due to differences in the ionic strength, protein concentration and arrangement between muscle and protein solution. Also

the differences in protein stoichiometry of intact muscle and our preparations, the lower troponin C content in the latter in particular, could be responsible for the lack of cooperativity in the observed changes in charge. The gradual change observed for the RTFs and Tm-tn may be enhanced and become cooperative in the structural and environmental conditions that pertain in muscle.

### 6.1.3 Electrode techniques for protein solutions

The microelectrode technique has been found superior to the macroelectrode technique when applied to low viscosity protein solutions of BSA, viscous protein solutions of Tm-tn and dilute gels of F-actin and RTFs.

Microelectrodes with tip diameter approximately 5–20 $\mu$m and resistance less than 1 M$\Omega$, which are obtained from sharp electrodes by removing the tips with forceps, give reproducible results, provided their tip does not become clogged with the protein. Blockage can be recognized by an increase in the resistance and erratic potential readings. Such an electrode can be made functional again by renewing the liquid junction, which can be achieved by tightening the electrode holder a very small fraction of a turn. This slightly increases pressure of the filling solution and pushes out the protein obstructing the tip. The main advantage of the microelectrode technique compared to the macroelectrode technique, is the small size of the electrode in relation to the sample and small KCl leakage rate. The leakage rate out of microelectrodes with tip diameter up to 25 $\mu$m was found to be approximately an order of magnitude lower than the leakage rate out of the three types of macroelectrodes used. Hence a microelectrode does not affect the sample as much as a macroelectrode does. The immersion of the microelectrode into the sample does not cause leakage of KCl that would lead to drifts in potentials. The transfer of the tip between the sample and outer buffer causes negligible sample dilution. The measurements can thus be repeated several times to achieve greater accuracy and the protein concentration can be determined afterwards.

The KCl leakage out of macroelectrodes can lead to large uncertainties both in the reference potential and the potential recorded with the electrode in the protein solution. This can give rise to large experimental error of the resulting Donnan potentials.

When one of the macroelectrodes was placed in a compartment with a semi-permeable membrane containing the same solution as was outside the compartment, and the reference electrode was placed in the outer buffer, negative potentials were usually observed in respect to the potential recorded when both electrodes were in the outer buffer. The magnitude and time course of these potentials depended on the KCl leakage rate out of the electrodes and on the membrane area of the compartment. Experiments in which these were varied suggest that there is a KCl accumulation inside the compartment to a concentration, at which the diffusion rate through the membrane is equal to the outflow rate through the porous pin of the electrode. The observed potentials were up to about 2 mV in solutions of 10–20 mM ionic strength, i.e. could be of the same order as the Donnan potentials. Only for the electrodes with the smallest leakage rate (approximately 1 $nmol \cdot s^{-1}$) and compartments entirely made of dialysis tubing, were these potentials less than 0.5 mV.

When the reference electrode was in the outer buffer and the measuring electrode was placed in a protein solution, the time course of the observed potentials depended on the same factors as when there was buffer in the sample compartment, and also on the sample viscosity. Under most conditions, drifts in the potentials were observed. The experiments suggest that the KCl leakage rate decreases when the protein absorbs onto the electrode surface and porous pin, and this results in registering more positive potentials. This effect was most prominent for viscous samples of F-actin and RTFs for which the initial potentials were close to zero or even positive for periods of minutes. It is not clear whether the subsequent slow-rate changes in the potentials for these samples were due to slow response time of the electrodes in such a medium or the leakage and accumulation of KCl. The potentials for these samples changed so slowly that the initial potentials could have been interpreted as equilibrium potentials leading

to reduced, or even positive, values of the net charge on negatively charged proteins, as comparison with the results obtained with microelectrodes revealed.

Since the experiments suggest that there is an accumulation of KCl which causes additional potentials, placing the reference electrode inside a small compartment where the accumulation can occur is generally not beneficial. The potentials stemming from the KCl leakage will not cancel since it is most likely that the leakage rate will be different in the buffer and protein. In fact, placing the reference electrode inside a compartment will just obscure these potentials. Relatively small errors in the Donnan potential values were obtained when the set-up with two dialysis sacks was applied to BSA in solutions of various pH. The value of the pI obtained from these measurements was in good agreement with literature values. This is probably because the leakage rate may not be substantially different for the buffer and BSA solution and also because the buffer in the reference compartment was changed at the same time as the protein solution was applied in the other compartment.

The general conclusion on the macroelectrode technique is that it can be applied to protein solutions of low viscosity but precautions have to be taken in order to minimize the effects of KCl leakage. The use of electrodes with KCl leakage rates not greater than 1 $nmol \cdot s^{-1}$ in a set-up with one sample compartment made of dialysis tubing, would minimize the errors in the resulting Donnan potentials. Obtaining a time course of the potentials is crucial in order to detect changes occurring over time which result from the leakage and accumulation of KCl.

The Donnan potential measurements for isolated proteins usually have to be conducted at protein concentrations lower than in muscle. As a result experimental solutions of ionic strength lower than physiological have to be used in order to obtain measurable Donnan potentials. Both the protein concentration and the media are thus far from the physiological conditions in living muscle. This is the main limitation of the technique for protein solutions compared to the technique applied to muscle fibres. The measurements in protein solutions have the advantage, however,

that one can study the charge of individual proteins or their combinations.

### 6.1.4 Summary of the main observations

1. The Donnan potential measurements and theoretical charge calculations do not suggest a significant difference between the net charge of HMM and methylated HMM at pH 6.7. Neither do the charge calculations indicate a possibility of a local change in the charge of some lysine residues at this pH. The ATPase activity of methylated HMM is consistent with changes in the vicinity of the SH1 group.

2. A significant change in charge of RTFs, Tm-tn and F-actin has been observed with $[Ca^{2+}]$ between pCa 6.5 and 3 (approximately), at ionic strength 0.02 M and pH 7.0. The change is more prominent for RTFs and Tm-tn than in the case of F-actin, for which the change in charge occurs only between pCas 4 and 3. No significant change in charge was observed for BSA in the whole range of pCas (3–9 approximately).

3. The macroelectrode technique is generally not suited for samples of high viscosity. In the case of low viscosity samples, KCl leakage from macroelectrodes can lead to large errors in the Donnan potentials. These can be minimized if electrodes with leakage rates of 1 $nmol \cdot s^{-1}$ or less are used in a set-up with one sample compartment entirely made of dialysis tubing. The analysis of the time course of the potentials is crucial for the detection of the effects caused by KCl leakage and accumulation.

4. Reproducible Donnan potentials can be obtained with microelectrodes of resistance less than 1 $M\Omega$ and tip size approximately 5–20 $\mu m$ for protein solutions of low and high viscosity. The electrodes tend to get clogged up with protein which results in an increase in resistance and erratic potentials, but this problem can be overcome by renewing the liquid junction of the electrode by tightening its holder.

5. The main limitation of the Donnan potential method for isolated proteins is that the protein concentrations are usually lower than in muscle, and the ionic strength of the experiments has to be lowered below physiological conditions to achieve measurable Donnan potentials. The main advantage of this method is that it enables measuring the charge of individual proteins or their combinations, which may shed light on the role of the individual proteins.

## 6.2 Suggestions for future studies

Several lines of further study emerge from the research of this thesis:

1. It is possible that the gradual and uncooperative change in charge observed for the RTFs with $[Ca^{2+}]$, could be a result of a partial dissociation of the Tm-tn from F-actin at the ionic strength of the experiment (0.02 M). The ultracentrifuging studies did not reveal detectable dissociation, but the proteins may not have been in such close contact as under more physiological conditions. This could be tested by carrying out an actomyosin ATPase assay at high and low levels of free $Ca^{2+}$. This assay would reveal whether Tm-tn confers the $Ca^{2+}$ sensitivity on actomyosin. In the case of finding that the ionic strength of 0.02 M was weakening or abolishing the regulatory effect of Tm-tn, this assay could be used to determine the sufficient ionic strength for repeating the Donnan potential measurements.

2. An attempt could be made to obtain the Tm-tn and RTFs in a pure form, with the stoichiometry of the components as found in intact muscle. It would also be interesting to obtain the tropomyosin, troponin C, troponin I and troponin T in separation and measure the charge on these proteins at various $[Ca^{2+}]$ levels.

3. It would be also interesting to measure the net electric charge of nebulin and the thin filament containing actin, Tm-tn and nebulin at various levels of $[Ca^{2+}]$.

4. The measurements of the net charge on the regulatory light chains of scallop myosin could shed light on the mechanism of the $Ca^{2+}$ regulation in molluscan muscle and the mechanism of the regulation in general.

5. With the knowledge of the limitations of the macroelectrode technique and the microelectrode technique giving accurate results for protein solutions, one could proceed to determine the charge on the subfragment-1 of myosin in the presence of nucleotides and their analogues that mimic transient intermediates of ATP hydrolysis. These could include: ATP, ADP, $PP_i$, $V_i$, ADP-$V_i$, AMP-PNP and AMP.

6. An extension of the study of the theoretical charge on muscle proteins calculated from their sequence could be carried out. This would involve the analysis of the distribution of the charged groups in muscle proteins of known three-dimensional structure. A study based on the methodology used by Barlow and Thornton (1986) could provide information on the local surface charge density, polarity and dipole moments. Their study showed that in the majority of proteins that interact with a charged ligand, the charge distributions are relatively asymmetric and the orientation of the dipoles acts to aid the ligand binding. A similar study for muscle proteins could provide insight into the functioning of the S1 ATPase. The location of the specific charged groups could also provide information on the interactions between muscle proteins involving closer contact.

# Appendix A

# Stability constants

The ionic composition of the experimental solutions was determined using the PERRIN program (Abbott, 1976). Input files for this program were formed for each particular solution using stability constants available in literature. The stability constants are defined as $\log_{10}K$, where K is an association constant in $M^{-1}$.

There are often large discrepancies between the published data referring to the formation of the same complexes as can be seen in compilations of Sillen and Martell (1971), Högfeldt (1982) and Perrin (1979) listing the stability constants and the experimental conditions under which they were determined. It is difficult to decide which values are more accurate and reliable than others listed in those tables without referring to the original publications, which can be very abundant for some of the complexes. This problem has been addressed in compilations listing the so-called critical stability constants (Martell and Smith, 1974, 1977, 1982; Smith and Martell, 1975, 1976, 1989). These tables contain values of stability constants selected from literature by the compiling research team employing rigorous selection criteria. For the above mentioned compilations of critical stability constants the selection criteria included omitting data obtained with a ligand of unspecified purity and/or under experimental conditions where the temperature or ionic strength were not accurately controlled, or even specified at all (Martell and Motekaitis, 1992). It was decided to use critical stability constants whenever possible. Values chosen had been determined at tem-

perature and ionic strength as close as possible to 25°C and 0.1 M respectively. The values of the constants used for the determination of the composition of our solutions are given in table A.1 below.

## References for table A.1

*a.* Smith and Martell (1989)

*b.* Sillen and Martell (1971)

*c.* Sigel *et al.* (1982)

*d.* Smith and Martell (1976)

*e.* Martell and Smith (1982)

*f.* Abbott (1976)

*g.* Martell and Smith (1974)

Table A.1: Stability constants for the formation of the complexes for ligands and metals present in the experimental solutions. Stability constants are expressed as $\log_{10}$K, where K is an association constant in $M^{-1}$.

| Ligand L | Metal/$H^+$ | Equilibrium | $\log_{10}$K | Reference |
|---|---|---|---|---|
| Acetate $C_2H_3O_2^-$ | $H^+$ | $HL/H \cdot L$ | 4.56 | *a* |
| | $K^+$ | $ML/M \cdot L$ | -0.41 | *a* |
| Azide $N_3^-$ | $H^+$ | $HL/H \cdot L$ | 4.64 | *b* |
| Bistris $C_8H_{19}O_5N$ | $H^+$ | $HL/H \cdot L$ | 6.56 | *a* |
| | $Na^+$ | $ML/M \cdot L$ | -0.8 | *a* |
| | $K^+$ | $ML/M \cdot L$ | -0.9 | *c* |
| Chloride $Cl^-$ | $Na^+$ | $ML/M \cdot L$ | -0.4 | *a* |
| | $K^+$ | $ML/M \cdot L$ | -0.7 | *d* |
| | $Ca^{2+}$ | $ML/M \cdot L$ | 0.08 | *e* |
| | $Mg^{2+}$ | $ML/M \cdot L$ | 0.2 | *a* |
| Citrate $C_6H_5O_7^{3-}$ | $H^+$ | $HL/H \cdot L$ | 5.70 | *a* |
| | | $H_2L/H \cdot HL$ | 4.35 | *a* |
| | | $H_3L/H \cdot H_2L$ | 2.90 | *a* |
| | $Na^+$ | $ML/M \cdot L$ | 0.71 | *a* |
| EGTA $C_{14}H_{20}O_{10}N_2^{4-}$ | $H^+$ | $HL/H \cdot L$ | 9.40 | *a* |
| | | $H_2L/H \cdot HL$ | 8.78 | *a* |
| | | $H_3L/H \cdot H_2L$ | 2.66 | *e* |
| | | $H_4L/H \cdot H_3L$ | 2.0 | *e* |
| | | $H_5L/H \cdot H_4L$ | 0.9 | *a* |
| | $Na^+$ | $ML/M \cdot L$ | 1.38 | *b* |
| | $K^+$ | $ML/M \cdot L$ | 0.96 | *f* |
| | $Ca^{2+}$ | $ML/M \cdot L$ | 10.86 | *g* |
| | | $MHL/ML \cdot H$ | 3.79 | *g* |
| | $Mg^{2+}$ | $ML/M \cdot L$ | 5.28 | *g* |
| | | $MHL/ML \cdot H$ | 7.62 | *g* |
| Phosphate $PO_4^{3-}$ | $H^+$ | $HL/H \cdot L$ | 11.79 | *a* |
| | | $H_2L/H \cdot HL$ | 6.75 | *a* |
| | | $H_3L/H \cdot H_2L$ | 1.9 | *a* |
| | $Na^+$ | $ML/M \cdot L$ | 0.82 | *a* |
| | | $MHL/M \cdot HL$ | 0.49 | *a* |
| | | $MH_2L/M \cdot H_2L$ | 0.2 | *a* |
| | $K^+$ | $ML/M \cdot L$ | 0.54 | *a* |
| | | $MHL/M \cdot HL$ | 0.35 | *a* |
| | | $MH_2L/M \cdot H_2L$ | 0.2 | *a* |
| | $Ca^{2+}$ | $ML/M \cdot L$ | 6.46 | *d* |
| | | $MHL/M \cdot HL$ | 2.66 | *a* |
| | | $MH_2L/M \cdot H_2L$ | 1.41 | *a* |
| | $Mg^{2+}$ | $ML/M \cdot L$ | 3.4 | *d* |
| | | $MHL/M \cdot HL$ | 1.86 | *a* |
| | | $MH_2L/M \cdot H_2L$ | 1.66 | *a* |
| Tris $C_4H_{11}O_3N$ | $H^+$ | $HL/H \cdot L$ | 8.11 | *a* |
| | $Na^+$ | $ML/M \cdot L$ | -0.72 | *a* |

# Appendix B

# Sequence derived properties of muscle proteins and BSA

This appendix contains values of parameters characterizing physical properties of muscle proteins and BSA, derived from their amino acid sequences. Sequences were analysed for all the main proteins found in rabbit muscle that were available in the protein sequence database OWL (Bleasby and Wootton, 1990) or in literature. When the rabbit sequence had not been determined, but a sequence for another species could be obtained, that sequence was used (human C-protein, titin and nebulin). The sequence of the chicken myosin subfragment-1 was also analysed. The protein sequences used are listed in table B.1 together with the source from which they were obtained.

Table B.2 lists the values of the following parameters: number of amino acid residues $N_{aa}$, molecular weight MW, molecular charge $q_{mol}$ at pH 7.0, specific charge $q_{spe}$ at pH 7.0 and isoelectric point pI. The molecular weight was calculated using the program PEPTIDESORT contained in the GCG package (Devereux *et al.*, 1984). The molecular charge was calculated as described in section 2.6. The specific charge, which is a useful parameter characterizing the density of electric charge on proteins, was obtained by dividing the molecular charge by the molecular weight. The isoelectric point was determined from the pH dependence of the molecular charge.

Table B.1: Protein sequence database OWL (Bleasby and Wootton, 1990) codes (in capitals) or literature references for the analysed protein sequences. **R**, **H**, **C** and **B** denote rabbit, human, chicken and bovine proteins respectively. 'Fast' and 'slow' denote isoforms from fast and slow skeletal muscle respectively, other isoforms are also indicated. Two numbers separated with an arrow symbolize the beginning and end of a fragment of the cited sequence.

| Protein | Species | Isoform | OWL CODE / literature |
|---|---|---|---|
| ELC1 | R | fast | MLE1_RABIT |
| | C | fast | MLE1_CHICK |
| ELC3 | R | fast | MLE3_RABIT |
| | C | fast | MLE3_CHICK |
| RLC | R | fast, 1 | MLRT_RABIT |
| | | fast, 2 | MLRS_RABIT |
| | C | fast | MLRS_CHICK |
| S1 | R | skeletal | Tong and Elzinga (1990) 1→204[a] |
| | | | A35557[b] |
| | | | Tong and Elzinga (1990) 647→809[c] |
| | C | fast | MYSS_CHICK 1→843[d] |
| myosin rod | R | skeletal | MYSS_RABIT |
| S2 | R | skeletal | MYSS_RABIT 1→428 |
| LMM | R | skeletal | MYSS_RABIT 429→1084 |
| actin | R | skeletal, $\alpha$ | ACTS_HUMAN |
| tropomyosin | R | skeletal, $\alpha$ | TPMA_RABIT |
| | | skeletal, $\beta$ | TPMB_RABIT |
| troponin C | R | fast | TPCS_RABIT |
| | | slow | TPCC_RABIT |
| troponin I | R | fast | TRIF_RABIT |
| | | slow | TRIS_RABIT |
| troponin T | R | fast, 2 | TRTB_RABIT |
| C protein | H | fast | S36845 |
| | | slow | CPSS_HUMAN |
| titin | H | cardiac | I38344 |
| nebulin | H | skeletal | S55024 |
| KMLC | R | skeletal | KMLC_RABIT |
| BSA | B | – | ALBU_BOVIN 25→607 |

[a] 23 kDa fragment of myosin S1.
[b] 50 kDa fragment of myosin S1.
[c] 20 kDa fragment of myosin S1.
[d] Residues 1→204, 205→646, 647→843 for the 23, 50 and 20 kDa fragments respectively.

Table B.2: Number of amino acid residues $N_{aa}$, values of the molecular weight MW, molecular charge $q_{mol}$ at pH 7.0, specific charge $q_{spe}$ at pH 7.0 and isoelectric point pI of muscle proteins and BSA as calculated from their amino acid sequences (listed in table B.1). **R**, **H**, **C**, **B** denote rabbit, human, chicken and bovine proteins respectively, protein isoforms are also indicated. MW is expressed in kDa, $q_{mol}$ and $q_{spe}$ are expressed in the units of electronic charge per molecule and per $10^5$ Da respectively.

| Protein | Species | Isoform | $N_{aa}$ | MW | $q_{mol}$ | $q_{spe}$ | pI |
|---|---|---|---|---|---|---|---|
| ELC1 | R | fast | 191 | 20.817 | -7.9 | -37.7 | 4.7 |
| | C | fast | 190 | 20.696 | -7.9 | -37.9 | 4.7 |
| ELC3 | R | fast | 149 | 16.527 | -10.9 | -65.7 | 4.3 |
| | C | fast | 149 | 16.579 | -12.9 | -77.5 | 4.2 |
| RLC | R | fast, 1 | 169 | 18.897 | -8.0 | -42.4 | 4.5 |
| | | fast, 2 | 169 | 18.895 | -8.0 | -42.4 | 4.5 |
| | C | fast | 166 | 18.637 | -9.0 | -48.3 | 4.5 |
| S1 (23 kDa) | R | skeletal | 204 | 22.898 | 1.2 | 5.4 | 8.4 |
| | C | fast | 204 | 22.916 | 0.3 | 1.4 | 7.4 |
| S1 (50 kDa) | R | skeletal | 442 | 49.945 | -5.4 | -10.8 | 5.8 |
| | C | fast | 442 | 49.906 | -6.3 | -12.6 | 5.8 |
| S1 (20 kDa) | R | skeletal | 163 | 18.765 | 10.3 | 55.0 | 10.1 |
| | C | fast | 197 | 23.234 | 16.4 | 70.4 | 10.5 |
| S1 heavy chain | R | skeletal | 809 | 91.571 | 6.2 | 6.7 | 8.2 |
| | C | fast | 843 | 96.020 | 10.4 | 10.9 | 8.6 |
| S1* | R | † | 1155 | 129.854 | -10.7 | -8.2 | 6.0 |
| | C | fast | 1179 | 133.295 | -8.9 | -6.7 | 6.2 |
| S2 | R | skeletal | 856 | 98.690 | -63.1 | -63.9 | 4.6 |
| LMM | R | skeletal | 1312 | 152.321 | -49.0 | -32.2 | 5.2 |
| myosin rod | R | skeletal | 2168 | 250.975 | -112.0 | -44.6 | 4.9 |
| HMM* | R | † | 3166 | 358.362 | -84.4 | -23.6 | 5.1 |
| myosin* | R | † | 4478 | 510.647 | -133.4 | -26.1 | 5.2 |
| actin | R | skeletal, $\alpha$ | 377 | 42.051 | -12.5 | -29.7 | 5.0 |
| tropomyosin | R | skeletal, $\alpha$ | 284 | 32.680 | -26.8 | -82.0 | 4.4 |
| | | skeletal, $\beta$ | 284 | 32.836 | -28.0 | -85.1 | 4.4 |
| troponin C | R | fast | 159 | 17.965 | -28.9 | -161.0 | 3.8 |
| | | slow | 161 | 18.402 | -29.1 | -158.1 | 3.7 |
| troponin I | R | fast | 181 | 21.083 | 4.2 | 20.0 | 9.2 |
| | | slow | 184 | 21.143 | 14.2 | 67.2 | 10.4 |
| troponin T | R | fast, 2 | 260 | 30.618 | 3.6 | 11.9 | 9.4 |
| C protein | H | fast | 1142 | 128.142 | 1.3 | 1.0 | 7.3 |
| | | slow | 1138 | 127.789 | -23.5 | -18.4 | 5.3 |
| titin | H | cardiac | 26926 | 3364.110 | -131.7 | -3.9 | 6.3 |
| nebulin | H | skeletal | 6669 | 773.208 | 186.7 | 24.1 | 9.4 |
| KMLC | R | skeletal | 607 | 65.336 | -20.6 | -31.5 | 4.9 |
| BSA | B | – | 583 | 66.409 | -17.7 | -26.6 | 5.4 |

⋆ The ratio of ELC1 to ELC3 in S1 was taken as 2:1 for rabbit and 1:1 for chicken (Wagner, 1982).

† S1, HMM and myosin consist of the skeletal heavy chain and light chains from fast type muscle.

# Appendix C

# Donnan potentials

This appendix contains tables with the values of Donnan potential $U_D$, protein concentration $c_p$, temperature $T$ and specific charge $q_{spe}$ for F-actin, tropomyosin-troponin complex (Tm-tn), reconstituted thin filaments (RTFs) and bovine serum albumin (BSA) in solutions of various pCa. The measurements were performed as described in chapter 5.

Table C.1: Donnan potential $U_D$, protein concentration $c_p$, temperature $T$ and specific charge $q_{spe}$ (in electronic charge units per $10^5$ Da) for F-actin in solutions of various pCa. The number of Donnan potential measurements was n.

| pCa | $U_D \pm$ SD (mV) | $c_p$ (mg/ml) | $T$ (°C) | $q_{spe}$ | n |
|---|---|---|---|---|---|
| 8.7 | -0.95±0.04 | 6.5 | 19.5 | -21.9 | 14 |
| | -1.08±0.07 | 6.4 | 20.4 | -25.1 | 11 |
| | -1.09±0.02 | 6.7 | 20.9 | -24.3 | 10 |
| | -1.19±0.06 | 7.7 | 21.1 | -23.3 | 10 |
| | -1.34±0.04 | 7.8 | 21.4 | -25.6 | 14 |
| | -1.24±0.05 | 7.7 | 21.5 | -23.9 | 14 |
| 7.9 | -1.32±0.06 | 7.8 | 20.3 | -25.3 | 12 |
| | -1.12±0.05 | 7.4 | 20.3 | -22.5 | 13 |
| | -1.10±0.05 | 7.2 | 20.6 | -22.8 | 15 |
| | -1.20±0.10 | 6.8 | 20.7 | -26.3 | 15 |
| | -1.09±0.03 | 7.1 | 21.0 | -22.9 | 11 |
| | -1.14±0.05 | 7.1 | 21.1 | -23.9 | 11 |
| 7.1 | -1.17±0.04 | 6.3 | 18.4 | -27.9 | 13 |
| | -1.10±0.07 | 6.5 | 19.0 | -25.0 | 12 |
| | -1.03±0.07 | 7.0 | 19.5 | -21.8 | 11 |
| | -1.01±0.07 | 6.6 | 19.8 | -22.7 | 13 |
| | -1.05±0.09 | 7.0 | 20.1 | -22.1 | 17 |
| | -1.08±0.08 | 6.7 | 20.4 | -23.7 | 15 |
| 6.4 | -1.09±0.05 | 7.0 | 20.8 | -22.8 | 11 |
| | -1.09±0.06 | 7.1 | 20.8 | -22.5 | 11 |
| | -1.15±0.08 | 6.6 | 20.7 | -25.3 | 13 |
| | -1.10±0.05 | 7.2 | 20.8 | -22.3 | 10 |
| | -1.15±0.04 | 6.7 | 20.9 | -25.4 | 12 |
| | -1.11±0.04 | 7.0 | 20.9 | -23.1 | 14 |
| 5.1 | -1.04±0.06 | 5.2 | 18.8 | -29.4 | 8 |
| | -0.96±0.13 | 6.5 | 18.3 | -21.6 | 10 |
| | -1.07±0.06 | 6.4 | 19.0 | -24.5 | 13 |
| | -1.03±0.06 | 7.2 | 19.8 | -21.1 | 16 |
| | -1.10±0.05 | 7.8 | 20.1 | -20.6 | 10 |
| | -1.18±0.05 | 7.7 | 20.5 | -22.3 | 13 |
| 3.9 | -0.85±0.12 | 5.1 | 19.0 | -24.5 | 19 |
| | -0.99±0.10 | 5.2 | 19.7 | -27.7 | 17 |
| | -0.97±0.04 | 5.3 | 19.9 | -26.8 | 12 |
| | -0.89±0.12 | 6.9 | 20.0 | -18.8 | 18 |
| | -1.45±0.08 | 8.9 | 19.3 | -23.8 | 13 |
| | -1.38±0.08 | 9.8 | 19.5 | -20.6 | 11 |
| 3.2 | -0.72±0.03 | 6.1 | 21.0 | -16.9 | 12 |
| | -0.72±0.03 | 5.9 | 21.0 | -17.4 | 11 |
| | -0.73±0.05 | 6.2 | 21.0 | -16.8 | 11 |
| | -0.84±0.04 | 6.4 | 21.0 | -18.7 | 11 |
| | -0.97±0.05 | 6.3 | 20.9 | -21.8 | 12 |
| | -0.84±0.10 | 6.5 | 21.0 | -18.5 | 9 |

Table C.2: Donnan potential $U_D$, protein concentration $c_p$, temperature $T$ and specific charge $q_{spe}$ (in electronic charge units per $10^5$ Da) for Tm-tn in solutions of various pCa. The number of Donnan potential measurements was n.

| pCa | $U_D \pm$ SD (mV) | $c_p$ (mg/ml) | $T$ (°C) | $q_{spe}$ | n |
|---|---|---|---|---|---|
| 8.7 | -1.56±0.06 | 9.1 | 19.6 | -25.8 | 11 |
| | -1.08±0.07 | 7.5 | 18.8 | -21.7 | 13 |
| | -1.39±0.06 | 9.1 | 19.0 | -22.9 | 12 |
| | -1.54±0.04 | 9.2 | 19.2 | -25.1 | 10 |
| | -1.62±0.05 | 8.9 | 19.3 | -27.4 | 10 |
| | -1.72±0.04 | 9.1 | 19.4 | -28.5 | 11 |
| 7.9 | -1.40±0.04 | 8.9 | 20.8 | -23.3 | 10 |
| | -1.47±0.04 | 8.8 | 20.5 | -24.9 | 10 |
| | -1.47±0.02 | 8.7 | 20.3 | -25.1 | 9 |
| | -1.54±0.05 | 9.0 | 20.1 | -25.6 | 11 |
| | -1.59±0.04 | 8.7 | 19.9 | -27.4 | 12 |
| | -1.51±0.04 | 8.7 | 19.8 | -25.9 | 11 |
| 7.1 | -1.83±0.06 | 10.1 | 18.5 | -27.0 | 11 |
| | -1.76±0.10 | 10.2 | 18.0 | -25.9 | 11 |
| | -1.81±0.03 | 9.9 | 17.9 | -27.4 | 10 |
| | -1.76±0.04 | 10.1 | 18.0 | -26.2 | 10 |
| | -1.74±0.04 | 9.1 | 18.5 | -28.3 | 11 |
| | -1.79±0.07 | 10.1 | 18.8 | -26.5 | 13 |
| 6.4 | -1.62±0.02 | 8.6 | 18.7 | -27.8 | 9 |
| | -1.81±0.02 | 9.9 | 18.4 | -27.0 | 10 |
| | -1.66±0.17 | 9.7 | 18.4 | -25.4 | 15 |
| | -1.70±0.08 | 9.6 | 18.5 | -26.2 | 11 |
| | -1.73±0.06 | 9.9 | 18.9 | -25.7 | 12 |
| | -1.79±0.03 | 10.1 | 19.0 | -25.9 | 11 |
| 5.1 | -1.78±0.05 | 10.0 | 20.9 | -25.9 | 10 |
| | -1.67±0.04 | 10.5 | 20.5 | -23.3 | 11 |
| | -1.72±0.05 | 9.9 | 20.2 | -25.3 | 12 |
| | -1.81±0.04 | 9.8 | 20.1 | -27.0 | 11 |
| | -1.61±0.02 | 9.3 | 20.0 | -25.4 | 9 |
| | -1.69±0.15 | 10.1 | 20.0 | -24.5 | 14 |
| 3.9 | -1.86±0.02 | 10.8 | 19.3 | -25.0 | 12 |
| | -1.82±0.04 | 10.9 | 19.4 | -24.3 | 10 |
| | -1.79±0.04 | 11.1 | 19.7 | -23.4 | 11 |
| | -1.83±0.03 | 11.2 | 19.9 | -23.9 | 10 |
| | -1.81±0.04 | 10.1 | 20.2 | -25.9 | 10 |
| | -1.91±0.01 | 10.8 | 20.3 | -25.7 | 10 |
| 3.2 | -1.63±0.04 | 10.7 | 21.1 | -21.6 | 10 |
| | -1.64±0.03 | 10.7 | 21.0 | -21.8 | 11 |
| | -1.60±0.04 | 10.8 | 21.0 | -21.2 | 12 |
| | -1.70±0.06 | 10.7 | 21.1 | -22.6 | 11 |
| | -1.61±0.02 | 10.1 | 21.4 | -22.7 | 11 |
| | -1.74±0.03 | 10.7 | 21.5 | -23.2 | 11 |

Table C.3: Donnan potential $U_D$, protein concentration $c_p$, temperature $T$ and specific charge $q_{spe}$ (in electronic charge units per $10^5$ Da) for RTFs in solutions of various pCa. The number of Donnan potential measurements was n.

| pCa | $U_D \pm$ SD (mV) | $c_p$ (mg/ml) | $T$ (°C) | $q_{spe}$ | n |
|---|---|---|---|---|---|
| | -1.29±0.07 | 6.4 | 20.0 | -30.0 | 9 |
| | -1.33±0.02 | 6.5 | 20.6 | -30.6 | 11 |
| 8.7 | -1.22±0.04 | 6.9 | 20.9 | -26.5 | 11 |
| | -1.26±0.02 | 6.6 | 21.0 | -28.5 | 11 |
| | -1.26±0.05 | 6.3 | 21.2 | -29.9 | 12 |
| | -1.39±0.04 | 6.4 | 21.2 | -32.7 | 14 |
| | -0.89±0.04 | 5.2 | 20.6 | -25.9 | 11 |
| | -0.98±0.04 | 5.1 | 20.7 | -28.7 | 13 |
| 7.9 | -0.93±0.05 | 4.9 | 20.6 | -28.3 | 13 |
| | -0.94±0.03 | 4.5 | 20.8 | -31.0 | 10 |
| | -0.91±0.04 | 4.5 | 20.9 | -30.3 | 13 |
| | -1.71±0.08 | 7.8 | 20.1 | -32.9 | 15 |
| | -1.16±0.06 | 6.4 | 19.4 | -26.7 | 13 |
| | -0.95±0.05 | 6.2 | 19.7 | -22.8 | 12 |
| 7.1 | -0.96±0.04 | 6.0 | 20.1 | -24.0 | 11 |
| | -0.98±0.04 | 5.7 | 20.2 | -25.6 | 11 |
| | -0.88±0.03 | 5.2 | 20.5 | -25.3 | 13 |
| | -0.93±0.04 | 5.1 | 20.8 | -26.9 | 13 |
| | -1.47±0.10 | 7.5 | 19.3 | -29.0 | 17 |
| | -1.60±0.07 | 7.5 | 20.0 | -31.2 | 12 |
| 6.4 | -1.66±0.04 | 7.0 | 20.2 | -34.8 | 12 |
| | -1.38±0.06 | 7.1 | 20.5 | -28.7 | 12 |
| | -1.25±0.04 | 5.4 | 20.8 | -34.2 | 12 |
| | -1.46±0.04 | 6.2 | 21.0 | -34.5 | 12 |
| | -0.81±0.08 | 4.2 | 17.4 | -28.4 | 17 |
| | -0.84±0.04 | 4.2 | 18.0 | -29.9 | 13 |
| 5.1 | -0.77±0.07 | 4.9 | 18.6 | -23.3 | 13 |
| | -0.76±0.08 | 4.7 | 18.9 | -23.9 | 11 |
| | -0.86±0.04 | 4.5 | 20.6 | -27.7 | 13 |
| | -0.71±0.05 | 3.1 | 19.8 | -33.6 | 13 |
| | -1.12±0.09 | 5.9 | 20.7 | -27.5 | 12 |
| | -0.85±0.03 | 5.8 | 20.6 | -21.4 | 11 |
| 3.9 | -0.89±0.03 | 5.9 | 20.6 | -21.8 | 13 |
| | -0.94±0.03 | 5.3 | 17.5 | -26.1 | 13 |
| | -0.94±0.04 | 6.0 | 17.9 | -23.0 | 10 |
| | -0.96±0.06 | 5.7 | 18.5 | -24.9 | 18 |
| | -0.92±0.05 | 6.4 | 20.5 | -20.3 | 11 |
| | -0.81±0.12 | 6.6 | 20.2 | -17.4 | 10 |
| 3.2 | -0.63±0.12 | 5.6 | 20.3 | -16.0 | 9 |
| | -0.67±0.05 | 5.8 | 20.5 | -16.4 | 10 |
| | -0.82±0.06 | 6.1 | 20.7 | -19.2 | 11 |
| | -0.94±0.06 | 6.1 | 21.0 | -21.9 | 11 |

Table C.4: Donnan potential $U_D$, protein concentration $c_p$, temperature $T$ and specific charge $q_{spe}$ (in electronic charge units per $10^5$ Da) for BSA in solutions of various pCa. The Donnan potential values represent single measurements.

| pCa | $U_D$ (mV) | $c_p$ (mg/ml) | $T$ (°C) | $q_{spe}$ |
|---|---|---|---|---|
| 8.7 | -0.77 | 6.6 | 24.0 | -17.4 |
| | -0.72 | 6.6 | | -16.2 |
| | -0.75 | 6.9 | | -16.1 |
| | -0.77 | 6.2 | | -18.4 |
| | -0.68 | 6.4 | | -15.7 |
| | -0.64 | 6.3 | | -15.0 |
| 7.9 | -1.27 | 9.4 | 23.2 | -20.0 |
| | -1.06 | 9.2 | | -17.1 |
| | -1.06 | 9.5 | | -16.4 |
| | -1.00 | 9.8 | | -15.2 |
| | -1.04 | 9.7 | | -16.0 |
| | -1.19 | 9.8 | | -17.9 |
| 7.1 | -1.19 | 10.4 | 22.0 | -16.9 |
| | -1.13 | 10.3 | | -16.1 |
| | -1.15 | 10.5 | | -16.2 |
| | -1.09 | 10.3 | | -15.7 |
| | -1.11 | 10.0 | | -16.4 |
| | -1.11 | 9.8 | | -16.8 |
| 6.4 | -1.24 | 10.5 | 22.0 | -17.2 |
| | -1.15 | 10.5 | | -16.0 |
| | -1.21 | 10.6 | | -16.6 |
| | -1.01 | 10.4 | | -14.2 |
| | -1.03 | 10.5 | | -14.3 |
| | -1.14 | 10.4 | | -16.0 |
| 5.1 | -1.28 | 9.8 | 22.5 | -18.9 |
| | -1.18 | 9.7 | | -17.7 |
| | -1.09 | 9.9 | | -16.0 |
| | -1.01 | 9.6 | | -15.2 |
| | -1.16 | 9.6 | | -17.5 |
| | -1.10 | 9.8 | | -16.3 |
| 3.9 | -1.23 | 10.6 | 22.0 | -16.7 |
| | -1.12 | 10.2 | | -15.8 |
| | -1.09 | 10.2 | | -15.5 |
| | -1.17 | 10.2 | | -16.5 |
| | -1.17 | 10.4 | | -16.2 |
| | -1.13 | 10.3 | | -15.9 |
| 3.2 | -1.30 | 12.6 | 18.6 | -14.8 |
| | -1.25 | 12.4 | | -14.5 |
| | -1.33 | 12.3 | | -15.5 |
| | -1.27 | 12.6 | | -14.5 |
| | -1.25 | 12.4 | | -14.4 |
| | -1.38 | 12.3 | | -16.1 |

# Bibliography


Abbott, R. H. (1976). PERRIN. Computer program (ALGOL) based on the algorithm of Perrin and Sayce (1967). Personal communication to G.F.Elliott.

Abola, E. E., Bernstein, F. C., Bryant, S. H., Koetzle, T. F., and Weng, J. (1987). *Crystallographic Databases - information content, software systems, scientific applications*, pages 107–132. Data Commission of the International Union of Crystallography.

Aldoroty, R. A. and April, E. W. (1984). Donnan potentials from striated muscle liquid crystals: A-band and I-band measurements. *Biophys. J.*, **46**, 769–779.

Ammann, D. (1986). *Ion-selective microelectrodes*. Springer-Verlag.

Applied Biosystems Inc. (1989). *Applied Biosystems model 420A amino acid analysis system user manual version 3.22*.

April, E. W., Brandt, P. W., and Elliott, G. F. (1969). X-ray diffraction measurements of the lattice dimensions of crayfish single muscle fibers. *Anat. Record*, **163**, 148.

Bagshaw, C. R. (1993). *Muscle contraction*. Chapman & Hall.

Barlow, D. J. and Thornton, J. M. (1986). The distribution of charged groups in proteins. *Biopolymers*, **25**, 1717–1733.

Bartels, E. M. and Elliott, G. F. (1981). Donnan potentials from the A- and I-bands of skeletal muscle, relaxed and in rigor. *J. Physiol.*, **317**, 85–87P.

Bartels, E. M. and Elliott, G. F. (1982). Donnan potentials in rat muscle: differences between skinning and glycerination. *J. Physiol.*, **327**, 72–73P.

Bartels, E. M. and Elliott, G. F. (1983). Donnan potentials in glycerinated rabbit skeletal muscle: the effects of nucleotides and of pyrophosphate. *J. Physiol.*, **343**, 32–33P.

Bartels, E. M. and Elliott, G. F. (1985). Donnan potentials from the A- and I-bands of glycerinated and chemically skinned muscles, relaxed and in rigor. *Biophys. J.*, **48**, 61–76.

Bartels, E. M., Cooke, P. H., Elliott, G. F., and Hughes, R. A. (1984). Donnan potential changes in rabbit muscle A-bands are associated with myosin. *J. Physiol.*, **358**, 80P.

Bartels, E. M., Cooke, P. H., Elliott, G. F., and Hughes, R. A. (1993). The myosin molecule - charge response to nucleotide binding. *Biochim. Biophys. Acta*, **1157**, 63–73.

Bernstein, F. C., Koetzle, T. F., Williams, G. J. B., Meyer, Jr., E. F., Brice, M. D., Rodgers, J. R., Kennard, O., Shimanouchi, T., and Tasumi, M. (1977). The protein data bank: A computer-based archival file for macromolecular structures. *J. Mol. Biol.*, **112**, 535–542.

Bleasby, A. J. and Wootton, J. C. (1990). Construction of validated, non-redundant composite protein sequence databases. *Prot. Eng.*, **3**, 153–159.

Bradbury, J. H. and Brown, L. R. (1973). Determination of the dissociation constants of the lysine residues of lysozyme by Proton-Magnetic-Resonance Spectroscopy. *Eur. J. Biochem.*, **40**, 565–576.

Bull, H. B. (1971). *An introduction to physical biochemistry.* F.A.Davis Company, Philadelphia.

Cantiello, H. F., Patenaude, C., and Zaner, K. (1991). Osmotically induced electrical signals from actin filaments. *Biophys. J.*, **59**, 1284–1289.

Celio, M. R., Pauls, T. L., and Schwaller, B. (1996). *Guidebook to the calcium-binding proteins.* Oxford University Press.

Collins, Jr., E. W. and Edwards, C. (1971). Role of Donnan equilibrium in the resting potentials in glycerol-extracted muscle. *Amer. J. Physiol.*, **221**, 1130–1133.

Cooke, R. (1975). The role of the bound nucleotide in the polymerization of actin. *Biochem.*, **14**, 3250–3256.

Coomber, S. J. and Elliott, G. F. (1995). Electrical measurements of calcium activation in isolated rabbit muscle myofilaments. *J. Physiol.*, **487P**, 157P.

Coomber, S. J. and Elliott, G. F. (1996). Sarcomere length (SL) dependence of Donnan potential measurements in calcium-activated isolated rabbit psoas muscle. *J. Physiol.*, **494P**, 131–132P.

Davis, J. S. and Harrington, W. F. (1987). Force generation by muscle fibers in rigor: A laser temperature-jump study. *Proc. Natl. Acad. Sci. USA*, **84**, 975–979.

Deshayes, C. (1994). *Measurements of net electrical charge on skeletal muscle proteins.* Ph.D. thesis, Open University.

Deshayes, C., Elliott, G. F., Jennison, K., Bartels, E. M., and Lambert, T. W. (1993). Electrical charge measurements on F- and G-actin from rabbit muscle at physiological ionic strengths. *J. Physiol.*, **459**, 275P.

Devereux, J., Haeberli, P., and Smithies, O. (1984). A comprehensive set of sequence analysis programs for the VAX. *Nucl. Acids Res.*, **12**, 387–395.

Donnan, F. G. (1911). Theorie der membrangleichgewichte und membranpotentiale bei vorhandensein von nicht dialysierenden elektrolyten. *Zeitschr. Elektrochem.*, **17**, 572–581.

Eisenberg, E. and Kielley, W. W. (1970). Native tropomyosin: effect on the interaction of actin with heavy meromyosin and subfragment-1. *Biochem. Biophys. Res. Comm.*, **40**, 50–56.

Elliott, G. F. (1968). Force-balances and stability in hexagonally-packed polyelectrolyte systems. *J. Theor. Biol.*, **21**, 71–87.

Elliott, G. F. (1973). Donnan and osmotic effects in muscle fibres without membranes. *J. Mechanochem. Cell Motil.*, **2**, 83–89.

Elliott, G. F. (1993). The contractile process. *Biophys.*, **12**, 149–159.

Elliott, G. F. and Bartels, E. M. (1982). Donnan potential measurements in extended hexagonal polyelectrolyte gels such as muscle. *Biophys. J.*, **38**, 195–199.

Elliott, G. F. and Worthington, C. R. (1994). How muscle may contract. *Biochim. Biophys. Acta*, **1200**, 109–116.

Elliott, G. F. and Worthington, C. R. (1995). Electrical forces in muscle contraction. *Biophys. J.*, **68**, 327S.

Elliott, G. F., Naylor, G. R. S., and Woolgar, A. E. (1978). Measurements of the electric charge on the contractile proteins in glycerinated rabbit psoas using microelectrode and diffraction effects. In D. H. Everett and B. Vincent, editors, *Ions in macromolecular and biological systems*, pages 329–339.

Elliott, G. F., Bartels, E. M., and Hughes, R. A. (1985). The myosin filament; charge amplification and charge condensation. In M. Blank, editor, *Electrical double layers in biology*, pages 277–285. Plenum Publishing Corp.

Fisher, A. J., Smith, C. A., Thoden, J. B., Smith, R., Sutoh, K., Holden, H. M., and Rayment, I. (1995). X-ray structures of the myosin motor domain of *Dictyostelium discoideum* complexed with MgADP•$BeF_x$ and MgADP•$AlF_4^{--}$. *Biochem.*, **34**, 8960–8972.

Fretheim, K. S., Iwai, R. E., and Feeney, R. E. (1979). Extensive modification of protein amino groups by reductive addition of different sized substituents. *Int. J. Pept. Protein Res.*, **14**, 451–456.

Gerken, T. A. (1984). Amino group environments and metal binding properties of Carbon-13 reductively methylated bovine $\alpha$-lactalbumin. *Biochem.*, **23**, 4688–4697.

Gerken, T. A., Jentoft, J. E., Jentoft, N., and Dearborn, D. G. (1982). Intramolecular interactions of amino groups in $^{13}C$ reductively methylated hen egg-white lysozyme. *J. Biol. Chem.*, **257**, 2894–2900.

Goa, J. (1952). A microbiuret method for protein determination. *Scand. J. Clin. Lab. Invest.*, **5**, 218–222.

Hames, B. D. and Rickwood, D. (1981). *Gel electrophoresis of proteins: a practical approach*. IRL Press Ltd.

Harafuji, H. and Ogawa, Y. (1980). Re-examination of the apparent binding constant of ethylene glycol bis($\beta$-aminoethyl ether)-N,N,N',N'-tetraacetic acid with calcium around neutral pH. *J. Bioch.*, **87**, 1305–1312.

Haselgrove, J. C. (1973). X-ray evidence for a conformational change in the actin-containing filaments of vertebrate striated muscle. *Cold Spring Harbor Symp. Quantit. Biol.*, **37**, 341–352.

Hinke, J. A. M. (1980). Water and electrolyte content of the myofilament phase in the chemically skinned barnacle fiber. *J. Gen. Physiol.*, **75**, 531–551.

Högfeldt, E. (1982). *Stability constants of metal-ion complexes.Part A: Inorganic ligands*. Pergamon Press.

Holmes, K. C., Popp, D., Gebhard, W., and Kabsch, W. (1990). Atomic model of the actin filament. *Nature*, **347**, 44–49.

Huxley, A. F. and Niedergerke, R. (1954). Structural changes in muscle during contraction. *Nature*, **173**, 971–973.

Huxley, H. and Hanson, J. (1954). Changes in the cross-striations of muscle during contraction and stretch and their structural interpretation. *Nature*, **173**, 973–976.

Huxley, H. E. (1957). The double array of filaments in cross-striated muscle. *J. Biophys. Bioch. Cytol.*, **3**, 631–647.

Huxley, H. E. (1973). Structural changes in the actin- and myosin-containing filaments during contraction. *Cold Spring Harbor Symp. Quantit. Biol.*, **37**, 361–376.

Ishikawa, T. and Wakabayashi, T. (1994). Calcium induced change in three-dimensional structure of thin filaments of rabbit skeletal muscle as revealed by cryo-electron microscopy. *Biochem. Biophys. Res. Comm.*, **203**, 951–958.

Israelachvili, J. N. (1985). *Intermolecular and surface forces: With applications to colloidal and biological systems*. Academic Press.

Jennison, K. (1992). *The electrical charge characteristics of muscle proteins*. Ph.D. thesis, Open University.

Jentoft, J. E., Jentoft, N., Gerken, T. A., and Dearborn, D. G. (1979). $^{13}$C NMR studies of ribonuclease A methylated with [$^{13}$C] formaldehyde. *J. Biol. Chem.*, **254**, 4366–4370.

Kabsch, W., Mannherz, H. G., Suck, D., Pai, E. F., and Holmes, K. C. (1990). Atomic structure of the actin:DNase I complex. *Nature*, **347**, 37–44.

Kanal, K. M., Fullerton, G. D., and Cameron, I. L. (1994). A study of the molecular sources of nonideal osmotic pressure of bovine serum albumin solutions as a function of pH. *Biophys. J.*, **66**, 153–160.

Kishino, A. and Yanagida, T. (1988). Force measurements by micromanipulation of a single actin filament by glass needles. *Nature*, **334**, 74–76.

Koretz, J. F. (1979). Effects of C-protein on synthetic myosin filament structure. *Biophys. J.*, **27**, 433–446.

Koretz, J. F., Irving, T. C., and Wang, K. (1993). Filamentous aggregates of native titin and binding of C-protein and AMP-deaminase. *Arch. Biochem. Biophys.*, **304**, 305–309.

Kraulis, J. (1991). Molscript: a program to produce both detailed and schematic plots of protein structures.

Labeit, S. and Kolmerer, B. (1995). Titins: giant proteins in charge of muscle ultrastructure and elasticity. *Science*, **270**, 293–296.

Labeit, S., Gautel, M., Lakey, A., and Trinick, J. (1992). Towards a molecular understanding of titin. *EMBO J.*, **11**, 1711–1716.

Lehman, W., Craig, R., and Vibert, P. (1994). $Ca^{2+}$-induced tropomyosin movement in *Limulus* thin filaments revealed by three-dimensional reconstruction. *Nature*, **368**, 65–67.

Ling, G. and Gerard, R. W. (1949). The normal membrane potential of frog sartorius fibers. *J. Cell. Compar. Physiol.*, **34**, 383–396.

Longsworth, L. G. and Jacobsen, C. F. (1949). An electrophoretic study of the binding of salt ions by $\beta$-lactoglobulin and bovine serum albumin. *J. Phys. Colloid Chem.*, **53**, 126–135.

Lorenz, M., Poole, K. J. V., Popp, D., Rosenbaum, G., and Holmes, K. C. (1995). An atomic model of the unregulated thin filament obtained by X-ray fiber diffraction on oriented actin-tropomyosin gels. *J. Mol. Biol.*, **246**, 108–119.

Lowey, S., Waller, G. S., and Trybus, K. M. (1993). Skeletal muscle myosin light chains are essential for physiological speeds of shortening. *Nature*, **365**, 454–456.

Margossian, S. S. and Lowey, S. (1982). Preparation of myosin and its subfragments from rabbit skeletal muscle. *Meth. Enzymol.*, **85**, 55–71.

Martell, A. E. and Motekaitis, R. J. (1992). *Determination and use of stability constants*. VCH Publishers, Inc.

Martell, A. E. and Smith, R. M. (1974). *Critical stability constants. Volume 1:Amino Acids*. Plenum Press.

Martell, A. E. and Smith, R. M. (1977). *Critical stability constants. Volume 3: Other organic ligands*. Plenum Press.

Martell, A. E. and Smith, R. M. (1982). *Critical stability constants. Volume 5:First supplement*. Plenum Press.

Minton, A. P. (1995). A molecular model for the dependence of the osmotic pressure of bovine serum albumin upon concentration and pH. *Biophys. Chem.*, **57**, 65–70.

Moos, C., Offer, G., Starr, R., and Bennett, P. (1975). Interaction of C-protein with myosin, myosin rod and light meromyosin. *J. Mol. Biol.*, **97**, 1–9.

Murray, J. M. (1982). Hybridization and reconstitution of the thin filament. *Meth. Enzymol.*, **85B**, 15–17.

Nastuk, W. L. and Hodgkin, A. L. (1950). The electrical activity of single muscle fibers. *J. Cell. Compar. Physiol.*, **35**, 39–71.

Naylor, G. R. S. (1977). *X ray and microelectrode studies of glycerinated rabbit psoas muscle*. Ph.D. thesis, Open University.

Naylor, G. R. S. (1978). A simple circuit for automatic continuous recording of microelectrode resistance. *Pflügers Arch. Eur. J. Physiol.*, **378**, 107–110.

Naylor, G. R. S., Bartels, E. M., Bridgman, T. S., and Elliott, G. F. (1985). Donnan potentials in rabbit psoas muscle in rigor. *Biophys. J.*, **48**, 47–59.

Ojteg, G., Lundahl, P., and Wolgast, M. (1989). The net electric charge of proteins. A comparison of determinations by Donnan potential measurements and by gel electrophoresis. *Biochim. Biophys. Acta*, **991**, 317–323.

Overbeek, J. T. G. (1956). The Donnan equilibrium. *Prog. Biophys. Biophys. Chem.*, **6**, 58–84.

Pardee, J. D. and Spudich, J. A. (1982). Purification of muscle actin. *Meth. Enzymol.*, **85**, 164–181.

Parry, D. A. D. and Squire, J. M. (1973). Structural role of tropomyosin in muscle regulation: analysis of the X-ray diffraction patterns from relaxed and contracting muscles. *J. Mol. Biol.*, **75**, 33–55.

Pemrick, S. M. and Edwards, C. (1974). Differences in the charge distribution of glycerol-extracted muscle fibers in rigor, relaxation, and contraction. *J. Gen. Physiol.*, **64**, 551–567.

Perrin, D. D. (1979). *Stability constants of metal-ions complexes. Part B Organic ligands*. Pergamon Press.

Perrin, D. D. and Sayce, I. G. (1967). Computer calculation of equilibrium concentrations in mixtures of metal ions and complexing species. *Talanta*, **14**, 833–842.

Peters, Jr., T. (1996). *All about albumin. Biochemistry, Genetics and Medical Applications*. Academic Press.

Phan, B. C., Cheung, P., Miller, C. J., Reisler, E., and Muhlrad, A. (1994). Extensively methylated myosin subfragment-1:Examination of local structure, interactions with nucleotides and actin, and ligand-induced conformational changes. *Biochem.*, **33**, 11286–11295.

Phillips, Jr., G. N., Lattman, E. E., Cummins, P., Lee, K. Y., and Cohen, C. (1979). Crystal structure and molecular interactions of tropomyosin. *Nature*, **278**, 413–417.

Pollard, T. D. (1982). Assays for myosin. *Meth. Enzymol.*, **85**, 123–130.

Pollard, T. D. and Weeds, A. G. (1984). The rate constant for ATP hydrolysis by polymerized actin. *FEBS Lett.*, **170**, 94–98.

Poole, K. J. V., Lorenz, M., Evans, G., Rosenbaum, G., and Holmes, K. C. (1994). The effect of calcium on the regulated thin filament structure. *Biophys. J.*, **66**, A347.

Potter, J. D. and Gergely, J. (1975). The calcium and magnesium binding sites on troponin and their role in the regulation of myofibrillar adenosine triphosphatase. *J. Biol. Chem.*, **250**, 4628–4633.

Rashin, A. A. and Honig, B. (1984). On the environment of ionizable groups in globular proteins. *J. Mol. Biol.*, **173**, 515–521.

Rayment, I., Rypniewski, W. R., Schmidt-Bäse, K., Smith, R., Tomchick, S. R., Benning, M. M., Winkelmann, D. A., Wesenberg, G., and Holden, H. M. (1993). Three-dimensional structure of myosin subfragment-1: A molecular motor. *Science*, **26**, 50–58.

Rees, M. K. and Young, M. (1967). Studies on the isolation and molecular properties of homogeneous globular actin. *J. Biol. Chem.*, **242**, 4449–4458.

Reuben, J. P., Brandt, P. W., Berman, M., and Grundfest, H. (1971). Regulation of tension in the skinned crayfish muscle fiber. I. Contraction and relaxation in the absence of Ca (pCa $>$ 9). *J. Gen. Physiol.*, **57**, 385–407.

Rome, E. (1967). Light and X-ray diffraction studies of the filament lattice of glycerol-extracted rabbit psoas muscle. *J. Mol. Biol.*, **27**, 591–602.

Rome, E. (1968). X-ray diffraction studies of the filament lattice of striated muscle in various bathing media. *J. Mol. Biol.*, **37**, 331–344.

Rypniewski, W. R., Holden, H. M., and Rayment, I. (1993). Structural consequences of reductive methylation of lysine residues in hen egg white lysozyme: An X-ray analysis at 1.8 Å resolution. *Biochem.*, **32**, 9851–9858.

Scordilis, S. P., Tedeschi, H., and Edwards, C. (1975). Donnan potential of rabbit skeletal muscle myofibrils I: electrofluorochromometric detection of potential. *Proc. Natl. Acad. Sci. USA*, **72**, 1325–1329.

Sellers, J. R. and Goodson, H. V. (1995). Motor proteins 2: myosin. *Protein Profile*, **2**, 1323–1423.

Sheterline, P. and Sparrow, J. C. (1994). Actin. *Protein Profile*, **1**, 1–121.

Sigel, H., Scheller, K. H., and Prijs, B. (1982). Metal ion/buffer interactions. *Inorg. Chim. Acta*, **66**, 147–155.

Sillen, L. G. and Martell, A. E. (1971). *Stability constants of metal-ion complexes.* The Chemical Society.

Sleep, J. A., Trybus, K. M., Johnson, K. A., and Taylor, E. W. (1981). Kinetic studies of normal and modified heavy meromyosin and subfragment-1. *J. Muscle Res. Cell Mot.*, **2**, 373–399.

Smillie, L. B. (1982). Preparation and identification of $\alpha$- and $\beta$-tropomyosins. *Meth. Enzymol.*, **85B**, 234–241.

Smith, C. A. and Rayment, I. (1995). X-ray structure of the magnesium(II)-pyrophosphate complex of the truncated head of *Dictyostelium discoideum* myosin to 2.7 Å resolution. *Biochem.*, **34**, 8973–8981.

Smith, C. A. and Rayment, I. (1996). X-ray structure of the magnesium(II)·ADP·vanadate complex of the *Dictyostelium discoideum* myosin motor domain to 1.9 Å resolution. *Biochem.*, **35**, 5404–5417.

Smith, R. M. and Martell, A. E. (1975). *Critical stability constants. Volume 2:Amines.* Plenum Press.

Smith, R. M. and Martell, A. E. (1976). *Critical stability constants. Volume 4:Inorganic complexes.* Plenum Press.

Smith, R. M. and Martell, A. E. (1989). *Critical stability constants. Volume 6:Second supplement.* Plenum Press.

Starr, R. and Offer, G. (1982). Preparation of C-protein, H-protein , and phosphofructokinase. *Meth. Enzymol.*, **85**, 130–138.

Strasburg, G. M., Greaser, M. L., and Sundaralingam, M. (1980). X-ray diffraction studies of troponin-C crystals from rabbit and chicken skeletal muscle. *J. Biol. Chem.*, **255**, 3806–3808.

Stryer, L. (1988). *Biochemistry.* W. H. Freeman and Company.

Tong, S. W. and Elzinga, M. (1990). Amino acid sequence of rabbit skeletal muscle myosin. *J. Biol. Chem.*, **265**, 4893–4901.

Toyoshima, Y. Y., Kron, S. J., McNally, E. M., Niebling, K. R., Toyoshima, C., and Spudich, J. A. (1987). Myosin subfragment-1 is sufficient to move actin filaments *in vitro*. *Nature*, **328**, 536–539.

Tumminia, S. J., Koretz, J. F., and Landau, J. V. (1989). Hydrostatic pressure studies of native and synthetic thick filaments: *in vitro* myosin aggregates at pH 7.0 with and without C-protein. *Biochim. Biophys. Acta*, **999**, 300–312.

Tumminia, S. J., Koretz, J. F., and Landau, J. V. (1990). Hydrostatic pressure studies of native and synthetic thick filaments: II. native thick filaments from rabbit skeletal muscle. *Biochim. Biophys. Acta*, **1040**, 373–381.

Wagner, P. D. (1982). Preparation and fractionation of myosin light chains and exchange of the essential light chains. *Meth. Enzymol.*, **85B**, 72–81.

Wang, K. (1982). Purification of titin and nebulin. *Meth. Enzymol.*, **85B**, 264–274.

Wang, K. (1996). Titin/connectin and nebulin: giant protein rulers of muscle structure and function. *Adv. Biophys.*, **33**, 123–134.

Weast, R. C. (1974). *Handbook of chemistry and physics.* CRC Press.

Weeds, A. G. and Taylor, R. S. (1975). Separation of subfragment-1 isoenzymes from rabbit skeletal muscle myosin. *Nature*, **257**, 54–56.

Wegner, A. (1976). Head to tail polymerization of actin. *J. Mol. Biol.*, **108**, 139–150.

White, H. D. and Rayment, I. (1993). Kinetic characterization of reductively methylated myosin subfragment 1. *Biochem.*, **32**, 9859–9865.